Dissertation zur Erlangung des Doktorgrades
der Fakultät für Chemie und Pharmazie
der Ludwig-Maximilians-Universität München

In Search of Vicinal, Carbon-Centered Superelectrophiles

Alan Virmani

aus

München, Deutschland

2022

Erklärung

Diese Dissertation wurde im Sinne von § 7 der Promotionsordnung vom 28. November 2011 von Herrn Prof. Dr. Andreas J. Kornath betreut.

Eidesstattliche Versicherung

Diese Dissertation wurde selbstständig und ohne unerlaubte Hilfe erarbeitet.

München, den 31.08.2022

…...................................
Alan Virmani

Dissertation eingereicht am   05.09.2022

1. Gutachter: Prof. Dr. Andreas J. Kornath

2. Gutachter: Prof. Dr. Konstantin Karaghiosoff

Mündliche Prüfung am   28.09.2022

Danksagung

Mein erster Dank gilt natürlich meinem Doktorvater Herrn Prof. Andreas J. Kornath für die freundliche Aufnahme in seine Arbeitsgruppe und die Möglichkeit, meine Dissertation unter seiner Anleitung anzufertigen. Ich bedanke mich auch für die fachliche Unterstützung sowie den Raum, auch meine eigenen Ideen verfolgen zu können.

Herrn Prof. Dr. Konstantin Karaghiosoff danke ich für die freundliche Bereitschaft, als Zweitgutachter zur Verfügung zu stehen.

Ein großer Dank gilt dem gesamten Arbeitskreis, allen voran Steffi, Chris, Alex, Marie, Domi, Flo, Basti, Dirk, Valentin, Ulli, Julian, Gaby aber auch Manu, Ines und Yvonne. Ihr habt dazu beigetragen, dass ich sowohl die Zeit im Labor als auch die Zeit außerhalb genießen konnte.

Hervorzuheben sind hierbei sowohl Alex und am Ende auch Dirk für die Hilfe mit meinen NMR-Spektren, als auch Gaby, die mir bei administrativen Dingen und mit Ratschlägen für alle Lebenslagen zur Seite stand.

Ein ganz besonderer Dank geht an Chris, der sich nachweislich an meinen Kristallansätzen aufgerieben hat. Ich hatte viel Spaß, mich mit dir über alles Mögliche zu unterhalten, dein Zimmerpartner auf Konferenzen zu sein, aber auch mit all den Themen inner- und außerhalb der Universität.

Ein weiterer Dank geht an meine Studierenden Martina, Constantin, Melis und Timo. Auch wenn nicht immer alles geklappt hat, eure Mithilfe leistete ein großen Beitrag zu meiner Doktorarbeit.

Zusätzlich möchte ich mich beim AK Daumann für die nette und lustige Nachbarschaft bedanken.

Auch außerhalb der Universität haben viele Menschen meinen Dank verdient. Meine Familie, insbesondere meine immer unterstützenden Eltern. Meine alten Schulfreunde Sophia, Daniel, Fabio, Michi und Kai. Meine WYBs Tobi, Niklas, Michi, Ralf, Daan, Juri, Steffi, Lara, Denise, Flo, Peter, Elli, Fionan, David, Tom, die dafür gesorgt haben, dass ich im Studium die beste Zeit meines Lebens hatte. Ganz besonders danke ich Vera. Danke für deine Unterstützung in allen Lebenslagen. Ohne dich wäre ich nicht so weit gekommen.

Table of Contents

1. Introduction

Electrophilic and nucleophilic reactions play a fundamental role in a great number of reactions in organic chemistry. The terms "electrophile" and "nucleophile" were first established by Ingold and derive from "electron-seeking" and "nucleus-seeking" compounds.[1,2] A distinct role is played by carbon-centered electrophiles, especially carbocations that are mostly formed intermediately. At the beginning of the 20th century, the triphenylmethylium ion, one of the first stable carbenium ions, was synthesized from triphenylmethyl alcohol or chloride, respectively (Equations 1 and 2).[3–5]

$$\text{(1)}$$

$$\text{(2)}$$
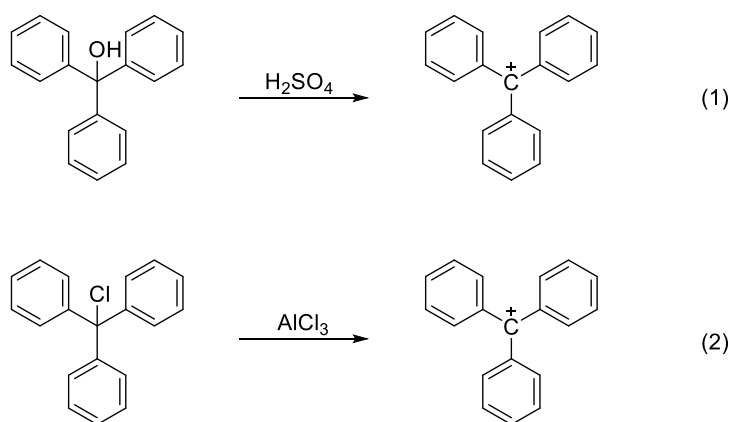
Two original types of carbocations are known. The "non-classical" carbonium ions are tetra- or pentacoordinated and thus have a full valence shell. The trivalent carbenium ions are defined as "classical" carbocations with an sp^2-hybridized central carbon atom and formally six electrons.[6] The general Lewis structures are illustrated in Figure 1.

Tetracoordinated Carbonium Ion   Pentacoordinated Carbonium Ion   Trivalent Carbenium Ion
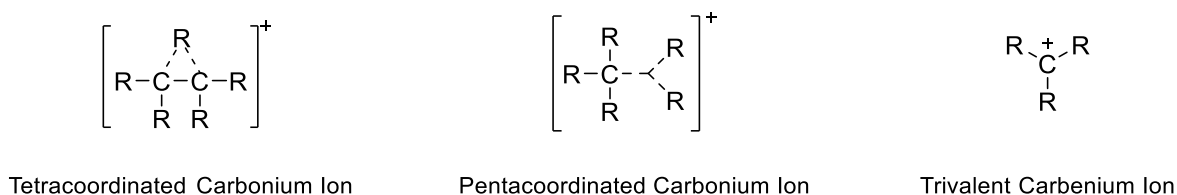
Figure 1. General Lewis structures of non-classical (tetra-/pentacoordinated) carbonium ions and classical (trivalent) carbenium ions (R = H, alkyl).

In organic chemistry, carbenium ions take an important role in electrophilic reactions. In a very large number of reactions, the reactive carbenium ion is generated intermediately by catalysis, e.g. with Brønsted acids in esterification reactions[7] or with Lewis acids in Friedel-Crafts alkylations.[8] The importance of intermediate carbenium ions was first discussed by Meerwein in 1922 when he investigated the rearrangement of camphene hydrochloride to isobornyl chloride.[9] Time after time, the concept of short-lived intermediate carbocations was established, and the interest in stabilizing these intermediates rose. One of the first examples

was the acetylium ion synthesized by Seel in 1943 by reacting acetyl fluoride with boron trifluoride.[10] Olah and co-workers found a way to generate and stabilize a great variety of carbocations in the 1960s by the use of superacids.[11] Olah's seminal work in this field helped to understand the pathways of electrophilic reactions. The importance of his contribution was emphasized when he was awarded the Nobel Prize in 1994.

But Olah was not the first one to work with superacids. The term "superacid solution" was first used by Hall and Conant in 1927,[12] and its definition as acids stronger than 100% sulfuric acid proposed by Gillespie in 1971[13] is generally accepted. Olah and his co-workers mostly used the binary superacidic system FSO_3H/SbF_5 ("magic acid") with solvents like SO_2, SO_2ClF, and SO_2F_2.[14] The low melting points and low nucleophilicity of these solvents and FSO_3H allowed them to study the thermally labile and highly electrophilic carbocations by NMR spectroscopy at low temperatures. Later, they even succeeded in stabilizing the first dicationic carbon-centered species.[15–17] However, the designation "electrophile" does not live up to the extreme reactivity of carbodications, which is why the term "superelectrophile" is much more appropriate.[18] Superelectrophiles are categorized into two types. In "gitonic" superelectrophiles the charges are in close proximity. Subcategories of gitonic carbodications are geminal (1,1), vicinal (1,2), and 1,3-superelectrophiles, whereas in "distonic" superelectrophiles the positive charges are separated by at least two atoms (>1,3-superelectrophiles). The classification is illustrated in Figure 2.[18]
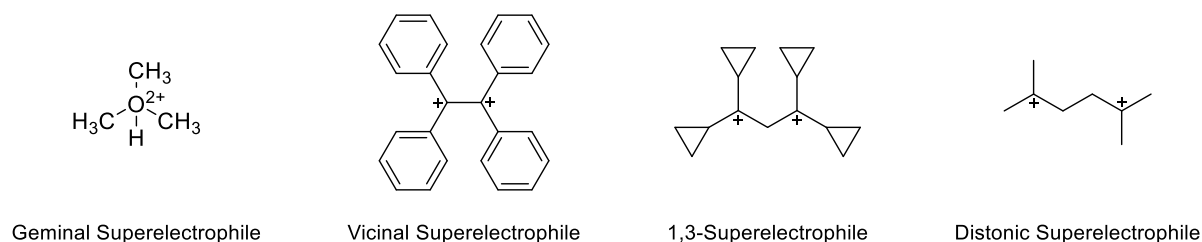

Geminal Superelectrophile   Vicinal Superelectrophile   1,3-Superelectrophile   Distonic Superelectrophile

Figure 2. Categories of superelectrophiles.[18]

Especially the generation of vicinal carbodications opened up new possibilities in organic chemistry. Distinct examples are the electrophilic reactions of 1,2-dicarbonyl compounds with benzene in highly acidic media (trifluoromethanesulfonic acid or trifluoroacetic acid), leading to geminal diphenylated products. The yield usually raised when the acidity of the medium was increased, which indicated the intermediate formation of the respective vicinal superelectrophile.[19–23] This resulted in different products and higher yields in reactions with deactivated and thus very weak nucleophiles.[21,24,25]

The simplest possible carbon-centered superelectrophile with vicinal charges is the ethylene dication $[C_2H_4]^{2+}$, which is a discrete species in the gas phase.[26] Its properties have been subject to theoretical studies in the literature. The most efficient way to delocalize the positive charges via hyperconjugation is found to be the perpendicular D_{2d} structure, resulting in a shortened CC distance.[27–29] Introducing second-row substituents like NH_2, OH, or F leads to a planar structure due to a significant donating effect of π-electrons into the $CC(\pi)$ bond according to quantum chemical calculations.[30] The Lewis structures are shown in Figure 3.
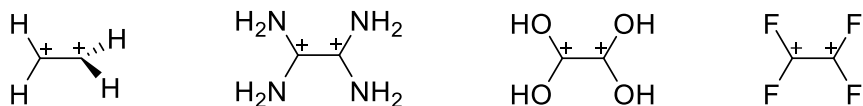
Figure 3. Lewis structures of the ethylene dication and selected derivatives.

In 2018, Schickinger and Kornath achieved the synthesis of the to-date simplest superelectrophile, the tetrahydroxydicarbenium ion $[C_2(OH)_4]^{2+}$. They were able to synthesize and isolate the dication by diprotonation of oxalic acid with the superacidic systems HF/MF_5 (M = As, Sb), allowing a structural characterization by vibrational spectroscopy and X-ray diffraction (Equation 3).[31]
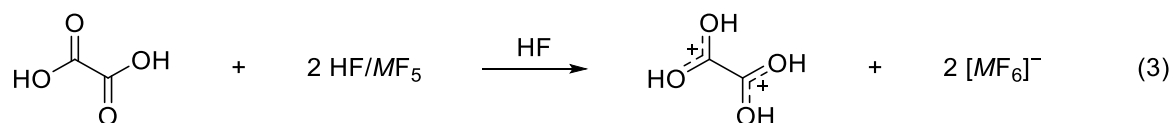
Applying anhydrous hydrogen fluoride (aHF) as a solvent does not compromise the acidity of the system compared to magic acid.[14] However, its low boiling point allows the isolation of thermally labile carbocations *in vacuo* at low temperatures, making it a powerful tool for the syntheses and characterizations of superelectrophilic compounds.[31,32]
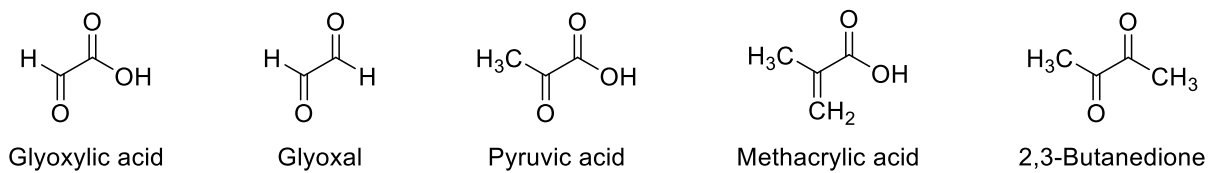
2. Objectives

The simplest vicinal carbon-centered superelectrophile that has been structurally analyzed so far is $[C_2(OH)_4]^{2+}$. As the calculations predict, it exhibits a planar C_{2h} structure, which is stabilized by π-donation.[31] To what extent this stabilization can be reduced and what happens to the carbon scaffold when this occurs can be investigated by reducing the number of heteroatoms of $[C_2(OH)_4]^{2+}$. The subsequent influence of the substituents on the geometry and what specific impact hydrogen atoms or methyl groups have are of particular interest.

By formally successively substituting the hydroxy groups of $[C_2(OH)_4]^{2+}$ for either hydrogen atoms or methyl groups, the simplest superelectrophiles without any heteroatoms and π-electrons are reached, $[C_2H_4]^{2+}$ and $[C_2(CH_3)_4]^{2+}$. The formal pathway is illustrated in Figure 4.

Figure 4. A schematic pathway from the structurally analyzed $[C_2(OH)_4]^{2+}$ cation to the plain dications $[C_2H_4]^{2+}$ and $[C_2(CH_3)_4]^{2+}$.

In search of vicinal, carbon-centered superelectrophiles even simpler than $[C_2(OH)_4]^{2+}$, a reasonable approach is the protonation of non-conjugating π-systems containing fewer heteroatoms than oxalic acid. To investigate the specific impact hydrogen atoms or methyl groups may or may not have, the substituents should be varied differently. Following this train of thought, suitable substrates to investigate first in superacidic systems are glyoxylic acid, glyoxal, pyruvic acid, methacrylic acid, and 2,3-butanedione. The Lewis structures are shown in Figure 5.

| Glyoxylic acid | Glyoxal | Pyruvic acid | Methacrylic acid | 2,3-Butanedione |

Figure 5. Lewis structures of the potential substrates to investigate in superacids in the search for vicinal, carbon-centered superelectrophiles.

3. Summary

3.1. Properties of Pyruvic Acid in Superacids

Substituting one hydroxy group of oxalic acid for a methyl group leads to the compound pyruvic acid. Protonating pyruvic acid is a promising way to generate a small, carbon-centered, and vicinal superelectrophile with fewer π-electrons than $[C_2(OH)_4]^{2+}$. The general reactions with the binary systems HF/MF_5 (M = As, Sb) are given below (Equations 4 and 5). Depending on the employed amount of Lewis acid, a single or double protonation is achieved.[33]

$$\text{(4)}$$

$$\text{(5)}$$
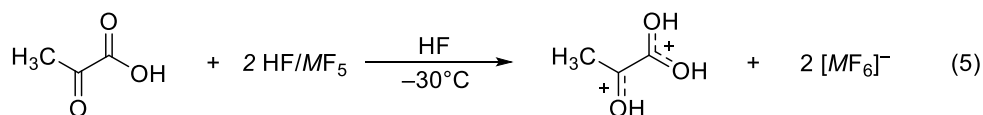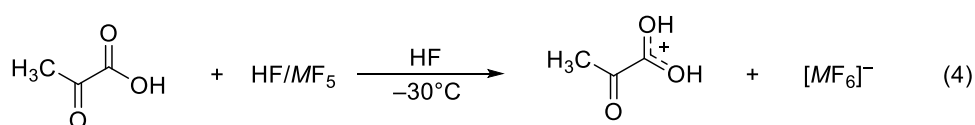
M = As, Sb

Implementing pyruvic acid with equimolar amounts of Lewis acid leads to the monoprotonated species $[C_2(O)(OH)_2Me][MF_6]$. The resulting salts are characterized by vibrational spectroscopy and in the case of the $[SbF_6]^-$ salt by single-crystal X-ray diffraction. Besides forming cation-cation chains via hydrogen bonding (Figure 6), a short non-hydrogen bridged C···F contact between a protonated carboxy group and a close-by anion is observed in the solid state (Figure 7).
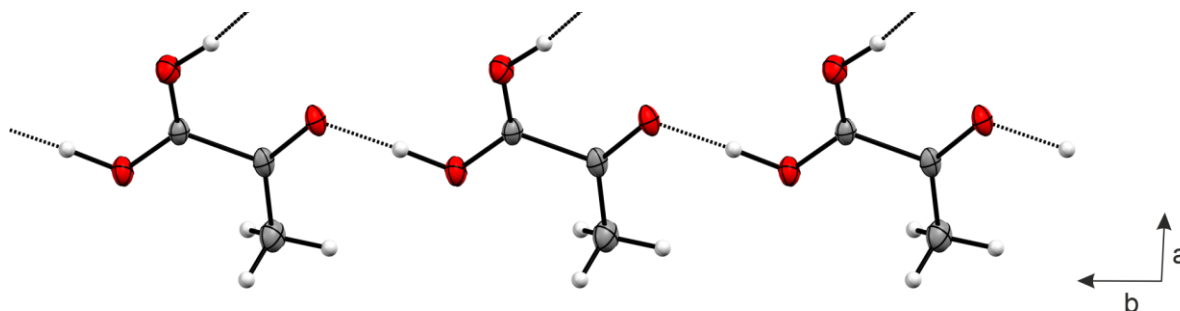

Figure 6. Cationic chain of $[C_2(O)(OH)_2Me][SbF_6]$ (50% probability displacement ellipsoids, hydrogen atoms shown as spheres of arbitrary radius).
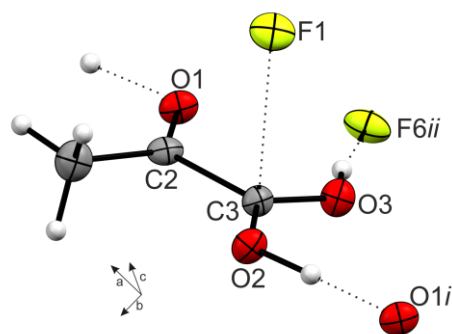
Figure 7. Interionic interactions of the cation in the crystal packing of $[C_2(O)(OH)_2Me][SbF_6]$. (50% probability displacement ellipsoids, hydrogen atoms shown as spheres of arbitrary radius). Symmetry codes: $i = -1+x, y, z$; $ii = -1-x, -y, 3-z$.

By applying a twofold amount of Lewis acid, the diprotonated salts $[C_2(OH)_3Me][MF_6]_2$ are formed. The vibrational mode as well as the bond distance of the central C−C bond remain unaffected by successive protonation.[34,35] The X-ray structure analysis of the $[SbF_6]^-$ salt reveals two short non-hydrogen bridged C···F contacts of adjacent anions with each carboxonium moiety, similar to the monoprotonated species (Figure 8).
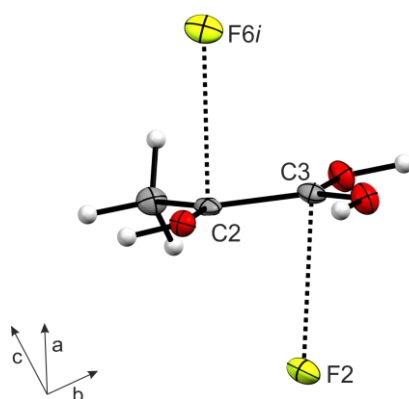

Figure 8. Non-hydrogen bridged C···F contacts in $[C_2(OH)_3Me][SbF_6]_2$ (50% probability displacement ellipsoids, hydrogen atoms as spheres of arbitrary radius). Symmetry code: $i = 1+x, y, z$.

To explain the remarkable stability of the central C−C bond of diprotonated pyruvic acid, quantum chemical calculations on the MP2/aug-cc-pVTZ level of theory were applied. Adding five HF molecules to the optimized gas-phase structure to simulate all donor-acceptor interactions of the dication has a significant impact on the carbon scaffold compared to the calculated structure of the naked cation. The structures and the respective C−C bond lengths are illustrated in Figure 9. The perpendicular $[SbF_6]^-$ anions interact directly with the formally empty p(π) orbitals of the superelectrophile, stabilizing the C−C bond.
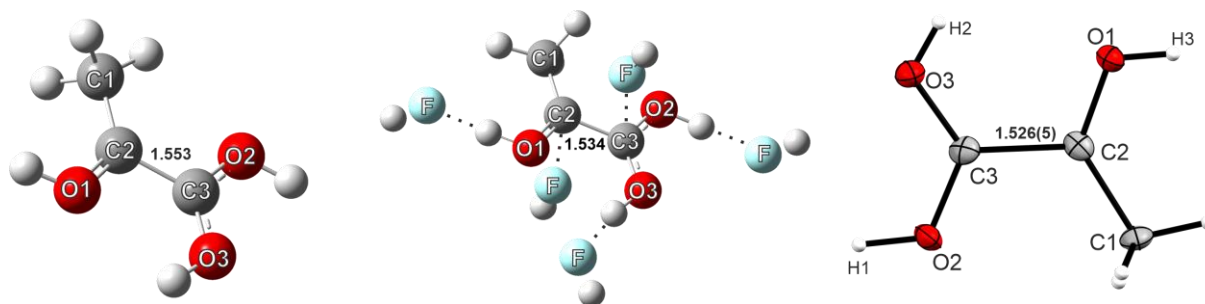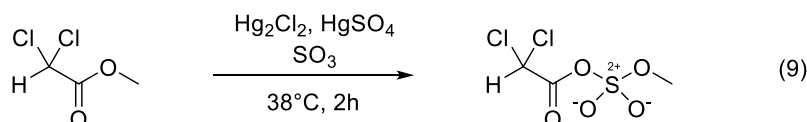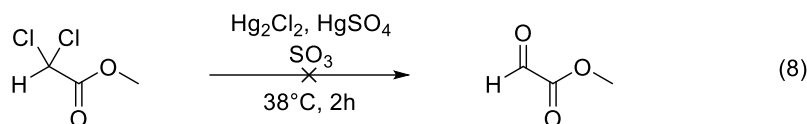
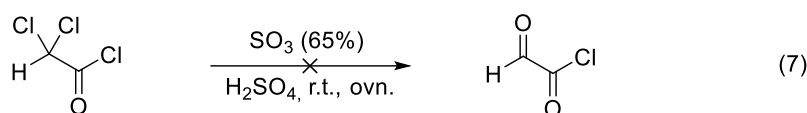**Figure 9.** Comparison of the central C−C bond distance [Å] of the calculated gas-phase structures [C2(OH)3Me]2+ (left), [C2(OH)3Me]2+·5 HF (middle), and the X-ray structure of [C2(OH)3Me][SbF6]2 (right, 50% probability displacement ellipsoids, hydrogen atoms as spheres of arbitrary radius). Calculated on the MP2/aug-cc-pVTZ level of theory.

3.2. Glyoxylic Acid Monohydrate in Superacids – the Unexpected Synthesis of an α-Fluoroalcohol
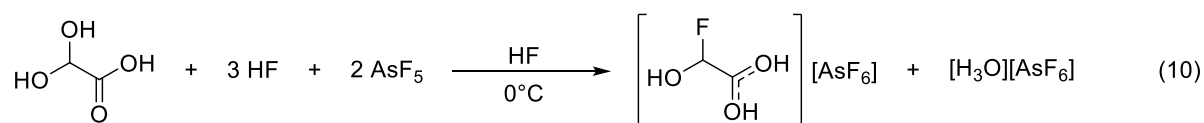
In this part of the thesis, the generation of the vicinal dication $[C_2(OH)_3H]^{2+}$ is attempted. The basic idea is to keep the same number of π-electrons as in diprotonated pyruvic acid but to reduce the σ-conjugation by substituting the methyl group for a hydrogen atom. A reasonable approach is investigating glyoxylic acid (GA) in superacidic media. However, GA is accessible only in its monohydrate form (GAM) which implies not co-crystallized but chemically bound water (Equation 6). GAM is thus better described as dihydroxyacetic acid.
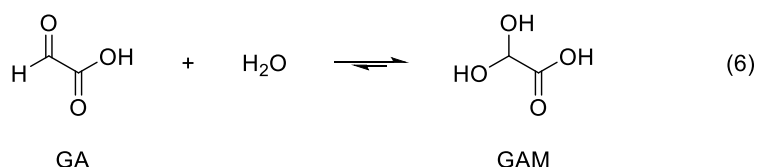
Attempts to prepare GA by dehydration of GAM were not successful. Another approach was to generate the acyl chloride and the methyl ester of GA directly under anhydrous conditions. For that, 2,2-dichloroacetyl chloride and methyl-2,2-dichloroacetate were reacted with oleum (Equations 7–9). Unfortunately, this did not succeed either. The reaction of the acyl chloride led to the decomposition products CO and CO_2. Implementing the methyl ester with oleum on the other hand resulted in the insertion of SO_3 into the ester group.

$$\text{(7)}$$

SO$_3$ (65%)
H$_2$SO$_4$, r.t., ovn.

$$\text{(8)}$$

Hg$_2$Cl$_2$, HgSO$_4$
SO$_3$
38°C, 2h

$$\text{(9)}$$

Hg$_2$Cl$_2$, HgSO$_4$
SO$_3$
38°C, 2h

The final approach to synthesizing the aimed superelectrophile [C$_2$(OH)$_3$H]$^{2+}$ was to react GAM directly with HF/AsF$_5$. The idea was to protonate one of the hydroxy groups and subsequently raise the temperature of the reaction to 0°C to eliminate the OH$_2^+$ moiety as H$_3$O$^+$. However, [C$_2$(OH)$_3$H]$^{2+}$ cannot be isolated. Instead, the [AsF$_6$]$^-$ salt of protonated α-fluorohydroxyacetic acid [FHA-1H][AsF$_6$] is formed according to Equation 10.

HO—CH(OH)—C(=O)—OH + 3 HF + 2 AsF$_5$ $\xrightarrow[0°C]{\text{HF}}$ [HO—CHF—C(OH)$_2$]$^+$ [AsF$_6$] + [H$_3$O][AsF$_6$]
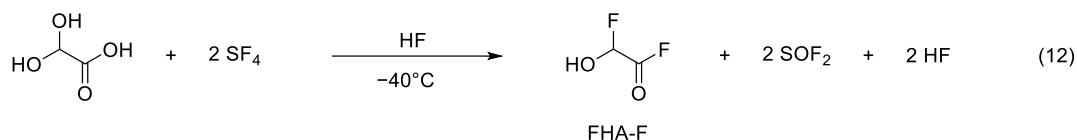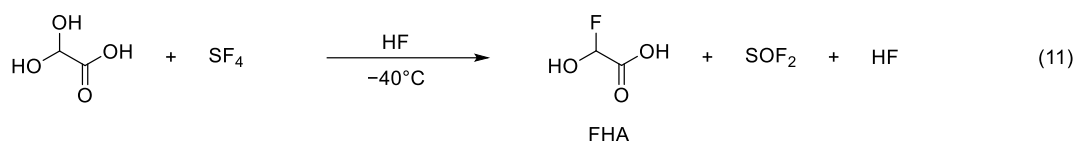
$$\text{(10)}$$

Formally, a two-to-one ratio of AsF$_5$ to GAM would suffice to form [FHA-1H][AsF$_6$]. However, full conversion takes place only when three equivalents of Lewis acid are applied. This leads to the conclusion that the superelectrophile [C$_2$(OH)$_3$H]$^{2+}$ must be formed intermediately. [C$_2$(OH)$_3$H]$^{2+}$ reacts electrophilically with the superacidic solvent HF to form the fluorinated compound, that, in this case, can be isolated. The reaction pathway is proposed in Scheme 1. [FHA-1H][AsF$_6$] is found as a racemic mixture of the two enantiomers, strongly indicating an S$_N$1 mechanism. Additionally, no second protonation or desoxyfluorination occurs despite an excess Lewis acid.
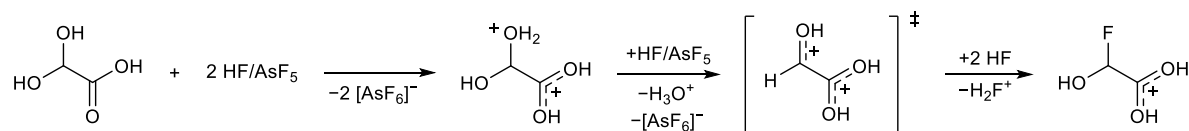
Scheme 1. Proposed mechanism of the synthesis of [FHA-1H][AsF$_6$] from GAM with the binary superacid HF/AsF$_5$. The superelectrophilic intermediate [C$_2$(OH)$_3$H]$^{2+}$ is shown in square brackets.

[FHA-1H][AsF$_6$] is a representative of the rare class of α-fluoroalcohols. These compounds are known to be labile under normal conditions. The stability of [FHA-1H][AsF$_6$] piqued our interest in the neutral species α-fluorohydroxyacetic acid (FHA). To generate α-fluorohydroxyacetic acid (FHA), GAM has reacted with SF$_4$ in aHF solution, a known

9

desoxyfluorination agent.[36–38] Employing an equimolar amount of SF_4 leads to FHA, a twofold amount of SF_4 to the acyl fluoride FHA-F (Equations 11 and 12). FHA is identified by NMR spectroscopy, and FHA-F by NMR and vibrational spectroscopy.

$$\text{GAM} + SF_4 \xrightarrow[-40°C]{HF} \text{FHA} + SOF_2 + HF \quad (11)$$

$$\text{GAM} + 2\,SF_4 \xrightarrow[-40°C]{HF} \text{FHA-F} + 2\,SOF_2 + 2\,HF \quad (12)$$

The first desoxyfluorination with SF_4 (Equation 19) occurs at the tetrahedral C atom under the formation of FHA, as confirmed by NMR spectroscopy (^1H, ^{19}F, ^{13}C). Based on literature-reported reactions of SF_4 with carbonyl compounds and alcohols,[36,38] the reaction pathway follows an S_N1 mechanism, resulting in a racemic mixture. The proposed reaction pathway is illustrated in Scheme 2.
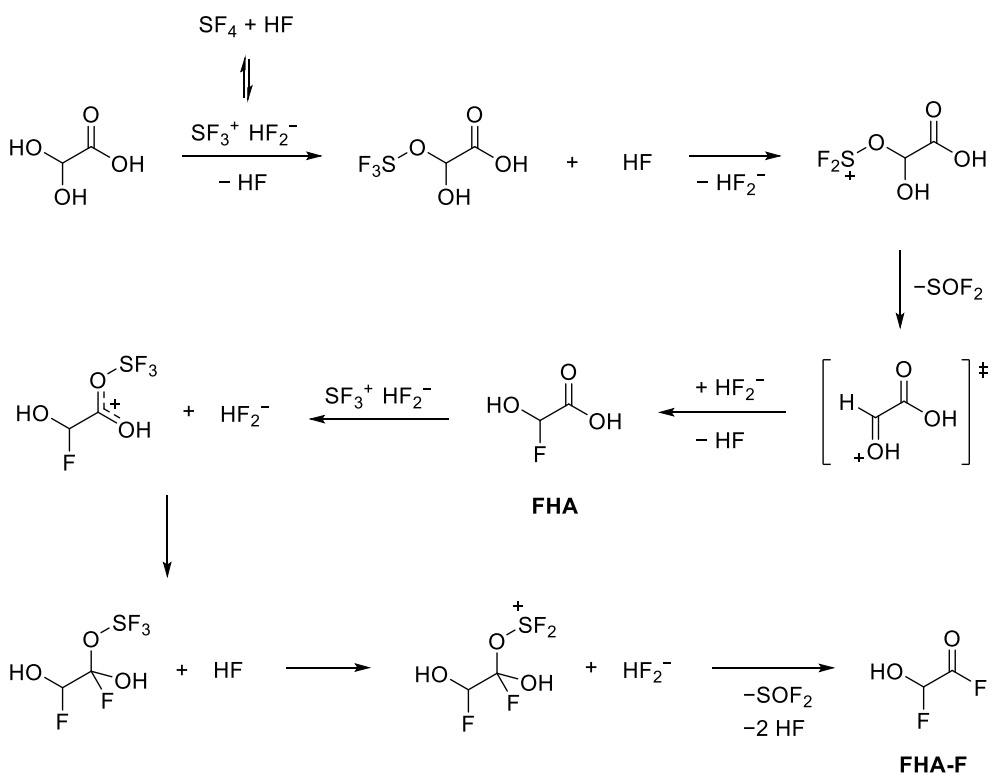
Scheme 2. Proposed mechanism of the successive desoxyfluorination of GAM in HF/SF4.

In the case of [FHA-1H][AsF6], single crystals suitable for X-ray structure analysis grew as racemic twins from aHF. In the following, the *S*-enantiomer is presented (Figure 10). Since the C−F and the C−O bond lengths are quite similar, a crystallographic disorder could be assumed.

However, considering the environment of the cation, this assumption can be discarded. The cation exhibits hydrogen bridges via the hydroxy group to an adjacent anion, whereas no interactions of the fluorine atom are found. The asymmetric unit is illustrated in Figure 10.
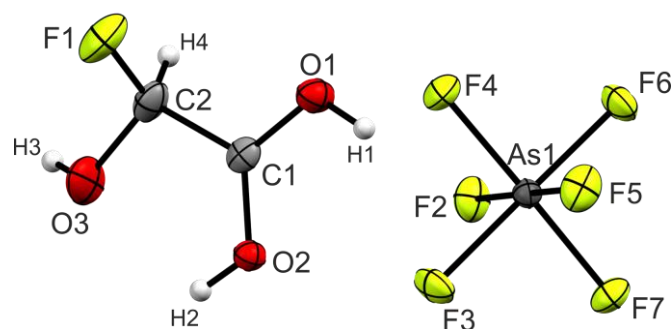

Figure 10. Projection of the asymmetric unit of [FHA-1H][AsF$_6$] (50% probability displacement ellipsoids, hydrogen atoms shown as spheres of arbitrary radius).

Interestingly, the C−OH of the α-fluoroalcohol group is significantly shorter than a regular C−O single bond while the C−F distance coincides with a regular single bond length.[39] According to NBO calculations (MP2/aug-cc-pVTZ level of theory) of FHA, FHA-F, and the naked cation [FHA-1H]$^+$, a lone-pair of the oxygen atom interacts with the antibonding σ^*(C−F) orbital, elongating the C−F distance. In the cation, the C−F bond is in turn shortened by interactions of a fluorine lone-pair into the σ^*(C−C) orbital. The quantum chemically optimized gas-phase structures are displayed in Figure 11.
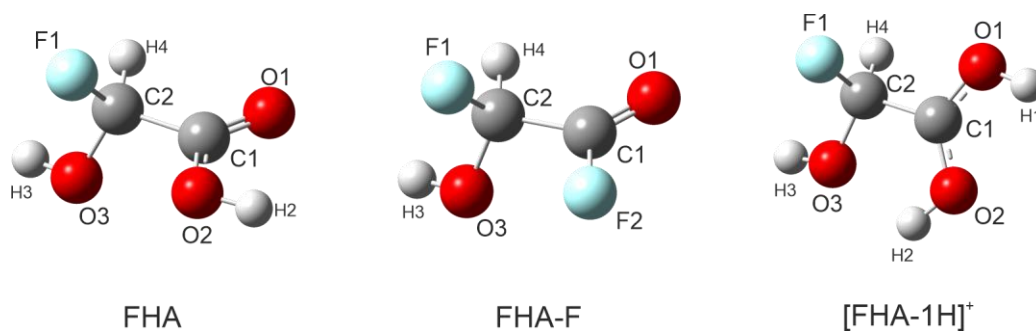

Figure 11. Optimized gas-phase structures of FHA, FHA-F, and [FHA-1H]$^+$. Calculated on the B3LYP/aug-cc-pVTZ level of theory.

3.3.　Properties of 2,3-Butanedione in Superacids

2,3-Butanedione is a member of the class of 1,2-dicarbonyl compounds. Their reactivity towards nucleophiles in highly acidic media has been reported in the literature.[19,21] It reacts with the superacidic media HF/MF$_5$ (M = As, Sb) under the formation of the monoprotonated species [C$_2$(O)(OH)Me$_2$][MF$_6$] when equimolar amounts of Lewis acid are employed. The respective equation is given below (Equation 13).

$$M = \text{As, Sb} \quad (13)$$
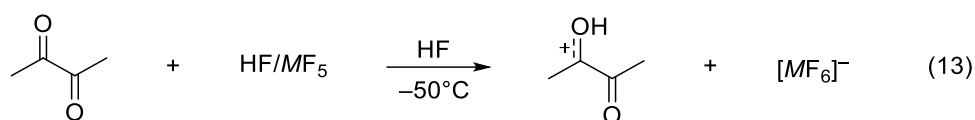
The generation and stabilization of the superelectrophile $[C_2(OH)_2Me_2]^{2+}$ by reacting 2,3-butanedione with a twofold amount of HF/MF_5 are not possible in aHF solution. Instead, a ketal-like product of two single-protonated compounds is formed among others and analyzed via single-crystal X-ray diffraction. A reaction pathway of this condensation product is illustrated in Scheme 3.
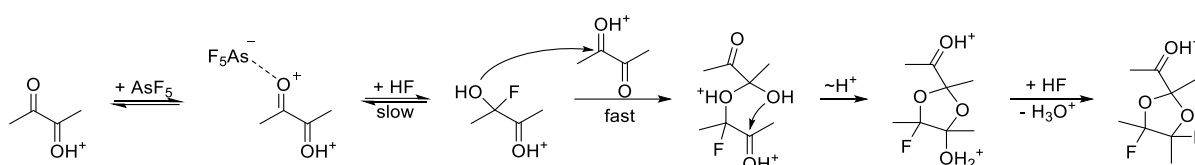

Scheme 3. Proposed mechanism of the formation of the ketal-like product from monoprotonated 2,3-butanedione with excess AsF$_5$ in aHF.

To avoid the addition of HF to $[C_2(OH)_2Me_2]^{2+}$, aHF cannot be used as a solvent for the superacid. However, by the application of SO$_2$, $[C_2(OH)_2Me_2]^{2+}$ could be isolated. 2,3-Butanedione was dissolved with two equivalents of both HF and SbF$_5$ in SO$_2$ at $-55°C$. The reaction is given in Equation 14. Employing SO$_2$ instead of aHF as a solvent is necessary to prevent the superelectrophile from a consecutive reaction.

$$(14)$$
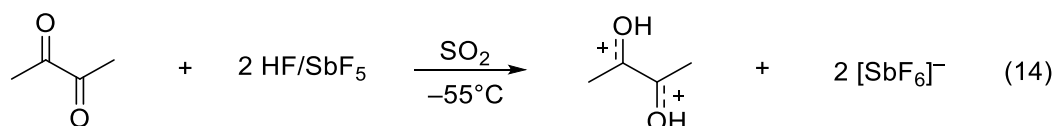
$[C_2(OH)_2Me_2][SbF_6]_2 \cdot 2\,SO_2$ is analyzed by Raman spectroscopy and single-crystal X-ray diffraction. Similar to $[C_2(OH)_4][SbF_6]_2$[31] and $[C_2(OH)_3Me][SbF_6]_2$, short non-hydrogen bridged C···F contacts are observed in the crystal phase (Figure 12).

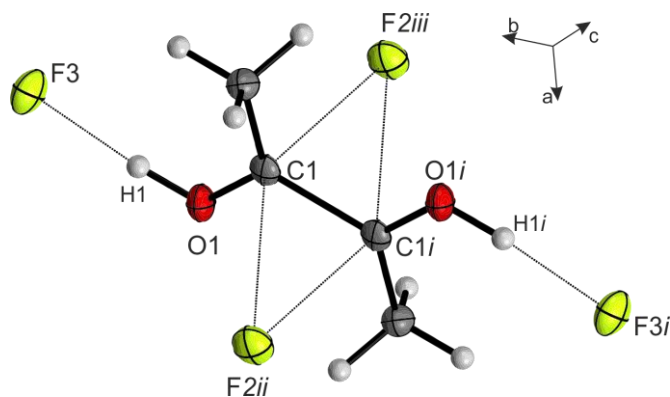**Figure 12.** Donor-acceptor interactions of the cation in the crystal phase of $[C_2(OH)_2Me_2][SbF_6]_2 \cdot 2\,SO_2$ (50% probability displacement ellipsoids, hydrogen atoms as spheres of arbitrary radius). Symmetry operations: $i = -x$, $-y$, $-z$; $ii = -x$, $0.5+y$, $1.5-z$; $iii = x$, $1.5-y$, $-0.5+z$.

Quantum chemical calculations of the naked dication on the B3LYP/aug-cc-pVQZ level of theory predict a C_2 symmetry with a twist of 37.48° around the central C−C bond. However, Raman spectroscopic and X-ray structure analyses reveal a planar C_{2h} structure of the superelectrophile. The question arises why in the solid-state C_{2h} symmetry is formed, whereas the calculated optimization of the bare cation has a twisted geometry. Either the cation is constrained into C_{2h} symmetry by the crystal packing or intermolecular interactions have a stabilizing effect on the planar structure. To answer this question, HF molecules are added to the gas-phase structure to simulate the cation-anion interactions. Re-optimization of the complex resulted in a planar geometry. This intermolecular hyperconjugation is illustrated in Figure 13. Hence, the simulated interactions stabilize the central C−C bond. The stabilization energy is quantified by Natural Bond Orbital (NBO) theory calculations on the MP2/aug-cc-pVTZ level of theory. It is about twice as big as the calculated energy of the π-donation by the OH groups, which has been declared as the main source of stabilizing energy in previous theoretical investigations of the geometry of similar vicinal dications.[30]
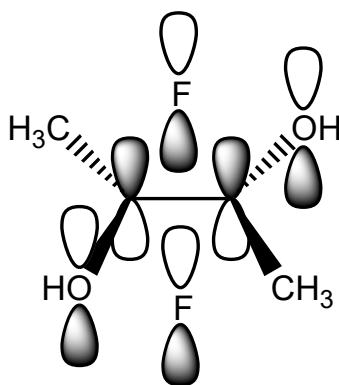

Figure 13. Illustration of the intermolecular hyperconjugation by the coordinated HF molecules into the p(π) orbitals of the carbon atoms.

After clarification of the geometry, Mapped Electrostatic Potentials (MEP) are calculated together with Natural Population Analysis (NPA) charges on the MP2/aug-cc-pVTZ level of

theory to discuss the location of the positive charges. A comparison of 2,3-butanedione with the superelectrophile $[C_2(OH)_2Me_2]^{2+}$ is depicted in Figure 14.

The highest positive electrostatic potential (blue) of 2,3-butanedione is located on the central C−C bond, while the methyl groups have a slightly less positive potential. After diprotonation, the highest electrostatic potential is more focused on the central carbon atoms, forming a π-hole directly above the C−C bond. This is consistent with the increase in the NPA charges.
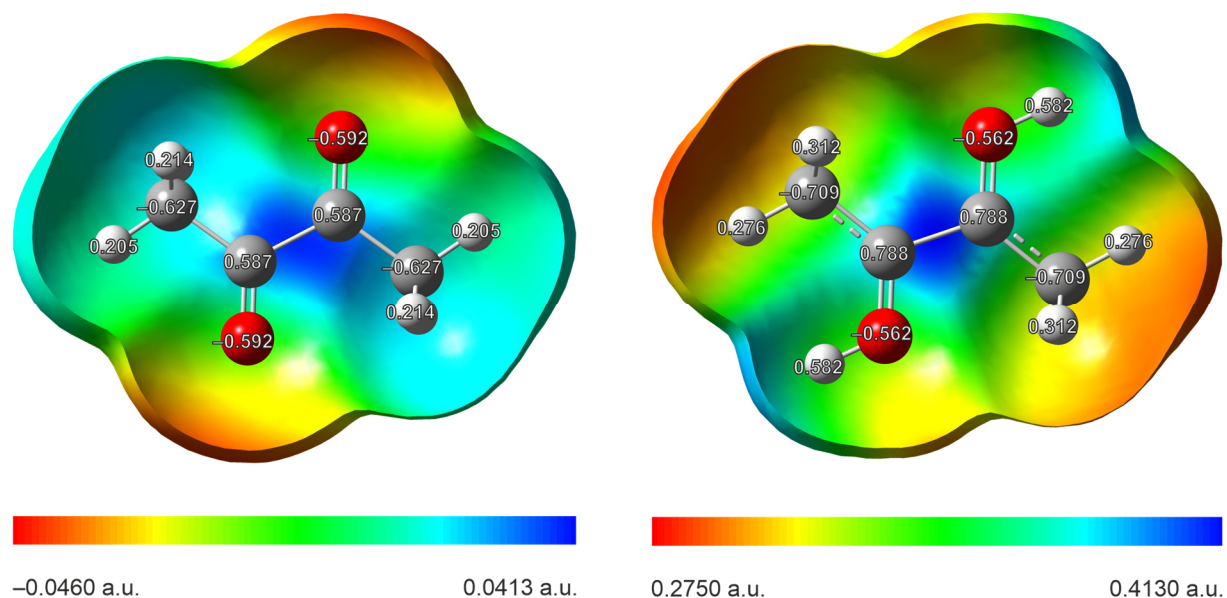

−0.0460 a.u.   0.0413 a.u.   0.2750 a.u.   0.4130 a.u.

Figure 14. Molecular 0.0004 bohr^{-3} 3D isosurfaces with mapped electrostatic potential as a color scale from −0.0460 a.u. (red) to 0.0413 a.u. (blue) for 2,3-butanedione on the left and from 0.2750 a.u. (red) to 0.4130 a.u. (blue) for the diprotonated species on the right. The calculated NPA charges are shown on the respective atoms.

3.4. α-Hydroxyisobutyric Acid in Superacids – Cleavage or not?

Since diprotonated 2,3-butanedione can be stabilized, the next targeted superelectrophile is the isomeric dication $[Me_2CC(OH)_2]^{2+}$, in which both methyl groups are on one side of the dication and the hydroxy groups on the other. A suitable candidate would be 2-methyl-2-propenoic acid, also known as methacrylic acid. However, methacrylic acid tends to polymerize under acidic conditions,[40] which is why α-hydroxyisobutyric acid (HIBA) was chosen as the starting material. The idea was similar to the protonation of glyoxylic acid monohydrate (Chapter 3.2), in which the starting material was diprotonated and H_3O^+ was subsequently eliminated.

Applying the binary superacid HF/SbF$_5$ leads to the mono- ([HIBA-1H]$^+$) and diprotonated species ([HIBA-2H]$^{2+}$) (Equations 15 and 16). Employing the weaker superacidic system HF/GeF$_4$ does not lead to a protonated form of HIBA but a chelate adduct with the Lewis acid (Equation 17). The compounds [HIBA-1H][SbF$_6$], [HIBA-2H][SbF$_6$]$_2$, and [HIBA]·GeF$_4$ were characterized by single-crystal X-ray diffraction and NMR spectroscopy.

$$\text{(15)}$$

$$\text{(16)}$$

$$\text{(17)}$$
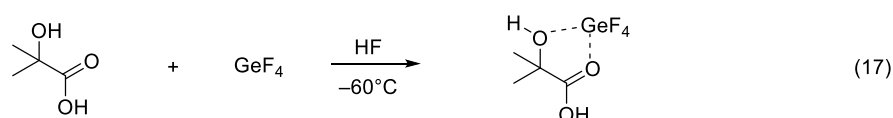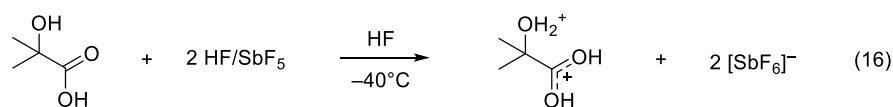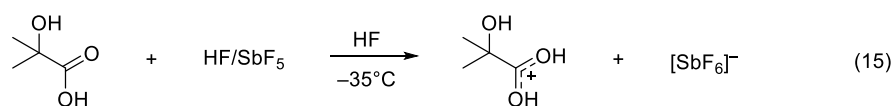
The idea was to synthesize the superelectrophile $[\text{Me}_2\text{CC(OH)}_2]^{2+}$ by diprotonation of HIBA with excess Lewis acid in aHF solution and successively raise the temperature of the reaction to room temperature to eliminate the OH_2^+ moiety as H_3O^+ (Equation 18). However, despite the use of a sixfold amount of SbF_5, NMR spectra showed remarkable thermal stability of diprotonated HIBA in aHF solution.

$$\text{(18)}$$
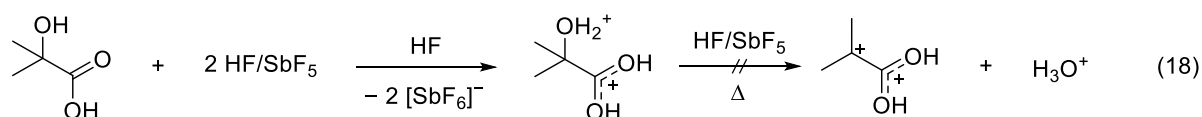
The ^1H and ^{13}C NMR studies confirm the formation of $[\text{HIBA-1H}][\text{SbF}_6]$, $[\text{HIBA-2H}][\text{SbF}_6]_2$, and $[\text{HIBA}]\cdot\text{GeF}_4$. The X-ray structure analysis of the starting material HIBA shows an intramolecular hydrogen bond $\text{O}(-\text{H})\cdots\text{O}$, in which the hydroxy group serves as the donor and the doubly bonded oxygen atom of the carboxy group as the acceptor. The result is a five-membered ring-like structure. Upon single protonation, the donor and acceptor sites are reversed. The second protonation breaks the hydrogen bond completely. The structures of the compounds HIBA, $[\text{HIBA-1H}][\text{SbF}_6]$, $[\text{HIBA-2H}][\text{SbF}_6]_2$, and $[\text{HIBA}]\cdot\text{GeF}_4$ from the respective X-ray structure analysis are shown in Figure 15.
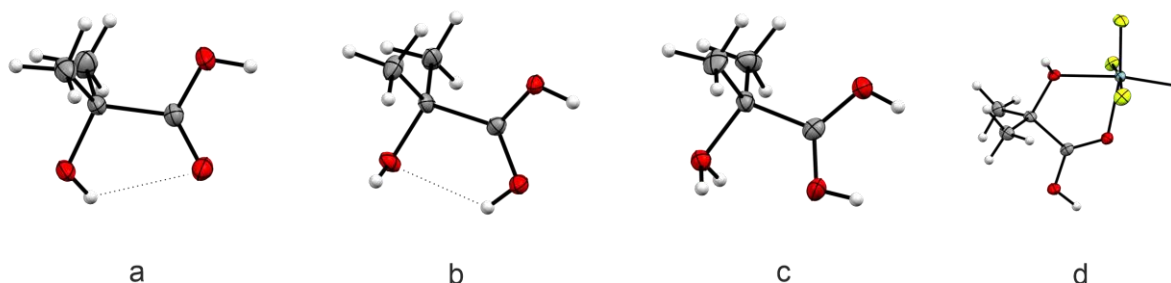

Figure 15. Structures of HIBA (a), $[\text{HIBA-1H}]^+$ (b), $[\text{HIBA-2H}]^{2+}$ (c), and $[\text{HIBA}]\cdot\text{GeF}_4$ (d), as obtained from the respective X-ray structure analysis (50% probability displacement ellipsoids, hydrogen atoms shown as spheres of arbitrary radius, and hydrogen bonds as dashed lines).

4. Conclusion

In search of simple, carbon-centered, and vicinal superelectrophiles, this thesis aimed specifically at the syntheses of the dications $[C_2(OH)_3Me]^{2+}$, $[C_2(OH)_3H]^{2+}$, $[C_2(OH)_2Me_2]^{2+}$, and the isomeric $[Me_2CC(OH)_2]^{2+}$. The objective was to generate and structurally analyze them in the solid state and to investigate the influence hydrogen atoms or methyl groups have on the carbon scaffold.

Proceeding from oxalic acid, the first substrate investigated in superacids was pyruvic acid, in which one hydroxy group of oxalic acid is formally substituted for a methyl group. By the application of the superacidic systems HF/MF$_5$ (M = As, Sb), a successive protonation was achieved and the resulting salts were isolated for the first time. The diprotonated species $[C_2(OH)_3Me]^{2+}$ was found to be significantly stabilized by unusually close anions in the solid state, interacting directly with the formally empty π-orbitals of the central carbon atoms. The introduced methyl group has an electron-donating effect via hyperconjugation.

The next step was to remove the possibility of hyperconjugation by introducing a hydrogen atom instead of a methyl group. This leads to glyoxylic acid (GA) as the starting material. However, GA is not accessible in its pure aldehyde but in its monohydrate form (GAM). Reacting GAM directly with superacids still leads to the desired superelectrophile $[C_2(OH)_3H]^{2+}$ under H$_3$O$^+$ cleavage. However, its electrophilicity is so high it even reacts with anhydrous hydrogen fluoride, resulting in the protonated species of α-fluorohydroxyacetic acid, a representative of the rare class of α-fluoroalcohols.

Since hyperconjugation of the methyl group is necessary, it piqued our interest to formally substitute another hydroxy group for a second methyl group. The resulting substrate 2,3-butanedione has only four π-electrons. A single protonation was possible in the superacidic systems HF/MF$_5$ with an equimolar amount of Lewis acid and aHF as a solvent. Employing a twofold amount, however, resulted in a condensation product under the addition of HF. To solve this problem, a novel preparative approach was introduced. By implementation of 2,3-butanedione with two equivalents of each HF and SbF$_5$ with SO$_2$ as a solvent, the desired superelectrophile $[C_2(OH)_2Me_2]^{2+}$ was not only synthesized but also isolated to perform a single-crystal X-ray structure analysis. In the solid state, the dication exhibits non-hydrogen bridged C$\cdots$F contacts, in which the adjacent anions donate electron density directly into the CC(π) bond, similar to diprotonated pyruvic acid. The impact of this intermolecular hyperconjugation is even stronger in the case of $[C_2(OH)_2Me_2]^{2+}$, in which it influences the quantum chemically calculated global minimum structure of the dication.

In the last part of this thesis, the synthesis of the isomeric superelectrophile $[Me_2CC(OH)_2]^{2+}$ was attempted. For that, diprotonation of methacrylic acid seems to be a reasonable approach. Unfortunately, methacrylic acid polymerizes under acidic conditions,[40] which is why a strategy similar to the protonation GAM was chosen, in which α-hydroxyisobutyric acid (HIBA) was reacted with the superacidic system HF/SbF$_5$. Diprotonation was possible, however, no

cleavage of H_3O^+ was observed as it was for the protonation of GAM. In summary, the second hydroxy group of GAM compared to HIBA is necessary to stabilize the carbenium ion for cleavage, but not sufficiently for persistence.

In conclusion, diprotonated 2,3-butanedione is now the simplest vicinal carbon-centered superelectrophile that has been structurally analyzed so far. In our search for small carbodications, we found a way to stabilize a superelectrophile that even reacts with HF at low temperatures.

5. References

[1] C. K. Ingold, *J. Chem. Soc.* **1933**, 1120.

[2] C. K. Ingold, *Chem. Rev.* **1934**, *15*, 225.

[3] F. Kehrmann, F. Wentzel, *Ber. Dtsch. Chem. Ges.* **1901**, *34*, 3815.

[4] A. Baeyer, V. Villiger, *Ber. Dtsch. Chem. Ges.* **1902**, *35*, 1189.

[5] A. Baeyer, *Ber. Dtsch. Chem. Ges.* **1905**, *38*, 569.

[6] G. A. Olah, *Angew. Chem. Int. Ed. Engl.* **1973**, *12*, 173.

[7] A. Hädener, H. Kaufmann, *Grundlagen der organischen Chemie*, Birkhäuser Verlag, Basel, Boston, Berlin, **2006**.

[8] A. Wollrab, *Organische Chemie. Eine Einführung für Lehramts- und Nebenfachstudenten*, Springer, Berlin, Heidelberg, **2009**.

[9] H. Meerwein, K. van Emster, *Ber. dtsch. Chem. Ges. A/B* **1922**, *55*, 2500.

[10] F. Seel, *Z. Anorg. Allg. Chem.* **1943**, *250*, 331.

[11] G. A. Olah, *Chem. Eng. News Archive* **1967**, *45*, 76.

[12] N. F. Hall, J. B. Conant, *J. Am. Chem. Soc.* **1927**, *49*, 3047.

[13] R. J. Gillespie, T. E. Peel in *Advances in Physical Organic Chemistry*, Elsevier, **1971**, pp. 1–24.

[14] George A. Olah, G. K. Surya Prakash, Árpád Molnár, Jean Sommer, *Superacid Chemistry*, Wiley, Hoboken, NJ, **2009**.

[15] G. A. Olah, J. L. Grant, R. J. Spear, J. M. Bollinger, A. Serianz, G. Sipos, *J. Am. Chem. Soc.* **1976**, *98*, 2501.

[16] H. Hart, C.-Y. Wu, R. H. Schwendeman, R. H. Young, *Tetrahedron Lett.* **1967**, *8*, 1343.

[17] J. M. Bollinger, C. A. Cupas, K. J. Friday, M. L. Woolfe, G. L. Olah, *J. Am. Chem. Soc.* **1967**, *89*, 156.

[18] G. A. Olah, *Superelectrophiles and their chemistry*, John Wiley, Hoboken, N.J, **2007**.

[19] T. Yamazaki, S. Saito, T. Ohwada, K. Shudo, *Tetrahedron Lett.* **1995**, *36*, 5749.

[20] D. A. Klumpp, S. Lau, M. Garza, B. Schick, K. Kantardjieff, *J. Org. Chem.* **1999**, *64*, 7635.

[21] T. Ohwada, T. Yamazaki, T. Suzuki, S. Saito, K. Shudo, *J. Am. Chem. Soc.* **1996**, *118*, 6220.

[22] D. A. Klumpp, K. Y. Yeung, G. K. Surya Prakash, G. A. Olah, *Synlett* **1998**, *1998*, 918.

[23] D. A. Klumpp, K. Y. Yeung, G. K. S. Prakash, G. A. Olah, *J. Org. Chem.* **1998**, *63*, 4481.

[24] T. Ohwada, T. Suzuki, K. Shudo, *J. Am. Chem. Soc.* **1998**, *120*, 4629.

[25] G. S. Prakash, F. Paknia, A. Kulkarni, A. Narayanan, F. Wang, G. Rasul, T. Mathew, G. A. Olah, *J. Fluorine Chem.* **2015**, *171*, 102.

[26] C. Benoit, J. A. Horsley, *Mol. Phys.* **1975**, *30*, 557.

[27] G. Hossein Shafiee, *OJPC* **2012**, *02*, 176.

[28] R. H. Nobes, M. W. Wong, L. Radom, *Chem. Phys. Lett.* **1987**, *136*, 299.

[29] K. Lammertsma, M. Barzaghi, G. A. Olah, J. A. Pople, A. J. Kos, P. v. R. Schleyer, *J. Am. Chem. Soc.* **1983**, *105*, 5252.

[30] G. Frenking, *J. Am. Chem. Soc.* **1991**, *113*, 2476.

[31] M. Schickinger, T. Saal, F. Zischka, J. Axhausen, K. Stierstorfer, Y. Morgenstern, A. J. Kornath, *ChemistrySelect* **2018**, *3*, 12396.

[32] S. Beck, M. Raljic, C. Jessen, A. J. Kornath, *Eur. J. Org. Chem.* **2020**, *2020*, 4521.

[33] A. Virmani, M. Pfeiffer, C. Jessen, Y. Morgenstern, A. J. Kornath, *Z. Anorg. Allg. Chem.* **2022**, *648*, e202200005.

[34] W. J. Ray, J. E. Katon, D. B. Phillips, *J. Mol. Struct.* **1981**, *74*, 75.

[35] K. Harata, N. Sakabe, J. Tanaka, *Acta Crystallogr., Sect. B: Struct. Sci.* **1977**, *33*, 210.

[36] W. R. Hasek, W. C. Smith, V. A. Engelhardt, *J. Am. Chem. Soc.* **1960**, *82*, 543.

[37] J. Kollonitsch, S. Marburg, L. Perkins, *J. Org. Chem.* **1975**, *40*, 3808.

[38] D. G. Martin, F. Kagan, *J. Org. Chem.* **1962**, *27*, 3164.

[39] E. Wiberg, N. Wiberg, G. Fischer, *Lehrbuch der anorganischen Chemie*, Walter de Gruyter, Berlin, New York, **2007**.

[40] J. Brandrup (Ed.) *Polymer handbook*, Wiley, Hoboken, N. J., **1999**.

6. Appendix

Publications and conference contributions are listed in this appendix. Furthermore, it contains the manuscripts, supporting information, and cover pictures published in the scope of this dissertation. The first manuscript has been peer-reviewed and published in a scientific journal. The publications of the other three manuscripts are in process. The manuscripts are sorted thematically in the same way as they are summarized in this thesis.

6.1. List of Publications and Conference Contributions

6.1.1. Publications

1. A. Virmani, M. Pfeiffer, C. Jessen, Y. Morgenstern, A. J. Kornath*, Protonation of Pyruvic Acid – Synthesis of a plain Superelectrophile*, *Z. Anorg. Allg. Chem.* **2022**, *648*, e202200005.
   DOI: 10.1002/zaac.202200005   Cover DOI: 10.1002/zaac.202200212

2. A. Virmani, C. Jessen, A. Nitzer, A. J. Kornath, *Desoxyfluorination with Superacids – Synthesis and Characterization of Protonated α-Fluorohydroxyacetic Acid*, *publication in preparation.*

3. A. Virmani, C. Jessen, A. J. Kornath, *It Takes Two to Tango – Synthesis and Structure of the Small Superelectrophile $[C_2(OH)_2Me_2]^{2+}$*, *publication in preparation.*

4. A. Virmani, T. F. Manitz, A. Nitzer, C. Jessen, A. J. Kornath, *Reversing the Intramolecular Hydrogen Bond – Successive Protonation of α-Hydroxyisobutyric Acid, publication in preparation.*

6.1.2. Conference Contributions

1. Poster Presentation
   A. Virmani, M. Pfeiffer, C. Jessen, Y. Morgenstern, A. J. Kornath, *Pyruvic Acid in Superacids – Formation of a Superelectrophile*, 19th European Symposium on Fluorine Chemistry, Warsaw (Poland), August 25–31, **2019**.

2. Oral Presentation
   A. Virmani, C. Jessen, M. Pfeiffer, A. J. Kornath, *Vicinal, carbon-centered Superelectrophiles: Synthesis, Characterization, Stability*, 20th European Symposium on Fluorine Chemistry, Berlin (Germany), August 15–19, **2022**.

HF/MF₅ Constructions

Front Cover: Protonation of Pyruvic Acid – Synthesis of a Plain Superelectrophile

Alan Virmani, Martina Pfeiffer, Christoph Jessen, Yvonne Morgenstern, Andreas J. Kornath

Protonation of Pyruvic Acid – Synthesis of a plain Superelectrophile

Alan Virmani,[a] Martina Pfeiffer,[a] Christoph Jessen,[a] Yvonne Morgenstern,[a] and Andreas J. Kornath*[a]

The syntheses of $[H_3C(O)CC(OH)_2][MF_6]$ and $[H_3C(OH)CC(OH)_2]_2[MF_6]_2$ (M=As, Sb) by reacting pyruvic acid in the super-acidic systems HF/AsF_5 and HF/SbF_5 are reported. The salts were characterized by low-temperature vibrational spectroscopy and in the cases of $[H_3C(O)CC(OH)_2][SbF_6]$ and $[H_3C(OH)CC(OH)_2]_2[SbF_6]_2 \cdot HF$ by X-ray crystal structure analyses. The exper-imental results are discussed together with quantum chemical calculations. Remarkably, the bond distance and the twisting angle around the central C–C bond are unaffected by the protonations despite increasing coulombic repulsion. The crystal structure reveals short interionic interactions that have a considerable influence on the C–C bond.

Introduction

The geometry of ethylene dications of the type $[C_2X_2Y_2]^{2+}$ (X; Y=H, F, OH, NH_2, SH) has been a subject of various theoretical studies as it is the simplest vicinal superelectrophile. It has only been observed in the gas phase.[1–6] The first study on the potential energy surface of $[C_2H_4]^{2+}$ by *Schleyer et al.* suggests a perpendicular structure (D_{2d}) to be most stable with a rotational barrier of 28.1 kcal/mol. This result was explained by hyper-conjugation, leading to a significantly shortened C–C bond.[4] The influence of substituents has been pointed up by *Frenking*, who found out that ethylene dications containing second-row substituents (X, Y=F, OH, NH_2) prefer a planar structure if steric repulsion of adjacent moieties is absent. This is due to π-donation, resulting in a decrease of both the C–C and the C–X distances.[2] The crystal structures of the chloro and bromo salts of $[C_2(NMe_2)_4]^{2+}$, which are obtained by two-electron-oxidation of the neutral ethylene derivative, have a twisting angle of 76° and 67°, respectively. These results by *Bock et al.*[7] are an attempt of experimental validation of the geometry of ethylene dications, however, the substituents are too big to exclude steric repulsion.

A method other than ionization of neutral ethylene derivatives was established in seminal work by *Olah* and *Prakash*, who stabilized a large number of carbocations in superacidic solutions and characterized them mainly by ^1H and ^{13}C NMR spectroscopy.[8–10] Superacids turn out to be a powerful agent to generate and stabilize ethylene dications by protonating non-conjugating π-systems like adjacent carbonyl or carboxyl groups.[11,12] The same approach was chosen in a recent work, in which the tetrahydroxyethylene dication $[C_2(OH)_4][SbF_6]_2$ was obtained by diprotonation of oxalic acid in the superacidic system HF/SbF_5 and the solid-state structure was determined.[13] Hereby, a planar structure of the dication with two vicinal, carbon-centered positive charges was found. The next step towards the ethylene dication is reducing the number of π-electrons by formally substituting one hydroxy group of $[C_2(OH)_4]^{2+}$ for a methyl group. *Olah et al.* already generated diprotonated pyruvic acid $[C_2(OH)_3Me]^{2+}$ in super-acidic solution.[11] Still, to better understand the geometry of ethylene dications, a structural analysis is yet to be performed. For that, we investigated the behavior of pyruvic acid in the superacidic systems HF/AsF_5 and HF/SbF_5.

Results and Discussion

Syntheses and properties of $[H_3C(O)CC(OH)_2][MF_6]$ and $[H_3C(OH)CC(OH)_2]_2[MF_6]_2$ (M=As, Sb)
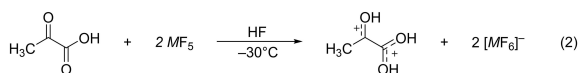
Salts containing the mono- and diprotonated species of pyruvic acid were prepared in the superacidic systems HF/AsF_5 and HF/SbF_5 at $-30°C$, where anhydrous hydrogen fluoride (aHF) served as both reagent and solvent. Depending on the stoichiometry of the respective Lewis acid, salts of mono-(Equation 1) or diprotonated (Equation 2) pyruvic acid were obtained containing the corresponding anion. The deuterated salts $[H_3C(O)CC(OD)_2][AsF_6]$ and $[H_3C(OD)CC(OD)_2]_2[AsF_6]_2$ are generated using anhydrous deuterium fluoride (aDF) as a solvent. Due to the excess of aDF, nearly complete substitution of acidic protons for deuterium is observed.

[a] A. Virmani, M. Pfeiffer, C. Jessen, Y. Morgenstern,
     Prof. Dr. A. J. Kornath
     Department Chemie
     Ludwig-Maximilians-Universität München
     Butenandtstr. 5–13,
     81377 München, Germany
     E-mail: andreas.kornath@cup.uni-muenchen.de
     Homepage: http://www.org.chemie.uni-muenchen.de/ac/
               kornath/

All four salts, [H₃C(O)CC(OH)₂][AsF₆] (**1**), [H₃C(O)CC-(OH)₂][SbF₆] (**2**), [H₃C(OH)CC(OH)₂][AsF₆]₂ (**3**) and [H₃C(OH)CC-(OH)₂][SbF₆]₂ (**4**) are soluble in aHF. Isolated, **1** and **2** are stable up to room temperature, **3** and **4** decompose at −28 °C. In the case of **2** and **4**, colorless crystals grew in aHF at −55 °C after 36 h (**2**) and 72 h (**4**), respectively. The solvent was then slowly removed at −78 °C.

$$H_3C-C(=O)-C(=O)-OH + MF_5 \xrightarrow[-30°C]{HF} H_3C-C(=O)-C(OH)_2^+ + [MF_6]^- \quad (1)$$

$$H_3C-C(=O)-C(=O)-OH + 2\,MF_5 \xrightarrow[-30°C]{HF} H_3C-C(OH)^+-C(OH)_2^+ + 2\,[MF_6]^- \quad (2)$$
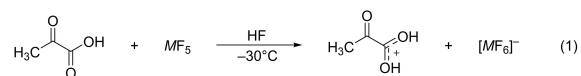
M = As, Sb

Crystal structure of [H₃C(O)CC(OH)₂][SbF₆]

Monoprotonated pyruvic acid [H₃C(O)CC(OH)₂][SbF₆] (**2**) crystallizes in the triclinic space group P$\bar{1}$ with two formula units per unit cell with two symmetrically independent anions. Selected bond lengths, bond angles, dihedral angles, and interionic contacts are listed in Table 1. The cation is displayed in Figure 1.

Table 1. Selected bond lengths, interionic distances [Å], bond angles [deg], and dihedral angles [deg] of **2**. Symmetry codes $i = -1+x, -y, z$; $ii = -1-x, 1-y, -z$.

Bond lengths [Å]		Interionic distances D···A [Å]	
C1–C2	1.462(6)	O3···F6ii	2.587(4)
C2–C3	1.541(5)	O2···O1i	2.518(4)
C2–O1	1.211(4)	C3···F1	2.567(5)
C3–O2	1.249(4)		
C3–O3	1.265(5)		
Bond angles [deg]		**Dihedral angles [deg]**	
C1–C2–C3	118.0(3)	O1–C2–C3–O2	178.8(3)
O3–C3–O2	122.2(4)	C1–C2–C3–O3	177.4(3)
O3–C3–C2	120.5(3)	O1–C2–C3–O3	−2.9(5)
O2–C3–C2	117.3(3)	C1–C2–C3–O2	−0.9(5)
O1–C2–C1	128.1(4)		
O1–C2–C3	113.9(3)		

The crystal packing (Figure S1) and a list of all bond lengths and angles (Table S1) are given in the Supporting Information.

In the cation, the C3–O2 bond is shortened from 1.311(6) Å to 1.249(4) Å, while the C3–O3 bond is elongated from 1.218(6) Å to 1.265(5) Å compared to the starting material.[14] This is due to π-resonance of the [C(OH)₂]⁺ moiety and has been found in various protonated carboxylic acids.[13,15] Consequently, both CO bonds do not differ significantly. Both the C1–C2 (1.462(6) Å) and the C2–O1 (1.211(4) Å) distances remain approximately unchanged after the protonation. The C2–C3
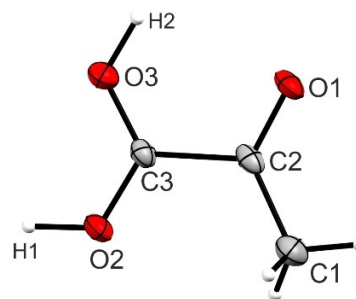
Figure 1. Bare cation [H₃C(O)CC(OH)₂]⁺ of **2**. Probability displacement ellipsoids are set at 50 %. Hydrogen atoms are set as spheres of arbitrary radius.

bond length of 1.541(5) Å is only slightly longer compared to the corresponding bond of the starting material (1.529(7) Å).[14]

As a result of the protonation, the angles O1–C2–C1 and O3–C3–C2 increase whereas the angles O2–C3–C2 and O1–C2–C3 decrease compared to the starting material. The angles C1–C2–C3 and O3–C3–O2 do not change in the course of the protonation. Still, the sums of the respective angles around the C2, and the C3 atom amount to 360°, pointing up sp² hybridization of said carbon atoms. The dihedral angle of 2.9(5)° remains approximately the same as in pyruvic acid (3.5°).[14]

The crystal packing shows hydrogen bonds O2···O1i (2.518(4) Å), which connects the individual cations to chains. Two antiparallel chains are linked to each other via an anion, forming O3···F6ii (2.587(4) Å) hydrogen bonds (Figure 2).
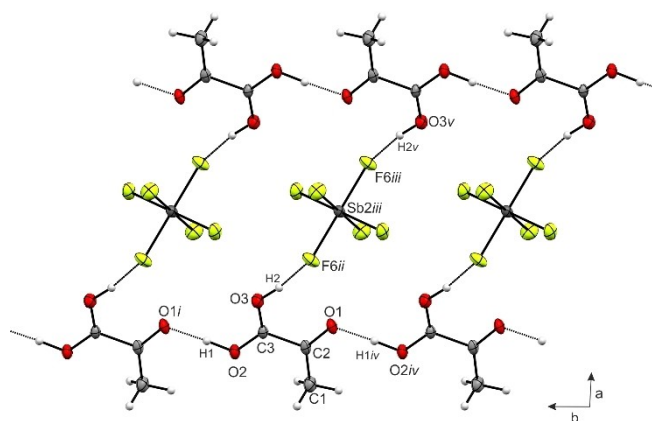
Figure 2. Intermolecular hydrogen bonds (represented as dashed lines) in **2**. Symmetry codes $i = -1+x, -y, z$; $ii = 1-x, -y, 3-z$; $iii = x, 1+y, z$; $iv = 1+x, y, z$; $v = -1-x, -1-y, 3-z$.

Additionally, a strong, non-hydrogen bridged contact between the carboxylic C3 atom and the F1 atom of the anion is observed (Figure 3). This C3···F1 distance of 2.567(5) Å is approximately 19 % below the sum of the van-der-Waals radii
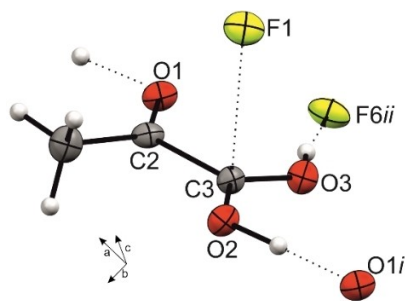
Figure 3. Interionic surroundings of the cation in the crystal packing of **2**. Symmetry codes: $i = -1 + x, y, z$; $ii = -1 - x, -y, 3 - z$.

Figure 4. Low-temperature vibrational spectra of [H₃C(O)CC-(OD)₂][AsF₆]: a) IR, f) Ra; [H₃C(O)CC(OH)₂][SbF₆]: b) IR, e) Ra; [H₃C(O)CC(OH)₂][AsF₆]: c) IR, d) Ra.

(3.17 Å),[16] and the C2–C3···F1 angle adds up to 80.0(2)°. Such interactions are rare but have been reported in literature.[17]

The antimony atoms Sb1 and Sb2 of the two symmetrically independent anions are located in the inversion centers of the crystal packing. Both anions deviate slightly from the ideal O_h symmetry due to the interionic interactions.

Vibrational spectra of the monoprotonated salts 1 and 2

Low-temperature infrared and Raman spectra of [H₃C(O)CC-(OH)₂][AsF₆] (**1**), [H₃C(O)CC(OH)₂][SbF₆] (**2**), and the deuterated species [H₃C(O)CC(OD)₂][AsF₆] are displayed in Figure 4. For the cation, C_s symmetry and 27 fundamental vibrations, all of which are Raman and IR active, are expected. For the assignment, vibrational frequencies of the geometry-optimized structure of [H₃C(O)CC(OH)₂]⁺ were calculated at the MP2/aug-cc-pVDZ level of theory. Observed frequencies of pyruvic acid were assigned based on results obtained by *Ray et al.*[18] A list of selected quantum chemically calculated, and observed frequencies of **1** and **2** are shown in Table 2. The complete assignment is summarized in Table S4.

For the cation, two OH stretching vibrations are expected. In the IR spectra of **1** and **2**, the OH stretching vibrations are superposed by water condensed on the CsBr plate due to our measuring method. Therefore, the OD stretching vibrations of [H₃C(O)CC(OD)₂][AsF₆] are more meaningful. Those are observed at 2343 cm⁻¹, 2215 cm⁻¹ (IR), 2320 cm⁻¹, and 2219 cm⁻¹ (Ra).

The out-of-phase CO stretching vibration of the carboxy group of **1** and **2** occurs between 1652 cm⁻¹ and 1673 cm⁻¹. The in-phase CO stretching vibration is observed between 1520 cm⁻¹ and 1540 cm⁻¹. The corresponding frequencies of the parent compound pyruvic acid are reported at 1771 cm⁻¹ (C=O) and 1209 cm⁻¹ (C–O).[18] This observed alignment of the CO frequencies is anticipated due to the protonation. It has to be noted that the carbonylic C=O, as well as the central C–C stretching vibrations of **1** and **2**, remain approximately unchanged.

The frequencies of the anions occur between 186 cm⁻¹ and 696 cm⁻¹ for the [AsF₆]⁻ salt and between 178 cm⁻¹ and 670 cm⁻¹ for the [SbF₆]⁻ salt. For both anions more vibrations are observed than expected for an ideal O_h symmetry,

Table 2. Selected observed vibrational frequencies [cm⁻¹] of [H₃C-(O)CC(OH)₂][MF₆] (M = As, Sb) and calculated vibrational frequencies [cm⁻¹] of [H₃C(O)CC(OH)₂]⁺.

[C₃H₅O₃][AsF₆]		[C₃H₅O₃][SbF₆]		[C₃H₅O₃]⁺[a]	Assignment
IR	Ra	IR	Ra	(IR/Ra)	
1733 (vw)	1729 (41)	1738 (vw)	1737 (21)	1735 (59/8)	$\nu(CO_k)$
1652 (vw)	1663 (2)	1662 (vw)	1673 (13)	1688 (272/1)	$\nu_{oop}(CO_a)$
1520 (vw)	1526 (1)	1523 (vw)	1540 (6)	1557 (144/9)	$\nu_{ip}(CO_a)$
797 (vw)	797 (54)	798 (w)	799 (21)	731 (31/10)	$\nu(CC)$

[a] Calculated at the MP2/aug-cc-pVDZ level of theory. [b] IR intensities in km·mol⁻¹ and Raman intensities in Å⁴·μ⁻¹. Experimental Raman intensity is scaled to the most intensive mode to be 100. [c] Abbreviations: v = very, w = weak, m = medium, ν = stretch, ip = in-phase, oop = out-of-phase, k = keto, a = acid.

suggesting a distorted octahedral structure. This is confirmed by the X-ray structure analysis for **2**.

Crystal Structure of [H₃C(OH)CC(OH)₂][SbF₆]₂·HF

Diprotonated pyruvic acid [H₃C(OH)CC(OH)₂][SbF₆]₂·HF (**4**) crystallizes in the triclinic space group $P\bar{1}$ with two formula units per unit cell. Selected bond lengths, interionic contacts, bond angles, and dihedral angles are listed in Table 3. The cation of **4**

Table 3. Selected bond lengths, interionic interactions [Å], bond angles [deg], and dihedral angels [deg] of **4**. Symmetry codes $i = 1-x, 1-y, -z$; $ii = 1-x, -y, -z$; $iii = 1+x, y, z$.

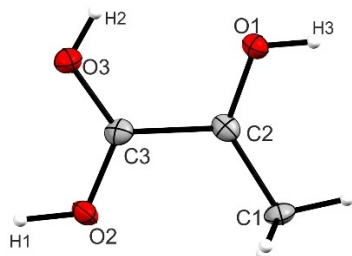| Bond lengths [Å]		Interionic distances D···A [Å]	
C1–C2	1.451(5)	F13···F3i	2.494(3)
C2–C3	1.526(5)	O3···F12iii	2.554(4)
C2–O1	1.243(4)	O1···F7ii	2.453(4)
C3–O2	1.254(5)	O2···F13	2.492(4)
C3–O3	1.260(4)	C2···F6i	2.598(5)
		C3···F2	2.608(5)
Bond angles [deg]		**Dihedral angles [deg]**	
C1–C2–C3	119.8(3)	O1–C2–C3–O2	179.6(3)
O3–C3–O2	121.9(4)	C1–C2–C3–O3	−178.6(3)
O3–C3–C2	123.1(3)	O1–C2–C3–O3	−0.2(5)
O2–C3–C2	115.0(3)	C1–C2–C3–O2	1.2(5)
O1–C2–C1	128.1(4)		
O1–C2–C3	112.1(3)		

Figure 5. Bare cation [H₃C(OH)CC(OH)₂]²⁺ of **4**. Probability displacement ellipsoids are set at 50%. Hydrogen atoms are set as spheres of arbitrary radius.

is shown in Figure 5. All bond lengths and angles are listed in Table S2. An asymmetrical unit comprising a co-crystallized HF molecule is displayed in Figure S2, the crystal packing in Figure S3.

The C1–C2 bond length (1.451(5) Å) of the cation is in good agreement with known C(sp³)–C(sp²) distances,[19,20] but it is shortened significantly compared to pyruvic acid (1.487(5) Å). The C2–O1 distance of the keto group of pyruvic acid (1.206(6) Å)[14] is elongated by the protonation to 1.243(4) Å due to π-resonance of the protonated carbonyl group. The CO bond is significantly shorter than in previously reported protonated carbonyl groups,[21] probably because of the protonated carboxy group as an electron-withdrawing group in the direct vicinity.

The C2–C3 bond distance of 1.526(5) Å is unchanged compared to pyruvic acid (1.529(7) Å)[14] and **2** (1.541(5) Å). The dihedral angle of 1.2(5)° does not significantly deviate from C_s symmetry. This is rather surprising since no intramolecular hydrogen bonds are observed. *Yanai et al.* found that polarized push-pull ethylene derivatives tend to twist around the C–C bond if the moieties do not interact while increasing the C–C distance significantly.[22] In our case, the bond length between the two positively polarized C atoms is unchanged relative to the starting material, although coulombic repulsion is present.[23]

Regarding the bond angles, only the angles O2–C3–C2, which decreases from 117.3(3)° to 115.0(3)°, and O3–C3–C2 that increases from 120.5(3)° to 123.1(3)°, change slightly compared to **2**. The sum of the respective angles around both the carbon atoms amount to 360°, pointing up sp² hybridization of the central C atoms.

The cation of **4** exhibits three strong hydrogen bonds to F atoms of two [SbF₆]⁻ anions (O1···F7ii and O3···F12iii) and one co-crystallized HF molecule (O2···F13) (Figure S4). Interionic interactions are observed between the central C atoms and F atoms of the [SbF₆]⁻ anion, shown in Figure 6. The distances of
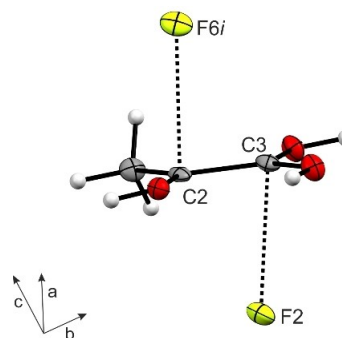
Figure 6. Non-hydrogen bridged C···F contacts in **4**. Symmetry code: $i = 1+x, y, z$.

C2···F6i (2.598(5) Å) and C3···F2 (2.608(5) Å) are approximately 18% below the sum of the van-der-Waals radii (3.17 Å).[16] The corresponding angles F6i···C2–C3 (84.4(2)°) and F2···C3–C2 (80.4(2)°) are close to a linear geometry.

Bond lengths of the anions range between 1.853(2) Å and 1.941(2) Å. The distortion of the ideal O_h symmetry is caused by strong interionic interactions.

Vibrational spectra of the diprotonated salts 3 and 4

Low-temperature infrared and Raman spectra of [H₃C(OH)CC(OH)₂][AsF₆]₂ (**3**), [H₃C(OH)CC(OH)₂][SbF₆]₂ (**4**) and [H₃C(OD)CC(OD)₂][AsF₆]₂ are displayed in Figure 7. Selected observed vibrational frequencies are summarized in Table 4 along with selected calculated values of the cation [H₃C(OH)CC(OH)₂]²⁺ (MP2/aug-cc-pVDZ level of theory). In addition, the quantum
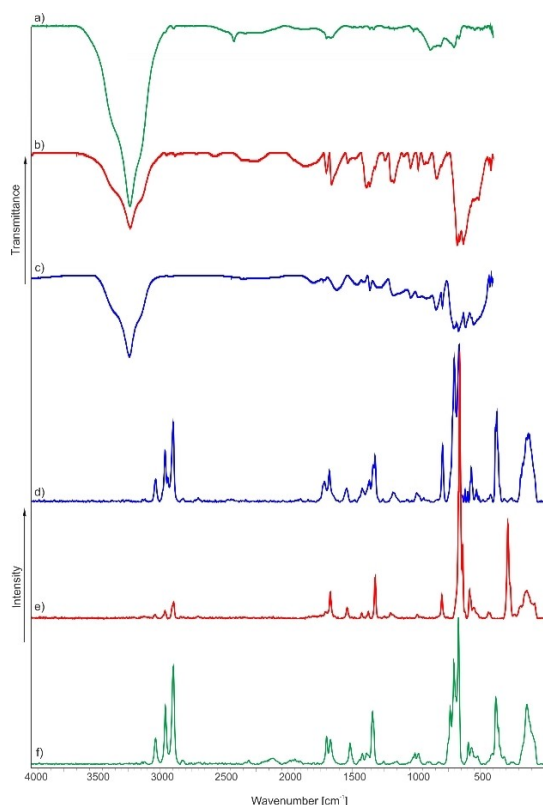
Figure 7. Low-temperature vibrational spectra of [H₃C(OD)CC-(OD)₂][AsF₆]₂: a) IR, f) Ra. [H₃C(OH)CC(OH)₂][SbF₆]₂: b) IR, e) Ra; [H₃C(OH)CC(OH)₂][AsF₆]₂: c) IR, d) Ra.

Table 4. Selected observed vibrational frequencies [cm⁻¹] of [H₃C-(OH)CC(OH)₂][MF₆]₂ (M=As, Sb) and calculated vibrational frequencies [cm⁻¹] of [H₃C(OH)CC(OH)₂]²⁺.

| [C₃H₆O₃][AsF₆]₂ | | [C₃H₆O₃][SbF₆]₂ | | [C₃H₆O₃]²⁺ | Assignment |
IR	Ra	IR	Ra	(IR/Ra)	
1708 (vw)	1717 (13)	1705 (w)	1710 (3)	1731 (172/5)	$\nu_{oop}(CO_a)$
	1678 (20)	1662 (m)	1671 (10)	1661 (155/32)	$\nu(CO_k)$
	1542 (9)	1537 (w)	1540 (4)	1537 (73/14)	$\nu_{ip}(CO_a)$
796 (m)	793 (36)	804 (w)	799 (9)	747 (25/7)	$\nu(CC)$

[a] Calculated at the MP2/aug-cc-pVDZ level of theory. [b] IR intensities in km·mol⁻¹ and Raman intensities in Å⁴·μ⁻¹. Experimental Raman intensity is scaled to the most intensive mode to be 100. [c] Abbreviations: v=very, w=weak, m=medium, ν=stretch, ip=in-phase, oop=out-of-phase, k=keto, a=acid.

Due to the poor polarizability of the OH bond, respective stretching modes are not detected in the Raman spectra. In the IR spectra broad bands of water, which condensed on the CsBr plate because of our measuring method, superpose the ν(OH) vibrations of diprotonated pyruvic acid. The thus more meaningful OD stretching modes are detected in the spectra of [H₃C(OD)CC(OD)₂][AsF₆]₂ at 2343 cm⁻¹ and 2120 cm⁻¹ in the IR spectrum and 2307 cm⁻¹, 2118 cm⁻¹, and 1949 cm⁻¹ in the Raman spectrum.

Regarding the second protonation, the shifts of frequencies of the CO bonds are examined. A blue-shift of the carboxylic $\nu_{oop}(CO)$ mode of approximately 50 cm⁻¹ compared to the monocations is observed, whereas $\nu_{ip}(CO)$ remains unaffected. The CO stretching mode of the keto group occurs between 1662 cm⁻¹ and 1678 cm⁻¹. This indicates a significant red-shift relative to the monoprotonated salts and the parent compound pyruvic acid of between 51 cm⁻¹ and 76 cm⁻¹. The stretching vibration of the central C–C bond remains unchanged relative to the monoprotonated species **1** and **2** as well as the starting material.

The frequencies of the anions occur between 128 cm⁻¹ and 707 cm⁻¹ for the [AsF₆]⁻ salt and between 184 cm⁻¹ and 681 cm⁻¹ for the [SbF₆]⁻ salt. For both salts more vibrations are observed than expected for the ideal O_h symmetry of the anion, confirming the distorted octahedral structure shown in the crystal packing of **4**.

Theoretical Studies

Calculations on the naked cations [H₃C(O)CC(OH)₂]⁺ and [H₃C-(OH)CC(OH)₂]²⁺ were carried out at the MP2/aug-cc-pVDZ level of theory. Compared to the data acquired from the X-ray structure analyses, the bond distances are overestimated. To assess the possible influence of adjacent anions on the stability of the carbon scaffold, we performed additional calculations on the MP2/aug-cc-pVTZ level of theory. For that, the optimized structures of the naked dication [H₃C(OH)CC(OH)₂]²⁺ (**A**) and the cation containing five added HF molecules to simulate all adjacent ionic interactions (**D**) as in the crystal structure of **4** were calculated. To quantify the different effects, the cation with three added in-plane HF molecules to simulate hydrogen bonding (**B**) and the cation including two added perpendicular HF molecules to feign C···F interactions (**C**) were also investigated separately. The structures are displayed in Figure 8, the respective bond lengths are listed in Table 5.

The optimized structure of the naked cation **A** overestimates particular bond lengths compared to the X-ray data of **4**. Certain improvements are made when intermolecular interactions are simulated. The C2–O1 distances of the calculated structures containing hydrogen bonds (**B** and **D**) best represent the X-ray structure. Regarding the C2–C3 bond, the calculation of the bare cation considerably overestimates the distance. When simulating all intermolecular interactions as in the crystal structure of **4** (**D**), the best match for the central C–C bond was obtained.

chemically calculated vibrational modes of [H₃C(OH)CC(OH)₂]²⁺·3 HF are summarized in Table S9 (Supporting Information). The cation has C_s symmetry and 30 fundamental vibrations, all of which are Raman and IR active. For a complete analysis of the vibrational frequencies, see Table S5 in the Supporting Information.

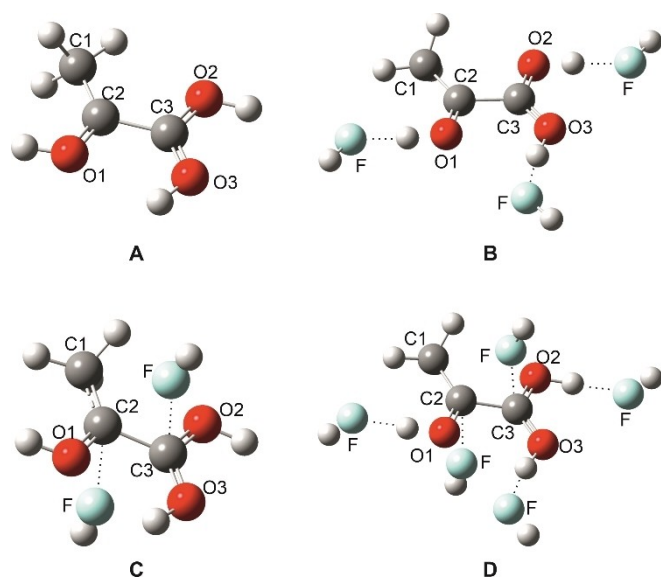**Figure 8.** Comparison of the optimized gas-phase structures of $[H_3C(OH)CC(OH)_2]^{2+}$, calculated on the MP2/aug-cc-pVTZ level of theory. Respective interactions are visualized as dashed lines.

Table 5. Comparison of the bond distances [Å] of the calculated structures **A**, **B**, **C**, and **D** with X-ray data of **4**.

	A[a]	**B**[a]	**C**[a]	**D**[a]	X-ray (4)
C1—C2	1.447	1.452	1.445	1.453	1.451(5)
C2—C3	1.548	1.541	1.538	1.534	1.526(5)
C2—O1	1.261	1.251	1.257	1.249	1.243(4)
C3—O2	1.261	1.259	1.262	1.259	1.254(5)
C3—O3	1.263	1.259	1.262	1.259	1.260(4)

[a] Calculated on the MP2/aug-cc-pVTZ level of theory.

All optimizations of the dication reveal C_s symmetry. The C1—C2 bond is shorter than the usual C(sp^3)–C(sp^2) bond.[20] The hyperconjugation of the methyl group becomes more important if the p-orbital is formally empty. The same conclusion is pulled up in a theoretical study on the ethylene dication to explain the perpendicular D_{2d} structure as the most stable one.[4] A consistent observation was made by *Olah et al.*, who investigated pyruvic acid in the superacidic system FSO$_3$H/SbF$_5$/SO$_2$ and characterized it by ^{1}H NMR spectroscopy.[11] They reported a deshielded singlet methyl absorption at 3.75 ppm. These observations indicate a distribution of the positive charge over both the hydroxy and the methyl group.

Comparing the calculated structures **A** and **B**, added in-plane HF molecules lead to a shortening of the C—O bonds, consistent with previous results in our group.[13,24] Regarding the C2—C3 distance, a slight improvement towards the X-ray data is noted. That means that the strong hydrogen bonds, simulated by HF molecules, facilitate the π-donation of the hydroxy groups into the C(p) orbitals while shortening the C—O distance, similar to the results of a theoretical study on substituted ethylene dications.[2]

A further stabilizing effect of the C—C bond is found when comparing the naked cation **A** to the optimized structure with two additional HF molecules to simulate the nearly perpendicular interaction with adjacent anions (**C**). All bond lengths of **A** and **C** are in fair agreement except for the C2—C3 distance, which is in **C** more similar to the X-ray data than in **A**, and a better fit than in **B**, where hydrogen bonds are imitated. This indicates that the greater electron-donating effect into the C(p) orbitals is based on the perpendicular interactions, where the formally unoccupied p(π) orbitals receive electron-density from neighboring anions.

These stabilizations are combined in structure **D**, where the central C—C bond of 1.534 Å is satisfyingly close to the solid-state structure of **4** (1.526(5) Å), suggesting that hydrogen bonding and C···F interactions are the main stabilizing effects on the central C—C bond.

Conclusions

In this work, we report the syntheses and isolation of $[H_3C-(O)CC(OH)_2][MF_6]$ and $[H_3C(OH)CC(OH)_2][MF_6]_2$ by reacting pyruvic acid with MF_5 ($M = As$, Sb) in aHF. The compounds were characterized by vibrational spectroscopy and in the cases of the respective $[SbF_6]^-$ salts by single-crystal X-ray structure analyses. The experimental results are discussed together with quantum chemical calculations. The central C—C bond appears to be unaffected by diprotonation, even though an elongation is expected as former theoretical studies on ethylene dications indicate.[2,4] In the solid-state, strong hydrogen bonds are observed, facilitating electron donation of the hydroxy groups into the carbon p(π) orbitals. Non-hydrogen bridged C···F interactions between a positively charged carbon and a fluorine atom of the anion of nearly perpendicular geometry have an additional significant stabilizing effect on the carbon scaffold.

Experimental Section

Caution! Avoid contact with any of these materials. Hydrogen fluoride will be formed by the hydrolysis of these compounds. HF burns the skin and causes irreparable damage. Safety precautions should be taken when using and handling these materials.

Apparatus and Materials. All reactions were carried out under standard Schlenk conditions by using FEP/PFA reactors closed with a stainless-steel valve and a stainless-steel vacuum line. All vessels were dried with fluorine prior to use. Low-temperature IR measurements were performed with a Bruker Vertex-80 V FTIR spectrometer. A small sample was placed on a CsBr single-crystal plate in a cooled cell. The IR spectra were recorded in a range between 350 cm^{-1} and 4000 cm^{-1}. Raman spectroscopic analysis was performed at −196 °C with a Bruker MultiRAM FT-Raman spectrometer with an Nd:YAG laser excitation up to 1000 mW ($\lambda = 1064$ nm) in the range between 250 cm^{-1} and 4000 cm^{-1}. Single-crystal X-ray structure investigations were carried out with an Oxford Xcalibur3 diffractometer equipped with a Spellman generator (50 kV, 40 mA) and a KappaCCD detector. The measurements were performed with Mo-K_α radiation ($\lambda = 0.71073$ Å). For data collection, the software CrysAlis CCD,[25] for data reduction the software CrysAlis RED[26] was used. The solution and refinement

were performed with the programs SHELXT[27] and SHELXL-97[28] implemented in the WinGX software package[29] and checked with the software PLATON.[30] The absorption correction was achieved with the SCALE3 ABSPACK multi-scan method.[31] Quantum chemical calculations were performed with the Gaussian 09 program package.[32] Calculations were carried out employing the method MP2 and the base sets aug-*cc*-pVDZ and aug-cc-pVTZ. For visualization of the structures and vibrational modes, the program GaussView 5.0[33] was employed. Pyruvic acid (abcr) was used as purchased, antimony pentafluoride (VWR) was distilled three times prior to use. Arsenic pentafluoride was synthesized from the elements and purified by fractionated distillation.

Syntheses of [H$_3$C(O)CC(OX)$_2$][*M*F$_6$] and [H$_3$C(O*X*)CC(O*X*)$_2$][*M*F$_6$]$_2$ (*X*=H, D; *M*=As, Sb). For the syntheses of [H$_3$C(O)CC(OX)$_2$][*M*F$_6$], first arsenic pentafluoride (170 mg, 1.00 mmol) or antimony pentafluoride (217 mg. 1.00 mmol), respectively, were condensed into a reactor (FEP tube), followed by anhydrous *X*F (*X*=H; D) at −196 °C. Pyruvic acid (88.1 mg, 1.00 mmol) was added under an inert nitrogen atmosphere. The mixture was warmed up to −30 °C for 10 min before being cooled down to −78 °C again. After removing excess *X*F in dynamic vacuum overnight, [H$_3$C(O)CC(O*X*)$_2$][AsF$_6$] or [H$_3$C(O)CC(O*X*)$_2$][SbF$_6$], respectively, were obtained as colorless solids in quantitative yields. The syntheses of [H$_3$C(O*X*)CC-(O*X*)$_2$][*M*F$_6$]$_2$ (*X*=H, D; *M*=As, Sb) were carried out by using three equivalents of the respective Lewis acid.

Acknowledgments

Conflict of Interest

The authors declare no conflict of interest.

Data Availability Statement

The data that support the findings of this study are available in the supplementary material of this article.

[1] G. Frenking, W. Koch, H. Schwarz, *J. Comput. Chem.* **1986**, *7*, 406.
[2] G. Frenking, *J. Am. Chem. Soc.* **1991**, *113*, 2476.
[3] G. Hossein Shafiee, *OJPC* **2012**, *02*, 176.
[4] K. Lammertsma, M. Barzaghi, G. A. Olah, J. A. Pople, A. J. Kos, P. v R Schleyer, *J. Am. Chem. Soc.* **1983**, *105*, 5252.
[5] T. Ohwada, K. Shudo, *J. Am. Chem. Soc.* **1989**, *111*, 34.
[6] G. A. Olah, D. A. Klumpp, *Superelectrophiles and their chemistry*, Wiley, Hoboken, NJ **2008**.

[7] H. Bock, K. Ruppert, K. Merzweiler, D. Fenske, H. Goesmann, *Angew. Chem.* **1989**, *101*, 1715.
[8] G. A. Olah, *Angew. Chem. Int. Ed. Engl.* **1973**, *12*, 173.
[9] G. K. S. Prakash, *Pure Appl. Chem.* **1998**, *70*, 2001.
[10] G. K. S. Prakash, T. N. Rawdah, G. A. Olah, *Angew. Chem. Int. Ed. Engl.* **1983**, *22*, 390.
[11] G. A. Olah, A. T. Ku, J. Sommer, *J. Org. Chem.* **1970**, *35*, 2159.
[12] G. A. Olah, A. M. White, *J. Am. Chem. Soc.* **1967**, *89*, 4752.
[13] M. Schickinger, T. Saal, F. Zischka, J. Axhausen, K. Stierstorfer, Y. Morgenstern, A. J. Kornath, *ChemistrySelect* **2018**, *3*, 12396.
[14] K. Harata, N. Sakabe, J. Tanaka, *Acta Crystallogr. Sect. B* **1977**, *33*, 210.
[15] R. Minkwitz, S. Schneider, M. Seifert, H. Hartl, *Z. Anorg. Allg. Chem.* **1996**, *622*, 1404.
[16] A. Bondi, *J. Phys. Chem.* **1964**, *68*, 441.
[17] K. O. Christe, X. Zhang, R. Bau, J. Hegge, G. A. Olah, G. K. S. Prakash, J. A. Sheehy, *J. Am. Chem. Soc.* **2000**, *122*, 481.
[18] W. J. Ray, J. E. Katon, D. B. Phillips, *J. Mol. Struct.* **1981**, *74*, 75.
[19] K. Eriks, T. D. Hayden, S. H. Yang, I. Y. Chan, *J. Am. Chem. Soc.* **1983**, *105*, 3940.
[20] H. Dietrich, *Angew. Chem.* **1961**, *73*, 511.
[21] D. Stuart, S. D. Wetmore, M. Gerken, *Angew. Chem. Int. Ed. Engl.* **2017**, *56*, 16380.
[22] H. Yanai, T. Suzuki, F. Kleemiss, H. Fukaya, Y. Dobashi, L. A. Malaspina, S. Grabowsky, T. Matsumoto, *Angew. Chem. Int. Ed. Engl.* **2019**, *58*, 8839.
[23] D. A. Klumpp, *Chemistry (Weinheim an der Bergstrasse, Germany)* **2008**, *14*, 2004.
[24] T. Soltner, N. R. Goetz, A. Kornath, *Eur. J. Inorg. Chem.* **2011**, *2011*, 3076.
[25] CrysAlisCCD, Version 1.171.35.11 (release 16–05-2011 CrysAlis 171.NET), Oxford Diffraction Ltd, UK **2011**.
[26] CrysAlisRED, Version 1.171.35.11 (release 16–05-2011 CrysAlis 171.NET), Oxford Diffraction Ltd, UK **2011**.
[27] G. M. Sheldrick, *Acta Crystallogr. Sect. A* **2015**, *71*, 3.
[28] G. M. Sheldrick, *SHELXL-97, Program for Crystal Structure Solution*, University of Göttingen, Germany **1997**.
[29] L. J. Farrugia, *J. Appl. Crystallogr.* **1999**, *32*, 837.
[30] A. L. Spek, *PLATON, A Multipurpose Crystallographic Tool*, Utrecht University, Utrecht, Netherlands **1999**.
[31] SCALE3 ABSPACK, An Oxford Diffraction Program, Oxford Diffraction Ltd, UK **2005**.
[32] M. J. Frisch, G. W. Trucks, H. B. Schlegel, G. E. Scuseria, M. A. Robb, J. R. Cheeseman, G. Scalmani, V. Barone, B. Mennucci, G. A. Petersson, H. Nakatsuji, M. Caricato, X. Li, H. P. Hratchian, A. F. Izmaylov, J. Bloino, G. Zheng, J. L. Sonnenberg, M. Hada, M. Ehara, K. Toyota, R. Fukuda, J. Hasegawa, M. Ishida, T. Nakajima, Y. Honda, O. Kitao, H. Nakai, T. Vreven, J. A. Montgomery, J. E. Peralta, F. Ogliaro, M. Bearpark, J. J. Heyd, E. Brothers, K. N. Kudin, V. N. Staroverov, R. Kobayashi, J. Normand, K. Raghavachari, A. Rendell, J. C. Burant, S. S. Iyengar, J. Tomasi, M. Cossi, N. Rega, J. M. Millam, M. Klene, J. E. Knox, J. B. Cross, V. Bakken, C. Adamo, J. Jaramillo, R. Gomperts, R. E. Stratmann, O. Yazyev, A. J. Austin, R. Cammi, C. Pomelli, J. W. Ochterski, R. L. Martin, K. Morokuma, V. G. Zakrzewski, G. A. Voth, P. Salvador, J. J. Dannenberg, S. Dapprich, A. D. Daniels, O. Farkas, J. B. Foresman, J. V. Ortiz, J. Cioslowski, D. J. Fox, *Gaussian09, Revision A.02*, Gaussian, Inc., Wallingford CT **2009**.
[33] T. K. J. M. R. Dennington, *GaussView, Version 5*, Semichem Inc., Shawnee Mission KS **2009**.

RESEARCH ARTICLE
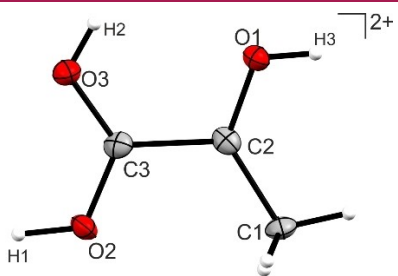
A. Virmani, M. Pfeiffer, C. Jessen, Y. Morgenstern, Prof. Dr. A. J. Kornath*

1 – 8

Protonation of Pyruvic Acid – Synthesis of a plain Superelectrophile

Supporting Information

Protonation of Pyruvic Acid – Synthesis of a plain Superelectrophile

Alan Virmani, Martina Pfeiffer, Christoph Jessen, Yvonne Morgenstern, and Andreas J. Kornath*

Content

Figures:

Tables:

Crystal structure of [H₃C(O)CC(OH)₂][SbF₆]

Figure S1. Crystal packing of [H₃C(O)CC(OH)₂][SbF₆] (**2**). Probability displacement ellipsoids are set at 50%. Hydrogen atoms are set as spheres of arbitrary radius.

Table S1. Bond lengths [Å], bond angles [°], and dihedral angles [°] of **2**.

Bond distances [Å]			
C1–C2	1.462(6)	Sb1–F1	1.893(2)
C2–C3	1.541(5)	Sb1–F2	1.864(3)
C3–O2	1.249(4)	Sb1–F3	1.864(3)
C3–O3	1.265(5)	Sb2–F4	1.858(2)
C2–O1	1.211(4)	Sb2–F5	1.879(3)
		Sb2–F6	1.897(3)
Bond angles [°]			
C1–C2–C3	118.0(3)	F3–Sb1–F2	90.66(13)
O3–C3–O2	122.2(4)	F2–Sb1–F1	90.04(11)
O3–C3–C2	120.5(3)	F3–Sb1–F1	90.10(11)
O2–C3–C2	117.3(3)	F4–Sb2–F5	90.78(12)
O1–C2–C1	128.1(4)	F5–Sb2–F6	89.73(12)
O1–C2–C3	113.9(3)	F4–Sb2–F6	89.15(11)
Dihedral angle [°]			
O1–C2–C3–O2	178.8(3)		
C1–C2–C3–O2	−0.9(5)		
O1–C2–C3–O3	−2.9(5)		
C1–C2–C3–O3	177.4(3)		

Crystal structure of [H₃C(OH)CC(OH)₂][SbF₆]₂·HF
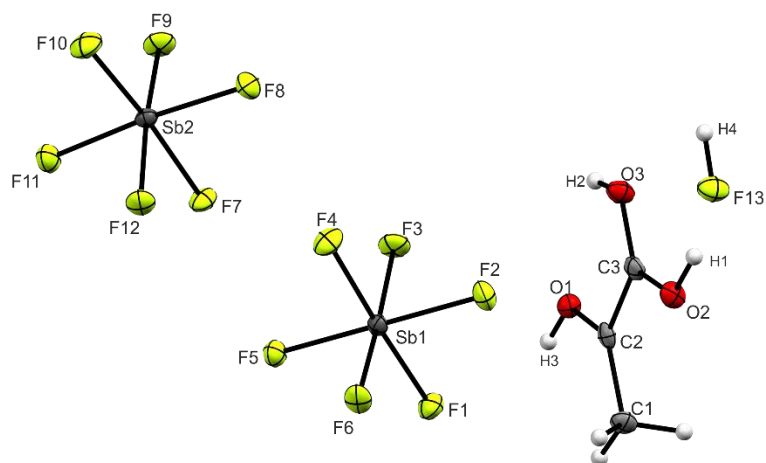
Figure S2. Asymmetrical unit of **4**. Probability displacement ellipsoids are set at 50%. Hydrogen atoms are set as spheres of arbitrary radius.
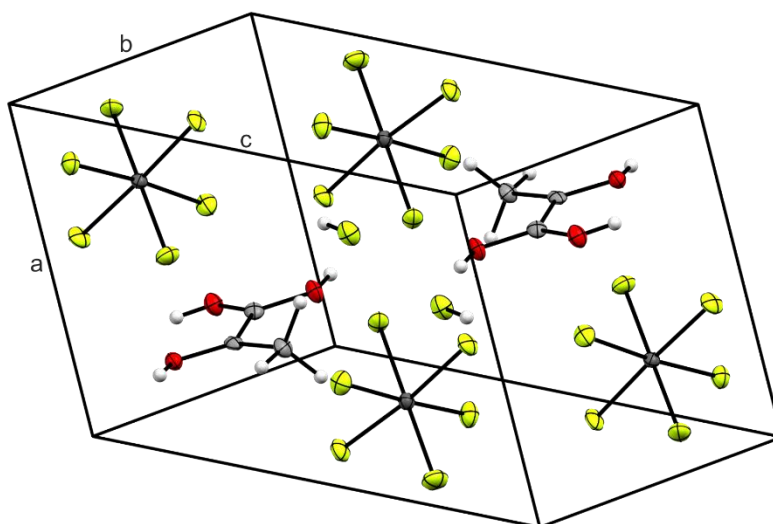
Figure S3. Crystal packing of [H₃C(OH)CC(OH)₂][SbF₆]₂·HF (**4**). Probability displacement ellipsoids are set at 50%. Hydrogen atoms are set as spheres of arbitrary radius.
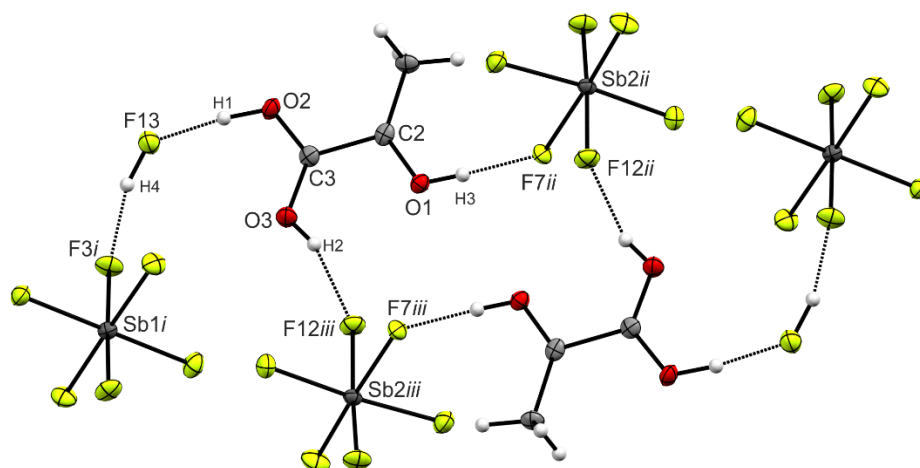
Figure S4. Hydrogen bonds (represented as dashed lines) in **4**. Symmetry codes: *i* = 1−*x*, 1−*y*, −*z*; *ii* = 1−*x*, −*y*, −*z*; *iii* = 1+*x*, *y*, *z*.

Table S2. Bond lengths [Å], bond angles [°], and dihedral angles [°] of **4**.

Bond distances [Å]			
C1–C2	1.451(5)	Sb1–F1	1.870(2)
C2–C3	1.526(5)	Sb1–F2	1.886(2)
C3–O2	1.254(5)	Sb1–F3	1.905(2)
C3–O3	1.260(4)	Sb1–F6	1.877(2)
C2–O1	1.243(4)	Sb1–F5	1.866(2)
		Sb1–F4	1.862(2)
		Sb2–F7	1.941(2)
		Sb2–F8	1.855(2)
		Sb2–F9	1.865(2)
		Sb2–F10	1.853(2)
		Sb2–F11	1.867(2)
		Sb2–F12	1.909(2)

Bond angles [°]			
C1–C2–C3	119.8(3)	F4–Sb1–F5	91.01(11)
O3–C3–O2	121.9(4)	F4–Sb1–F1	177.7(9)
O3–C3–C2	123.1(3)	F5–Sb1–F1	90.68(10)
O2–C3–C2	115.0(3)	F4–Sb1–F6	88.17(11)
O1–C2–C1	128.1(4)	F5–Sb1–F6	90.15(10)
O1–C2–C3	112.1(3)	F1–Sb1–F6	93.40(11)
		F4–Sb1–F2	91.34(11)
		F5–Sb1–F2	175.8(10)
		F1–Sb1–F2	86.88(11)
		F6–Sb1–F2	93.30(10)
		F4–Sb1–F3	88.51(11)
		F5–Sb1–F3	89.81(10)
		F1–Sb1–F3	89.92(11)
		F6–Sb1–F3	176.6(10)
		F2–Sb1–F3	86.87(10)
		F10–Sb2–F8	93.82(11)
		F10–Sb2–F9	95.71(11)
		F8–Sb2–F9	90.67(11)
		F10–Sb2–F11	90.86(11)
		F8–Sb2–F11	175.1(9)
		F9–Sb2–F11	90.14(10)
		F10–Sb2–F12	90.95(11)
		F8–Sb2–F12	88.69(10)
		F9–Sb2–F12	173.3(10)
		F11–Sb2–F12	89.95(10)
		F10–Sb2–F7	175.8(9)
		F8–Sb2–F7	89.57(10)
		F9–Sb2–F7	86.62(11)
		F11–Sb2–F7	85.70(10)
		F12–Sb2–F7	86.74(10)

Dihedral angle [°]	
O1–C2–C3–O2	179.6(3)
C1–C2–C3–O2	1.2(5)
O1–C2–C3–O3	− 0.2(5)
C1–C2–C3–O3	− 178.6(3)

Table S3. X-ray data and parameters of **2** and **4**.

	[H₃C(O)CC(OH)₂][SbF₆]	[H₃C(OH)CC(OH)₂][SbF₆]₂·HF
Formula	$C_3H_5F_6O_3Sb$	$C_3H_7F_{13}O_3Sb_2$
M_r [g/mol]	324.82	581.59
Crystal size, mm³	0.18 × 0.17 × 0.12	0.17 × 0.10 × 0.04
Crystal system	triclinic	triclinic
Space group	$P\bar{1}$	$P\bar{1}$
a [Å]	5.621(5)	7.469(5)
b [Å]	6.264(5)	9.486(5)
c [Å]	12.313(5)	9.523(5)
α [°]	104.483(5)	80.637(5)
β [°]	94.218(5)	76.201(5)
γ [°]	91.739(5)	72.650(5)
V [Å³]	418.1(5)	622.4(6)
Z	2	2
ρ_{calc} [g cm⁻³]	2.580	3.103
μ [mm⁻¹]	3.379	4.514
$\lambda_{MoK\alpha}$ [Å]	0.71073	0.71073
F(000)	304	536
T [K]	130	143
hkl range	−7:7; −8:7; −14:16	−9:10; −12:12; −12:13
Reflections measured	2249	3329
Reflections unique	1679	2835
R_{int}	0.0399	0.0252
parameters	130	207
R(F)/*w*R(F²)[a]	0.0427/0.0837	0.0350/ 0.0628
Weighting scheme[b]	0.0360/0.0000	0.0227/0.0000
S (GooF)[c]	1.038	1.042
Residual [e Å⁻³]	1.079/−1.816	0.996/−1.467
Device type	Oxford XCalibur	Oxford XCalibur
Solution	SHELXT[25]	SHELXT[25]
Refinement	SHELXL-97[26]	SHELXL-97[26]
CCDC	2002472	2002473

[a] $R_1 = \Sigma||F_o|-|F_c||/\Sigma|F_o|$
[b] $wR_2 = [\Sigma[w(F_o^2-F_c^2)^2]/\Sigma[w(F_o)^2]]^{1/2}$; $w = [\sigma_c^2(F_o^2)+(0.0360P)^2]^{-1}$, $w = [\sigma_c^2(F_o^2) + (0.0227P)^2]^{-1}$; $P = (F_o^2+2F_c^2)/3$
[c] GooF = $\{\Sigma[w(F_o^2-F_c^2)^2]/(n-p)\}^{1/2}$ (n = number of reflections; p = total number of parameters).

Vibrational spectroscopy

Table S4. Observed vibrational frequencies [cm⁻¹] of **1**, **2**, and the deuterated species of **1**, as well as the calculated vibrational frequencies of the respective species.

[H₃C(O)CC(OH)₂][AsF₆]		[H₃C(O)CC(OH)₂][SbF₆]		[H₃C(O)CC(OD)₂][AsF₆]		[H₃C(O)CC(OH)₂]⁺ calc.[a] (IR/Ra)	[H₃C(O)CC(OD)₂]⁺ calc.[b] (IR/Ra)	Assignment
IR	Ra	IR	Ra	IR	Ra			
				2343 (w)	2320 (2)	3601 (276/96)	2622 (160/46)	ν(OX)
				2215 (m)	2219 (4)	3356 (277/37)	2441 (148/17)	ν(OX)
					3140 (3)			1641 + 1500
				3137 (vw)				
3045 (vw)	3040 (19)	3040 (vw)	3042 (9)	3040 (vw)	3040 (27)	3218 (5/49)	3218 (5/49)	ν_{asym}(CH₃)
	2982 (23)		2979 (11)	2981 (vw)	2982 (33)	3149 (3/45)	3149 (3/45)	ν_{asym}(CH₃)
2935 (vw)	2940 (71)		2934 (36)	2938 (vw)	2940 (88)	3065 (17/163)	3065 (17/164)	ν_{sym}(CH₃)
					2832 (3)			2 × 1418
					2707 (5)			1500 + 1200
				2409 (w)				2 × 1205 = 2410
1733 (vw)	1729 (41)	1738 (vw)	1737 (21)	1723 (w)	1723 (20)	1735 (59/8)	1731 (51/9)	ν(CO$_k$)
1652 (vw)	1663 (2)	1662 (vw)	1673 (13)	1645 (w)	1641 (4)	1688 (272/1)	1679 (333/1)	ν_{asym}(CO$_a$)
1520 (vw)	1526 (1)	1523 (vw)	1540 (6)	1516 (vw)	1500 (10)	1557 (144/9)	1504 (46/8)	ν_{sym}(CO$_a$)
1421 (vw)	1420 (1)	1404 (vw)	1417 (14)	1406 (vw)	1418 (17)	1448 (17/5)	1448 (17/5)	δ_{asym}(CH₃)
1362 (vw)	1364 (35)	1362 (vw)	1364 (16)	1361 (w)	1364 (34)	1436 (17/9)	1434 (11/10)	δ_{asym}(CH₃)
1459 (m)	1447 (7)	1454 (vw)	1445 (7)			1387 (58/4)	1386 (51/5)	δ_{sym}(CH₃)
1306 (vw)	1303 (3)	1301 (vw)	1318 (12)			1228 (218/5)	1016 (45/3)	δ(COX)
						1206 (75/4)	921 (50/2)	δ(COX)
1179 (w)	1183 (15)	1180 (w)	1183 (4)	1205 (w)	1200 (4)	1179 (65/2)	1199 (88/1)	δ(CCH)
1026 (vw)	1023 (1)	1024 (vw)	1023 (1)	1024 (w)	1033 (5)	1036 (1/0)	1035 (1/0)	γ(CH₃)
997 (vw)	996 (9)	993 (vw)	992 (4)	993 (w)	994 (13)	989 (6/1)	990 (35/4)	ν(H₃CC(O))
				903 (w)	903 (14)			
847 (vw)		847 (w)				878 (68/0)	641 (43/0)	γ(OX)
						757 (161/0)	553 (74/0)	γ(OX)
797 (vw)	797 (54)	798 (w)	799 (21)			731 (31/10)	690 (29/9)	ν((O)CC(O))
613 (w)	618 (17)	625 (w)	620 (7)	777 (w)	778 (6)	668 (27/1)	715 (17/0)	γ(CO$_a$)
						593 (18/2)	567 (17/2)	δ(CCO)
						479 (8/1)	466 (10/0)	δ(CCO)
	375 (54)				375 (1)	373 (0/0)	352 (2/0)	γ(CC)
						369 (31/2)	349 (28/2)	δ(CCO)
						224 (16/0)	216 (16/0)	ρ(CO$_a$)
	137 (24)		137 (19)			141 (0/0)	141 (0/0)	τ(CH₃)
						106 (4/0)	104 (4/0)	τ(CC)
				759 (m)	759 (34)			[MF₆]⁻
696 (vs)	695 (58)				701 (40)			[MF₆]⁻
	676 (100)	668 (w)	670 (39)	673 (s)	678 (100)			[MF₆]⁻
		656 (w)	653 (100)					[MF₆]⁻
572 (s)	579 (29)	570 (m)	579 (9)	627 (m)				[MF₆]⁻
	560 (30)	547 (w)	562 (8)	595 (m)	580 (21)			[MF₆]⁻
		469 (vw)	466 (4)	546 (m)	559 (17)			[MF₆]⁻
451 (vw)								[MF₆]⁻
417 (w)	421 (14)		434 (6)		412 (23)			[MF₆]⁻
390 (s)	375 (54)			390 (m)	375 (57)			[MF₆]⁻
		287 (vw)	282 (51)					[MF₆]⁻
	186 (39)		178 (12)		184 (26)			[MF₆]⁻

[a] Calculated at the MP2/aug-cc-pVDZ level of theory [b] IR intensities in km·mol⁻¹ and Raman intensities in Å⁴·µ⁻¹. Experimental Raman intensity is scaled to the most intensive mode to be 100. [c] Abbreviations: v = very, w = weak, m = medium, sh = shoulder ν = stretch, δ = deformation sym = symmetric, asym = antisymmetric, k = keto, a = acid. [d] X = H, D; M = As, Sb.

Table S5. Observed vibrational frequencies [cm^{-1}] of **3**, **4**, and the deuterated species of **3**, as well as the calculated vibrational frequencies of the respective species.

$[H_3C(OH)CC(OH)_2][AsF_6]_2$ IR	Ra	$[H_3C(OH)CC(OH)_2][SbF_6]_2$ IR	Ra	$[H_3C(OD)CC(OD)_2][AsF_6]_2$ IR	Ra	$[H_3C(OH)CC(OH)_2]^{2+}$ calc.[a] (IR/Ra)	$[H_3C(OD)CC(OD)_2]^{2+}$ calc.[b] (IR/Ra)	Assignment
				2343 (vw)	2307 (3)	3567 (340/37)	2604 (195/15)	$\nu(OX)$
				2120 (vw)	2118 (4)	3461 (771/81)	2524 (482/33)	$\nu(OX)$
					1949 (4)	3449 (217/23)	2516 (99/8)	$\nu(OX)$
	3034 (14)		3040 (2)		3036 (18)	3180 (47/52)	3180 (47/52)	$\nu_{asym}(CH_3)$
2945 (vw)	2961 (33)	2954 (vw)	2961 (3)	2960 (vw)	2959 (40)	3047 (44/60)	3047 (45/60)	$\nu_{asym}(CH_3)$
	2939 (16)							
2895 (vw)	2897 (51)	2885 (vw)	2894 (6)	2896 (vw)	2897 (67)	2977 (160/197)	2977 (143/205)	$\nu_{sym}(CH_3)$
	2701 (3)							
		2579 (vw)						
2361 (vw)		2357 (vw)						
2339 (vw)								
		2237 (vw)						
		1894 (w)						
1817 (vw)								
	1678 (20)	1662 (m)	1671 (10)	1703 (vw)	1701 (17)	1731 (172/5)	1719 (171/5)	$\nu_{oop}(CO_a)$
1708 (vw)	1717 (13)	1705 (w)	1710 (3)	1668 (vw)	1671 (19)	1661 (155/32)	1649 (195/30)	$\nu(CO_k)$
1606 (w)								
	1542 (9)	1537 (w)	1540 (4)	1506 (vw)	1516 (14)	1537 (73/14)	1506 (40/16)	$\nu_{ip}(CO_a)$
1466 (sh)	1480 (2)	1464 (sh)	1482 (1)					
1419 (w)	1422 (9)	1409 (sh)	1426 (2)	1423 (vw)	1422 (7)	1414 (9/5)	1413 (18/5)	$\delta_{asym}(CH_3)$
1361 (sh)	1366 (14)	1363 (m)	1374 (3)	1364 (vw)	1374 (7)	1395 (27/5)	1395 (28/5)	$\delta_{asym}(CH_3)$
	1337 (24)			1335 (vw)	1343 (37)	1369 (141/15)	1338 (111/31)	$\delta_{sym}(CH_3)$
	1322 (24)	1323 (w)	1320 (16)	1252 (vw)	1256 (2)	1298 (188/20)	1267 (84/6)	$\delta_{sym}(CH_3)$
1260 (w)	1260 (2)	1248 (vw)	1249 (1)					
		1198 (m)	1200 (2)					
				1155 (vw)	1150 (2)			
				1024 (vw)	1025 (5)			
1180 (w)	1181 (6)	1176 (m)	1181 (1)	999 (vw)		1179 (141/3)	993 (83/3)	$\delta(COX)$
1139 (sh)	1171 (6)	1143 (sh)						
		1103 (vw)	1107 (1)	892 (w)	903 (2)	1116 (130/8)	870 (18/4)	$\delta(COX)$
1043 (w)		1047 (w)		814 (w)	824 (2)	1097 (208/0)	840 (154/0)	$\delta(COX)$
				1007 (vw)	1011 (8)	1012 (1/1)	997 (3/1)	$\gamma(CH_3)$
989 (w)	996 (6)	987 (w)	992 (2)		982 (7)	985 (22/2)	991 (1/2)	$\nu(H_3CC(O))$
928 (w)		918 (w)		608 (vw)	597 (15)	855 (90/0)	604 (107/0)	$\gamma(OX)$
847 (m)		847 (w)			523 (6)	765 (122/1)	540 (6/0)	$\gamma(OX)$
796 (m)	793 (36)	804 (w)	799 (9)		738 (38)	747 (25/7)	693 (14/6)	$\nu((O)CC(O))$
						653 (19/1)	750 (0/0)	$\gamma_{oop}(CC)$
617 (s)	620 (8)	634 (s)		495 (vw)		616 (222/0)	462 (115/0)	$\gamma(OX)$
						578 (46/1)	537 (53/1)	$\delta(CCO)$
						482 (4/3)	454 (9/2)	$\delta(CCO)$
						389 (5/2)	370 (4/2)	$\delta(CCO)$
						375 (2/0)	359 (1/0)	$\gamma_{ip}(CC)$
						240 (11/0)	229 (11/0)	$\rho(CO_a)$
	138 (41)		138 (11)		140 (41)	144 (7/1)	144 (7/1)	$\tau(CCH_3)$
						53 (2/0)	51 (2/0)	$\tau(CC)$
707 (s)	705 (92)			708 (w)	709 (69)			$[MF_6]^-$
671 (s)		681 (vs)	672 (47)	667 (vw)	672 (100)			$[MF_6]^-$
	666 (100)	663 (vs)	662 (100)		597 (15)			$[MF_6]^-$
567 (sh)	572 (22)	574 (sh)	585 (11)		572 (11)			$[MF_6]^-$
553 (s)		514 (m)	557 (4)					$[MF_6]^-$
		436 (w)	437 (2)	415 (vw)	408 (7)			$[MF_6]^-$
425 (w)	420 (5)	419 (w)						$[MF_6]^-$
406 (vw)	382 (48)			386 (w)	383 (46)			$[MF_6]^-$
	371 (57)	355 (m)			360 (25)			$[MF_6]^-$
			286 (36)		315 (5)			$[MF_6]^-$
	186 (17)		184 (5)		262 (2)			$[MF_6]^-$
	128 (43)							$[MF_6]^-$

[a] Calculated at the MP2/aug-cc-pVDZ level of theory [b] IR intensities in km·mol^{-1} and Raman intensities in Å^4·μ^{-1}. Experimental Raman intensity is scaled to the most intensive mode to be 100. [c] Abbreviations: v = very, w = weak, m = medium, sh = shoulder, ν = stretch, δ = deformation sym = symmetric, asym = antisymmetric, ip = in-phase, oop = out-of-phase, k = keto, a = acid. [d] *X* = H, D; *M* = As, Sb.

Theoretical investigation
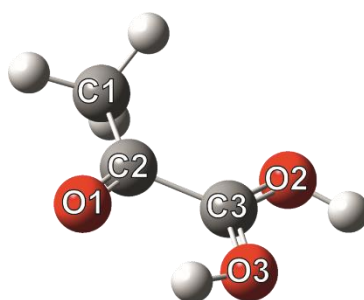
Figure S5. Optimized gas-phase structure of [C$_2$(O)(OH)$_2$Me]$^+$. Calculated on the MP2/aug-cc-pVDZ level of theory.

Table S6. Standard orientation of [C$_2$(O)(OH)$_2$Me]$^+$. Calculated on the MP2/aug-cc-pVDZ level of theory.

Atomic Type	Coordinates (Angstroms)		
	X	Y	Z
C	0.000000	0.744426	0.000000
O	-1.141763	1.329741	0.000000
O	1.094365	1.403960	0.000000
H	1.828388	0.725515	0.000000
C	0.104888	-0.805562	0.000000
O	1.274525	-1.173349	0.000000
C	-1.140254	-1.620980	0.000000
H	-1.744320	-1.370928	0.888545
H	-1.744320	-1.370928	-0.888545
H	-0.877335	-2.685269	0.000000
H	-1.067230	2.311477	0.000000
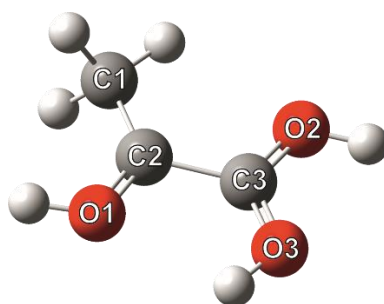
Figure S6. Optimized gas-phase structure of [C$_2$(OH)$_3$Me]$^{2+}$. Calculated on the MP2/aug-cc-pVTZ level of theory.

Table S7. Standard orientation of [C$_2$(OH)$_3$Me]$^{2+}$. Calculated on the MP2/aug-cc-pVTZ level of theory.

Atomic Type	Coordinates (Angstroms)		
	X	Y	Z
C	0.000000	0.748636	0.000000
O	1.175056	1.205418	0.000000
C	0.045328	-0.798815	0.000000
O	-1.092716	-1.343029	0.000000
O	1.117189	-1.466134	0.000000
H	1.965637	-0.966508	0.000000

C	-1.235063	1.503986	0.000000
H	-1.239416	2.171207	0.878137
H	-1.239416	2.171207	-0.878137
H	-2.117690	0.872376	0.000000
H	1.263044	2.193066	0.000000
H	-1.089976	-2.334229	0.000000

Figure S7. Optimized gas-phase structure of [C$_2$(OH)$_3$Me]$^{2+}$·3 HF. Donor-acceptor distances are shown next to the respective hydrogen bond. Calculated on the MP2/aug-cc-pVTZ level of theory.

Table S8. Standard orientation of [C$_2$(OH)$_3$Me]$^{2+}$·3 HF. Calculated on the MP2/aug-cc-pVTZ level of theory.

	Coordinates (Angstroms)		
Atomic Type	X	Y	Z
C	-0.652477	-0.679943	0.000036
O	-1.470314	0.266526	-0.000344
C	0.805329	-0.181653	-0.000086
O	1.659154	-1.107514	0.000174
O	1.113791	1.038906	-0.000401
H	0.386520	1.749340	-0.000534
C	-0.947954	-2.102047	0.000605
H	-0.457780	-2.558424	-0.869678
H	-0.457664	-2.557792	0.871149
H	-2.015093	-2.305207	0.000738
H	-2.468511	0.002148	-0.000253
H	2.640218	-0.799359	0.000094
F	-3.832622	-0.499806	-0.000084
H	-4.654351	-0.047904	-0.000285
F	-0.528594	2.943831	0.000073
H	-0.273942	3.844616	0.000369
F	4.008022	-0.267564	-0.000040
H	4.828909	-0.717040	0.000096

Table S9. Calculated frequencies of $[H_3C(OH)CC(OH)_2]^{2+}\cdot 3$ HF. Calculated on the MP2/aug-cc-pVDZ level of theory.

$[H_3C(OH)CC(OH)_2]^{2+}\cdot 3$ HF (IR/Ra) calc.[a][b]	Assignment[c]
3876 (301/70)	ν(HF)
3871 (359/54)	ν(HF)
3847 (369/59)	ν(HF)
3207 (21/45)	$\nu_{asym}(CH_3)$
3080 (38/57)	$\nu_{asym}(CH_3)$
3018 (44/225)	$\nu_{sym}(CH_3)$
2973 (1741/91)	ν(OH)
2801 (1624/177)	ν(OH)
2729 (3947/43)	ν(OH)
1748 (259/4)	$\nu_{asym}(CO_a)$
1680 (129/30)	$\nu(CO_k)$
1571 (20/17)	$\nu_{sym}(CO_a)$
1454 (387/3)	δ(COH)
1426 (54/4)	$\delta_{sym}(CH_3)$
1400 (20/4)	$\delta_{asym}(CH_3)$
1341 (63/1)	δ(COH)
1318 (40/33)	$\delta_{sym}(CH_3)$
1236 (373/9)	δ(COH)
1209 (59/0)	δ(CCH)
1110 (91/0)	γ(OH)
1027 (41/0)	γ(OH)
982 (5/0)	$\delta(CH_3)$
975 (16/2)	$\nu(H_3CC(O))$
927 (142/0)	γ(OH)
810 (0/11)	$\nu((O)CC(O))$
696 (3/0)	γ_{oop}(CC)
639 (10/2)	δ(CCO)
568 (1/3)	δ(CCO)
526 (115/2)	δ(HF)
480 (129/0)	δ(HF)
462 (206/1)	δ(HF)
415 (4/0)	γ_{ip}(CC)
406 (32/1)	δ(HF)
337 (59/0)	δ(CCO)
274 (29/0)	ν(H⋯FH)
258 (294/1)	δ(HF)
215 (18/0)	ν(H⋯FH)
210 (156/1)	δ(HF)
207 (165/1)	δ(HF)
202 (16/0)	ν(H⋯FH)
148 (7/1)	$\tau(CH_3)$
124 (2/0)	δ(HFH)
108 (0/1)	τ(CC)
96 (2/0)	δ(HFH)
72 (0/0)	δ(HFH)
62 (2/0)	δ(HFH)
55 (1/0)	γ(HF)
23 (0/1)	τ(CC)

[a] Calculated on the MP2/aug-cc-pVDZ level of theory [b] IR intensities in km·mol^{-1} and Raman intensities in Å^4·µ^{-1}. [c] Abbreviations: ν = stretch, δ = deformation sym = symmetric, asym = antisymmetric, ip = in-phase, oop = out-of-phase, k = keto, a = acid.
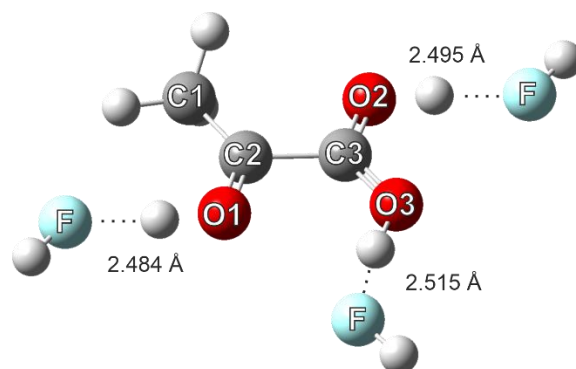
Figure S8. Optimized gas-phase structure of [C$_2$(OH)$_3$Me]$^{2+}$·2 HF. Donor-acceptor distances are shown next to the respective interaction. Calculated on the MP2/aug-cc-pVTZ level of theory.

Table S10. Standard orientation of [C$_2$(OH)$_3$Me]$^{2+}$·2 HF. Calculated on the MP2/aug-cc-pVTZ level of theory.

Atomic Type	Coordinates (Angstroms)		
	X	Y	Z
F	2.416879	-0.007100	-0.108770
O	0.001220	-1.141266	1.324473
O	-0.003894	-1.602955	-0.837669
O	-0.001265	1.031924	-1.308949
C	0.000641	0.747622	-0.084115
C	0.004303	1.654723	1.040218
H	0.003797	2.699001	0.735723
H	0.881477	1.423938	1.659997
H	-0.868552	1.424620	1.666159
C	-0.000891	-0.777168	0.116500
H	-0.005724	-1.217639	-1.740848
H	-0.000372	1.996881	-1.517351
H	0.000588	-2.119122	1.457958
F	-2.417265	-0.003094	-0.105336
1	-3.347897	-0.080709	-0.091469
1	3.347345	-0.087902	-0.101681
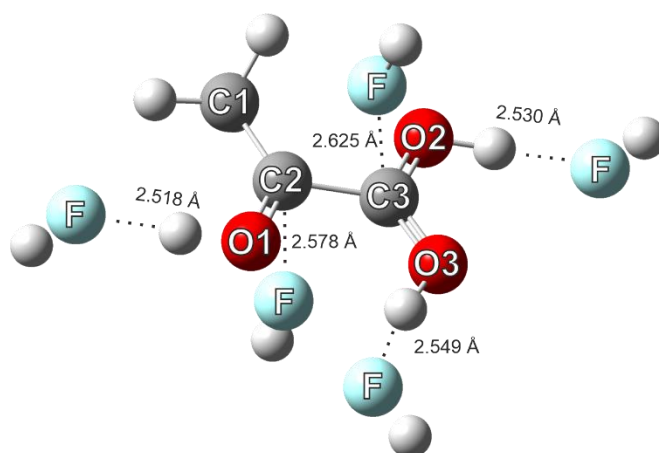
Figure S9. Optimized gas-phase structure of [C$_2$(OH)$_3$Me]$^{2+}$·5 HF. Donor-acceptor distances are shown next to the respective interaction. Calculated on the MP2/aug-cc-pVTZ level of theory.

Table S11. Standard orientation of [C$_2$(OH)$_3$Me]$^{2+}$·5 HF. Calculated on the MP2/aug-cc-pVTZ level of theory.

Atomic Type	Coordinates (Angstroms)		
	X	Y	Z
F	-0.030009	-0.291602	2.486716
O	1.658355	-1.047753	0.010905
O	1.129757	1.099140	0.002025
O	-1.456897	0.355993	-0.004126
C	-0.648773	-0.596951	0.002281
C	-0.958887	-2.016486	0.006736
H	-2.028659	-2.203264	0.002547
H	-0.483485	-2.463744	0.886186
H	-0.475304	-2.471199	-0.864350
C	0.808527	-0.118193	0.005229
H	0.397146	1.790563	-0.002509
H	-2.441163	0.091833	-0.006777
H	2.624545	-0.734083	0.011659
F	-0.013155	-0.311060	-2.480226
H	0.084280	-0.308995	-3.406161
H	0.060697	-0.288654	3.413335
F	-3.850738	-0.423705	-0.009895
H	-4.678048	0.013594	-0.014943
F	4.036302	-0.185082	-0.006629
H	4.864235	-0.617538	0.005840
F	-0.531402	3.032603	-0.008832
H	-0.278157	3.931847	-0.010951

ARTICLE

Desoxyfluorination with Superacids – Synthesis and Characterization of Protonated α-Fluorohydroxyacetic Acid

Alan Virmani,[a] Christoph Jessen,[a] Alexander Nitzer,[a] and Andreas J. Kornath*[a]

Abstract: α-Fluoroalcohols describe a rare and unstable class of compounds, accessible mainly by fluorination of highly electrophilic carbonyl compounds. In this work, we report the syntheses of α-fluorohydroxyacetic acid (FHA) and its acyl fluoride (FHA-F) by reacting the dihydroxy species glyoxylic acid monohydrate (GAM) with SF_4. Surprisingly, only one of the geminal hydroxy groups is substituted when excess SF_4 is employed. Implementing GAM with the binary superacid HF/AsF_5 also leads to a single yet quantitative desoxyfluorination at the diol group. The reaction pathways are discussed based on NMR experiments, the characterization was carried out using NMR and vibrational spectroscopy as well as single-crystal X-ray diffraction.

Introduction

Organic compounds containing carbon atoms with more than one hydroxy group are known to be labile under regular conditions. According to the rule of Erlenmeyer, they undergo facile dehydration under the formation of the respective carbonyl compound.[1] This also applies to alcohols with a geminal halogen atom, where the hydrogen halide is easily eliminated.[2] In the case of fluorinated compounds, only a few examples of α-fluoroalcohols are known. Fluoromethanol CFH_2OH, the simplest representative, was synthesized by Olah and Pavláth as early as 1953.[3] In 1977, Seppelt was able to generate the perfluorinated alcohol trifluoromethanol CF_3OH by reacting CF_3OCl with HCl. He operated at low temperatures to prevent decay under the formation of COF_2 and HF.[4] 30 years later, Christe et al. investigated this equilibrium.[5] The addition of HF or F^- to a carbonyl group is a convenient way to access (per-)fluorinated alcohols, first shown by Andreades and England in 1961,[6] followed by others in recent studies.[7,8] The general equation is given below (Equation 1).

However, the α-fluoroalcohol is only stable when the electrophilicity of the carbonyl group is high enough, similar to the

rule of Erlenmeyer.[1] The equilibrium of Equation 1 can be shifted to the right by transforming the alcohol into stable derivatives like acetals or oxonium ions.[5,9,10] The oxonium ions were generated by reacting the carbonyl compounds with the superacidic system HF/SbF_5 in anhydrous hydrogen fluoride (aHF). In this way, the perfluorinated oxonium ions of methanol, ethanol, n-propanol,[10] and isopropanol[11] have been synthesized.

An example of an exception to the rule of Erlenmeyer is glyoxylic acid (GA). The purchasable monohydrate form (GAM) does not imply co-crystallized but chemically bound water and is better described as dihydroxyacetic acid. Its reactivity toward highly acidic systems, in which it can be activated for electrophilic reactions, has been described by Prakash et al.[12] The high electrophilicity makes it an interesting target for generating an α-fluorohydroxy compound with an additional functional group in the direct vicinity. To exploit this possibility or to determine if a difluorinated product is formed, we have implemented GAM with the desoxyfluorinating agent SF_4 as well as the superacidic medium HF/AsF_5. We wish to report the results herein.

Results and Discussion

Syntheses and Properties

α-Fluorohydroxyacetic acid (FHA, **1**) is synthesized by reacting glyoxylic acid monohydrate (also dihydroxyacetic acid, GAM) with an equimolar amount of sulfur tetrafluoride (Equation 2). For the synthesis of α-fluorohydroxyacetyl fluoride (FHA-F, **2**), a twofold amount of SF_4 is applied (Equation 3)
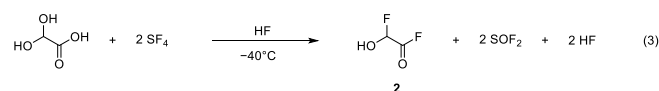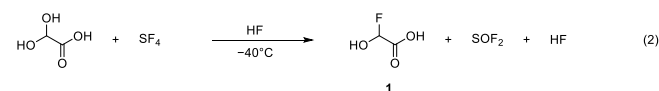
The mechanism of GAM in the system HF/SF_4 is proposed based on the literature-reported pathways of similar reactions.[13–15] In the first step, SF_4 dissociates in aHF according to Equation 4.
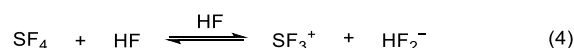
We confirm that the alcohol moiety is more nucleophilic than the carboxy group, which is why the first desoxyfluorination takes place there (Scheme 1). The reactive intermediate is a planar

[a]   A. Virmani, C. Jessen, A. Nitzer, Prof. Dr. A. J. Kornath
      Department Chemie
      Ludwig-Maximilians-Universität München
      Butenandtstraße 5-13 (D)
      D-81377 München
      E-mail: andreas.kornath@cup.uni-muenchen.de

Supporting information for this article is given via a link at the end of the document.

oxonium ion. Since the addition of a nucleophile in this mechanism is not stereoselective, a racemic mixture is expected.
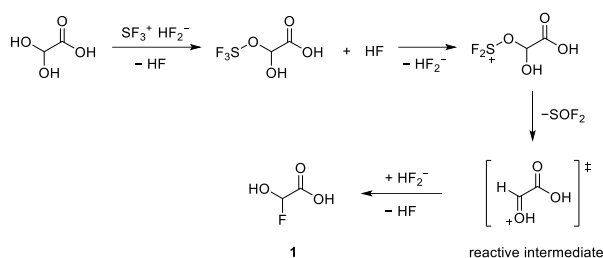
Scheme 1. Proposed reaction pathway of GAM with equimolar amounts of SF_4.

The second desoxyfluorination of the carboxylic group proceeds in a similar fashion. However, in this case, the formation of a tetrahedral intermediate is likely, as has been suggested in previous studies about the reactions of carbonyl compounds with HF/SF_4.[13,15] The proposed mechanism is illustrated in Scheme 2.
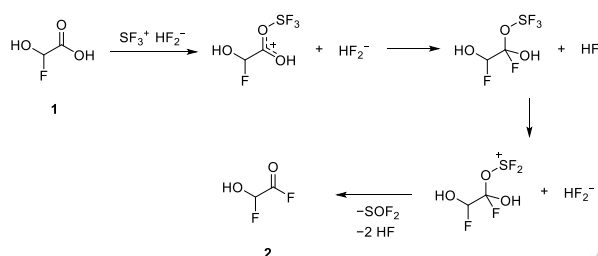
Scheme 2. Proposed reaction pathway of the desoxyfluorination reaction at the carboxy group.

Employing three or more equivalents of SF_4 did not result in a second desoxyfluorination at the tetrahedral C atom, hence in 2,2-difluoroacetyl fluoride or 2,2-difluoroacetic acid. Since the cationic intermediate would be a fluoro carbenium ion, it is presumably not sufficiently stabilized.

The desoxyfluorination agent SF_4 has been investigated in the past.[13],[15] Interestingly, a similar reaction is observed for GAM reacting with superacids. Protonated α-fluorohydroxyacetic acid [FHA-1H]+ is generated from GAM in the superacidic system HF/AsF_5, resulting in [FHA-1H][AsF$_6$] (**3**). The reaction is visualized in Equation 5.

Formally, a two-to-one ratio of AsF_5 to GAM would suffice to form [FHA-1H][AsF$_6$]. However, full conversion takes place only when three equivalents of Lewis acid are applied. By first dissolving three equivalents of Lewis acid (compared to GAM) in aHF, the superacidic medium is formed, which reacts with GAM to [FHA-1H][AsF$_6$] in quantitative yields. The carboxy group is more basic than the hydroxy groups due to a better resonance stabilization, which is why it is likely protona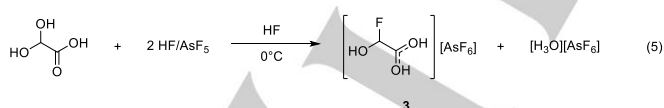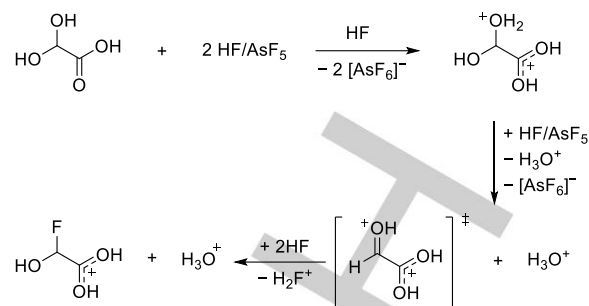ted in the first step. The second protonation occurs at one of the hydroxy groups that subsequently is substituted for fluoride. **3** is found as a racemic mixture of the two enantiomers, strongly indicating an S_N1 mechanism. The proposed mechanism is displayed in Scheme 3.

Scheme 3. Proposed mechanism of the synthesis of [FHA-1H]+ from GAM.

The necessity of three equivalents of Lewis acid to form **3** leads to the conclusion that a superelectrophilic carbodication is formed as the reactive intermediate.

NMR spectroscopy

The reactivity of glyoxylic acid monohydrate (GAM) in the systems HF/SF_4, HF/AsF_5, or solely aHF can be traced by ^1H, ^{19}F, and ^{13}C NMR spectroscopy. The samples were dissolved either in aHF or SO_2, and acetone-*d6* was employed for external referencing. For more details of the experimental procedure, see the Supporting Information. The chemical shifts of **1**, **2**, and **3** are listed in Table 1. The respective solvent used for the measurements is given in the table footnote. A reference of GAM in D_2O is displayed in Figures S1 and S2.

Table 1. ^1H, ^{19}F, and ^{13}C chemical shifts [ppm] including coupling constants [Hz] of **1**, **2**, and **3**. Measured at −40°C.

	FHA[a]	FHA-F[b]	[FHA-1H][AsF$_6$][a]
δ [^1H] (C−H)	5.57 (d), J=54.4	7.00 (d) J=51.2	5.61 (d) J=56.9
δ [^{19}F] (C−F)	−130.38 (d) J=54.4	−134.67 (d) J=53.7	−128.88 (d) J=53.9
δ [^{19}F] (COF)		23.63 (d) J=16.3 22.97 (d) J=14.1	
δ [^{13}C] (carboxylic)	170.98 (d) J=32.7	154.33 (dd) J=368.7, 34.8	184.90 (d) J=34.0
δ [^{13}C] (tetrahedral)	96.95 (d) J=225.1	92.59 (dd) J=241.3, 82.4	97.00 (d) J=227.1

[a] aHF as a solvent. [b] SO_2 as a solvent.

GAM has proven very reactive to HF. When dissolved in aHF, NMR spectra (Figures S3–S5, Supporting Information) show a variety of fluorinated compounds. Doublets in both the ^1H (5.65 ppm, J = 61.2 Hz) and the ^{13}C NMR spectra (171.57 ppm, J = 32.6 Hz and 97.99 ppm, J = 225.2 Hz) are very similar to those assigned to **1**. This means that desoxyfluorination occurs in aHF, albeit uncontrolled. By first dissolving equimolar amounts of SF_4 (compared to GAM) in aHF and secondly adding GAM, **1** becomes the main product with an amount of roughly 74% (NMR spectra displayed in Figures S6–S8, Supporting Information), as the doublet at 5.57 ppm is the most intensive one in the ^1H NMR spectrum. The ^{19}F signal at −130.38 ppm is assigned to the

fluorine atom in FHA since the coupling constant is the same as for the ^{1}H signal. The ^{13}C shift of the carboxy group is observed at 170.98 ppm, and the tetrahedral carbon shift at 96.95 ppm.

By employing two equivalents of SF_4, **2** is the most abundant species. The NMR spectra recorded in aHF showed an equilibrium of **2** and its HF-adduct **4** (see Equation 6). The spectra are displayed in Figures S9–S11 in the Supporting Information.

$$\text{HO}\overset{\displaystyle O}{\underset{\displaystyle F}{-}}\text{F} \xleftarrow{\text{HF}} \text{HO}\overset{\displaystyle F\ \ F}{\underset{\displaystyle F}{-}}\text{OH} \qquad (6)$$

<center>**2**   **4**</center>
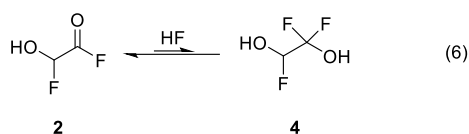
The equilibrium is shifted to **2** by removing all volatile products at −78°C, successively warming up the residue to 0°C, and trapping the gas phase into a second vessel at −196°C. The condensate was dissolved in SO_2, and NMR spectra (Figures S12–S14) show **2** as the only organic compound, as shown by the intensive doublet at 7.00 ppm in the ^{1}H NMR spectrum. The ^{13}C signal of the acyl fluoride is observed at 154.33 ppm. The dd-splitting pattern shows the coupling to two fluorine atoms, just like the ^{13}C shift of the tetrahedral carbon at 92.59 ppm. In the ^{19}F NMR spectrum, these signals occur at −134.67, 23.63, and 22.97 ppm. Additional signals at 65.17 ppm and 64.48 ppm are assigned to residual SF_4 that has not been removed.[16]

A different approach to generating a derivative of α-fluorohydroxyacetic acid is the desoxyfluorination of GAM with superacids. By dissolving the Lewis acid in aHF in the first step, the superacidic medium is formed. Subsequently adding GAM to the solution led to a quantitative synthesis of [FHA-1H][AsF$_6$] (**3**) (NMR spectra displayed in Figures S15–S17, Supporting Information). The ^{13}C signal of the carboxy group (184.90 ppm) is shifted downfield compared to GAM and **1** due to the protonation in the superacidic system, similar to reported protonated carboxy groups.[17] The doublet at 97.00 ppm is assigned to the CHF(OH) group. The ^{19}F signal is observed at −128.88 ppm and the ^{1}H resonance at 5.61 ppm.

Vibrational Spectroscopy

The synthesis of FHA-F and [FHA-1H][AsF$_6$] is confirmed by vibrational spectroscopy. FHA-F (**2**) was generated by reacting GAM with a twofold amount of SF_4 in aHF. The solvent and other volatile products were removed *in vacuo* overnight at −78°C. The sample was warmed up to 0°C and an infrared spectrum of the gas phase was measured at room temperature. In the case of [FHA-1H]$^+$, the [AsF$_6$]$^-$ salt (**3**) was synthesized by reacting GAM with HF/AsF$_5$ in aHF and successively removing the solvent *in vacuo* at −78°C. Infrared and Raman spectroscopy of the colorless residue was performed at low temperatures (see Supporting Information for more details). The spectra are displayed in Figure 1 and selected observed frequencies are listed in Table 2. To support the assignment of the vibrational frequencies, quantum chemical calculations of the respective compounds were performed. The detailed characterization of the compounds is found in the Supporting Information. FHA (**1**) could not be isolated, which is why an experimental frequency analysis was not feasible. However, the quantum chemically calculated frequencies and their assignment are listed in Table S3 in the Supporting Information.
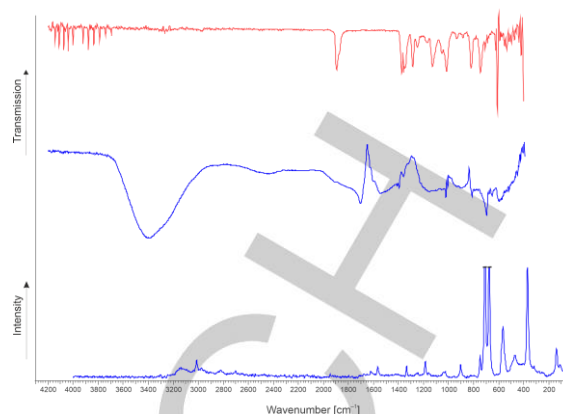

Figure 1. The infrared spectrum of gaseous **2** at room temperature (top, red). Low-temperature infrared (middle) and Raman spectrum (bottom) of **3** (blue).

Table 2. Selected observed vibrational frequencies [cm^{-1}] of **2** and **3**.

FHA-F	[FHA-1H][AsF$_6$]		Assignment
exp. IR[a]	exp. IR[a]	exp. Ra[b]	
1894 (m)	1705 (m)		ν(CO$_a$)
	1541 (m)	1567 (7)	ν(CO$_a$)
1173 (m)			ν(C(O)F)
1128 (m)	1151 (m)	1162 (3)	ν(C−OH)
1016 (m)	1022 (m)	1027 (4)	ν(CF)
822 (m)	897 (m)	903 (8)	ν(CC)

[a] Abbreviations: m = medium, a = acid. [b] Experimental Raman intensities are relative to a scale of 1 to 100.

The infrared spectrum of **2** shows rotational bands of remaining hydrogen fluoride between 3728 and 4143 cm^{-1}, which was not completely removed after the reaction. The ν(C=O) vibration is observed at 1894 cm^{-1}. This band is distinct for acyl fluorides[18–20] and is significantly blue-shifted compared to GAM (1742 cm^{-1}).[21] The stretching vibrations of the newly formed CF bonds occur at 1173 (acyl fluoride moiety) and 1016 cm^{-1} (fluorohydroxy group). The intensive bands down from 708 cm^{-1} are assigned to residual SF_4, which has been observed in the NMR study as well. A reference spectrum of SF_4 is illustrated in Figure S18 in the Supporting Information.

In the IR spectrum of **3**, a strong and broad band with its maximum at 3406 cm^{-1} is found. This might be assigned to H_3O^+, however, it cannot be excluded that this band is attributed to the measurement method at low temperatures, where water can condense onto the specimen, superposing the OH and CH stretching vibrations. The protonation of the carboxy group can be traced by the ν_{as}(CO) band at 1705 cm^{-1} (IR), which is red-shifted compared to ν(C=O) of GAM (1742 cm^{-1}).[21] The antisymmetric CO stretching mode of **3** occurs at 1541 (IR) and 1567 cm^{-1} and is in return blue-shifted concerning ν(C−O) of GAM (1101 cm^{-1}). This convergence of the carboxylic vibrations is a direct result of protonation and has been described in several studies.[22,23] The stretching vibration of the newly formed CF bond is observed at 1022 (IR) and 1027 cm^{-1} (Ra), similar to **2**.

Crystal Structure of 3

Single crystals of **3** were obtained by dissolving the colorless powder in aHF at −55°C. Colorless needles suitable for single-

<center>3</center>

crystal X-ray diffraction grew as racemic twins within three days. In the following, the *S*-enantiomer is discussed. **3** crystallizes in the orthorhombic space group $P2_12_12_1$ with four formula units per unit cell. The asymmetric unit is displayed in Figure 2. Table 3 contains selected geometric parameters.
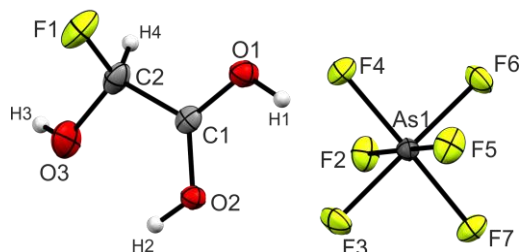

Figure 2. Projection of the asymmetric unit of **3** (50% probability displacement ellipsoids, hydrogen atoms displayed as spheres of arbitrary radius).

Table 3. Selected geometric parameters of **3**. Symmetry codes: *i* = *x*, 1+*y*, *z*; *ii* = 1.5−*x*, 2−*y*, 0.5+*z*.

Bond lengths [Å]		Intermolecular interactions D(−H)···A [Å]	
C1−O1	1.258(4)	O1(−H1)···F2	2.579(4)
C1−O2	1.272(4)	O2(−H2)···O3	2.587(4)
C1−C2	1.515(5)	O2(−H2)···F6*i*	2.669(3)
C2−O3	1.355(5)	O3(−H3)···F3*ii*	2.826(4)
C2−F1	1.376(5)	C1···F7	2.733(5)

Bond angles [deg]		Dihedral angles [deg]	
O1−C1−O2	120.6(3)	O3−C2−C1−O1	179.5(4)
O1−C1−C2	117.4(3)	F1−C2−C1−O1	−61.2(5)
O2−C1−C2	122.0(3)	O3−C2−C1−O2	−1.0(6)
O3−C2−C1	106.6(3)	F1−C2−C1−O2	118.3(4)
F1−C2−C1	106.1(4)		
O3−C2−F1	111.9(4)		

The C1−C2 bond of 1.515(5) Å is similar to the starting material glyoxylic acid monohydrate (GAM, 1.522(3) Å),[24] yet shorter than a regular C−C single bond (1.54 Å).[25] The C1−O1 (1.258(4) Å) and C1−O2 (1.272(4) Å) bond distances are approximately the same and between the length of a formal CO single (1.19 Å) and a double bond (1.43 Å),[25] as it has been observed in a variety of protonated carboxylic acids.[22,23,26] The C2−O3 bond (1.355(5) Å) is significantly shorter than the two C−OH bonds in GAM (1.400(4) and 1.404(3) Å) and even more significant than a regular C−O single bond in general (1.43 Å).[25] The newly formed C2−F1 of 1.376(5) Å is close to a regular C−F bond (1.36 Å).[27] The nature of this bond relation will be discussed below in the Theoretical Study.

The O1−C1−O2 angle of 120.6(3)° is significantly smaller than in GAM (125.1(2)°)[24] as a result of the protonated carboxy group. Subsequently, the O1−C1−C2 is widened from 111.9(2)° in GAM to 117.4(3)° in **3**, while the remaining bond angles remain approximately unchanged. Regarding the torsion angles, the O3−C2−C1−O2 dihedral is reduced from 9.9(9)° to −1.0(6)°. This is due to an intramolecular hydrogen bond O2(−H2)···O3 with a distance of 2.587(4) Å that is formed upon protonation. The cation exhibits three additional, moderately strong hydrogen bonds[28] (Figure 3) to form layers in the *bc*-plane (O1(−H1)···F2, O2(−H2)···F6, and O3(−H3)···F3). These layers are connected along the *a*-axis by nearly perpendicular C1···F7 interactions with a distance of 2.733(5) Å (Figure S21, Supporting Information), which is about 14% within the sum of the van-der-Waals radii (3.17 Å).[29]
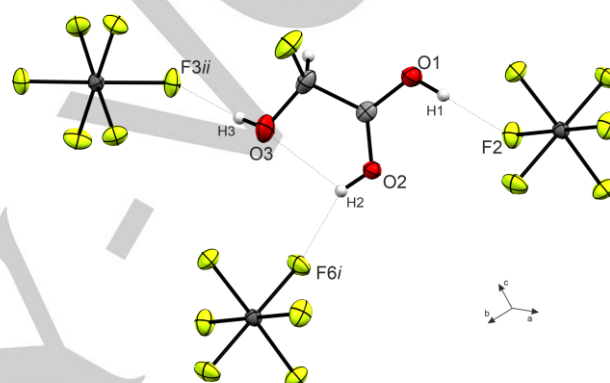
Figure 3. Hydrogen bonds in the crystal packing of **3** (50% probability displacement ellipsoids, hydrogen atoms displayed as spheres of arbitrary radius).

The bond distances of the anion range between 1.698(3) and 1.754(2) Å. As−F bonds involved in donor-acceptor interactions (As1−F2, As1−F2, and As1−F6) are slightly longer than the others, resulting in a distorted octahedral structure. These values have been observed for [AsF₆]⁻ anions in literature.[26],[30],[31]

Theoretical Study

For FHA (**1**), FHA-F (**2**), and the free [FHA-1H]⁺ cation, quantum chemical calculations were performed. The gas-phase structures were optimized and the vibrational frequencies were computed on the B3LYP/aug-cc-pVTZ level of theory. In the case of the cation, a direct comparison to the experimental X-ray values is possible. The bond lengths are listed in Table 4. The calculated structures are illustrated together with the cation of **3** in Figure 4. The labeling of the atoms is based on the crystal structure analysis for consistency.

Figure 4. Optimized gas-phase structures of FHA, FHA-F, [FHA-1H]+, and the cation [FHA-1H]+ of **3**. Calculated on the B3LYP/aug-cc-pVTZ level of theory.

.

Table 4. Calculated bond distances [Å] of FHA, FHA-F, and [FHA-1H]+ compared to the experimental values of **3** obtained from the X-ray structure analysis.

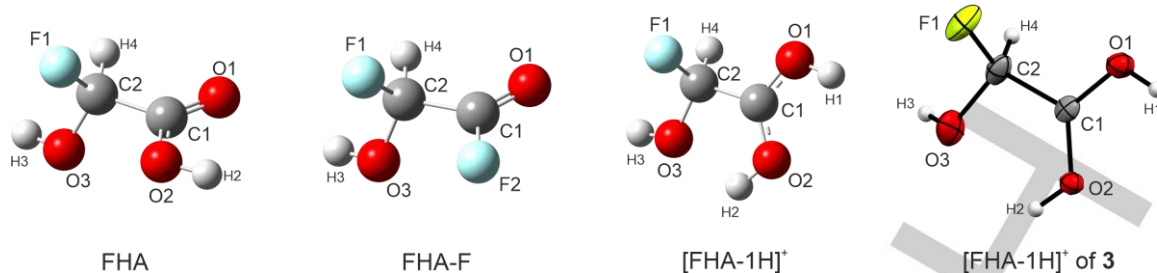|	FHA[a]	FHA-F[a]	[FHA-1H]+[a]	X-ray (3)
C1−O1	1.201	1.180	1.268	1.258(4)
C1−O2/F2	1.338	1.342	1.268	1.272(4)
C1−C2	1.532	1.529	1.538	1.515(5)
C2−O3	1.376	1.373	1.368	1.355(5)
C2−F1	1.392	1.389	1.367	1.376(5)

[a] Calculated on the B3LYP/aug-cc-pVTZ level of theory.

The C−O bond distances of the protonated carboxy group are in fair agreement with the experimental values. For FHA, the values are consistent with comparable carboxylic acids like GAM or difluoroacetic acid.[24,32] The C=O bond length of FHA-F is the shortest among the investigated, yet it is in agreement with the rare structural analyses of gaseous acyl fluorides reported in the literature, as well as the C(O)F bond.[33,34] The C2−O3 distances of all calculated structures (1.368–1.376 Å) are similar, while the X-ray data of **3** is a little shorter. However, all these values are shorter than a regular C−O single bond (1.43 Å).[25] The calculated C2−F1 bond lengths of FHA and FHA-F are longer than in the case of [FHA-1H]+. The bond distances of α-fluoroalcohols compared to a regular C−F (1.36 Å)[25] and C−OH bond have been discussed in a study by Krossing et al. Accordingly, the elongation of the C−F bond is a result of lone-pair conjugation of the oxygen atom into the antibonding σ*(C−F) orbital, subsequently shortening the C−OH bond.[8] This is in agreement with our DFT results, but not to this extent. We performed NBO calculations of all three investigated compounds (MP2/aug-cc-pVTZ level of theory) to assess this effect. The stabilization energies according to the second-order perturbation theory analyses of these interactions are summarized in Table 5.

Table 5. The stabilization energy by the lone-pairs (LP) of the O3 and the F1 atom. NBO calculations on the MP2/aug-cc-pVTZ level of theory.

	LP(O3)→σ*(C2−F1)	LP(F1)→σ*(C1−C2)
FHA	109.3 kJ·mol−1	16.8 kJ·mol−1
FHA-F	111.5 kJ·mol−1	19.3 kJ·mol−1
[FHA-1H]+	105.7 kJ·mol−1	29.0 kJ·mol−1

[a] Calculated on the MP2/aug-cc-pVTZ level of theory.

The interactions of the oxygen lone-pair with the σ*(C−F) orbital are similar among the investigated compounds, explaining the shortening of the C−OH bond. The C−F distance of the neutral compounds FHA and FHA-F is subsequently elongated. In the case of the protonated species, the calculated C−F bond length rather coincides with a regular distance. Since the protonation has no significant influence on the described interaction, there must be another that strengthens the C−F bond. This is found to be the σ-conjugation of a fluorine lone-pair into the σ*(C−C) orbital. The stabilization energy of this interaction in [FHA-1H]+ is calculated to be 12.2 kJ·mol−1 higher than in FHA. This also explains, why the C−C bond of the protonated species is the longest. However, the calculation estimates it longer than the experimental X-ray data shows. Similarly, the C−C bonds of FHA (1.532 Å) and FHA-F (1.529 Å) are longer than expected when compared to the corresponding bonds in difluoroacetic acid and difluoroacetyl fluoride.[34] This indicates that our DFT calculation generally expects these bonds to be longer.

Conclusions

For the first time, α-fluorohydroxyacetic acid (FHA), its acyl fluoride (FHA-F), and its protonated species ([FHA-1H]+) are generated. The syntheses of FHA and FHA-F are achieved by reacting glyoxylic acid monohydrate (GAM) with HF/SF4. By applying the binary superacid HF/AsF5, [FHA-1H][AsF6] is the only organic compound, allowing a complete characterization by NMR, vibrational spectroscopy, and single-crystal X-ray diffraction. The superacidic desoxyfluorination only occurs when three equivalents of Lewis acid are used, implying that the superelectrophile [C2(OH)3H]2+ is formed intermediately. NBO calculations reveal a complex relation between the C−F and the C−OH bond of the fluorohydroxy group. The use of superacids in aHF could enable convenient access to fluorinated compounds with a high electrophilicity and give desoxyfluorination reagents a new appeal.

Experimental Section

Caution! Avoid contact with any of these materials. Hydrogen fluoride will be formed by the hydrolysis of these compounds. HF burns the skin and causes irreparable damage. Safety precautions must be taken when using and handling these materials.

Apparatus and Materials. All reactions were carried out at standard Schlenk conditions by using FEP/PFA reactors closed with a stainless-

steel valve and a stainless-steel vacuum line. All vessels have been dried with fluorine prior to use. Raman spectroscopic analyses were rendered at −196°C with a Bruker MultiRAM FT-Raman spectrometer with an Nd:YAG laser excitation up to 1000 mW (λ = 1064 nm) in a usable range between 50 cm⁻¹ and 4000 cm⁻¹. Low-temperature IR-spectroscopic investigations were carried out with a Bruker Vertex-80V FTIR spectrometer using a cooled cell with a single-crystal CsBr plate on which small amounts of the samples were placed.[35] Single-crystal X-ray structure investigations were carried out with an Oxford Xcalibur3 diffractometer equipped with a Spellman generator (50 kV, 40 mA) and a KappaCCD detector. The measurements were performed with Mo-K_α radiation (λ = 0.71073 Å). For data collection, the software CrysAlis CCD,[36] for data reduction the software CrysAlis RED[37] was used. The solution and refinement were performed with the programs SHELXT[38] and SHELXL[39] implemented in the WinGX software package[40] and checked with the software PLATON. The absorption correction was achieved with the SCALE3 ABSPACK multi-scan method.[41] Quantum chemical calculations were performed with the Gaussian 16[42] program package. Structure optimization and frequency analyses were carried out employing the method B3LYP and the basis sets aug-cc-pVTZ. Natural Bond Orbital (NBO) calculations were performed at the MP2/aug-cc-pVTZ level of theory. For visualization, the program GaussView 6.0[43] was employed. NMR spectra were recorded either on a Jeol ECX400 NMR or a Bruker AV400 NMR instrument. The spectrometers were externally referenced to CFCl₃ for ¹⁹F and to tetramethylsilane for ¹H and ¹³C NMR spectra. For visualization and evaluation, the software MestReNova Version 14.0.0 was used.[44] The spectra were recorded inside 4 mm FEP NMR tube inliners. Acetone-*d6* was employed for external referencing when aHF or SO₂ were used as solvents for the respective compounds. Glyoxylic acid monohydrate (97%, abcr) was stored under a nitrogen atmosphere. SF₄ (abcr) was used as purchased. Arsenic pentafluoride was synthesized from the elements and purified by fractionated distillation.

Deposition number 2173682 ([FHA-1H][AsF₆]) contains the supplementary crystallographic data for this paper. These data are provided free of charge by the joint Cambridge Crystallographic Data Centre and Fachinformationszentrum Karlsruhe Access Structures service.

[1] L. F. Fieser, M. Fieser, *Organische Chemie*, Verl. Chemie, Weinheim/Bergstr., **1972**.

[2] W. A. Sheppard, C. M. Sharts, *Organic fluorine chemistry*, Benjamin, New York, **1969**.

[3] G. A. Olah, A. Pavláth, *Acta. Chim. Acad. Sci. Hung.* **1953**, *3*, 203.

[4] K. Seppelt, *Angew. Chem. Int. Ed. Engl.* **1977**, *16*, 322.

[5] K. O. Christe, J. Hegge, B. Hoge, R. Haiges, *Angew. Chem. Int. Ed. Engl.* **2007**, *46*, 6155.

[6] S. Andreades, D. C. England, *J. Am. Chem. Soc.* **1961**, *83*, 4670.

[7] A. F. Baxter, J. Schaab, K. O. Christe, R. Haiges, *Angew. Chem. Int. Ed. Engl.* **2018**, *57*, 8174.

[8] J. Schaab, M. Schwab, D. Kratzert, J. Schwabedissen, H.-G. Stammler, N. W. Mitzel, I. Krossing, *Chemical communications (Cambridge, England)* **2018**, *54*, 9294.

[9] G. A. Olah, G. D. Mateescu, *J. Am. Chem. Soc.* **1971**, *93*, 781.

[10] A. F. Baxter, J. Schaab, J. Hegge, T. Saal, M. Vasiliu, D. A. Dixon, R. Haiges, K. O. Christe, *Chemistry (Weinheim an der Bergstrasse, Germany)* **2018**, *24*, 16737.

[11] R. Minkwitz, S. Reinemann, *Z. Anorg. Allg. Chem.* **1999**, *625*, 121.

[12] G. S. Prakash, F. Paknia, A. Kulkarni, A. Narayanan, F. Wang, G. Rasul, T. Mathew, G. A. Olah, *J. Fluorine Chem.* **2015**, *171*, 102.

[13] W. R. Hasek, W. C. Smith, V. A. Engelhardt, *J. Am. Chem. Soc.* **1960**, *82*, 543.

[14] J. Kollonitsch, S. Marburg, L. Perkins, *J. Org. Chem.* **1975**, *40*, 3808.

[15] D. G. Martin, F. Kagan, *J. Org. Chem.* **1962**, *27*, 3164.

[16] T. V. Oommen, B. Gotthardt, T. R. Hooper, *Inorg. Chem.* **1971**, *10*, 1632.

[17] A. Nitzer, M. Regnat, C. Jessen, A. J. Kornath, *Eur. J. Org. Chem.* **2022**, *2022*.

[18] J. R. Durig, G. A. Guirgis, T. A. Mohamed, *J. Mol. Struct.* **1998**, *444*, 165.

[19] J. R. Durig, W. Zhao, D. Lewis, T. S. Little, *The Journal of Chemical Physics* **1988**, *89*, 1285.

[20] J. R. Durig, M. M. Bergana, H. V. Phan, *J. Raman Spectrosc.* **1991**, *22*, 141.

[21] K. L. Plath, J. L. Axson, G. C. Nelson, K. Takahashi, R. T. Skodje, V. Vaidaa, *React Kinet Catal Lett* **2009**, *96*, 209.

[22] C. Jessen, A. J. Kornath, *Eur. J. Inorg. Chem.* **2022**, *2022*.

[23] A. Virmani, M. Pfeiffer, C. Jessen, Y. Morgenstern, A. J. Kornath, *Z. Anorg. Allg. Chem.* **2022**.

[24] T. Lis, *Acta Crystallogr C Cryst Struct Commun* **1983**, *39*, 1082.

[25] E. Wiberg, N. Wiberg, G. Fischer, *Lehrbuch der anorganischen Chemie*, Walter de Gruyter, Berlin, New York, **2007**.

[26] M. Schickinger, T. Saal, F. Zischka, J. Axhausen, K. Stierstorfer, Y. Morgenstern, A. J. Kornath, *ChemistrySelect* **2018**, *3*, 12396.

[27] F. H. Allen, D. G. Watson, L. Brammer, A. G. Orpen, R. Taylor in *International Tables for Crystallography* (Eds.: E. Prince, H. Fuess, T. Hahn, H. Wondratschek, U. Müller, U. Shmueli, A. Authier, V. Kopský, D. B. Litvin, M. G. Rossmann et al.), International Union of Crystallography, Chester, England, **2006**, pp. 790–811.

[28] G. A. Jeffrey, *An introduction to hydrogen bonding*, Oxford Univ. Press, New York, **1997**.

[29] A. Bondi, *J. Phys. Chem.* **1964**, *68*, 441.

[30] R. Minkwitz, F. Neikes, U. Lohmann, *Eur. J. Inorg. Chem.* **2002**, *2002*, 27.

[31] D. Mootz, M. Wiebcke, *Inorg. Chem.* **1986**, *25*, 3095.

[32] J. Bijen, J. L. Derissen, *J. Mol. Struct.* **1975**, *27*, 233.

[33] Y. Berrueta Martínez, C. G. Reuter, Y. V. Vishnevskiy, Y. B. Bava, A. L. Picone, R. M. Romano, H.-G. Stammler, B. Neumann, N. W. Mitzel, C. O. Della Védova, *J. Phys. Chem. A* **2016**, *120*, 2420.

[34] B. P. van Eijck, P. Brandts, J. Maas, *J. Mol. Struct.* **1978**, *44*, 1.

[35] L. Bayersdorfer, R. Minkwitz, J. Jander, *Z. Anorg. Allg. Chem.* **1972**, *392*, 137.

[36] CrysAlisCCD, *Version 1.171.35.11 (release 16-05-2011 CrysAlis 171.NET)*, Oxford Diffraction Ltd, UK, **2011**.

[37] CrysAlisRED, *Version 1.171.35.11 (release 16-05-2011 CrysAlis 171.NET)*, Oxford Diffraction Ltd, UK, **2011**.

[38] G. M. Sheldrick, *Acta crystallographica. Section A, Foundations and advances* **2015**, *71*, 3.

[39] G. M. Sheldrick, *Acta crystallographica. Section C, Structural chemistry* **2015**, *71*, 3.

[40] L. J. Farrugia, *J. Appl. Crystallogr.* **1999**, *32*, 837.

[41] SCALE3 ABSPACK, *An Oxford Diffraction Program*, Oxford Diffraction Ltd, UK, **2005**.

[42] M. J. Frisch, G. W. Trucks, H. B. Schlegel, G. E. Scuseria, M. A. Robb, J. R. Cheeseman, G. Scalmani, V. Barone, G. A. Petersson, H. Nakatsuji et al., *Gaussian 16 Rev. C.01*, Wallingford, CT, **2016**.

[43] Roy Dennington, Todd A. Keith, John M. Millam, *GaussView 6*, Semichem Inc., Shawnee Mission KS, **2019**.

[44] Mestrelab Research S.L., *MestReNova*, Santiago de Compostela, Spain, **2019**.

Entry for the Table of Contents (Please choose one layout)

Layout 1:

FULL PAPER

α-Fluoroalcohols are usually synthesized by reacting an electrophilic carbonyl compound with HF. But what if the electrophilicity is so high that water is already bound to the carbonyl group? In this study, derivatives of α-fluorohydroxyacetic acid are generated from glyoxylic acid monohydrate with SF_4 and the binary superacid HF/AsF_5, showing a new side of the system HF/AsF_5 that gives both superacid and desoxyfluorination chemistry a new appeal.
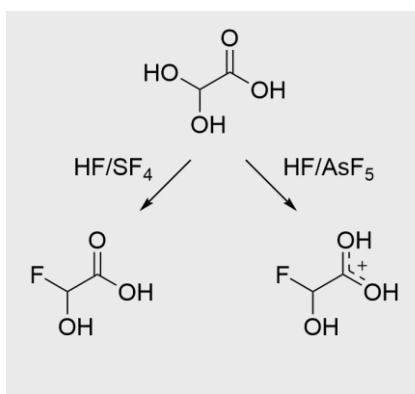
Alan Virmani, Christoph Jessen, Alexander Nitzer, and Andreas J. Kornath*

Page No. – Page No.

Desoxyfluorination with Superacids – Synthesis and Characterization of Protonated α-Fluorohydroxyacetic Acid

Desoxyfluorination with Superacids – Synthesis and Characterization of Protonated α-Fluorohydroxyacetic Acid

Alan Virmani, Christoph Jessen, Alexander Nitzer, and Andreas J. Kornath*

Abstract: α-Fluoroalcohols describe a rare and unstable class of compounds, accessible mainly by fluorination of highly electrophilic carbonyl compounds. In this work, we report the syntheses of α-fluorohydroxyacetic acid (FHA) and its acyl fluoride (FHA-F) by reacting the dihydroxy species glyoxylic acid monohydrate (GAM) with SF_4. Surprisingly, only one of the geminal hydroxy groups is substituted when excess SF_4 is employed. Implementing GAM with the binary superacid HF/AsF_5 also leads to a single yet quantitative desoxyfluorination at the diol group. The reaction pathways are elucidated by NMR experiments, the characterization was carried out using NMR and vibrational spectroscopy as well as single-crystal X-ray diffraction.

Table of Contents

SUPPORTING INFORMATION

List of Figures

SUPPORTING INFORMATION

List of Tables

Experimental Procedures

Caution! Avoid contact with any of these materials. Hydrogen fluoride will be formed by the hydrolysis of these compounds. HF burns the skin and causes irreparable damage. Safety precautions should be taken when using and handling these materials.

Apparatus and Materials

All reactions were carried out at standard Schlenk conditions by using sealed 6 mm FEP/PFA reactors closed with a stainless-steel valve and a stainless-steel vacuum line. All vessels have been dried with fluorine prior to each reaction or NMR measurement. Glyoxylic acid monohydrate (abcr) was stored under a nitrogen atmosphere. SF$_4$ (abcr) was used as purchased. Arsenic pentafluoride was synthesized from the elements and purified by fractionated distillation.

Raman spectra were rendered with a Bruker MultiRAM FT-Raman spectrometer with an Nd:YAG laser excitation up to 1000 mW (λ = 1064 nm) in a usable range between 200 cm^{-1} and 4000 cm^{-1}. A measurement was performed after transferring the sample into a cooled (−196°C) glass cell under a nitrogen atmosphere and subsequent evacuation of the glass cell.

Low-temperature IR-spectroscopic investigations were carried out with a Bruker Vertex-80V FTIR spectrometer using a cooled cell with a single-crystal CsBr plate on which small amounts of the samples were placed.[1]

Single-crystal X-ray structure investigations were carried out with an Oxford Xcalibur3 diffractometer equipped with a Spellman generator (50 kV, 40 mA) and a KappaCCD detector. The measurements were performed with Mo-K_α radiation (λ = 0.71073 Å). For data collection, the software CrysAlis CCD,[2] for data reduction the software CrysAlis RED[3] was used. The solution and refinement were performed with the programs SHELXT[4] and SHELXL-97[5] implemented in the WinGX software package[6] and checked with the software PLATON.[7] The absorption correction was achieved with the SCALE3 ABSPACK multi-scan method.[8]

Quantum chemical calculations were performed with the Gaussian 16[9] program package. Calculations were carried out employing the method B3LYP and the basis sets aug-cc-pVTZ. For visualization of the structures and vibrational modes, the program GaussView 6.0[10] was employed.

NMR spectra were recorded either on a Jeol ECX400 NMR or a Bruker AV400 NMR instrument. For visualization and evaluation, the software MestReNova Version 14.0.0 was used.[11] The spectrometers were externally referenced to CFCl$_3$ for ^{19}F and to tetramethylsilane for ^{1}H and ^{13}C NMR spectra. NMR measurements were prepared by dissolving the sample in aHF or SO$_2$ at the respective temperature and subsequently transferring the solution under a nitrogen atmosphere into a sealed 4 mm FEP tube at −78°C. After cooling down to −196°C the FEP tube was flame-sealed *in vacuo*. Immediately before the NMR measurement, the sealed FEP tube was put in a standard glass NMR tube loaded with 0.2 mL acetone-d$_6$ as an external reference and warmed to the designated temperature.

SUPPORTING INFORMATION

Synthesis of α-Fluorohydroxyacetic Acid

First, the FEP reactor was dried chemically with F_2. Sulfur tetrafluoride (108 mg, 1.00 mmol) and anhydrous hydrogen fluoride (approximately 0.5 mL) were then successively condensed into the reactions vessel at −196°C and agitated at −40°C. After cooling down to −196°C, glyoxylic acid monohydrate (92.05 mg, 1.00 mmol) was added under a nitrogen atmosphere and dissolved at −40°C. Volatile by-products and excess hydrogen fluoride were removed under a dynamic vacuum at −78°C overnight, leaving a colorless, amorphous glass-like residue.

Synthesis of α-Fluorohydroxyacetic Fluoride

First, the FEP reactor was dried chemically with F_2. Sulfur tetrafluoride (216 mg, 2.00 mmol) and anhydrous hydrogen fluoride (approximately 0.5 mL) were then successively condensed into the reactions vessel at −196°C and agitated at −40°C. After cooling down to −196°C, glyoxylic acid monohydrate (92.05 mg, 1.00 mmol) was added under a nitrogen atmosphere and dissolved at −40°C. Volatile by-products and excess hydrogen fluoride were removed under a dynamic vacuum at −78°C overnight, leaving a colorless, amorphous glass-like residue.

Synthesis of Protonated α-Fluorohydroxyacetic Acid

For the synthesis of protonated a-fluorohydroxyacetic acid, arsenic pentafluoride (510 mg, 3.00 mmol) (**3**) was condensed into a reactor (FEP tube), followed by excess anhydrous hydrogen fluoride (aHF) at −196°C. The mixture was warmed up to 0°C to form the superacidic medium. After cooling it down to −196°C again, glyoxylic acid monohydrate (92 mg, 1.00 mmol) was added and subsequently dissolved at −45°C. After warming up to 0°C, the mixture was agitated again and dried overnight at −78°C under a dynamic vacuum, leaving a colorless powder.

Results and Discussion

NMR Spectroscopy

Glyoxylic Acid Monohydrate (GAM) in D_2O

^{1}H NMR (400 MHz, Deuterium Oxide) δ [ppm] = 5.35 (s, 1H).
^{13}C NMR (101 MHz, Deuterium Oxide) δ [ppm] = 173.17, 86.14.

SUPPORTING INFORMATION

	Parameter	Value
1	Origin	Bruker BioSpin GmbH
2	Instrument	AV400
3	Solvent	D2O
4	Temperature	299.1
5	Experiment	1D
6	Number of Scans	16
7	Receiver Gain	210.4
8	Relaxation Delay	4.0000
9	Pulse Width	10.6000
10	Acquisition Time	6.5536
11	Acquisition Date	2022-04-27T19:48:03
12	Spectrometer Frequency	400.18
13	Spectral Width	10000.0
14	Nucleus	1H
15	Acquired Size	65536
16	Spectral Size	131072

Figure S1. ^{1}H NMR spectrum of GAM in D$_2$O at room temperature.

	Parameter	Value
1	Origin	Bruker BioSpin GmbH
2	Instrument	AV400
3	Solvent	D2O
4	Temperature	299.2
5	Experiment	1D
6	Number of Scans	2048
7	Receiver Gain	210.4
8	Relaxation Delay	0.5000
9	Pulse Width	9.3000
10	Acquisition Time	1.2976
11	Acquisition Date	2022-04-27T20:51:53
12	Spectrometer Frequency	100.64
13	Spectral Width	25252.5
14	Nucleus	13C
15	Acquired Size	32768
16	Spectral Size	65536

Figure S2. ^{13}C NMR spectrum of GAM in D$_2$O at room temperature.

Glyoxylic Acid Monohydrate (GAM) dissolved in aHF

¹H NMR (400 MHz, aHF) δ [ppm] = 5.96 (d, *J* = 6.0 Hz), 5.87 (d, *J* = 8.1 Hz), 5.78 (s), 5.72 (s), 5.63 (d, *J* = 5.6 Hz), 5.57 (s), 5.50 (s).
¹⁹F NMR (376 MHz, aHF) δ [ppm] = −129.63 (dd, *J* = 58.5, 22.3 Hz), −134.85 (d, *J* = 61.6 Hz).
¹³C NMR (101 MHz, aHF) δ [ppm] = 171.57 (d, *J* = 32.6 Hz), 169.11, 168.48, 168.32, 100.43 (d, *J* = 65.2 Hz), 99.11, 98.70, 98.07 (d, *J* = 64.8 Hz), 96.88.

	Parameter	Value
1	Origin	JEOL
2	Solvent	aHF
3	Temperature	0.0
4	Experiment	1D
5	Receiver Gain	16.0
6	Relaxation Delay	4.0000
7	Pulse Width	5.7000
8	Acquisition Time	2.6214
9	Acquisition Date	2022-04-21T09:08:56
10	Spectrometer Frequency	399.78
11	Spectral Width	10000.0
12	Lowest Frequency	-1991.3
13	Nucleus	1H
14	Acquired Size	32768
15	Spectral Size	104858
16	Digital Resolution	0.10

Figure S3. ¹H NMR spectrum of GAM in aHF at 0°C.

	Parameter	Value
1	Origin	JEOL
2	Solvent	aHF
3	Temperature	0.0
4	Experiment	1D
5	Receiver Gain	16.0
6	Relaxation Delay	4.0000
7	Pulse Width	5.3500
8	Acquisition Time	0.2176
9	Acquisition Date	2022-04-21T09:14:45
10	Spectrometer Frequency	376.17
11	Spectral Width	301204.8
12	Lowest Frequency	-150602.4
13	Nucleus	19F
14	Acquired Size	65536
15	Spectral Size	131072
16	Digital Resolution	2.30

Figure S4. ^{19}F NMR spectrum of GAM in aHF at 0°C.

	Parameter	Value
1	Origin	JEOL
2	Solvent	aHF
3	Temperature	0.0
4	Experiment	1D
5	Receiver Gain	58.0
6	Relaxation Delay	1.0000
7	Pulse Width	2.6667
8	Acquisition Time	0.8651
9	Acquisition Date	2022-04-21T14:27:19
10	Spectrometer Frequency	100.53
11	Spectral Width	30303.0
12	Lowest Frequency	-5024.2
13	Nucleus	13C
14	Acquired Size	32768
15	Spectral Size	52430
16	Digital Resolution	0.58

Figure S5. ^{13}C NMR spectrum of GAM in aHF at 0°C.

8

2,2-Fluorohydroxyacetic Acid (1)
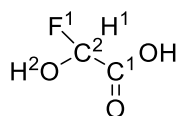
¹H NMR (400 MHz, aHF) δ [ppm] = 5.57 (d, *J* = 54.4 Hz, H1), 3.30 (s, br, H2).
¹⁹F NMR (376 MHz, aHF) δ [ppm] = −130.38 (d, *J* = 54.2 Hz, F1).
¹³C NMR (101 MHz, aHF) δ [ppm] = 170.98 (d, *J* = 32.7 Hz, C1), 96.95 (d, *J* = 225.1 Hz, C2).

	Parameter	Value
1	Title	an26
2	Origin	JEOL
3	Instrument	ECX400
4	Solvent	aHF
5	Temperature	-40.9
6	Experiment	1D
7	Number of Scans	16
8	Receiver Gain	14.0
9	Relaxation Delay	4.0000
10	Pulse Width	5.7000
11	Acquisition Time	2.6214
12	Acquisition Date	2020-10-23T10:52:49
13	Spectrometer Frequency	399.78
14	Spectral Width	10000.0
15	Nucleus	1H
16	Acquired Size	32768
17	Spectral Size	104858

Figure S6. ¹H NMR spectrum of GAM with equimolar amounts of SF₄ in aHF at −40°C.

	Parameter	Value
1	Title	an26
2	Origin	JEOL
3	Instrument	ECX400
4	Solvent	aHF
5	Temperature	-41.0
6	Experiment	1D
7	Number of Scans	64
8	Receiver Gain	14.0
9	Relaxation Delay	4.0000
10	Pulse Width	5.3500
11	Acquisition Time	0.2176
12	Acquisition Date	2020-10-23T10:59:17
13	Spectrometer Frequency	376.17
14	Spectral Width	301204.8
15	Nucleus	19F
16	Acquired Size	65536
17	Spectral Size	131072

Figure S7. ^{19}F NMR spectrum of GAM with equimolar amounts of SF_4 in aHF at −40°C.

	Parameter	Value
1	Origin	JEOL
2	Solvent	aHF
3	Temperature	-39.6
4	Experiment	1D
5	Receiver Gain	56.0
6	Relaxation Delay	1.0000
7	Pulse Width	2.6667
8	Acquisition Time	0.8651
9	Acquisition Date	2020-10-23T13:55:56
10	Spectrometer Frequency	100.53
11	Spectral Width	30303.0
12	Lowest Frequency	-5101.7
13	Nucleus	13C
14	Acquired Size	32768
15	Spectral Size	52430
16	Digital Resolution	0.58

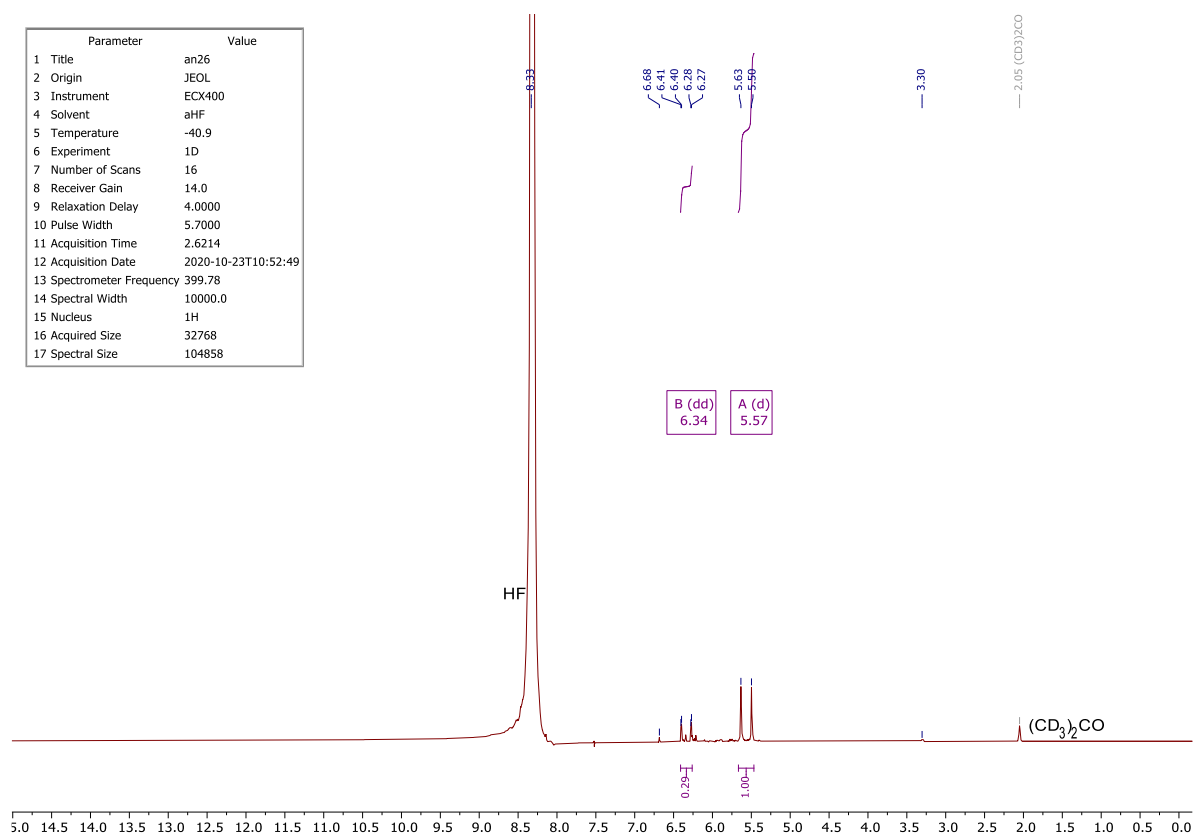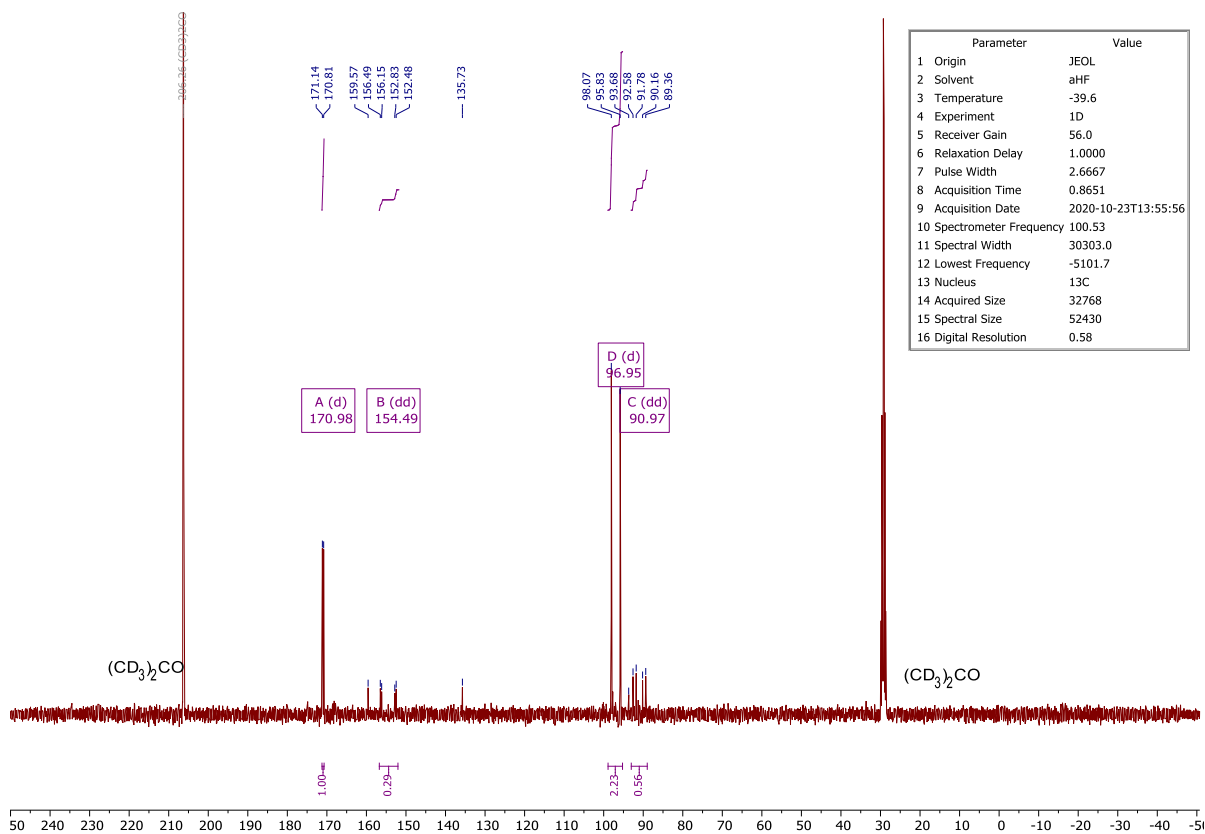**Figure S8.** ^{13}C NMR spectrum of GAM with equimolar amounts of SF_4 in aHF at −40°C.

SUPPORTING INFORMATION

*2,2-Fluorohydroxyacetyl Fluoride (**2**)*
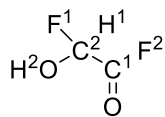
¹H NMR (400 MHz, SO₂) δ [ppm] = 7.00 (d, *J* = 51.2 Hz, H1).
¹⁹F NMR (376 MHz, SO₂) δ [ppm] = 23.63 (d, *J* = 16.3 Hz), 22.97 (d, *J* = 14.1 Hz, F2), −134.67 (d, *J* = 53.7 Hz F1).
¹³C NMR (101 MHz, SO₂) δ [ppm] = 154.33 (dd, *J* = 368.7 Hz, 34.8 Hz, C1), 92.59 (dd, *J* = 241.3 Hz, 82.4 Hz, C2).

2 is generated by dissolving a twofold amount of SF₄ (with respect to GAM) in aHF and successively adding GAM at −40°C. After removing all volatile products like SOF₂ and the solvent overnight, the residue was redissolved in aHF. ¹H, ¹⁹F, and ¹³C NMR spectra (Figure S9, Figure **S10**, and Figure **S11**) were measured at −40°C. The ¹⁹F NMR spectrum indicates an HF addition to **2**, illustrated in Equation S1.
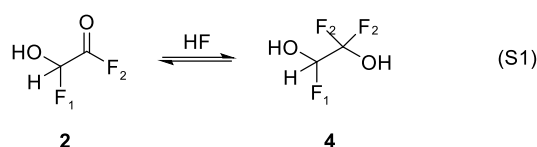
The signal at −138.79 ppm with a dt-splitting pattern (²*J*$_{HF}$ = 53.7 Hz, ³*J*$_{FF}$ = 9.35 Hz) is assigned to the F1 atom of the HF-adduct (**5**). The triplet coupling was calculated manually. The ¹⁹F signal of the F2 atom occurs at −83.46 ppm and is consistent with reported perfluorinated alcohols.[12] The respective proton signal is observed at 6.28 ppm with a dd-splitting pattern (²*J*$_{HF}$ = 51.0 Hz, ³*J*$_{HF}$ = 3.7 Hz). The ¹³C resonance of the CHF(OH) group is noticed at 91.31 ppm (dd, *¹J*$_{CF}$ = 242.9 Hz, ²*J*$_{CF}$ = 80.2 Hz). The equilibrium displayed in Equation S1 is shifted to **2** by removing the solvent, successively warming the residue up to 0°C, and trapping the gas phase into a second vessel at −196°C. The condensate was dissolved in SO₂, and NMR spectra (Figure S12, Figure S13, and Figure S14) show **2** as the only organic compound.

	Parameter	Value
1	Origin	Bruker BioSpin GmbH
2	Instrument	AV400TR
3	Solvent	aHF
4	Temperature	233.3
5	Experiment	1D
6	Number of Scans	16
7	Receiver Gain	18.2
8	Relaxation Delay	4.0000
9	Pulse Width	11.8500
10	Acquisition Time	6.5012
11	Acquisition Date	2020-11-12T09:03:02
12	Spectrometer Frequency	400.13
13	Spectral Width	10080.6
14	Nucleus	1H
15	Acquired Size	65536
16	Spectral Size	131072

Figure S9. ¹H NMR spectrum of GAM with a twofold amount of SF₄ in aHF at −40°C.

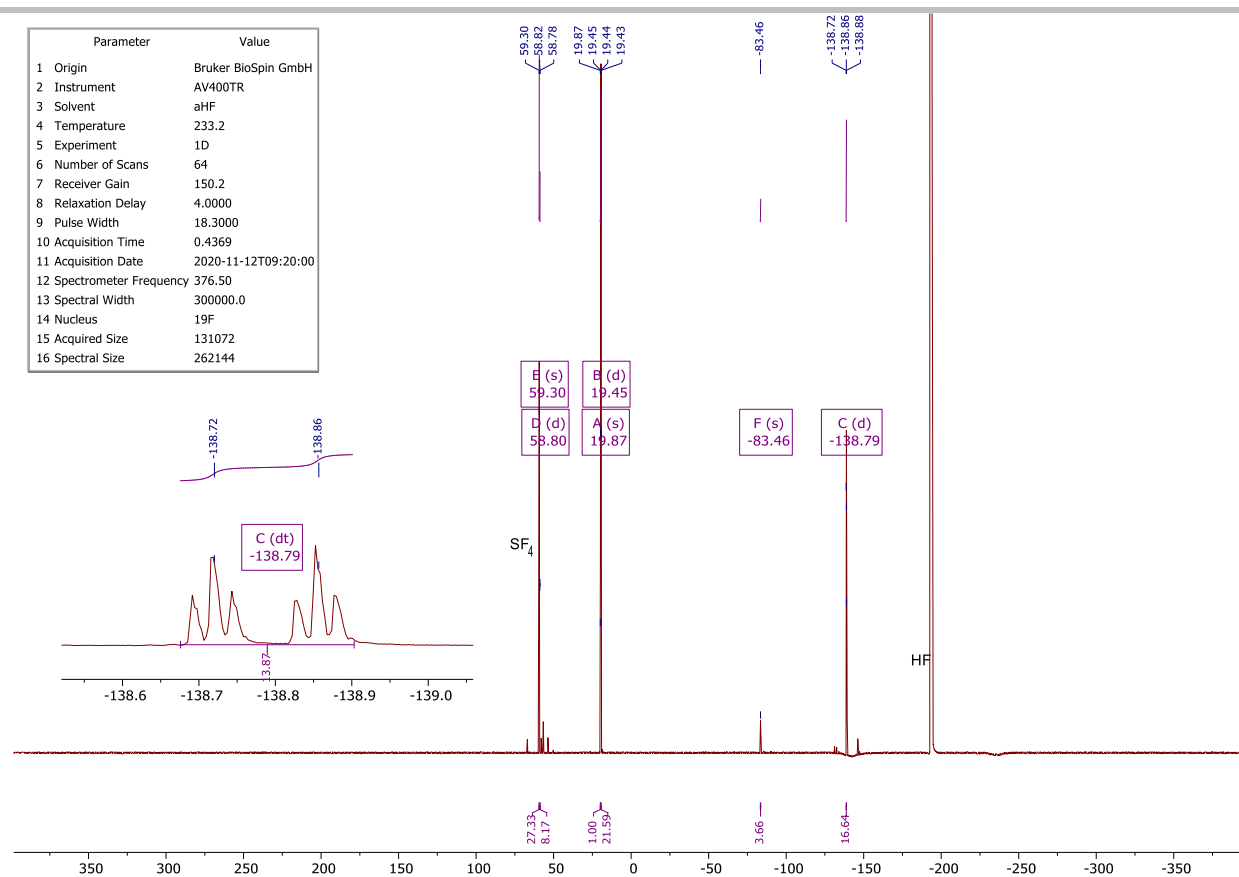|	Parameter	Value
1	Origin	Bruker BioSpin GmbH
2	Instrument	AV400TR
3	Solvent	aHF
4	Temperature	233.2
5	Experiment	1D
6	Number of Scans	64
7	Receiver Gain	150.2
8	Relaxation Delay	4.0000
9	Pulse Width	18.3000
10	Acquisition Time	0.4369
11	Acquisition Date	2020-11-12T09:20:00
12	Spectrometer Frequency	376.50
13	Spectral Width	300000.0
14	Nucleus	19F
15	Acquired Size	131072
16	Spectral Size	262144

Figure S10. ^{19}F NMR spectrum of GAM with a twofold amount of SF$_4$ in aHF at −40°C.

	Parameter	Value
1	Origin	Bruker BioSpin GmbH
2	Instrument	AV400TR
3	Solvent	aHF
4	Temperature	233.2
5	Experiment	1D
6	Number of Scans	2048
7	Receiver Gain	211.4
8	Relaxation Delay	0.5000
9	Pulse Width	10.0000
10	Acquisition Time	1.1010
11	Acquisition Date	2020-11-12T09:32:00
12	Spectrometer Frequency	100.62
13	Spectral Width	29761.9
14	Nucleus	13C
15	Acquired Size	32768
16	Spectral Size	65536
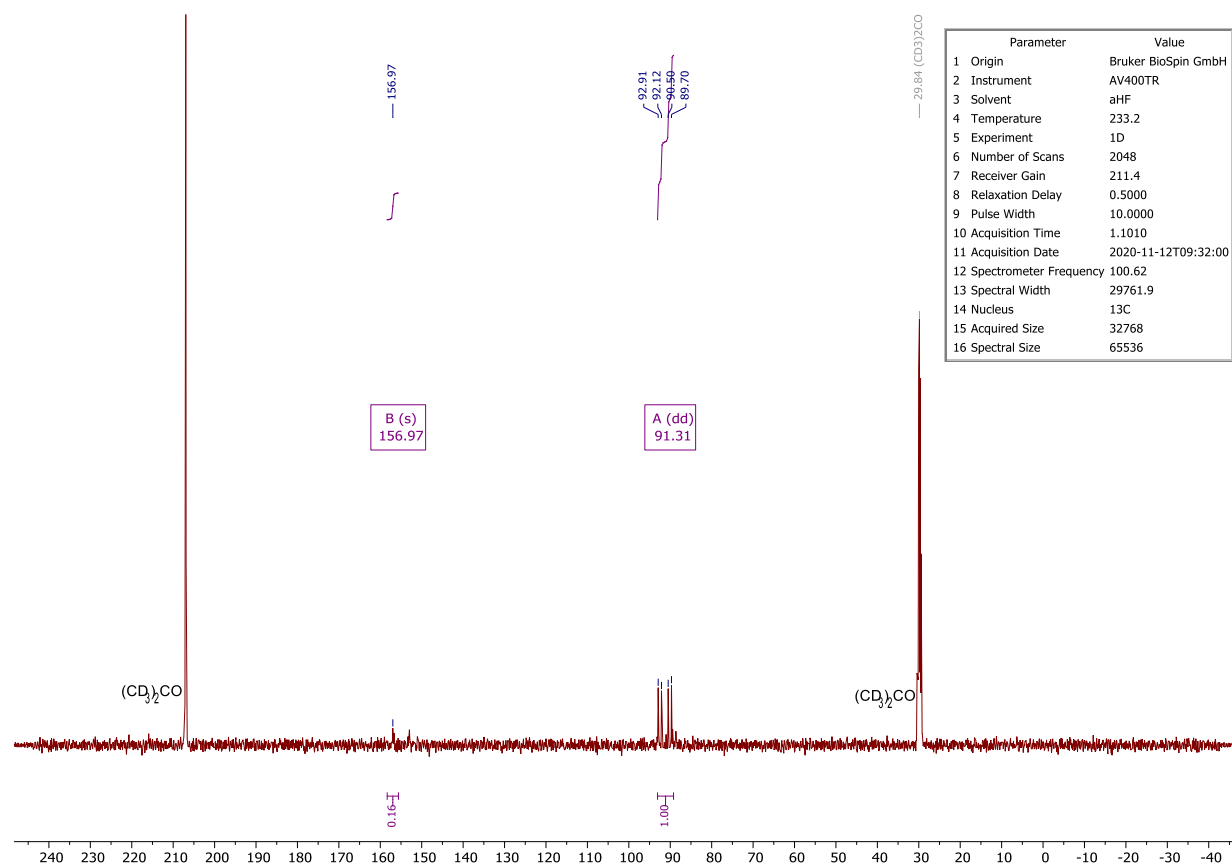
Figure S11. ^{13}C NMR spectrum of GAM with a twofold amount of SF$_4$ in aHF at −40°C.

	Parameter	Value
1	Origin	JEOL
2	Solvent	SO_2
3	Temperature	-40.0
4	Experiment	1D
5	Receiver Gain	36.0
6	Relaxation Delay	4.0000
7	Pulse Width	5.7000
8	Acquisition Time	3.6386
9	Acquisition Date	2020-12-09T08:45:34
10	Spectrometer Frequency	399.78
11	Spectral Width	7204.6
12	Lowest Frequency	-1195.6
13	Nucleus	1H
14	Acquired Size	32768
15	Spectral Size	52430
16	Digital Resolution	0.14

Figure S12. ^1H NMR spectrum of **2** in SO_2 at −40°C.

	Parameter	Value
1	Origin	JEOL
2	Solvent	SO_2
3	Temperature	-40.0
4	Experiment	1D
5	Receiver Gain	16.0
6	Relaxation Delay	4.0000
7	Pulse Width	5.3500
8	Acquisition Time	0.2176
9	Acquisition Date	2020-12-09T08:52:03
10	Spectrometer Frequency	376.17
11	Spectral Width	301204.8
12	Lowest Frequency	-150602.4
13	Nucleus	19F
14	Acquired Size	65536
15	Spectral Size	131072
16	Digital Resolution	2.30

Figure S13. ^{19}F NMR spectrum of **2** in SO_2 at −40°C.
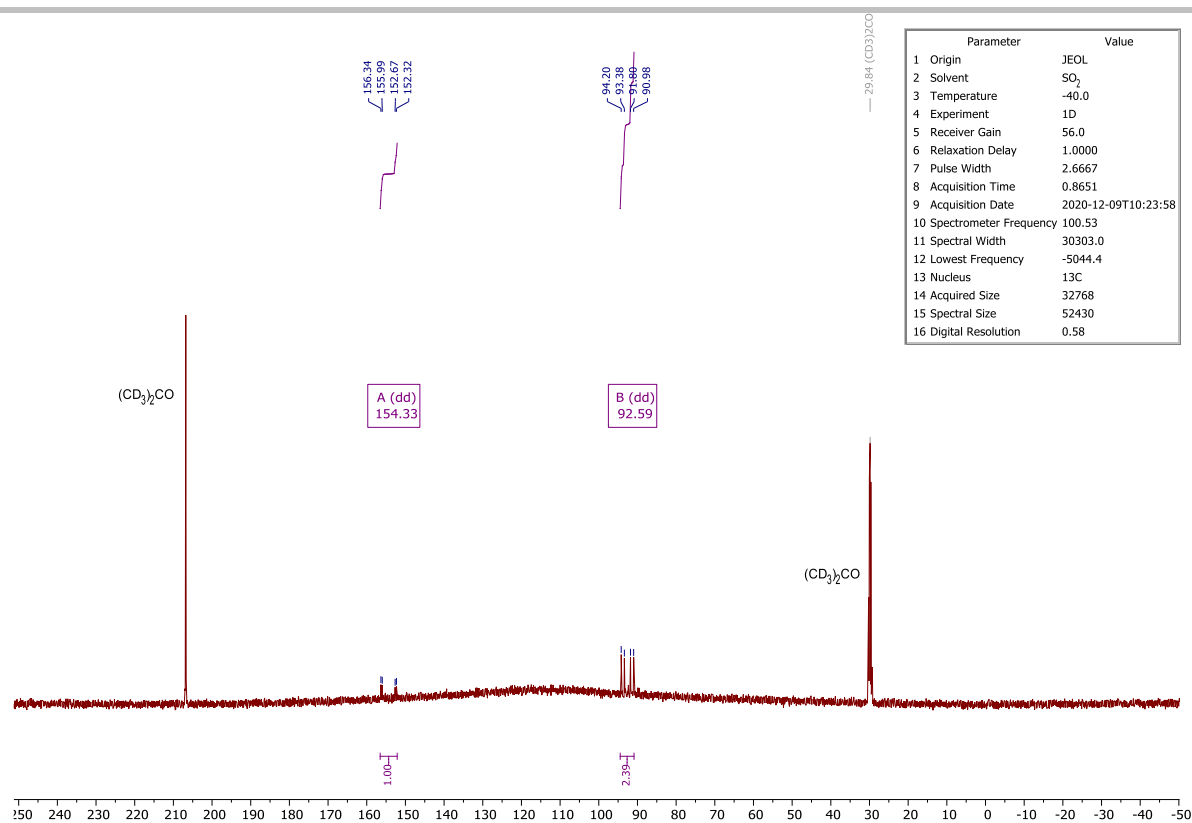
Figure S14. ^{13}C NMR spectrum of **2** in SO$_2$ at −40°C.

Protonated α-Fluorohydroxyacetic Acid [FHA-1H][AsF$_6$] (3)
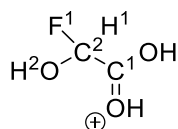
^{1}H NMR (400 MHz, aHF): δ [ppm] = 5.61 (d, J = 54.9 Hz; $^2J_{HF}$, H1).
^{19}F NMR (376 MHz, aHF): δ [ppm] = −128.88 (d, J = 53.9 Hz; $^2J_{HF}$, F1).
^{13}C NMR (101 MHz, aHF): δ [ppm] = 184.90 (d, J = 34.0 Hz; $^2J_{CF}$, C1), 97.00 (d, J = 227.1 Hz; $^1J_{CF}$, C2).

	Parameter	Value
1	Origin	JEOL
2	Solvent	aHF
3	Temperature	-40.0
4	Experiment	1D
5	Receiver Gain	16.0
6	Relaxation Delay	4.0000
7	Pulse Width	5.7000
8	Acquisition Time	3.6386
9	Acquisition Date	2020-01-22T08:41:13
10	Spectrometer Frequency	399.78
11	Spectral Width	7204.6
12	Lowest Frequency	-1195.7
13	Nucleus	1H
14	Acquired Size	32768
15	Spectral Size	52430
16	Digital Resolution	0.14
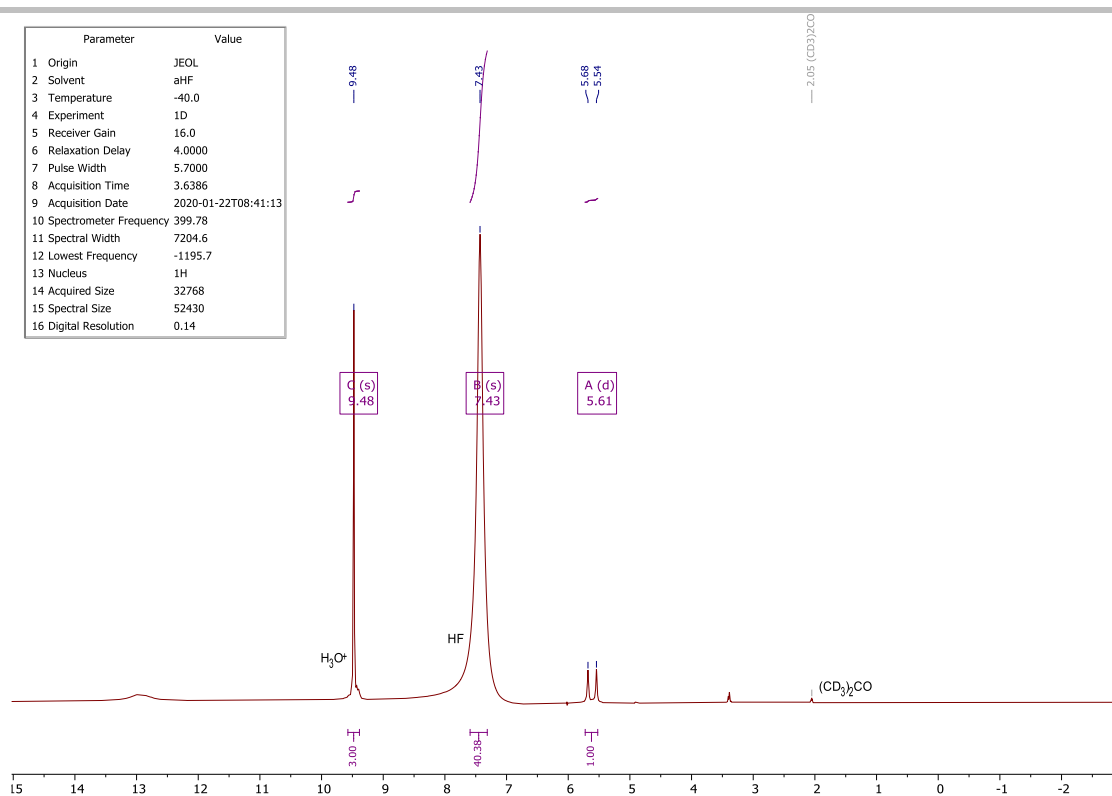
Figure S15. ^{1}H NMR spectrum of **3** in aHF at −40°C.

	Parameter	Value
1	Origin	JEOL
2	Solvent	aHF
3	Temperature	-40.0
4	Experiment	1D
5	Receiver Gain	12.0
6	Relaxation Delay	4.0000
7	Pulse Width	5.3500
8	Acquisition Time	0.2176
9	Acquisition Date	2020-01-22T08:48:36
10	Spectrometer Frequency	376.17
11	Spectral Width	301204.8
12	Lowest Frequency	-150602.4
13	Nucleus	19F
14	Acquired Size	65536
15	Spectral Size	131072
16	Digital Resolution	2.30

Figure S16. ^{19}F NMR spectrum of **3** in aHF at −40°C.

15
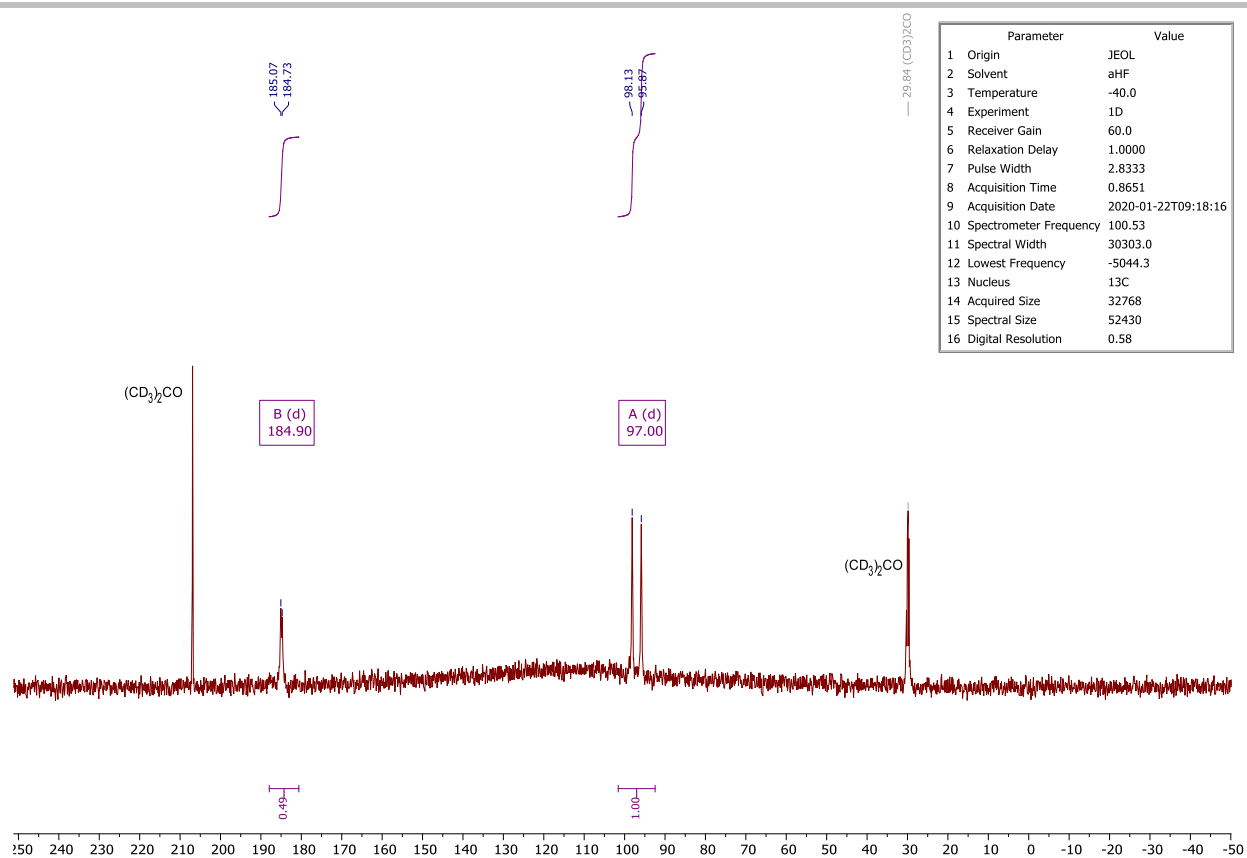
Figure S17. ^{13}C NMR spectrum of **3** in aHF at −40°C.

	Parameter	Value
1	Origin	JEOL
2	Solvent	aHF
3	Temperature	-40.0
4	Experiment	1D
5	Receiver Gain	60.0
6	Relaxation Delay	1.0000
7	Pulse Width	2.8333
8	Acquisition Time	0.8651
9	Acquisition Date	2020-01-22T09:18:16
10	Spectrometer Frequency	100.53
11	Spectral Width	30303.0
12	Lowest Frequency	-5044.3
13	Nucleus	13C
14	Acquired Size	32768
15	Spectral Size	52430
16	Digital Resolution	0.58

Vibrational Spectroscopy

Table S1. Experimental vibrational frequencies [cm^{-1}] of [FHA-1H][AsF$_6$] (**3**) and calculated frequencies of [FHA-1H]$^+$ (B3LYP/aug-cc-pVTZ level of theory).

[FHA-1H][AsF$_6$]		[FHA-1H]$^+$	
IR (exp.)[a]	Raman (exp.)[a]	$\tilde{\nu}$ (IR/Ra) (calc.)[b],[c]	Assignment
		3769 (212/82)	ν(OH)
		3615 (256/84)	ν(OH)
		3484 (336/31)	ν(OH)
	3127 (6)		
	3013 (11)	3067 (5/70)	ν(CH)
1705 (m)		1685 (268/1)	ν_{as}(CO)
	1623 (4)		
1541 (m)	1567 (7)	1567 (169/4)	ν_s(CO)
1412 (m)	1407 (2)	1422 (74/1)	ω(CH)
1362 (m)	1335 (7)	1354 (10/3)	δ(CCH)
1225 (m)	1247 (3)	1241 (198/6)	δ(COH)
	1206 (2)	1193 (33/4)	δ(COH)
1165 (m)	1185 (10)	1189 (175/2)	δ(FCH)
1151 (m)	1162 (3)	1154 (102/1)	ν(CO)
1022 (m)	1027 (4)	1066 (146/5)	ν(CF)
1007 (m)			
897 (m)	903 (8)	883 (27/4)	ν(CC)
854 (m)			
814 (m)		798 (25/0)	γ(OH)
764 (m)	747 (14)	760 (123/4)	δ(CCO$_2$)
696 (s)		693 (116/2)	δ(CCO)
		608 (5/1)	δ(CCO)
552 (m)		549 (49/1)	δ(COC)
	469 (13)	440 (0/1)	δ(CCO)
		324 (117/1)	γ(OH)
		303 (61/0)	δ(CCO)
		238 (1/1)	δ(CCF)
		58 (3/1)	τ(CC)
	711 (97)		[AsF$_6$]$^-$
675 (m)	676 (100)		[AsF$_6$]$^-$
	566 (31)		[AsF$_6$]$^-$
	369 (68)		[AsF$_6$]$^-$

[a] Abbreviations for IR intensities: s = strong, m = medium. Experimental Raman intensities are relative to a scale of 1 to 100.
[b] Calculated on the B3LYP/aug-cc-pVTZ level of theory. [c] IR intensities in km/mol; Raman intensities in Å^4/u.

Table S2. Experimental and calculated IR frequencies [cm^{-1}] of FHA-F (**2**). Calculated on the B3LYP/aug-cc-pVTZ level of theory.

FHA-F (exp.)[a]	FHA-F (calc.)[b],[c]	Assignment
	3800 (79)	ν(OH)
	3080 (19)	ν(CH)
1894 (m)	1907 (246)	ν(C=O)
	1453 (15)	δ(CH)
1373 (m)	1362 (10)	ω(CH)
1360 (m)		
1348 (m)		
1250 (m)	1278 (73)	δ(CCH)
1173 (w)	1189 (257)	ν(CF)
1128 (m)	1131 (84)	ν(C−O)
1051 (m)		
1016 (m)	1012 (177)	ν(CF)
822 (m)	832 (53)	ν(CC)
744 (m)	765 (42)	γ(COF)
689 (m)	693 (46)	δ(COF)
590 (w)		
581 (w)	579 (23)	δ(COF)
571 (w)		
517 (w)		
498 (m)		
474 (w)		
438 (m)		
420 (m)	418 (16)	δ(CCO)
	321 (98)	ω(OH)
	255 (3)	δ(CCF)
	235 (3)	δ(CCF)
	48 (4)	τ(CC)
1286 (m)		SF$_4$
885 (w)		SF$_4$
708 (m)		SF$_4$
623 (m)		SF$_4$
609 (vs)		SF$_4$
552 (m)		SF$_4$
534 (m)		SF$_4$

[a] Abbreviations for IR intensities: vs = very strong, s = strong, m = medium, w = weak. [b] Calculated on the B3LYP/aug-cc-pVTZ level of theory. [c] IR intensities in km/mol.
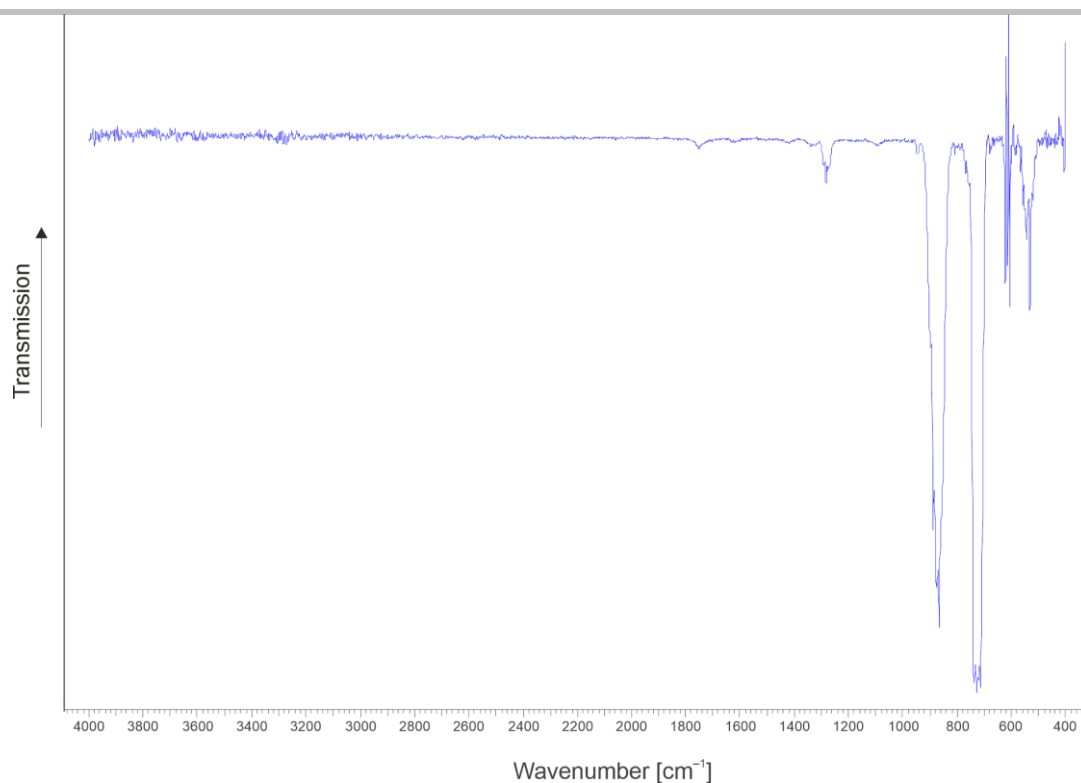
Figure S18. Reference spectrum of gaseous SF₄ at room temperature.

$\tilde{v}$ [cm^{-1}]= 1284 (m), 884 (w), 729 (vw), 622 (m), 612 (m), 603 (m), 555 (m), 544 (m), 532 (m), 406 (m), 397 (m).

Table S3. Quantum chemically calculated vibrational frequencies of **1**. Calculated on the B3LYP/aug-cc-pVTZ level of theory.

FHA

$\tilde{v}$ (IR/Ra)	Assignment
3799 (67/124)	ν(OH)
3732 (78/104)	ν(OH)
3080 (21/71)	ν(CH)
1823 (302/12)	ν(C=O)
1461 (20/2)	δ(CCH)
1381 (47/3)	δ(COH)
1360 (19/3)	ω(CH)
1250 (52/4)	δ(COH)
1170 (261/2)	ν(C–O)
1138 (88/4)	ν(C–O)
1011 (191/3)	ν(CF)
864 (23/10)	ν(CC)
789 (70/0)	γ(CO)
660 (65/3)	δ(CCO)
591 (74/1)	ω(OH)
571 (28/2)	δ(CCO)
419 (17/1)	δ(COF)
326 (94/2)	ω(OH)
267 (11/1)	δ(CCO)
240 (3/1)	δ(CCF)
40 (5/1)	τ(CC)

Single-Crystal X-ray Structure Analysis

Crystal Structure of [FHA-1H][AsF₆]
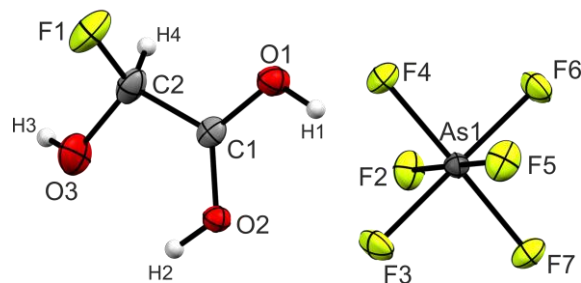
Figure S19. Projection of the asymmetric unit of **3** (50% probability displacement ellipsoids, hydrogen atoms displayed as spheres of arbitrary radius).
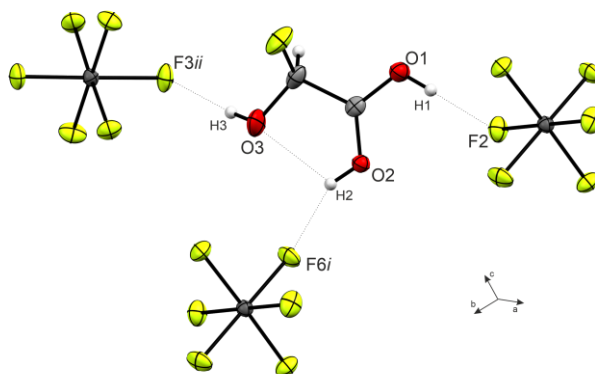
Figure S20. Hydrogen bonds of the cation in the crystal packing of **3** (50% probability displacement ellipsoids, hydrogen atoms displayed as spheres of arbitrary radius).
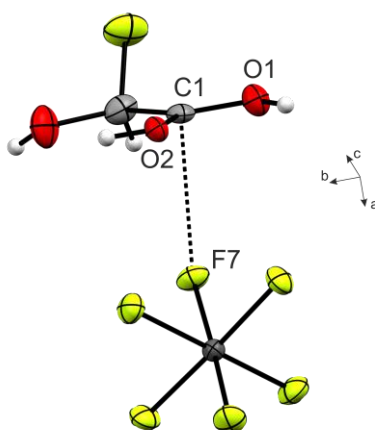
Figure S21. Non-hydrogen bonded cation-anion interaction in the crystal packing of **3** (50% probability displacement ellipsoids, hydrogen atoms displayed as spheres of arbitrary radius).
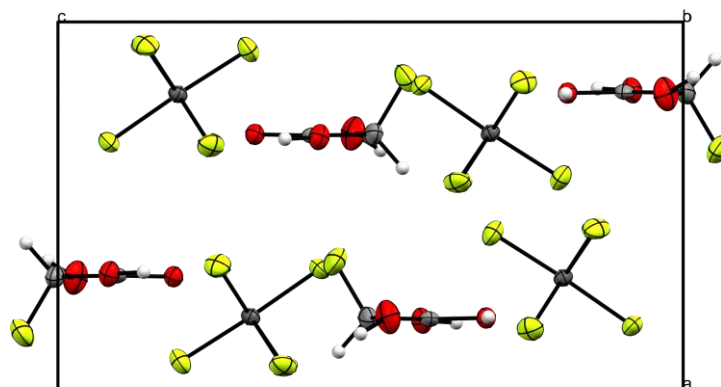
Figure S22. Crystal packing of **3** with a view along the *b*-axis (50% probability displacement ellipsoids, hydrogen atoms displayed as spheres of arbitrary radius).
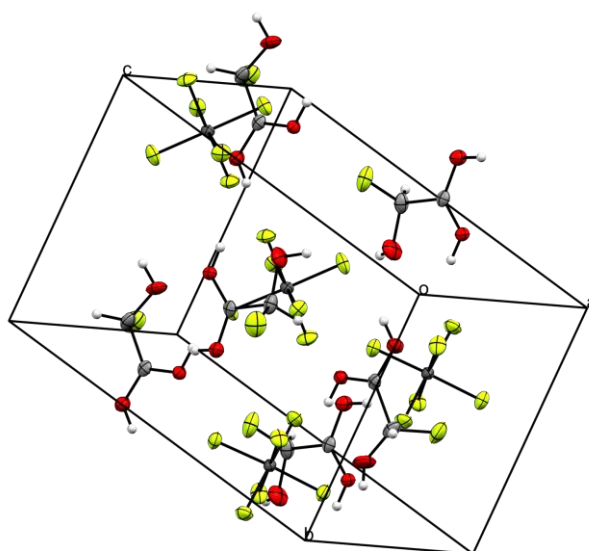
Figure S23. Crystal packing of **3** (50% probability displacement ellipsoids, hydrogen atoms displayed as spheres of arbitrary radius).

Table S4. Bond lengths [Å], bond angles, and torsion angles [°] of **3**.

Bond lengths [Å]

C1–C2	1.515(5)	As1–F2	1.754(2)
C1–O1	1.258(4)	As1–F3	1.727(2)
C1–O2	1.272(4)	As1–F4	1.703(2)
C2–O3	1.355(5)	As1–F5	1.698(3)
C2–F1	1.376(5)	As1–F6	1.727(2)
		As1–F7	1.716(2)

Bond angles [°]

O1–C1–C2	117.4(3)	F3–As1–F2	89.03(13)
O2–C1–C2	122.0(3)	F4–As1–F6	90.47(12)
O1–C1–O2	120.6(3)	F5–As1–F7	91.96(12)
O3–C2–C1	106.6(3)		
F1–C2–C1	106.1(4)		
O3–C2–F1	111.9(4)		

Dihedral angles [°]

O3–C2–C1–O1	179.5(4)
F1–C2–C1–O1	–61.2(5)
O3–C2–C1–O2	–1.0(6)
F1–C2–C1–O2	118.3(4)

Intermolecular interactions D(–H)···A [Å]

O1(–H1)···F2	2.579(4)
O2(–H2)···O3	2.587(4)
O2(–H2)···F6*i*	2.669(3)
O3(–H3)···F3*ii*	2.826(4)
C1···F7	2.733(5)

Table S5. Summary of the X-ray diffraction data collection and refinement.

|	$[C_2H_4FO_3][AsF_6]$
Formula	$C_2H_4F_7O_3As$
M_r [g mol^{-1}]	283.97
Crystal size [mm^3]	0.80 × 0.170 × 0.150
Crystal system	orthorhombisch
Space group	$P2_12_12_1$
a [Å]	7.4858(3)
b [Å]	8.0027(3)
c [Å]	12.7743(5)
α [deg]	90
β [deg]	90
γ [deg]	90
V [Å^3]	765.27(5)
Z	4
ρ_{calc} [g cm^{-3}]	2.465
μ [mm^{-1}]	4.549
λ(Mo-K$_\alpha$) [Å]	0.71073
F(000)	544
T [K]	121(2)
h,k,l range	–10:10, –11:11, –18:18
Refl. measured	2544
Refl. unique	2257
R$_{int}$	0.0437
Parameters	135
R(F)/wR(F^2) [a] (all reflexions)	0.0416/0.0631
Weighting scheme	calc
S (GooF)[d]	1.028
Residual density [e Å^{-3}]	0.797/–0.544
Device type	Oxford XCalibur
Solution	SHELXT[4]
Refinement	SHELXL-2018/1[5]
CCDC	2173682

SUPPORTING INFORMATION

Theoretical Study

α-Fluorohydroxyacetic Acid (FHA)
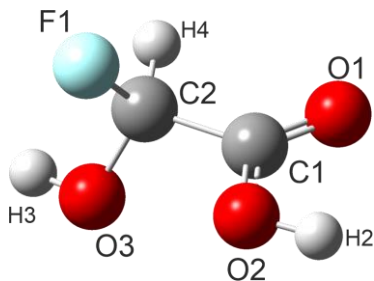
Figure S24. Optimization of the gas-phase structure of FHA. Calculated on the B3LYP/aug-cc-pVTZ level of theory.

Table S6: Standard orientation of FHA. Calculated on the B3LYP/aug-cc-pVTZ level of theory.

Atomic Type	X	Y	Z
F	−1.244502	0.840437	−0.813111
O	1.067135	0.952424	0.707265
O	1.637915	−0.829520	−0.548746
O	−1.270126	−0.612020	0.939554
C	−0.695407	−0.320106	−0.276339
C	0.807254	−0.108723	−0.065397
H	−2.144245	−0.993753	0.803175
H	−0.835056	−1.104689	−1.020467
H	2.029356	1.020418	0.801123

α-Fluorohydroxyacetic Acid (FHA-F)
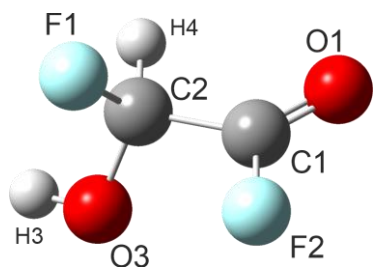
Figure S25. Optimization of the gas-phase structure of FHA-F. Calculated on the B3LYP/aug-cc-pVTZ level of theory.

Table S7. Standard orientation of FHA-F. Calculated on the B3LYP/aug-cc-pVTZ level of theory.

Atomic Type	X	Y	Z
F	−1.207018	0.951366	−0.689844
O	1.704702	−0.629905	−0.646942
O	−1.255582	−0.777422	0.790538
C	−0.671096	−0.284040	−0.349645
C	0.820887	−0.094466	−0.076235
H	−2.121126	−1.147330	0.583809
H	−0.791198	−0.930881	−1.219306
F	1.031532	0.782841	0.916734

Protonated α-Fluorohydroxyacetic Acid ([FHA-1H]⁺)
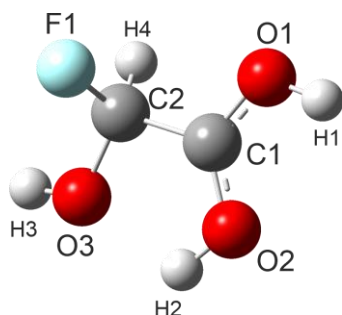
Figure S26. Optimization of the gas-phase structure of [FHA-1H]⁺. Calculated on the B3LYP/aug-cc-pVTZ level of theory.

Table S8. Standard orientation of [FHA-1H]⁺. Calculated on the B3LYP/aug-cc-pVTZ level of theory.

Atomic Type	X	Y	Z
F	−1.093802	−1.203964	−0.538907
O	1.072924	1.210624	−0.363999
O	1.592691	−0.841310	0.270649
O	−1.386180	0.937700	0.174918
C	−0.739742	−0.251522	0.375409
C	0.734321	0.072000	0.080148
H	0.281933	1.795160	−0.442466
H	−2.296761	0.932295	0.500484
H	2.509407	−0.597144	0.029094
H	−0.853324	−0.673612	1.377163

References

[1]   L. Bayersdorfer, R. Minkwitz, J. Jander, *Z. Anorg. Allg. Chem.* **1972**, *392*, 137.

[2]   CrysAlisCCD, *Version 1.171.35.11 (release 16-05-2011 CrysAlis 171.NET)*, Oxford Diffraction Ltd, UK, **2011**.

[3]   CrysAlisRED, *Version 1.171.35.11 (release 16-05-2011 CrysAlis 171.NET)*, Oxford Diffraction Ltd, UK, **2011**.

[4]   G. M. Sheldrick, *Acta crystallographica. Section A, Foundations and advances* **2015**, *71*, 3.

[5]   G. M. Sheldrick, *Acta crystallographica. Section C, Structural chemistry* **2015**, *71*, 3.

[6]   L. J. Farrugia, *J. Appl. Crystallogr.* **1999**, *32*, 837.

[7]   A. L. Spek, *J. Appl. Crystallogr.* **2003**, *36*, 7.

[8]   SCALE3 ABSPACK, *An Oxford Diffraction Program*, Oxford Diffraction Ltd, UK, **2005**.

[9]   M. J. Frisch, G. W. Trucks, H. B. Schlegel, G. E. Scuseria, M. A. Robb, J. R. Cheeseman, G. Scalmani, V. Barone, G. A. Petersson, H. Nakatsuji et al., *Gaussian 16 Rev. C.01*, Wallingford, CT, **2016**.

[10] Roy Dennington, Todd A. Keith, John M. Millam, *GaussView 6*, Semichem Inc., Shawnee Mission KS, **2019**.

[11] Mestrelab Research S.L., *MestReNova*, Santiago de Compostela, Spain, **2019**.

[12] A. F. Baxter, J. Schaab, K. O. Christe, R. Haiges, *Angew. Chem. Int. Ed. Engl.* **2018**, *57*, 8174.

ARTICLE

It Takes Two to Tango – Synthesis and Structure of the Small Superelectrophile [C2(OH)2Me2]2+

Alan Virmani,[a] Christoph Jessen,[a] and Andreas J. Kornath*[a]

Abstract: The acid-activation of 1,2-dicarbonyl compounds plays a key role in a variety of electrophilic reactions, some of which are only accessible in superacidic media when the superelectrophilic dication is formed. To obtain structural and electronic information about these elusive species, the vicinal dication $[C_2(OH)_2Me_2]^{2+}$ is synthesized and characterized by Raman spectroscopy and X-ray diffraction. Since this superelectrophile could not be stabilized in convenient superacids, the usage of liquid SO_2 turned out crucial. The experimental data are discussed together with quantum-chemical calculations on the B3LYP/aug-cc-pVTZ level of theory. Natural Bond Orbital (NBO) analyses quantify the superelectrophilic interactions found in the solid-state.

Introduction

The properties of the ethylene dication, the simplest vicinal carbon-centered superelectrophile, have been a subject of interest for a long time, especially in terms of geometry, charge repulsion, and the influence of substituents in the case of its derivatives.[1–3] *Schleyer* and others calculated different geometries of the parent compound $[C_2H_4]^{2+}$ and found that the perpendicular D_{2d} structure is the most efficient way to delocalize the vicinal positive charges.[4–6] *Frenking* compared different geometries of substituted ethylene dications of the formula $[C_2X_2Y_2]^{2+}$ (X, Y = F, OH, NH$_2$, SH).[7] He concluded that the introduction of second-row substituents led to a planar structure due to the overlap of π orbitals and hence an electron-donating effect on the CC(π) bond, provided the steric repulsion of the substituents is not too strong. To generate and stabilize superelectrophiles in condensed phase, superacids are one of the most efficient tools. The first stable carbon-centered dications synthesized in condensed phase contained large aromatic substituents to distribute the positive charges over the whole molecule.[8,9] In a recent study, we were able to determine the crystal structure of $[C_2(OH)_3Me][SbF_6]_2 \cdot HF$ by diprotonation of pyruvic acid and discussed the geometry of the carbon scaffold.[10] *Shudo et al.* investigated acid-catalyzed reactions of selected 1,2-dicarbonyl compounds like 2,3-butanedione with benzene, leading to geminal diphenylated ketones. The yield usually raised when the acidity of the medium was increased, which indicated the intermediate formation of the respective doubly-charged superelectrophile.[11,12] However, geminal double phenylation was only achieved when the electron deficiency of the starting material was high enough to react with benzene which is most likely deactivated.

[a] A. Virmani, C. Jessen, Prof. Dr. A. J. Kornath
Department Chemie
Ludwig-Maximilians-Universität München
Butenandtstraße 5-13 (D)
D-81377 München
E-mail: andreas.kornath@cup.uni-muenchen.de

With only four π-electrons in total, diprotonated 2,3-butanedione is a small and outstanding candidate to study the conflicting effects of steric repulsion by the methyl groups and π-donation by the hydroxy groups, as it is one of the simplest possible vicinal carbon-centered superelectrophile. Therefore, we investigated the conditions to generate and stabilize this compound. The results are reported herein.

Results and Discussion

Syntheses and Properties

Monoprotonated 2,3-butanedione $[C_2(O)(OH)Me_2]^+$ was isolated as the $[AsF_6]^-$ and $[SbF_6]^-$ salts by applying the superacidic systems HF/AsF$_5$ and HF/SbF$_5$ with one equivalent of the respective Lewis acid in anhydrous hydrogen fluoride (aHF) at −50°C. The general equation is given below (Equation 1).
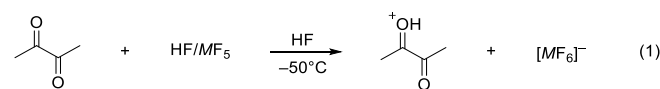

$$M = As, Sb$$

The isolation of the diprotonated species with a twofold amount of the mentioned Lewis acids did not succeed in aHF solution. When 2,3-butanedione is dissolved in aHF with two equivalents of SbF$_5$ at −70°C, a variety of side products is detected. The ^{19}F NMR spectrum (Figure S3, Supporting Information) shows a quartet shift at −83.8 ppm, indicating the addition of fluorine to at least one of the central carbon atoms, despite the presence of excess Lewis acid. Another side product found in the same sample is $[H_3CCO]^+$, as pointed up in the Raman (Figure S1) and the ^{13}C NMR spectrum at −70°C (Figure S4). The shifts occur at 146.9 ppm and 6.0 ppm as well as a Raman frequency at 2308 cm^{-1}.[13–15] When the solution is warmed up to room temperature, a singlet occurs at 182.0 ppm in the ^{13}C NMR spectrum (Figure S5) and is assigned to carbon

monoxide,[16,17] indicating an HF-induced disproportionation of 2,3-butanedione.

In the course of our studies, we tried diprotonation of 2,3-butanedione using the superacidic system HF/AsF$_5$ in aHF, but no quantitative diprotonation was observed. Instead, a ketal-like condensation product of the formula [C$_8$H$_{13}$F$_2$O$_3$][AsF$_6$] crystallized from aHF within ten minutes at −45°C. An attempted explanation, visualized in Scheme 1, is the AsF$_5$-induced addition of hydrogen fluoride to protonated 2,3-butanedione, increasing the nucleophilicity of the hydroxy group and allowing it to quickly react with another cation. The adduct formed then reacts further in a similar fashion. In the end, H$_3$O$^+$ is eliminated while formally adding another fluoride ion. The product was analyzed via single-crystal X-ray diffraction and is characterized in the Supporting Information.
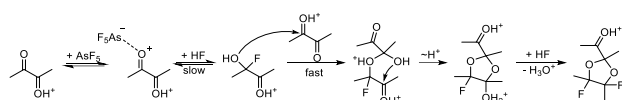
Scheme 1. Proposed mechanism of the formation of the ketal-like product from 2,3-butanedione with a twofold amount of AsF$_5$ in aHF.

To generate [C$_2$(OH)$_2$Me$_2$]$^{2+}$, 2,3-butanedione was dissolved with two equivalents of both HF and SbF$_5$ in SO$_2$ at −55°C. The reaction is given in Equation 2. Employing SO$_2$ instead of aHF as a solvent turned out necessary to prevent the superelectrophile from reacting further.

$$\text{(2)}$$
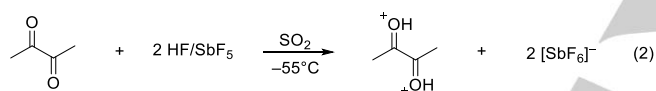
Raman Spectroscopy

Low-temperature Raman spectra of [C$_2$(OH)$_2$Me$_2$][SbF$_6$]$_2$·2 SO$_2$ and [C$_2$(O)(OH)Me$_2$][AsF$_6$] are displayed in Figure 1. Selected experimental and quantum-chemically calculated frequencies (B3LYP/aug-cc-pVTZ) of the dication are listed in Table 1. For a full assignment, see Table S3 in the Supporting Information. The cation [C$_2$(O)(OH)Me$_2$]$^+$ exhibits C_s symmetry and has 21 A' and 12 A" fundamental vibrations according to quantum-chemical calculations, and is discussed in the Supporting Information.

The quantum-chemical optimization of the naked dication [C$_2$(OH)$_2$Me$_2$]$^{2+}$ reveals C_2 symmetry with a tilt of 37.48° around the central C−C bond. In the later discussed X-ray structure analysis, a planar C_{2h} geometry is observed. Another structure optimization including four HF molecules added to the dication to simulate donor-acceptor interactions revealed C_{2h} symmetry (see Theoretical Study below). Subsequently, the frequency analysis was performed. For C_{2h}, 36 fundamental vibrations ($\Gamma_{vib} = 12 A_g + 7 A_u + 6 B_g + 11 B_u$) of the dication are expected, of which all vibrations of the races A$_g$ and B$_g$ are Raman active due to the rule of mutual exclusion.[18]

Compared to the starting material,[19,20] the symmetric CO stretching vibration is redshifted from 1719 cm^{-1} to 1667 cm^{-1} as a result of the protonation, caused by the significant importance of the hydroxycarbenium resonance structure.[10,21] Furthermore, the stretching vibration of the central CC bond is redshifted from 1288 cm^{-1} to 1216 cm^{-1}. On the other hand, ν_s((H$_3$C)C) occurs at

726 cm^{-1} and thus is blueshifted with respect to the parent compound 2,3-butanedione (693 cm^{-1}).

For the anion [SbF$_6$]$^-$, more frequencies than expected are detected (Table S3). This derives from a distorted O_h symmetry, as confirmed by the crystal structure analysis. The most intensive line at 1146 cm^{-1} is referred to ν(SO$_2$) of SO$_2$ which is co-crystallized in the solid-state.[22]
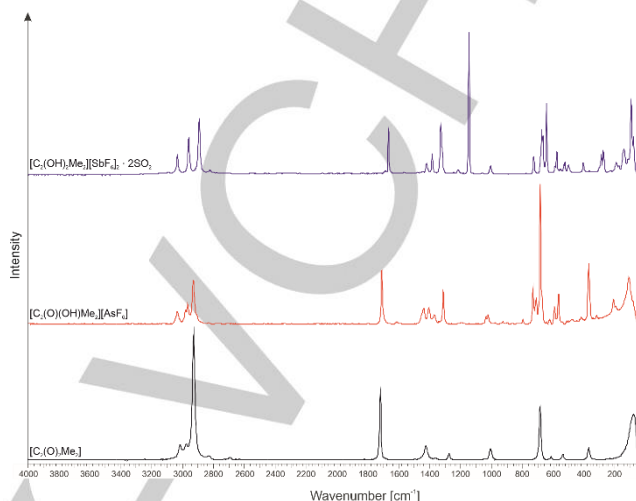
Figure 1. Stacked Raman spectra of 2,3-butanedione (bottom, black), [C$_2$(O)(OH)Me$_2$][AsF$_6$] (middle, red), and [C$_2$(OH)$_2$Me$_2$][SbF$_6$]$_2$·2 SO$_2$ (top, blue).

Table 1. Selected experimental and calculated vibrational frequencies of [C$_2$(OH)$_2$Me$_2$]$^{2+}$.

[C$_2$(OH)$_2$Me$_2$][SbF$_6$]$_2$	[C$_2$(OH)$_2$Me$_2$]$^{2+}$·4 HF	Assignment	
exp. Ra[b]	calc.[a] (IR/Ra)		
1667 (31)	1682 (0/19)	A$_g$	ν_s(CO)
1216 (2)	1232 (0/4)	A$_g$	ν(CC)
726 (12)	718 (0/10)	A$_g$	ν_s((H$_3$C)C)

[a] Calculated at the B3LYP/aug-cc-pVTZ level of theory. [b] Experimental Raman intensities are scaled to the most intensive line to be 100. [c] Abbreviations: ν = stretch, s = symmetric

Crystal Structure of [C$_2$(OH)$_2$Me$_2$][SbF$_6$]$_2$·2 SO$_2$

Single crystals of [C$_2$(OH)$_2$Me$_2$][SbF$_6$]$_2$·2 SO$_2$ were obtained by recrystallizing the colorless substance from a mixture of SO$_2$ and SO$_2$ClF at −70°C. [C$_2$(OH)$_2$Me$_2$][SbF$_6$]$_2$·2 SO$_2$ crystallizes in the monoclinic space group $P2_1/c$ with four formula units per unit cell. The cation with short contacts is displayed in Figure 2, Table 2 contains selected structural details. The formula unit is given in Figure S1, X-ray data and parameters are shown in Table S2 (see Supporting Information).

The C1−C2 bond with a distance of 1.443(4) Å shortens significantly compared to the starting material (1.476(6) Å).[23] The shortening of the C1−C2 bond of this dication is more considerable than in other protonated ketones,[10,21] even better comparable with fluorine-substituted carbenium ions.[24] Comparing the C1−C1i bond of [C$_2$(OH)$_2$Me$_2$]$^{2+}$ (1.549(4) Å) with that in parent 2,3-butanedione (1.540(6) Å),[23] surprisingly no significant difference can be noted. The distances are comparable to other non-conjugated C(sp^2)−C(sp^2) bonds like e.g. oxalic acid and oxamide.[25,26] The C1−O1 distance extends from

1.209(6) Å[23] to 1.250(4) Å as a result of charge delocalization and is shorter than other protonated ketones.[21]
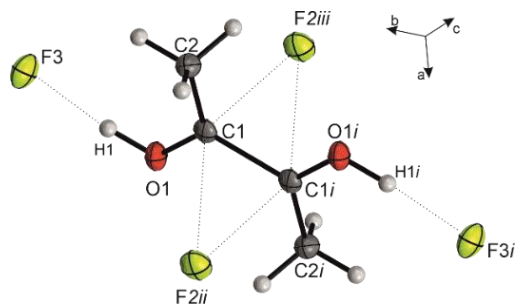

Figure 2. The dication of [C₂(OH)₂Me₂][SbF₆]₂·2SO₂ with its short interionic contacts, visualized as dashed lines (50% probability displacement ellipsoids). Symmetry operations: $i = -x, -y, -z$; $ii = -x, 0.5 + y, 1.5 - z$; $iii = x, 1.5 - y, -0.5 + z$.

Regarding the bond angles of the cation, several significant changes relative to 2,3-butanedione are observed. The C2−C1−O1 angle widens slightly from 124.5(3)° to 126.9(2)° as a direct result of the protonation, enhancing the repulsion between oxygen and the methyl group.[23] Consequently, the angle O1−C1−C1i is decreased from 118.8(2)° to 111.7(2)°, whereas the C2−C1−C1i angle expands from 116.7(2)° to 121.3(2)°. These angles amount to approximately 360°, underlining the sp^2 hybridization of the central carbon atoms. The dihedral angles of 2.1(4)° and −2.1(4)° are close to a planar C_{2h} structure of the carboxo skeleton.

In the crystal packing, the [C₂(OH)₂Me₂]²⁺ cation is surrounded by four anions, two of which form strong hydrogen bonds O1···F3 and O1i···F3i (Figure 2) with a distance of 2.476(3) Å. The other two anions are connected directly to the central carbon atoms, amounting to four C···F contacts in total. These interactions span a rhomboid with intermolecular distances of 2.520(3) Å (C1···F2ii and C1i···F2iii) and 2.625(4) Å (C1i···F2ii and C1···F2iii), which are approximately 21% and 17% respectively below the sum of the van-der-Waals radii (3.17 Å).[27]

Table 2. Selected bond distances, intermolecular interactions [Å], bond angles, and dihedral angles [°] of [C₂(OH)₂Me₂][SbF₆]₂·2SO₂. Symmetry operations: $i = -x, 2 - y, 1 - z$; $ii = -x, 0.5 + y, 1.5 - z$; $iii = x, 1.5 - y, -0.5 + z$.

Bond lengths [Å]		Intermolecular interactions D(−H)···A [Å]	
C1−C1i	1.549(4)	C1···F2ii	2.520(3)
C1−C2	1.443(4)	C1···F2iii	2.625(4)
C1−O1	1.250(4)	O1(−H1)···F3	2.476(3)
Bond angles [deg]		**Dihedral angles [deg]**	
C2−C1−C1i	121.3(2)	O1−C1−C1i−O1i	−180.0(3)
C2−C1−O1	126.9(3)	C2−C1−C1i−C2i	180.0(3)
O1−C1−C1i	111.7(2)	C2−C1−C1i−O1i	−2.1(4)
		O1−C1−C1i−C2i	2.1(4)

The Sb−F bonds of the anion with distances between 1.857(3) Å and 1.928(2) Å are in good agreement with previously observed values.[28–31] The Sb1−F2 and Sb1−F3 bonds, which are involved in donor-acceptor interactions, are significantly longer than the other Sb−F bonds, resulting in a distortion of the ideal O_h

symmetry. Co-crystallized SO₂ displays S−O bond lengths (both 1.425(3) Å) which are comparable to previously reported distances in literature.[32]

Theoretical Study

Structure optimizations and vibrational frequencies were calculated applying the DFT method B3LYP and the basis sets aug-cc-pVTZ and aug-cc-pVQZ, respectively. The quantum-chemically calculated gas-phase structure of the naked dication [C₂(OH)₂Me₂]²⁺ (B3LYP/aug-cc-pVQZ) has C_2 symmetry following from a tilt of 37.48° around the central CC bond. However, as shown by the Raman spectroscopic and X-ray structure analyses, the cation exhibits C_{2h} symmetry. To evaluate the difference between these conformers, we first calculated the rotational scan around the central C−C bond of the naked cation on the B3LYP/aug-cc-pVTZ level of theory. The structure was optimized after every rotation of 1°, starting from a dihedral angle (C1−C2−C3−O2 and O1−C2−C3−C4, respectively) of 0°. The energy scan is displayed in Figure 3.
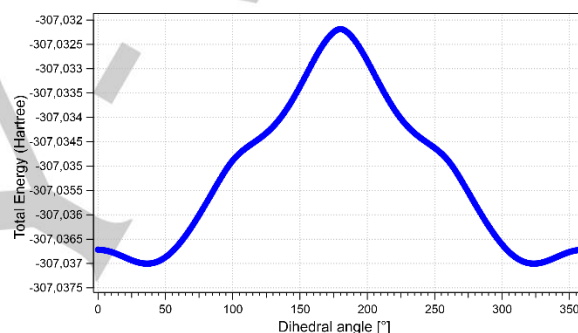
Figure 3. Energy scan of the rotation around the central C−C bond of naked [C₂(OH)₂Me₂]²⁺. Calculated at the B3LYP/aug-cc-pVTZ level of theory.

The energy scan shows a symmetrical curve with two minima, one local maximum, and one global maximum. After a rotation of 180°, the dication has C_s symmetry, representing the energy maximum. The lowest energies were calculated for a dihedral angle of 36° and −36°. The C_{2h} structure is represented at the local maximum at 0°.

The question arises why in the solid-state C_{2h} symmetry is formed, whereas the calculated optimization of the bare cation has a torsion angle of 37.48°. Either the cation is constrained into the C_{2h} symmetry by the crystal packing or intermolecular interactions have a stabilizing effect on the planar structure. Hence, for a more representative investigation, four HF molecules were added to the gas-phase structure of the dication to simulate donor-acceptor interactions, similar to the insights acquired from the X-ray structure analysis. The complex was optimized on the B3LYP/aug-cc-pVTZ level of theory, revealing C_{2h} symmetry. This indicates an electronic occupancy of the p(π) orbitals of the central carbon atoms. To evaluate the individual effects separately, we additionally calculated the optimized gas-phase structures of the cation with the two differently bonded HF molecules, hydrogen bridges and C···F interactions. The calculated structures are displayed in Figure 4.

The optimization of [C₂(OH)₂Me₂]²⁺ with two hydrogen-bonded HF molecules develops dihedral angles of 35.60°. Hydrogen bridges were expected to reduce the oxonium character of the

protonated keto groups, facilitating π-donation of the hydroxy groups. Yet, in our case, it only makes a difference of less than 2°. The optimization of the dication with two perpendicular HF molecules however exhibits a C1−C2−C3−O2 angle of 0.08° and an O1−C2−C3−C4 angle of −0.04°, thus very close to a planar structure. The energy gain by the electron donation into the central CC(π) bond solely by the C⋯F interactions is high enough to defy the sterical strain of the substituents.
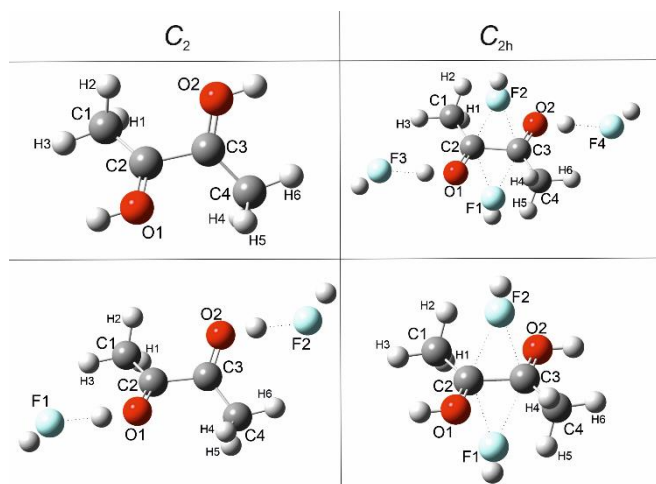
Figure 4. Optimized gas-phase structures of $[C_2(OH)_2Me_2]^{2+} \cdot n$HF ($n$ = 0, 2, 4). The left column shows calculated optimizations that reveal C_2 symmetry, C_{2h} on the right. Calculated on the B3LYP/aug-cc-pVTZ level of theory.

To quantify this effect, we performed NBO calculations of the optimized structure of $[C_2(OH)_2Me_2]^{2+}$ with two perpendicular HF molecules on the MP2/aug-cc-pVTZ level of theory, in which the two anti-bonding π^*(C−O) orbitals represent the bonding π(C−C) orbital (Figure 5). The occupation of both these orbitals (π^*(C2−O1) and π^*(C3−O2)) is 0.121 electrons. The second-order perturbation theory analysis shows donor-acceptor interactions into the π^*(C−O) orbitals, selected of which are displayed in Table S13 in the Supporting Information. For the F1 atom, stabilization energies of 16.7 (π^*(C2−O1)) and 17.2 kJ·mol^{-1} (π^*(C3−O2)) are calculated. For F2, the energies amount to 17.2 (π^*(C2−O1)) and 16.7 kJ·mol^{-1} (π^*(C3−O2)). The energy of this intermolecular hyperconjugation into the CC(π) bond sums up to 67.8 kJ·mol^{-1}. It is thus nearly twice as big as the contribution of π-donation (36.8 kJ·mol^{-1}), which was identified as the main source of stabilizing energy in previous theoretical investigations of the geometry of small superelectrophiles.[7]
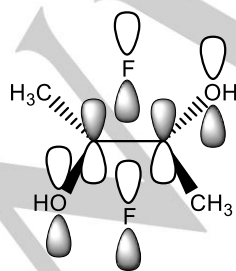
Figure 5. Intermolecular hyperconjugation of two perpendicular HF molecules into the π^*(C−O) orbitals.

Conclusions

The synthesis of the simple superelectrophile $[C_2(OH)_2Me_2]^{2+}$ in condensed phase by diprotonation of 2,3-butanedione is presented. The compound undergoes side reactions in anhydrous hydrogen fluoride and thus cannot be stabilized in convenient superacids, the usage of SO_2 as a solvent turned out crucial. The isolated product is analyzed by Raman spectroscopy and single-crystal X-ray diffraction. Quantum-chemical calculations quantify intermolecular interactions found in the solid-state, demonstrating a significant influence on the geometry of the superelectrophile. The formation of vicinal carbon-centered dications as intermediates is a key step in electrophilic superacid-catalyzed reactions. The presented results provide insights into this class of superelectrophiles.

Experimental Section

Caution! Avoid contact with any of these materials. Hydrogen fluoride will be formed by the hydrolysis of these compounds. HF burns the skin and causes irreparable damage. Safety precautions should be taken when using and handling these materials.

Apparatus and materials. All reactions were carried out at standard Schlenk conditions by using FEP/PFA reactors closed with a stainless-steel valve and a stainless-steel vacuum line. All vessels have been dried with fluorine prior to use. Raman spectroscopic analyses were rendered at −196°C with a Bruker MultiRAM FT-Raman spectrometer with an Nd:YAG laser excitation up to 1000 mW (λ = 1064 nm) in a usable range between 50 cm^{-1} and 4000 cm^{-1}. Single-crystal X-ray structure investigations were carried out with an Oxford Xcalibur3 diffractometer equipped with a Spellman generator (50 kV, 40 mA) and a KappaCCD detector. The measurements were performed with Mo-K_α radiation (λ = 0.71073 Å). For data collection, the software CrysAlis CCD,[33] for data reduction the software CrysAlis RED[34] was used. The solution and refinement were performed with the programs SHELXT[35] and SHELXL-97[36] implemented in the WinGX software package[37] and checked with the software PLATON.[38] The absorption correction was achieved with the SCALE3 ABSPACK multi-scan method.[39] Quantum-chemical calculations were performed with the Gaussian 09[40] and the Gaussian 16[41] program package. Calculations were carried out employing the method B3LYP and the basis sets aug-cc-pVTZ and aug-cc-pVQZ. NBO calculations were performed on the MP2/aug-cc-pVTZ level of theory. For visualization of the structures and vibrational modes, the program GaussView 6.0[42] was employed. NMR spectra were recorded either on a Jeol ECX400 NMR or a Bruker AV400 NMR instrument. The spectrometers were externally referenced to CFCl3 for ^{19}F and to tetramethylsilane for ^{1}H and ^{13}C NMR spectra. The spectra were recorded inside 4 mm FEP NMR tube inliners. Acetone-d6 was employed for external shimming when aHF was used as a solvent for the respective compounds. 2,3-Butanedione (Aldrich) was used as purchased, antimony pentafluoride (VWR) was distilled three times prior to use. Arsenic pentafluoride was synthesized from the elements and purified by fractionated distillation.

## Conflict of Interest

The authors declare no conflict of interest.

[1] T. Ohwada, K. Shudo, *J. Am. Chem. Soc.* **1989**, *111*, 34.

[2] D. A. Klumpp, *Chemistry (Weinheim an der Bergstrasse, Germany)* **2008**, *14*, 2004.

[3] G. Frenking, W. Koch, H. Schwarz, *J. Comput. Chem.* **1986**, *7*, 406.

[4] K. Lammertsma, M. Barzaghi, G. A. Olah, J. A. Pople, A. J. Kos, P. v. R. Schleyer, *J. Am. Chem. Soc.* **1983**, *105*, 5252.

[5] R. H. Nobes, M. W. Wong, L. Radom, *Chem. Phys. Lett.* **1987**, *136*, 299.

[6] G. Hossein Shafiee, *OJPC* **2012**, *02*, 176.

[7] G. Frenking, *J. Am. Chem. Soc.* **1991**, *113*, 2476.

[8] G. A. Olah, *Superelectrophiles and their chemistry*, Wiley-Interscience, Hoboken, N.J, **2008**.

[9] G. K. S. Prakash, T. N. Rawdah, G. A. Olah, *Angew. Chem. Int. Ed. Engl.* **1983**, *22*, 390.

[10] A. Virmani, M. Pfeiffer, C. Jessen, Y. Morgenstern, A. J. Kornath, *Z. Anorg. Allg. Chem.* **2022**, *14*.

[11] T. Ohwada, T. Yamazaki, T. Suzuki, S. Saito, K. Shudo, *J. Am. Chem. Soc.* **1996**, *118*, 6220.

[12] T. Yamazaki, S. Saito, T. Ohwada, K. Shudo, *Tetrahedron Lett.* **1995**, *36*, 5749.

[13] G. A. Olah, A. M. White, *J. Am. Chem. Soc.* **1967**, *89*, 7072.

[14] G. A. Olah, A. M. White, *J. Am. Chem. Soc.* **1969**, *91*, 5801.

[15] P. N. Gates, D. Steele, *J. Mol. Struct.* **1968**, *1*, 349.

[16] J. B. Stothers, *Appl. Spectrosc.* **1972**, *26*, 1.

[17] J. Firl, W. Runge, *Angew. Chem. Int. Ed. Engl.* **1973**, *12*, 668.

[18] P. F. Bernath, *Spectra of atoms and molecules*, Oxford University Press, Oxford, **2016**.

[19] J. R. Durig, S. E. Hannum, S. C. Brown, *J. Phys. Chem.* **1971**, *75*, 1946.

[20] A. Gómez-Zavaglia, R. Fausto, *J. Mol. Struct.* **2003**, *661-662*, 195.

[21] D. Stuart, S. D. Wetmore, M. Gerken, *Angew. Chem. Int. Ed.* **2017**, *56*, 16380.

[22] A. Anderson, R. Savoie, *Can. J. Chem.* **1965**, *43*, 2271.

[23] K. Eriks, T. D. Hayden, S. H. Yang, I. Y. Chan, *J. Am. Chem. Soc.* **1983**, *105*, 3940.

[24] K. O. Christe, X. Zhang, R. Bau, J. Hegge, G. A. Olah, G. K. S. Prakash, J. A. Sheehy, *J. Am. Chem. Soc.* **2000**, *122*, 481.

[25] J. L. Derissen, P. H. Smith, *Acta Crystallogr., Sect. B: Struct. Sci.* **1974**, *30*, 2240.

[26] G. de With, S. Harkema, *Acta Crystallogr., Sect. B: Struct. Sci.* **1977**, *33*, 2367.

[27] A. Bondi, *J. Phys. Chem.* **1964**, *68*, 441.

[28] R. Minkwitz, A. Kornath, R. Krause, H. Preut, *Z. Anorg. Allg. Chem.* **1994**, *620*, 632.

[29] R. Minkwitz, C. Hirsch, *Z. Anorg. Allg. Chem.* **1999**, *625*, 1674.

[30] R. Minkwitz, S. Schneider, *Angew. Chem. Int. Ed.* **1999**, *38*, 210.

[31] M. Schickinger, T. Saal, F. Zischka, J. Axhausen, K. Stierstorfer, Y. Morgenstern, A. J. Kornath, *ChemistrySelect* **2018**, *3*, 12396.

[32] S. Grabowsky, P. Luger, J. Buschmann, T. Schneider, T. Schirmeister, A. N. Sobolev, D. Jayatilaka, *Angew. Chem. Int. Ed.* **2012**, *51*, 6776.

[33] CrysAlisCCD, *Version 1.171.35.11 (release 16-05-2011 CrysAlis 171.NET)*, Oxford Diffraction Ltd, UK, **2011**.

[34] CrysAlisRED, *Version 1.171.35.11 (release 16-05-2011 CrysAlis 171.NET)*, Oxford Diffraction Ltd, UK, **2011**.

[35] G. M. Sheldrick, *Acta crystallographica. Section A, Foundations and advances* **2015**, *71*, 3.

[36] G. M. Sheldrick, *SHELXL-97, Program for Crystal Structure Solution*, University of Göttingen, Germany, **1997**.

[37] L. J. Farrugia, *J. Appl. Crystallogr.* **1999**, *32*, 837.

[38] A. L. Spek, *PLATON, A Multipurpose Crystallographic Tool*, Utrecht University, Utrecht, Netherlands, **1999**.

[39] *SCALE3 ABSPACK, An Oxford Diffraction Program*, Oxford Diffraction Ltd, UK, **2005**.

[40] M. J. Frisch, G. W. Trucks, H. B. Schlegel, G. E. Scuseria, M. A. Robb, J. R. Cheeseman, G. Scalmani, V. Barone, B. Mennucci, G. A. Petersson, H. Nakatsuji, M. Caricato, X. Li, H. P. Hratchian, A. F. Izmaylov, J. Bloino, G. Zheng, J. L. Sonnenberg, M. Hada, M. Ehara, K. Toyota, R. Fukuda, J. Hasegawa, M. Ishida, T. Nakajima, Y. Honda, O. Kitao, H. Nakai, T. Vreven, J. A. Montgomery, J. E. Peralta, F. Ogliaro, M. Bearpark, J. J. Heyd, E. Brothers, K. N. Kudin, V. N. Staroverov, R. Kobayashi, J. Normand, K. Raghavachari, A. Rendell, J. C. Burant, S. S. Iyengar, J. Tomasi, M. Cossi, N. Rega, J. M. Millam, M. Klene, J. E. Knox, J. B. Cross, V. Bakken, C. Adamo, J. Jaramillo, R. Gomperts, R. E. Stratmann, O. Yazyev, A. J. Austin, R. Cammi, C. Pomelli, J. W. Ochterski, R. L. Martin, K. Morokuma, V. G. Zakrzewski, G. A. Voth, P. Salvador, J. J. Dannenberg, S. Dapprich, A. D. Daniels, O. Farkas, J. B. Foresman, J. V. Ortiz, J. Cioslowski, D. J. Fox, *Gaussian09, Revision A.02*, Gaussian, Inc., Wallingford CT, **2009**.

[41] M. J. Frisch, G. W. Trucks, H. B. Schlegel, G. E. Scuseria, M. A. Robb, J. R. Cheeseman, G. Scalmani, V. Barone, G. A. Petersson, H. Nakatsuji et al., *Gaussian 16 Rev. C.01*, Wallingford, CT, **2016**.

[42] Roy Dennington, Todd A. Keith, John M. Millam, *GaussView 6*, Semichem Inc., Shawnee Mission KS, **2019**.

ARTICLE

Entry for the Table of Contents

Layout 1:

FULL PAPER

The synthesis of the small superelectrophile $[C_2(OH)_2Me_2]^{2+}$ turned out a challenging task since stabilizing it in convenient superacids was not possible. The origin of the experimentally observed yet unexpected C_{2h} structure of the dication is fathomed based on X-ray structure analysis together with quantum-chemical calculations.
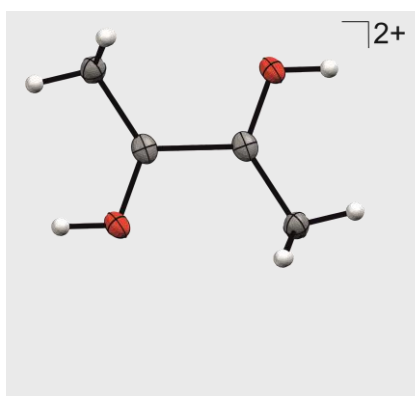
Alan Virmani, Christoph Jessen, Andreas J. Kornath*

Page No. – Page No.

It Takes Two to Tango – Synthesis and Structure of the Small Superelectrophile [C₂(OH)₂Me₂]²⁺

Supporting Information

It Takes Two to Tango – Synthesis and Structure of the Small Superelectrophile [C$_2$(OH)$_2$Me$_2$]$^{2+}$

Alan Virmani, Christoph Jessen, and Andreas J. Kornath*

List of Figures

List of Tables

Experimental procedure

Caution! Avoid contact with any of these materials. Hydrogen fluoride will be formed by the hydrolysis of these compounds. HF burns the skin and causes irreparable damage. Safety precautions should be taken when using and handling these materials.

<u>Apparatus and materials</u>

All reactions were carried out at standard Schlenk conditions by using FEP/PFA reactors closed with a stainless-steel valve and a stainless-steel vacuum line. All vessels have been dried with fluorine prior to use. Raman spectroscopic analyses were rendered at −196°C with a Bruker MultiRAM FT-Raman spectrometer with an Nd:YAG laser excitation up to 1000 mW (λ = 1064 nm) in a usable range between 50 cm^{-1} and 4000 cm^{-1}. Single-crystal X-ray structure investigations were carried out with an Oxford Xcalibur3 diffractometer equipped with a Spellman generator (50 kV, 40 mA) and a KappaCCD detector. The measurements were performed with Mo-K_α radiation (λ = 0.71073 Å). For data collection, the software CrysAlis CCD,[1] for data reduction the software CrysAlis RED[2] was used. The solution and refinement were performed with the programs SHELXT[3] and SHELXL-97[4] implemented in the WinGX software package[5] and checked with the software PLATON.[6] The absorption correction was achieved with the SCALE3 ABSPACK multi-scan method.[7] Quantum chemical calculations were performed with the Gaussian 09[8] and the Gaussian 16[9] program package. Calculations were carried out employing the method B3LYP and the basis sets aug-cc-pVTZ and aug-cc-pVQZ. NBO calculations were performed on the MP2/aug-cc-pVTZ level of theory. For visualization of the structures and vibrational modes, the program GaussView 6.0[10] was employed. NMR spectra were recorded either on a Jeol ECX400 NMR or a Bruker AV400 NMR instrument. The spectrometers were externally referenced to CFCl3 for ^{19}F and to tetramethylsilane for ^{1}H and ^{13}C NMR spectra. The spectra were recorded inside 4 mm FEP NMR tube inliners. Acetone-d6 was employed for external shimming when aHF was used as a solvent for the respective compounds. 2,3-butanedione (Aldrich) was used as purchased, antimony pentafluoride (VWR) was distilled three times prior to use. Arsenic pentafluoride was synthesized from the elements and purified by fractionated distillation.

<u>Synthesis of [C$_2$(O)(OH)Me$_2$][MF$_6$] (M = As, Sb)</u>

For the synthesis of [C$_2$(O)(OH)Me$_2$][MF$_6$] (M = As, Sb), arsenic pentafluoride (M = As; 170 mg, 1.00 mmol) or antimony pentafluoride (M = Sb; 217 mg, 1.00 mmol), respectively, was condensed into a reactor (FEP tube), followed by excess anhydrous hydrogen fluoride (aHF) at −196°C. The mixture was warmed up to −50°C to form the superacidic medium. After cooling it down to −196°C again, 2,3-butanedione (86 mg, 1.00 mmol) was added and subsequently dissolved at −50°C. When cooled down to −78°C, a white solid precipitated. Excess aHF was removed overnight under a dynamic vacuum.

<u>Synthesis of [C$_2$(OH)$_2$Me$_2$][SbF$_6$]$_2$</u>

For the synthesis of [C$_2$(OH)$_2$Me$_2$][SbF$_6$]$_2$, antimony pentafluoride (433 mg, 2.00 mmol) and hydrogen fluoride (40 mg, 2.00 mmol) were condensed into a reactor (FEP tube), followed by excess SO$_2$ at −196°C. The mixture was warmed up to −55°C to form the superacidic medium. After cooling it down to −196°C again, 2,3-butanedione (86 mg, 1.00 mmol) was added and subsequently dissolved at −55°C. When cooled down to −78°C, a white solid precipitated. Excess SO$_2$ was removed overnight under a dynamic vacuum.

<u>Synthesis of [C$_8$H$_{13}$F$_2$O$_3$][AsF$_6$]</u>

For the synthesis of [C$_8$H$_{13}$F$_2$O$_3$][AsF$_6$], arsenic pentafluoride (340 mg, 2.00 mmol) was condensed into a reactor (FEP tube), followed by excess anhydrous hydrogen fluoride (aHF) at −196°C. The mixture was warmed up to −52°C to form the superacidic medium. After cooling it down to −196°C again, 2,3-butanedione (86 mg, 1.00 mmol) was added, subsequently dissolved, and left for 10 minutes at −45°C. Colorless needles precipitated. Excess aHF was removed overnight at −78°C under a dynamic vacuum.

2,3-Butanedione with two equivalents of Lewis acid in aHF

While a single protonation of 2,3-butanedione with equimolar amounts of AsF$_5$ or SbF$_5$ takes place in anhydrous hydrogen fluoride (aHF), the presence of two or more equivalents of Lewis acid triggers a variety of side reactions, some of which are discussed in the main article. The identification was performed via single-crystal X-ray diffraction, Raman, and NMR spectroscopy.

2,3-butanedione was mixed with a solution of two equivalents of AsF$_5$ (with respect to 2,3-butanedione) in aHF at −50°C and the solvent was removed overnight. The resulting colorless powder was analyzed via low-temperature Raman spectroscopy, shown in Figure S1. A sharp line at 2308 cm^{-1} indicates the occurrence of an acylium cation, most likely [H$_3$CCO]$^+$.[11] The lines at 1726 cm^{-1} and 1668 cm^{-1} suggest the presence of (mono-)protonated carbonyl groups.
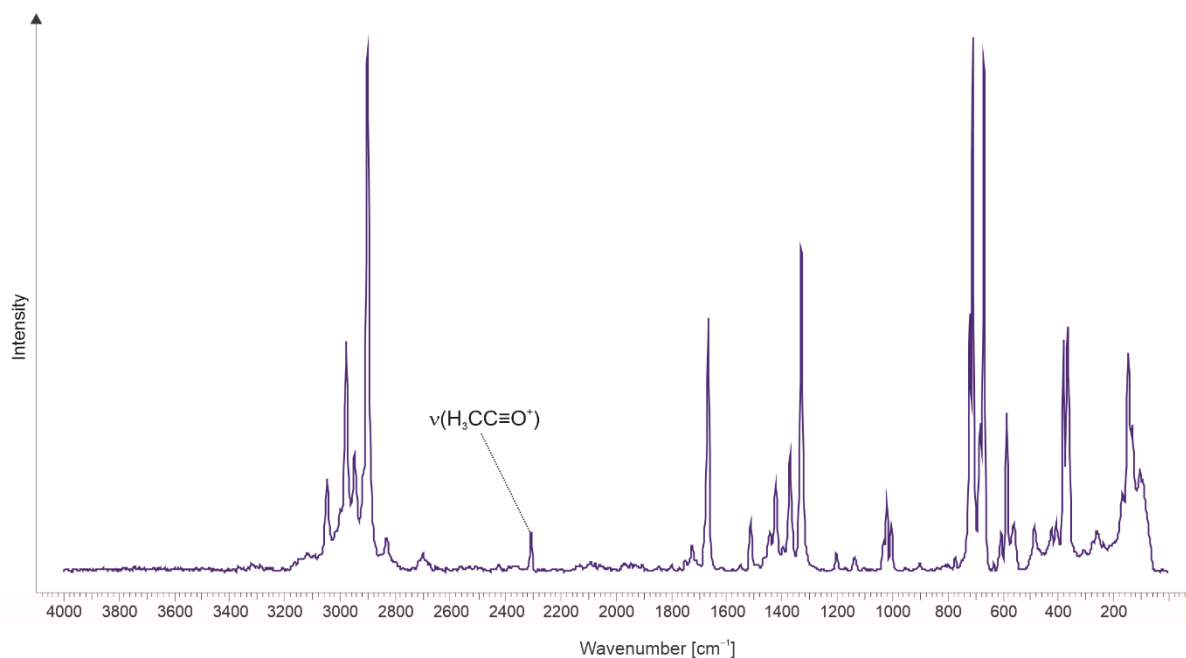
Figure S1. Raman spectrum of 2,3-butanedione in aHF with two equivalents of AsF$_5$.

In addition, ^{1}H, ^{13}C, and ^{19}F NMR spectra of a solution of 2,3-butanedione with two equivalents of SbF$_5$ in aHF with external acetone-d6 were recorded, each nucleus at −70°C, −45°C, −20°C, and room temperature. In Figure S2, the stacked ^{1}H NMR spectra with the respective temperatures are displayed. In the spectra from −70°C to −20°C, the signals right of HF (broad, ~8 ppm) show no significant changes in the distribution of the peaks, only slight yet consistent downfield shifts. The solution seems to be stable until it is warmed up to room temperature when decomposition starts.

At −70°C, the ^{19}F NMR spectrum (Figure S3) shows a quartet shift at −83.8 ppm, indicating the addition of fluorine to at least one of the central C atoms. The ^{13}C NMR spectrum (Figure S4) depicts a signal at 231.2 ppm, which likely is a protonated carbonyl group. However, signals at 146.9 ppm and 6.0 ppm are already detected at −70°C. These are assigned to [H$_3$CCO]$^+$,[12],[13] indicating an HF-induced disproportionation of the starting material.

When warmed up to room temperature, no protonated carbonyl group can be detected in the ^{13}C NMR spectrum (Figure S5). Instead, a signal at 182.0 ppm occurs that is assigned to carbon monoxide.[14],[15]
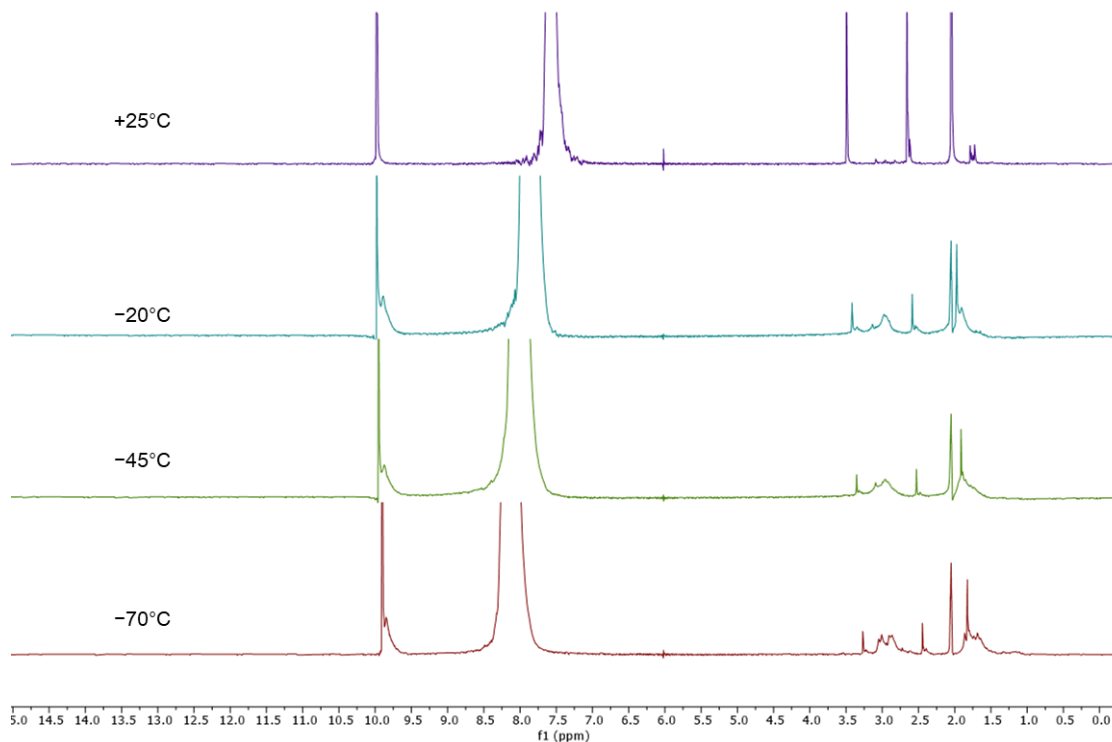
Figure S2. Stacked ^{1}H NMR spectra of 2,3-butanedione in aHF with two equivalents of SbF$_5$. The respective temperatures of the sample are shown on the left.
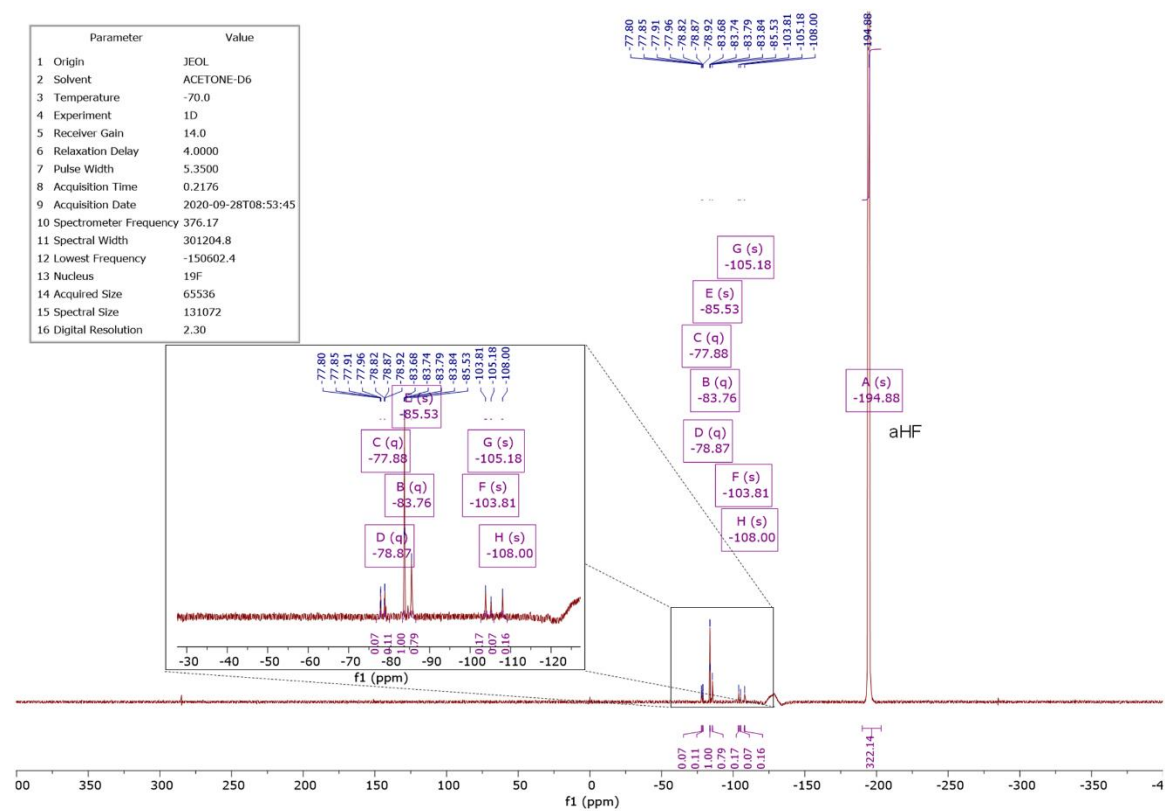

Figure S3. ^{19}F NMR spectrum of 2,3-butanedione with two equivalents of SbF$_5$ in aHF at −70°C. Several quartet signals indicate the addition of fluorine to the carbon scaffold.
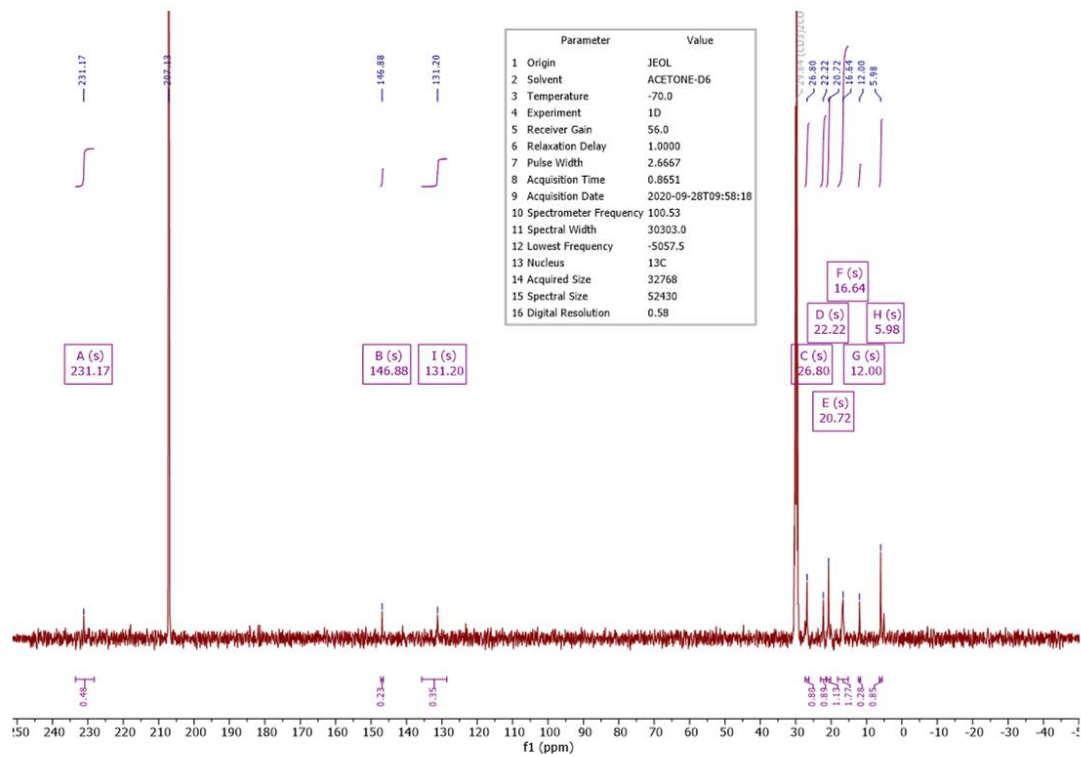
S5

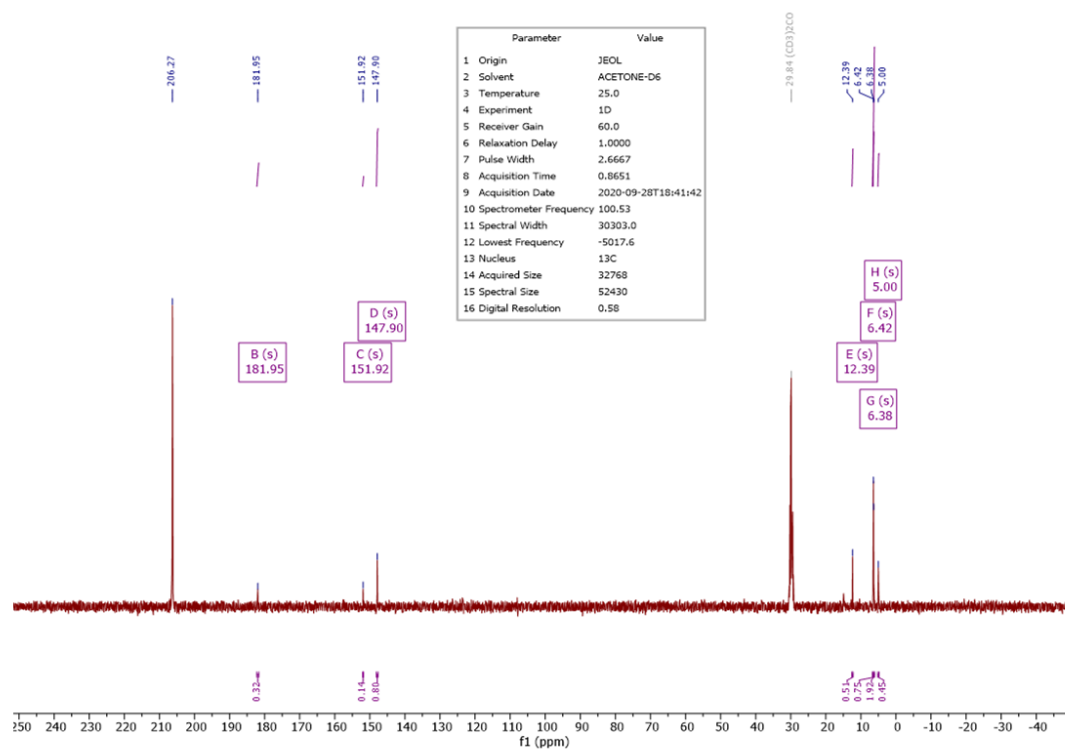**Figure S4.** ^{13}C NMR spectrum of 2,3-butanedione with two equivalents of SbF$_5$ in aHF at −70°C.

Figure S5. ^{13}C NMR spectrum of 2,3-butanedione with two equivalents of SbF$_5$ in aHF at room temperature.

S6

Crystal structure of [C$_8$H$_{13}$F$_2$O$_3$][AsF$_6$]

When 2,3-butanedione was dissolved in aHF with a twofold amount of AsF$_5$, a ketal-like condensation product of the formula [C$_8$H$_{13}$F$_2$O$_3$][AsF$_6$] crystallized within 10 minutes at −40°C. The solid-state structure was resolved via single-crystal X-ray diffraction. The salt crystallizes in the monoclinic space group $P2_1/c$ with four formula units per unit cell. All unique bond lengths, bond angles, and interionic contacts are listed in Table S1. Figure S6 shows the asymmetrical unit, short contacts are displayed in Figure S7. The crystal packing is given in Figure S8.
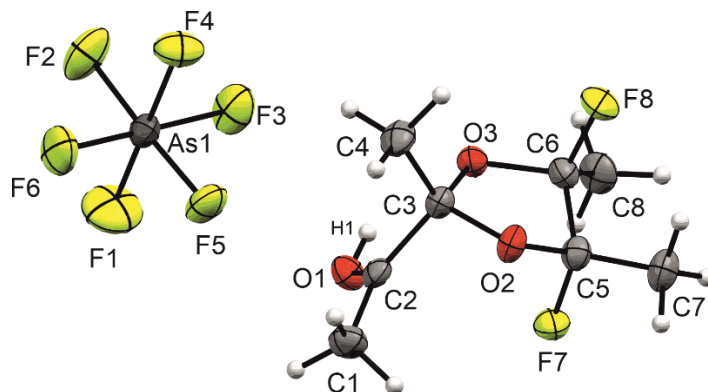
Figure S6. Asymmetrical unit of [C$_8$H$_{13}$F$_2$O][AsF$_6$]. Thermal ellipsoid displacement probability is set at 50%. Hydrogen atoms are set as spheres of arbitrary radius.

Figure S7. Short contacts of [C$_8$H$_{13}$F$_2$O][AsF$_6$], drawn as dashed lines. Thermal ellipsoid displacement probability is set at 50%. Hydrogen atoms are set as spheres of arbitrary radius. Symmetry operation: $i = 2−x, −0.5+y, 1.5−z$.

Figure S8. Crystal packing of [C$_8$H$_{13}$F$_2$O][AsF$_6$]. Thermal ellipsoid displacement probability is set at 50%. Hydrogen atoms are set as spheres of arbitrary radius.

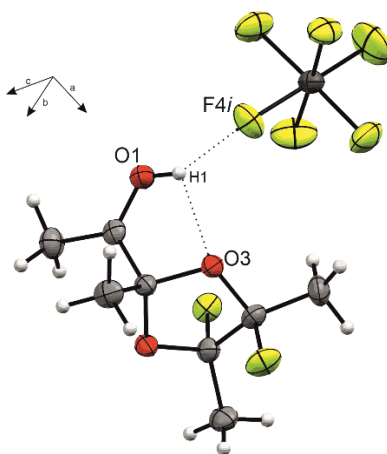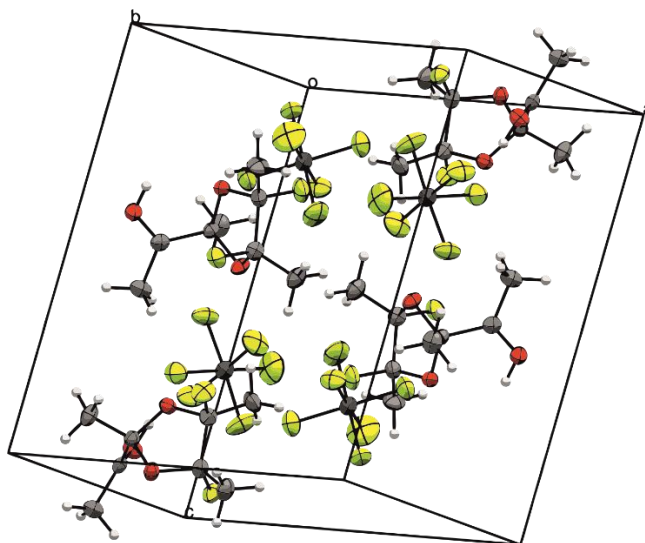**Table S1.** Bond lengths [Å], bond angles [°], and short contacts [Å] of [$C_8H_{13}F_2O_3$][AsF_6]. Symmetry operation: *i* = 2−*x*, −0.5+*y*, 1.5−*z*.

Bond lengths [Å]

C1−C2	1.454(3)	As1−F1	1.6966(18)
C2−C3	1.526(3)	As1−F6	1.7005(15)
C3−C4	1.504(3)	As1−F2	1.7034(15)
C5−C6	1.525(3)	As1−F3	1.7095(15)
C5−C7	1.487(3)	As1−F5	1.7127(15)
C6−C8	1.484(3)	As1−F4	1.7457(16)
C2−O1	1.256(2)		
C3−O2	1.420(2)		
C3−O3	1.423(2)		
C5−O2	1.393(3)		
C6−O3	1.414(3)		
C5−F7	1.406(2)		
C6−F8	1.395(3)		

Bond angles [°]

C1−C2−C3	121.57(19)	F1−As1−F2	91.33(9)
O1−C2−C1	118.2(2)	F1−As1−F3	90.65(10)
O1−C2−C3	120.19(19)	F1−As1−F5	91.57(9)
C4−C3−C2	112.28(18)	F1−As1−F6	91.98(10)
O2−C3−C2	108.09(17)	F2−As1−F3	89.97(8)
O3−C3−C2	106.82(16)	F2−As1−F4	88.27(8)
O2−C3−C4	110.32(17)	F2−As1−F6	91.36(9)
O3−C3−C4	112.15(17)	F3−As1−F4	88.77(8)
O2−C3−O3	106.93(16)	F3−As1−F5	88.91(8)
C7−C5−C6	119.2(2)	F4−As1−F5	88.82(7)
O2−C5−C6	103.00(17)	F4−As1−F6	88.61(8)
O2−C5−C7	112.22(18)	F5−As1−F6	89.62(8)
F7−C5−C6	105.19(16)	F1−As1−F4	179.30(8)
F7−C5−C7	109.64(18)	F2−As1−F5	176.90(8)
O2−C5−F7	106.72(17)	F3−As1−F6	177.03(8)
C8−C6−C5	119.69(19)		
O3−C6−C5	102.15(17)		
O3−C6−C8	112.41(19)		
F8−C6−C5	106.28(17)		
F8−C6−C8	108.94(19)		
F8−C6−O3	106.44(17)		
C5−O2−C3	106.96(15)		
C6−O3−C3	108.43(16)		

Short contacts D(−H)···A [Å]

O1(−H1)···F4*i*	2.619(2)
O1(−H1)···O3	2.606(2)

The bonds C2−C3, C3−C4, and C5−C6 are in the range of regular C−C single bonds (1.54 Å).[16] With 1.454(3) Å the C1−C2 bond is shorter than in 2,3-butanedione (1.476(6) Å),[17] yet comparable to other protonated keto groups with an adjacent methyl group.[18] This is due to hyperconjugation of the methyl group, similar to the C1−C2 bond in the superelectrophile $[C_2(OH)_2Me_2]^{2+}$ in the main article (1.443(4) Å). The C5−C7 bond distance amounts to 1.487(3) Å and the C6−C8 bond length to 1.484(3) Å as a result of hyperconjugation of the σ(C−H) bond into the σ*(C−F) orbital. The C2−O1 bond elongates from 1.209(6) Å in butanedione to 1.256(2) Å following protonation. The C3−O2 (1.420(2) Å) and C3−O3 bonds (1.423(2) Å) correspond to regular C−O single bond distances (1.43 Å).[16] On the other hand, the C5−O2 (1.393(3) Å) and the C6−O3 bond lengths (1.414(3) Å) are shorter than the standard C−O distance while the C−F bonds C5−F7 (1.406(2) Å) and C6−F8 (1.395(3) Å) are longer than expected C−F single bonds (1.36 Å).[16] This is due to the anomeric effect. The fluorine atoms are in the axial positions to reduce the coulombic strain[19] and thus negative hyperconjugation of the O2 and O3 atoms into the σ*(C−F) orbitals is possible. The C3−O3 bond is shorter than the C3−O2 distance, probably because of the intramolecular hydrogen bond O1(−H1)···O3 (2.606(2) Å) that reduces the negative hyperconjugation of the O3 atom. Regarding the bond angles in the ring of the cation, angles containing methyl groups stand out to be wider than expected tetrahedral angles, possibly because of steric repulsion. A formula unit of the salt is connected via the hydrogen bond O1(−H1)···F4i and amounts to 2.606(2) Å.

The anion $[AsF_6]^-$ is slightly distorted from an ideal O_h symmetry. With exception of the As1−F4 bond, the As−F bonds differ only slightly and are comparable to $[AsF_6]^-$ anions in literature. The As1−F4 distance is longer as a result of the O1(−H1)···F4i hydrogen bridge.[20],[21] The bond angles do not deviate more than 3.10° from the ideal octahedral angle.

Raman spectroscopy

Table S2. Experimental and calculated vibrational frequencies of $[C_2(OH)_2Me_2]^{2+}$.

$[C_2(OH)_2Me_2][SbF_6]_2$ exp. Raman [a]	$[C_2(OH)_2Me_2]^{2+}\cdot 2\,HF$ calc. (IR/Raman) [b]		Assignment [c]
	3152 (24/0)	B_u	$\nu_{as}(CH_3)$
3034 (12)	3152 (0/99)	A_g	$\nu_s(CH_3)$
2959 (24)	3042 (0/102)	B_g	$\nu_{as}(CH_3)$
	3042 (59/0)	A_u	$\nu_s(CH_3)$
2892 (36)	3010 (0/364)	A_g	$\nu_s(CH_3)$
	3004 (179/0)	B_u	$\nu_{as}(CH_3)$
2822 (2)	2916 (0/209)	A_g	$\nu_s(OH)$
	2885 (4471/0)	B_u	$\nu_{as}(OH)$
1667 (31)	1682 (0/19)	A_g	$\nu_s(CO)$
	1657 (239/0)	B_u	$\nu_{as}(CO)$
	1490 (0/2)	A_g	$\delta_s(OH)$
	1459 (77/0)	B_u	$\delta_{as}(CH_3)$
	1447 (0/7)	A_g	$\delta_s(CH_3)$
1420 (6)	1419 (0/9)	B_g	$\delta_{as}(CH_3)$
	1408 (477/0)	B_u	$\delta_{as}(OH)$
	1406 (30/0)	A_u	$\delta_s(CH_3)$
1384 (13)	1337 (0/40)	A_g	$\delta_s(CH_3)$
	1335 (96/0)	B_u	$\delta_{as}(CH_3)$
1216 (2)	1232 (0/4)	A_g	$\nu(CC)$
	1150 (88/0)	B_u	$\delta_{as}(CH_3)$
	1080 (197/0)	A_u	$\gamma_s(OH)$
	1070 (0/0)	B_g	$\gamma_{as}(OH)$
	1016 (0/1)	B_g	$\gamma_{as}(CO)$
1006 (6)	1016 (0/6)	A_g	$\rho_s(CH_3)$
	941 (16/0)	B_u	$\nu_{as}(H_3CC)$
	889 (11/0)	A_u	$\omega_s(CH_3)$
726 (12)	718 (0/10)	A_g	$\nu_s(H_3CC)$
	594 (0/0)	B_g	$\omega_{as}(CH_3)$

579 (11/0)	B_u	$\delta_{as}(CCO)$
551 (0/3)	A_g	$\delta_s(CCO)$
383 (1/0)	A_u	$\gamma_s(CO)$
380 (0/1)	A_g	$\delta_s(CCC)$
210 (21/0)	B_u	$\delta_{as}(CCC)$
146 (10/0)	A_u	$\tau_s(CH_3)$
116 (0/1)	B_g	$\tau_{as}(CH_3)$
82 (2/0)	A_u	$\tau(CC)$
1330 (34)	B_1	$\nu(SO_2)$[d]
1146 (99)	A_1	$\nu(SO_2)$[d]
523 (7)	A_1	$\nu(SO_2)$[d]
674 (31)		$[SbF_6]^-$
666 (25)		$[SbF_6]^-$
643 (49)		$[SbF_6]^-$
589 (4)		$[SbF_6]^-$
577 (14)		$[SbF_6]^-$
554 (2)		$[SbF_6]^-$
531 (5)		$[SbF_6]^-$
504 (7)		$[SbF_6]^-$
408 (6)		$[SbF_6]^-$
288 (11)		$[SbF_6]^-$
277 (14)		$[SbF_6]^-$
230 (1)		$[SbF_6]^-$
192 (7)		$[SbF_6]^-$
176 (5)		$[SbF_6]^-$
142 (17)		$[SbF_6]^-$
117 (10)		$[SbF_6]^-$

[a] Raman intensities are normalized to the most intensive line to be 100.
[b] Calculated on the B3LYP/aug-cc-pVTZ level of theory. IR intensities are given in km·mol^{-1} and Raman intensities in Å^4·μ^{-1}.
[c] The abbreviations denote symmetric (s), antisymmetric (as), stretch (ν), deformation (δ), twisting (τ), wagging (ω), rocking (ρ)
[d] Raman frequencies of SO_2 were assigned according to Ref. [22]

Table S3. Experimental and calculated vibrational frequencies of $[C_2(O)(OH)Me_2]^+$.

$[C_2(O)(OH)Me_2][AsF_6]_2$	$[C_2(O)(OH)Me_2]^+ \cdot HF$		
exp. Raman [a]	calc. (IR/Raman) [b]		Assignment [c]
	3239 (1375/174)	A'	ν(OH)
3034 (9)	3158 (1/53)	A'	$\nu_{as}(CH_3)$
	3155 (8/65)	A'	$\nu_{as}(CH_3)$
2980 (10)	3087 (0/49)	A"	$\nu_{as}(CH_3)$
2966 (14)	3051 (19/50)	A"	$\nu_{as}(CH_3)$
2929 (31)	3035 (10/161)	A'	$\nu_s(CH_3)$
	3017 (55/148)	A'	$\nu_s(CH_3)$
1710 (39)	1801 (89/21)	A'	ν(CO)
1612 (2)	1615 (133/6)	A'	ν(C(OH))
	1460 (12/6)	A"	$\omega(CH_3)$
1439 (11)	1457 (16/3)	A'	$\delta_{as}(CH_3)$
1406 (12)	1451 (123/1)	A'	$\delta_{as}(CH_3)$
	1441 (56/8)	A'	δ(COH)
	1413 (18/3)	A"	$\omega(CH_3)$
	1399 (77/5)	A'	$\delta(CH_3)$
	1348 (43/19)	A'	$\delta(CH_3)$
1194 (1)	1213 (60/2)	A'	ν(CC)
	1141 (70/1)	A'	δ(CCH)
1022 (6)	1071 (7/0)	A"	$\gamma(CH_3)$
	1037 (73/0)	A"	γ(CO)
	1012 (2/7)	A'	$\rho(CH_3)$
924 (2)	930 (13/1)	A'	ν_{as}(CC)
797 (3)			
731 (25)	734 (66/1)	A"	γ(OH)
	655 (10/10)	A'	ν_s(CC)
	593 (2/0)	A"	γ(CO)
	527 (27/1)	A'	δ(CCO)
	475 (2/1)	A'	δ(CCC)
	354 (3/3)	A'	δ(CCC)
	332 (1/0)	A"	γ(CO)
211 (18)	237 (8/0)	A'	δ(CCC)
	132 (0/0)	A"	$\tau(CH_3)$
110 (34)	93 (2/0)	A"	$\tau(CH_3)$
	17 (8/0)	A"	τ(CC)
711 (19)			$[AsF_6]^-$
685 (100)			$[AsF_6]^-$
592 (13)			$[AsF_6]^-$
565 (22)			$[AsF_6]^-$
370 (43)			$[AsF_6]^-$

[a] Raman intensities are normalized to the most intensive mode to be 100.
[b] Calculated on the B3LYP/aug-cc-pVTZ level of theory. IR intensities are given in $km \cdot mol^{-1}$ and Raman intensities in $Å^4 \cdot \mu^{-1}$.
[c] The abbreviations denote symmetric (s), antisymmetric (as), stretch (ν), deformation (δ), twisting (τ), wagging (ω), rocking (ρ)

X-ray diffraction of [C₂(OH)₂Me₂][SbF₆]·2 SO₂
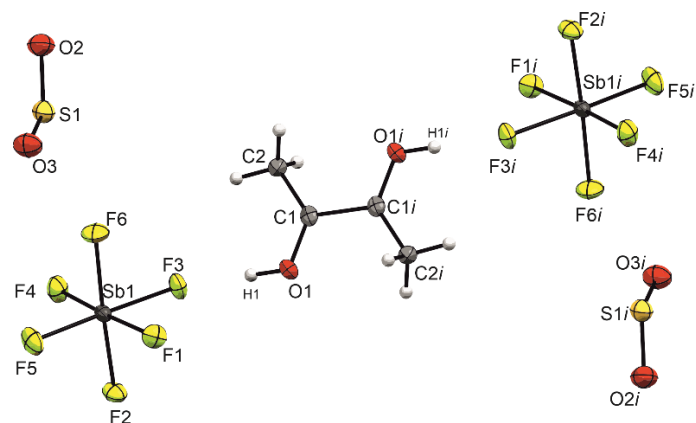
Figure S9. Formula unit of [C₂(OH)₂Me₂][SbF₆]·2 SO₂. Thermal ellipsoids displacement probability set at 50%, Hydrogen atoms are shown as spheres of arbitrary size. Symmetry operation: $i = -x, 2 - y, 1 - z$.

Table S4. Bond lengths, angles, and interionic distances of [C₂(OH)₂Me₂][SbF₆]₂·2 SO₂.

Bond lengths [Å]

C1–C1i	1.549(4)	Sb1–F1	1.867(2)
C1–C2	1.443(4)	Sb1–F2	1.881(2)
C1–O1	1.250(4)	Sb1–F3	1.928(2)
		Sb1–F4	1.867(2)
S1–O2	1.425(3)	Sb1–F5	1.861(2)
S1–O3	1.425(3)	Sb1–F6	1.857(3)

Bond angles [°]

C2–C1–C1i	121.3(2)	F1–Sb–F2	90.86(9)
C2–C1–O1	126.9(3)	F2–Sb–F4	88.41(9)
O1–C1–C1i	111.7(2)	F4–Sb–F6	89.9(1)
		F1–Sb–F6	90.5(1)
		F1–Sb–F5	91.02(9)
		F4–Sb–F5	93.52(9)
		F1–Sb–F3	87.15(8)
		F3–Sb–F4	88.30(8)
		F1–Sb–F4	175.42(9)
		F3–Sb–F5	178.08(9)
O2–S1–O3	117.3(2)	F2–Sb–F6	175.8(1)

Dihedral angles [°]

O1–C1–C1i–O1i	−180.0(3)
C2–C1–C1i–C2i	180.0(3)
C2–C1–C1i–O1i	−2.1(4)
O1–C1–C1i–C2i	2.1(4)

Intermolecular distances D(−H)···A [Å]

O1(−H1)···F3	2.476(3)
C1···F2ii	2.520(3)
C1i···F2	2.625(4)

Table S5. Structural parameters of [C₄H₈O₂][SbF₆]₂·2 SO₂ and [C₈H₁₃F₂O₃][AsF₆].

	$[C_4H_8O_2][SbF_6]_2\cdot 2\,SO_2$	$[C_8H_{13}F_2O_3][AsF_6]$
Formula	$C_4H_8F_{12}O_6S_2Sb_2$	$C_8H_{13}F_8O_3As$
M_r [g mol⁻¹]	687.72	384.10
Crystal size [mm³]	0.190 × 0.140 × 0.070	0.36 × 0.27 × 0.14
Crystal system	monoclinic	monoclinic
Space group	$P2_1/c$	$P2_1/c$
a [Å]	7.9166(5)	11.736(5)
b [Å]	13.3638(5)	8.994(5)
c [Å]	8.0768(4)	12.717(5)
α [deg]	90.0	90.000(5)
β [deg]	98.127(5)	97.480(5)
γ [deg]	90.0	90.000(0)
V [Å³]	845.91(8)	1330.9(11)
Z	4	4
ρ_{calc} [g cm⁻³]	2.700	1.917
μ [mm⁻¹]	3.586	2.654
λ(Mo-K$_\alpha$) [Å]	0.71073	0.71073
F(000)	644	760
T [K]	120(2)	173
h,k,l range	−11:11, −19:19. −10:11	−16:14, −12:11, −17:11
Refl. measured	2569	3571
Refl. unique	2072	2775
R_{int}	0.0406	0.0256
Parameters	124	189
R(F)/wR(F^2) [a] (all reflexions)	0.0440/0.0615	0.0501/0.0749
Weighting scheme	calc.[b]	calc.[c]
S (GooF)[d]	1.059	0.998
Residual density [e Å⁻³]	1.392/−0.660	0.557/−0.646
Device type	Oxford XCalibur	Oxford XCalibur
Solution	SHELXT[3]	SHELXL-97[4]
Refinement	SHELXL-2018/1[23]	SHELXL-97
CCDC	2123235	2123236

[a] $R_1 = \Sigma||F_0|-|F_c||/\Sigma|F_0|$
[b] $w = [\sigma_c^2(F_0^2) + (0.0213P)^2]^{-1}$; $P = (F_0^2 + 2F_c^2)/3$
[c] $w = [\sigma_c^2(F_0^2) + (0.0332P)^2]^{-1}$; $P = (F_0^2 + 2F_c^2)/3$
[d] $GooF = \{\Sigma[w(F_0^2 - F_c^2)^2]/(n-p)\}^{1/2}$ (n = number of reflections; p = total number of parameters)
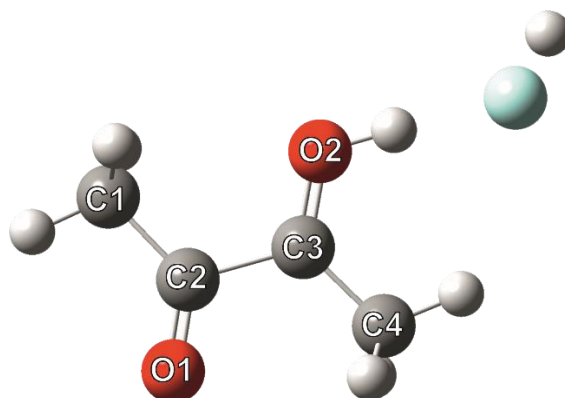
Theoretical Study

Figure S10. Optimized gas-phase structure of [C$_2$(O)(OH)$_2$Me]$^+$·HF, calculated on the B3LYP/aug-cc-pVTZ level of theory.

Table S6. Standard orientation of calculated [C$_2$(O)(OH)$_2$Me]$^+$·HF (B3LYP/aug-cc-pVTZ level of theory).

Atomic Type	Coordinates (Angstroms)		
	X	**Y**	**Z**
C	-0.018938	0.243127	0.002622
C	-1.550673	-0.019560	-0.003501
C	0.491089	1.610377	0.018527
H	0.053971	2.153179	-0.826737
H	0.080835	2.120112	0.898024
H	1.575683	1.667116	0.005318
C	-2.024259	-1.433092	0.014626
H	-1.644561	-1.975522	-0.854259
H	-1.648834	-1.952239	0.899442
H	-3.109930	-1.442362	0.011858
O	0.713126	-0.786060	-0.008284
O	-2.229590	0.971063	-0.024357
H	1.697149	-0.623487	-0.007356
H	4.038465	-0.897142	-0.015105
F	3.300624	-0.326088	-0.004856
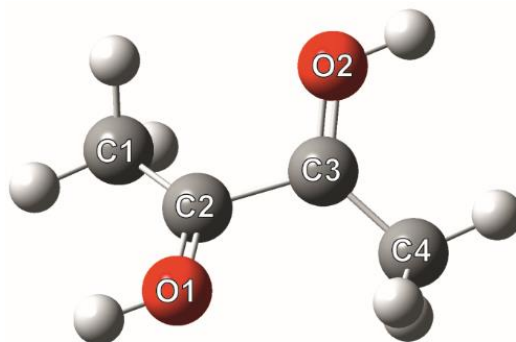
Figure S11. Optimized structure of [C$_2$(OH)$_2$Me$_2$]$^{2+}$. Calculated on the B3LYP/aug-cc-pVQZ level of theory.

Table S7. Standard orientation of calculated [C$_2$(OH)$_2$Me$_2$]$^{2+}$ (B3LYP/aug-cc-pVQZ level of theory).

Atomic Type	Coordinates (Angstroms)		
	X	Y	Z
C	0.015415	0.775900	-0.019760
O	1.134787	1.206190	-0.395228
C	-0.015415	-0.775900	-0.019760
O	-1.134787	-1.206190	-0.395228
C	-1.134787	1.560433	0.377222
H	-1.980634	1.306157	-0.285325
H	-1.480955	1.239351	1.373675
H	-0.947399	2.633054	0.364855
C	1.134787	-1.560433	0.377222
H	1.980634	-1.306157	-0.285325
H	1.480955	-1.239351	1.373675
H	0.947399	-2.633054	0.364855
H	1.248272	2.184473	-0.436150
H	-1.248272	-2.184473	-0.436150
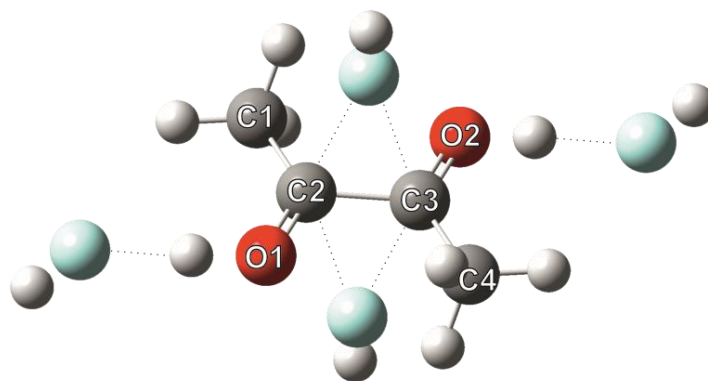
Figure S12. Optimized structure of [C₂(OH)₂Me₂]²⁺·4 HF. Interactions are displayed as dashed lines. Calculated on the B3LYP/aug-cc-pVTZ level of theory.

Table S8. Standard orientation of calculated [C₂(OH)₂Me₂]²⁺·4 HF (B3LYP/aug-cc-pVTZ level of theory).

| Atomic Type	Coordinates (Angstroms)		
	X	Y	Z
O	0.693201	1.554979	0.000000
C	-0.248667	0.734679	0.000000
C	-1.669081	1.051881	0.000000
H	-2.137846	0.578454	0.871737
H	-2.137846	0.578454	-0.871737
H	-1.855153	2.122548	0.000000
H	0.449313	2.543216	0.000000
O	-0.693201	-1.554979	0.000000
C	0.248667	-0.734679	0.000000
C	1.669081	-1.051881	0.000000
H	2.137846	-0.578454	-0.871737
H	2.137846	-0.578454	0.871737
H	1.855153	-2.122548	0.000000
H	-0.449313	-2.543216	0.000000
F	-0.000000	0.000000	2.601749
F	-0.000000	0.000000	-2.601749
H	0.000000	-0.000000	-3.534561
H	0.000000	-0.000000	3.534561
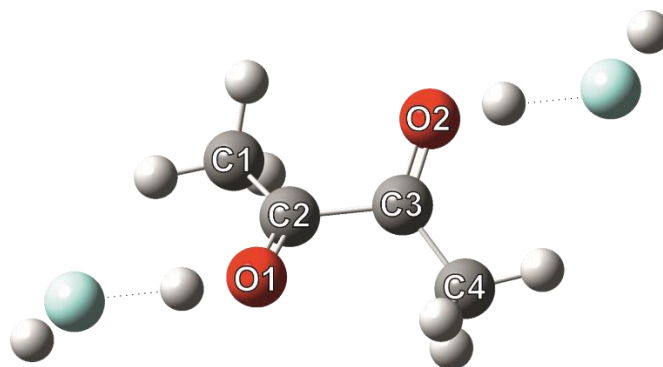
Figure S13. Optimized gas-phase structure of [C$_2$(OH)$_2$Me$_2$]$^{2+}$ with two hydrogen-bridged HF molecules. Interactions are displayed as dashed lines. Calculated on the B3LYP/aug-cc-pVTZ level of theory.

Table S9. Standard orientation of [C$_2$(OH)$_2$Me$_2$]$^{2+}$ with two hydrogen-bridged HF molecules (B3LYP/aug-cc-pVTZ level of theory).

Atomic Type	Coordinates (Angstroms)		
	X	Y	Z
F	-3.942334	0.148864	-0.311402
O	-1.503740	0.710694	-0.234753
C	-0.744174	-0.215638	0.118987
C	-1.131227	-1.566253	0.500173
H	-0.738138	-1.789792	1.503483
H	-0.616159	-2.281246	-0.158713
H	-2.207241	-1.720561	0.470635
H	-2.514685	0.515981	-0.281030
O	1.503843	-0.711320	-0.235270
C	0.744315	0.214867	0.118917
C	1.131531	1.565287	0.500651
H	0.616442	2.280613	-0.157855
H	0.738637	1.788426	1.504124
H	2.207563	1.719486	0.470998
H	2.514728	-0.516345	-0.281489
F	3.941789	-0.147094	-0.311430
H	4.699143	-0.639496	-0.568365
H	-4.698867	0.642441	-0.568489
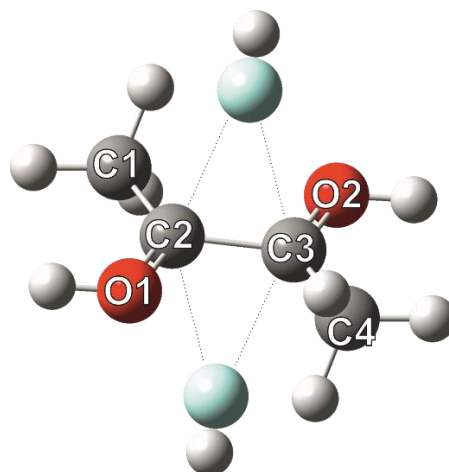
Figure S14. Optimized gas-phase structure of [C$_2$(OH)$_2$Me$_2$]$^{2+}$ with two perpendicular HF molecules. Interactions are displayed as dashed lines. Calculated on the B3LYP/aug-cc-pVTZ level of theory.

Table S10. Standard orientation of [C$_2$(OH)$_2$Me$_2$]$^{2+}$ with two perpendicular HF molecules (B3LYP/aug-cc-pVTZ level of theory).

Atomic Type	Coordinates (Angstroms)		
	X	Y	Z
O	-0.001058	-0.897705	1.443694
C	0.000715	-0.751279	0.195021
C	0.002454	-1.808502	-0.796140
H	0.870473	-1.678058	-1.457993
H	-0.871896	-1.684778	-1.451402
H	0.007313	-2.801858	-0.351075
H	-0.000696	-1.824755	1.771555
O	0.001896	0.898075	-1.445890
C	-0.000155	0.751582	-0.197200
C	-0.002705	1.808755	0.794026
H	-0.874120	1.680185	1.451946
H	0.868407	1.683029	1.452920
H	-0.003933	2.802174	0.349008
H	0.001610	1.825159	-1.773677
F	2.542639	0.000945	0.003777
F	-2.543213	-0.001859	0.001781
H	-3.477908	0.000315	-0.003475
H	3.477356	0.000512	0.005504

Table S11. Selected energies of donor-acceptor interactions from the second-order perturbation theory analysis of $[C_2(OH)_2Me_2]^{2+} \cdot 2\,HF$. Calculated on the MP2/aug-cc-pVTZ level of theory.

Donor NBO	Acceptor NBO	Stabilizing energy [kJ·mol⁻¹]	Assignment
$\pi(C2-O1)$	$\pi^*(C3-O2)$	18.4	π-donation
$\pi(C3-O2)$	$\pi^*(C2-O1)$	18.4	π-donation
LP(F1)	$\pi^*(C2-O1)$	16.7	Intermolecular hyperconjugation
LP(F1)	$\pi^*(C3-O2)$	17.2	Intermolecular hyperconjugation
LP(F2)	$\pi^*(C2-O1)$	17.2	Intermolecular hyperconjugation
LP(F2)	$\pi^*(C3-O2)$	16.7	Intermolecular hyperconjugation
$\sigma(C1-H1)$	$\pi^*(C2-O1)$	69.5	σ-conjugation
$\sigma(C1-H2)$	$\pi^*(C2-O1)$	68.2	σ-conjugation
$\sigma(C4-H4)$	$\pi^*(C3-O2)$	69.5	σ-conjugation
$\sigma(C4-H5)$	$\pi^*(C3-O2)$	68.2	σ-conjugation

References

[1] CrysAlisCCD, *Version 1.171.35.11 (release 16-05-2011 CrysAlis 171.NET)*, Oxford Diffraction Ltd, UK, **2011**.

[2] CrysAlisRED, *Version 1.171.35.11 (release 16-05-2011 CrysAlis 171.NET)*, Oxford Diffraction Ltd, UK, **2011**.

[3] G. M. Sheldrick, *Acta crystallographica. Section A, Foundations and advances* **2015**, *71*, 3.

[4] G. M. Sheldrick, *SHELXL-97, Program for Crystal Structure Solution*, University of Göttingen, Germany, **1997**.

[5] L. J. Farrugia, *J. Appl. Crystallogr.* **1999**, *32*, 837.

[6] A. L. Spek, *PLATON, A Multipurpose Crystallographic Tool*, Utrecht University, Utrecht, Netherlands, **1999**.

[7] *SCALE3 ABSPACK, An Oxford Diffraction Program*, Oxford Diffraction Ltd, UK, **2005**.

[8] M. J. Frisch, G. W. Trucks, H. B. Schlegel, G. E. Scuseria, M. A. Robb, J. R. Cheeseman, G. Scalmani, V. Barone, B. Mennucci, G. A. Petersson, H. Nakatsuji, M. Caricato, X. Li, H. P. Hratchian, A. F. Izmaylov, J. Bloino, G. Zheng, J. L. Sonnenberg, M. Hada, M. Ehara, K. Toyota, R. Fukuda, J. Hasegawa, M. Ishida, T. Nakajima, Y. Honda, O. Kitao, H. Nakai, T. Vreven, J. A. Montgomery, J. E. Peralta, F. Ogliaro, M. Bearpark, J. J. Heyd, E. Brothers, K. N. Kudin, V. N. Staroverov, R. Kobayashi, J. Normand, K. Raghavachari, A. Rendell, J. C. Burant, S. S. Iyengar, J. Tomasi, M. Cossi, N. Rega, J. M. Millam, M. Klene, J. E. Knox, J. B. Cross, V. Bakken, C. Adamo, J. Jaramillo, R. Gomperts, R. E. Stratmann, O. Yazyev, A. J. Austin, R. Cammi, C. Pomelli, J. W. Ochterski, R. L. Martin, K. Morokuma, V. G. Zakrzewski, G. A. Voth, P. Salvador, J. J. Dannenberg, S. Dapprich, A. D. Daniels, O. Farkas, J. B. Foresman, J. V. Ortiz, J. Cioslowski, D. J. Fox, *Gaussian09, Revision A.02*, Gaussian, Inc., Wallingford CT, **2009**.

[9] M. J. Frisch, G. W. Trucks, H. B. Schlegel, G. E. Scuseria, M. A. Robb, J. R. Cheeseman, G. Scalmani, V. Barone, G. A. Petersson, H. Nakatsuji et al., *Gaussian 16 Rev. C.01*, Wallingford, CT, **2016**.

[10] Roy Dennington, Todd A. Keith, John M. Millam, *GaussView 6*, Semichem Inc., Shawnee Mission KS, **2019**.

[11] P. N. Gates, D. Steele, *J. Mol. Struct.* **1968**, *1*, 349.

[12] G. A. Olah, A. M. White, *J. Am. Chem. Soc.* **1967**, *89*, 7072.

[13] G. A. Olah, A. M. White, *J. Am. Chem. Soc.* **1969**, *91*, 5801.

[14] J. Firl, W. Runge, *Angew. Chem. Int. Ed. Engl.* **1973**, *12*, 668.

[15] J. B. Stothers, *Appl. Spectrosc.* **1972**, *26*, 1.

[16] E. Wiberg, N. Wiberg, G. Fischer, *Lehrbuch der anorganischen Chemie*, Walter de Gruyter, Berlin, New York, **2007**.

[17] K. Eriks, T. D. Hayden, S. H. Yang, I. Y. Chan, *J. Am. Chem. Soc.* **1983**, *105*, 3940.

[18] D. Stuart, S. D. Wetmore, M. Gerken, *Angew. Chem. Int. Ed.* **2017**, *56*, 16380.

[19] K. B. Wiberg, W. F. Bailey, K. M. Lambert, Z. D. Stempel, *J. Org. Chem.* **2018**, *83*, 5242.

[20] D. Mootz, M. Wiebcke, *Inorg. Chem.* **1986**, *25*, 3095.

[21] M. Schickinger, T. Saal, F. Zischka, J. Axhausen, K. Stierstorfer, Y. Morgenstern, A. J. Kornath, *ChemistrySelect* **2018**, *3*, 12396.

[22] A. Anderson, R. Savoie, *Can. J. Chem.* **1965**, *43*, 2271.

[23] G. M. Sheldrick, *Acta crystallographica. Section C, Structural chemistry* **2015**, *71*, 3.

Reversing the Intramolecular Hydrogen Bond – Successive Protonation of α-Hydroxyisobutyric Acid

Alan Virmani,[a] Timo F. Manitz,[a] Alexander Nitzer,[a] Christoph Jessen,[a] and Andreas J. Kornath*[a]

Abstract: As multifunctional compounds, α-hydroxycarboxylic acids can react under acidic conditions to form polyesters or lactones. The respective protonated species have been invoked as intermediates. In order to obtain knowledge about the structure and reactivity of these key intermediates the mono- and diprotonated species of α-hydroxyisobutyric acid (HIBA), one of the simplest representatives, are generated. HIBA reacted with the superacidic medium HF/SbF$_5$ for the first time to form the salts [HIBA-1H][SbF$_6$] and [HIBA-2H][SbF$_6$]$_2$. The compounds are characterized by single-crystal X-ray diffraction and NMR spectroscopy. The experimental data are compared to quantum-chemical calculations on the B3LYP/aug-cc-pVTZ level of theory. By successive protonation, the intramolecular hydrogen bond is reversed before broken up completely.

Introduction

α-Hydroxycarboxylic acids, with their similarity to α-amino acids, are believed to be building blocks in polymers that may have been an element in the evolution of life.[1],[2] These small organic precursors can be formed under biological conditions, yet were most likely already available on the prebiotic earth.[3] Hydroxy carboxylic acids can form a variety of complex compounds by polymerization into polyesters, some of which are of interest in the chemical industry in terms of green polymer synthesis.[4] One specific example is α-hydroxyisobutyric acid, commonly abbreviated as aHIBA, 2-HIBA, or simply HIBA, which can be biotechnologically produced from accessible compounds and enzymes.[4,5] HIBA, thoroughly examined via vibrational spectroscopy and quantum-chemical calculations by *Fausto* and *Jarmelo*,[6] was found in a relatively high concentration on the Murchison meteorite that fell in Australia in 1969, pointing up that it is generated under extraterrestrial conditions as well.[7,8] It is believed that in space HIBA is formed in a *Strecker*-cyanohydrin synthesis from acetone, hydrogen cyanide, and ammonia in aqueous solutions.[7] For this mechanism, proton transfers in these intermediates are crucial. Protons are abundantly available in inner and outer space in the form of cosmic rays and solar winds.[9] Since HIBA is present on extraterrestrial objects, its protonated species may also be. This prompted us to investigate the chemical behavior of HIBA towards protonation in a laboratory

environment and generate data that can help provide information about the stability and reactivity of this bioorganic building block.

Results and Discussion

Syntheses and Properties

The successive protonation of α-hydroxyisobutyric acid (HIBA) was carried out in the superacidic system HF/SbF$_5$ with anhydrous hydrogen fluoride (aHF) as solvent. The monoprotonated species [HIBA-1H][SbF$_6$] (**1**) is obtained when one equivalent of SbF$_5$ is employed at −35°C. The protonation takes place at the carboxy group, shown in Equation 1.

$$\text{HIBA} + \text{HF/SbF}_5 \xrightarrow[-35°C]{HF} [\text{product}] + [\text{SbF}_6]^- \quad (1)$$
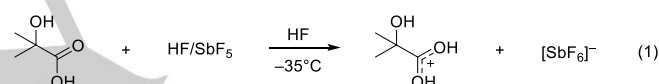
When HIBA is reacted with a twofold amount of SbF$_5$ in aHF, the acidity is not high enough for double protonation. ^{1}H and ^{13}C NMR spectra hint at a sesquiprotonation, discussed in the Supporting Information. Twofold protonation is achieved by employing three equivalents of SbF$_5$ at −40°C, resulting in [HIBA-2H][SbF$_6$]$_2$ (**2**). The second protonation occurs at the hydroxy group (Equation 2). When **2** is warmed up to room temperature in aHF solution, no desoxyfluorination at the tertiary carbon atom is observed.

$$\text{HIBA} + 2\,\text{HF/SbF}_5 \xrightarrow[-40°C]{HF} [\text{product}] + 2\,[\text{SbF}_6]^- \quad (2)$$

Furthermore, when the less acidic system HF/GeF$_4$ is employed, no protonation is observed at all. Instead, HIBA forms an adduct with GeF$_4$ despite excess Lewis acid (Equation 3). [HIBA]·GeF$_4$ (**3**) is analyzed via single-crystal X-ray diffraction and NMR spectroscopy.

$$\text{HIBA} + \text{GeF}_4 \xrightarrow[-60°C]{HF} [\text{product}] \quad (3)$$

X-ray structure analyses of 1 and 2

Single-crystals of [HIBA-1H][SbF$_6$] (**1**), [HIBA-2H][SbF$_6$]$_2$ (**2**), and [HIBA]·GeF$_4$ (**3**) suitable for X-ray diffraction were obtained by recrystallizing the colorless solids from aHF at −70°C. The compounds are thoroughly discussed in the Supporting Information, which also contains the crystal data and structure

[a]   A. Virmani, T. F. Manitz, A. Nitzer, C. Jessen, Prof. Dr. A. J. Kornath
       Department Chemie
       Ludwig-Maximilians-Universität München
       Butenandtstraße 5-13 (D)
       D-81377 München
       E-mail: andreas.kornath@cup.uni-muenchen.de

refinement. Lists of all bond lengths, angles, and donor-acceptor distances are also given in the Supporting Information. In the X-ray structure analyses, **1**, **2**, and **3** are compared to the starting material HIBA, which was first published by *Gaykema, Kanters,* and *Roelofsen*.[10] For a better comparison, we performed another crystal structure determination of HIBA at low temperatures. The starting material is discussed in the Supporting Information.

1 crystallizes in the monoclinic space group $P2_1/c$ with eight formula units per unit cell. The asymmetric unit contains two symmetrically independent formula units. The bond lengths and angles of the symmetrically independent cations do not differ significantly, whereas most of the donor-acceptor interactions do, likely due to packing effects. In the following, the effects of the protonation are explained by the example of one of the cations. The two symmetrically independent cations including the respective donor-acceptor interactions are displayed in Figure 1. Selected bond lengths, bond angles, torsion angles, and donor-acceptor interactions are shown in Table 1.
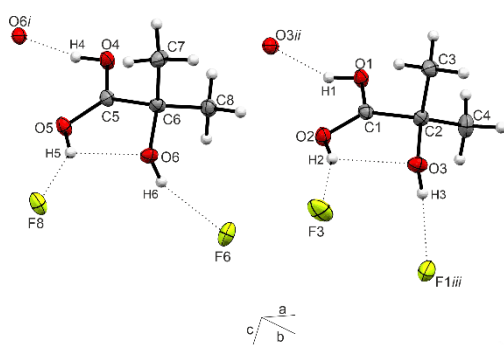
Figure 1. Symmetrically independent cations of **1**. Thermal ellipsoids displacement probability set at 50%, hydrogen atoms as spheres of arbitrary radius. Donor-acceptor interactions are visualized as dashed lines. $i = 1-x$, $-0.5+y$, $0.5-z$; $ii = 2-x$, $-0.5+y$, $0.5-z$; $iii = 2-x$, $2-y$, $1-z$.

Table 1. Selected bond lengths [Å], angles [°], torsion angle [°], and donor-acceptor interactions [Å] of the symmetrically independent cations of **1**. $i = 1-x$, $-0.5+y$, $0.5-z$; $ii = 2-x$, $-0.5+y$, $0.5-z$; $iii = 2-x$, $2-y$, $1-z$.

Bond lengths [Å]			
C1–C2	1.507(5)	C5–C6	1.511(5)
C1–O1	1.257(4)	C5–O4	1.269(4)
C1–O2	1.287(4)	C5–O5	1.276(4)
C2–O3	1.439(4)	C6–O6	1.442(4)
Bond and torsion angles [°]			
O1–C1–O2	119.4(3)	O4–C5–O5	118.4(3)
O1–C1–C2	117.5(3)	O4–C5–C6	118.1(3)
O2–C1–C2	123.0(3)	O5–C5–C6	123.4(3)
O2–C1–C2–O3	13.9(4)	O5–C5–C6–O6	11.3(4)
Donor-acceptor interactions D(−H)···A [Å]			
O1(–H1)···O3ii	2.519(3)	O4(–H4)···O6i	2.540(3)
O2(–H2)···O3	2.644(3)	O5(–H5)···O6	2.633(3)
O2(–H2)···F3	2.699(3)	O5(–H5)···F8	2.599(3)
O3(–H3)···F1iii	2.708(3)	O6(–H6)···F6	2.752(3)

The C1−C2 bond shortens from 1.529(1) Å in the starting material to 1.507(5) Å. Carboxylic CO bond lengths of 1.257(4) Å (C1−O1) and 1.289(4) Å (C1−O2) are between a formal single and double

bond, similar to previous studies in literature.[11–13] The C2−O3 bond remains unaffected by the protonation (1.439(4) Å against 1.429(1) Å in the starting material). The O1−C1−C2 angle widens from 112.7(1)° to 117.5(3)° and O1−C1−O2 decreases from 123.9(1)° to 119.4(3)°, whereas the O2−C1−C2 angle is the same as in the starting material.

The first symmetrically independent cation of [HIBA-1H]$^+$ has an O2–C1–C2–O3 torsion angle of 13.9(4)°, the respective O5–C5–C6–O6 angle in the second cation amounts to 11.3(4)°, thus deriving slightly from an ideal C_s symmetry. Both cations form a variety of hydrogen bonds, which are further examined in the Supporting Information. Additionally, both cations exhibit intramolecular hydrogen bonds of notable strength[11,14] as a stabilizing effect (see Theoretical Study), resulting in a five-membered, nearly planar ring-like structure. The donor-acceptor distances amount to 2.644(3) Å (O2···O3) and 2.633(3) Å (O5···O6), respectively. A similar hydrogen bridge is found in HIBA as well (O3···O2: 2.680(1) Å). However, this hydrogen bond is formed with the hydroxy group as the donor and a doubly bonded oxygen atom of the carboxy group as an acceptor.

The diprotonated species **2** crystallizes in the orthorhombic space group $Pca2_1$ with four formula units per unit cell. Similar to the crystal packing of **1**, the asymmetric unit contains two symmetrically independent formula units. Additionally, one HF molecule co-crystallizes per asymmetric unit, which is why the formula [HIBA-2H]$_2$[SbF$_6$]$_4$·HF is more appropriate to describe the crystal packing. In Figure 2, the two symmetrically independent cations including the respective short contacts are shown, Table 2 contains selected bond lengths, angles, torsion angle, and donor-acceptor interactions. A full list is found in the Supporting Information, together with a thorough X-ray structure analysis of **2**.
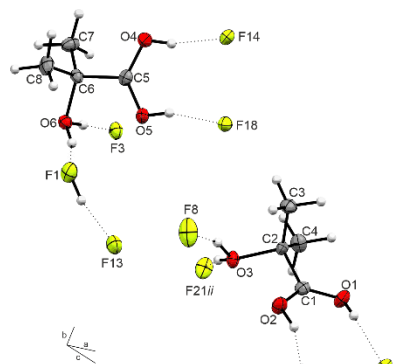

**Figure 2.** The two symmetrically independent cations of **2**. Thermal ellipsoids displacement probability set at 50%, hydrogen atoms as spheres of arbitrary radius. Donor-acceptor interactions are visualized as dashed lines. $i = 0.5+x$, $-y$, z; $ii = 1.5-x$, y, $-0.5+z$.

The CO bond distances of the alcohol group C2−O3 (1.501(5) Å) and C6−O6 (1.484(5) Å), respectively, are significantly elongated from a regular CO single bond length[15] in the starting material (1.429(1) Å) and the monoprotonated species (1.439(4) Å/1.442(4) Å). Compared to the monoprotonated species, no intramolecular hydrogen bridge is detected. The protons at the carboxy groups are pointed away from the carbon scaffold (Figure 2), which is very unusual.[16,17] It is to be noted that the position of protons in the X-ray structure analysis is not significant. Yet, donor-acceptor interactions (O1···F23i and

O2···F25) indicate a high probability of the presence of protons at these positions. Following this, it is not surprising that the O1−C1−O2 (and O4−C5−O6, respectively) widens from 119.5(3)°/118.4(3)° to 127.7(4)°/126.9(4)° while the O1−C1−C2/O4−C5−C6 and the O2−C1−C2/O5−C5−C6 angles decrease.

The biggest difference between the two symmetrically independent cations is the torsion angle around the central C−C bond, which is about 17° smaller in the first cation (O2−C1−C2−O3: −35.6(5)°) compared to the second cation (O5−C5−C6−O6: −18.0(5)°). Both cations, therefore, stray from the optimal C_s symmetry, likely due to sterical effects and intermolecular interactions, which are described in the Supporting Information.

Table 2. Selected bond lengths [Å], angles [°], torsion angle [°], and donor-acceptor interactions [Å] of the symmetrically independent cations of **2**. Symmetry operations: $i = 0.5+x, -y, z$; $ii = 1.5-x, y, -0.5+z$.

Bond lengths [Å]			
C1–C2	1.514(6)	C5–C6	1.516(6)
C1–O1	1.266(5)	C5–O4	1.266(5)
C1–O2	1.254(5)	C5–O5	1.259(5)
C2–O3	1.501(5)	C6–O6	1.484(5)
Bond and torsion angles [°]			
O1–C1–O2	127.7(4)	O4–C5–O5	126.9(4)
O1–C1–C2	115.1(4)	O4–C5–C6	115.7(4)
O2–C1–C2	117.2(4)	O5–C5–C6	117.4(4)
O2–C1–C2–O3	−35.6(5)	O5–C5–C6–O6	−18.0(5)
Donor-acceptor interactions D(−H)···A [Å]			
O1(–H1)···F23i	2.576(4)	O4(–H5)···F14	2.547(4)
O2(–H2)···F25	2.497(4)	O5(–H6)···F18	2.490(4)
O3(–H3)···F21ii	2.552(4)	O6(–H7)···F1	2.549(4)
O3(–H4)···F8	2.497(5)	O6(–H8)···F3	2.571(4)
F1(–H9)···F13	2.551(6)		

[HIBA]·GeF$_4$ (**3**) crystallizes in the monoclinic space group $P2_1/n$ with four formula units per unit cell. The asymmetric unit is shown in Figure 3. Selected bond lengths and angles are listed in Table 3. A full list is found in the Supporting Information, together with a thorough X-ray structure analysis of **3**.
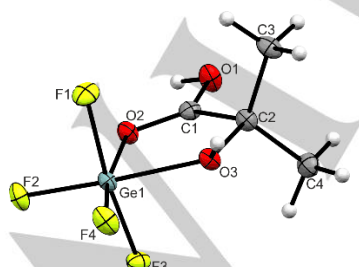
Figure 3. The asymmetric unit of [HIBA]·GeF$_4$ (**3**). Thermal ellipsoid displacement probability set at 50%, hydrogen atoms shown as spheres of arbitrary radius.

The C1−O1 distance amounts to 1.273(6) Å and C1−O2 to 1.236(5) Å. Similar to the protonated species **1** and **2**, the carboxylic CO bond lengths of **3** are approximated upon adduct formation. The C2−O3 bond of 1.442(6) Å is hardly affected in the

course of the reaction (1.429(1) Å in HIBA) and is thus similar to the respective distance in the cation of **1**. The Ge−F bond lengths are comparable to [GeF$_6$]$^{2-}$ octahedron.[18] The newly formed Ge1−O2 (1.944(3) Å) and Ge1−O3 (1.966(3) Å) bonds are similar to the reported structure of GeF$_4$·2 OEt$_2$.[19] The Ge1−F1 and the Ge1−F3 bonds are equally long within 3σ as well as the C2−C3 and the C2−C4 distances, all of which point away from the plane the adduct exhibits, indicating C_s symmetry. The bond angles of the carbon scaffold remain approximately unchanged compared to the starting material. However, the O3−C2−C1 angle is decreased from 108.24(8)° in HIBA to 104.0(4) in the adduct as well as the O2−C1−C2 angle from 123.4(0)° in HIBA to 121.3(4)°. For that, the O1−C1−C2 angle widens from 112.40(9)° to 115.9(4)°. The O2−C1−C2−O3 dihedral drops from 14.3(1)° to 2.2(6)°.

Table 3. Selected bond lengths [Å] and angles [°] of **3**.

Bond lengths [Å]			
C1–C2	1.515(6)	Ge1–F1	1.793(3)
C2–C3	1.509(7)	Ge1–F2	1.732(3)
C2–C4	1.515(7)	Ge1–F3	1.797(3)
C1–O1	1.236(5)	Ge1–F4	1.726(3)
C1–O2	1.273(6)	Ge1–O2	1.944(3)
C2–O3	1.442(6)	Ge1–O3	1.966(3)
Bond and torsion angles [°]			
O2–C1–C2	121.3(4)	O3–C2–C1	104.0(4)
O3–C2–C1	104.0(4)	O2–Ge1–O3	80.64(14)
O2–C1–C2–O3	2.2(6)	Ge1–O3–C2–C1	−2.1(4)
O1–C1–C2–O3	−178.7(4)	Ge1–O2–C1–O1	179.7(4)

NMR Spectroscopy

The protonation of α-hydroxyisobutyric acid (HIBA) can be traced by NMR spectroscopy, especially ^{13}C NMR data. Different results were obtained when 1.0, 2.0, or 3.0 equivalents of SbF$_5$ or excess GeF$_4$ with respect to the starting material HIBA were employed. The ^{1}H and ^{13}C NMR spectra of these species in aHF with external acetone-d6 are displayed together with the starting material HIBA in acetone-d6 in the Supporting Information, the ^{13}C NMR spectra of [HIBA-1H][SbF$_6$], [HIBA-2H][SbF$_6$]$_2$, and [HIBA]·GeF$_4$ are stacked in Figure 4. The respective NMR signals are listed in Table 4.

The usage of one equivalent of SbF$_5$ led to a single protonation at the carboxylic group (C1), as the ^{13}C signal is shifted from 178.35 ppm in HIBA to 193.01 ppm. Furthermore, the tertiary carbon atom (C2) is slightly moved downfield (76.44 ppm compared to 72.17 ppm) whereas the methyl groups (C3) are shifted upfield from 27.70 ppm to 23.68 ppm. The protons of the O−H groups are not observed, probably due to the rapid exchange in aHF. Double protonation is achieved when three equivalents of SbF$_5$ were used. This is pointed up by the ^{13}C signal of the C3 atom at 87.59 ppm. The respective proton signals are, unlike the other spectra, visible at 9.80 ppm, similar to NMR studies of protonated aliphatic alcohols in literature.[20,21] The ^{13}C methyl resonance (21.98 ppm) is even more moved upfield than in the monoprotonated species, while the carboxylic signal (186.76 ppm) occurs between the monocation and the starting

material. The ^{1}H and ^{13}C NMR spectra of [HIBA-1H][SbF$_6$] and [HIBA-2H][SbF$_6$]$_2$, especially the isogamous methyl signals, show that unlike the X-ray structure analyses suggest, both cations exhibit the point group C_s in aHF solution. To investigate whether an [OH$_2$]$^+$/F substitution takes place at the C3 atom, the solution of **2** was warmed up to room temperature. However, ^{1}H and ^{13}C NMR spectra show remarkable stability of **2** towards temperature (Figures S5 and S6 in the Supporting Information).

When HIBA was reacted with the system HF/GeF$_4$, a chelated adduct of GeF$_4$ and the two acceptor sites of HIBA is formed. The ^{13}C signal of the carboxy group occurs at 187.70 ppm, similar to [HIBA-2H]$^{2+}$, whereas the tertiary C2 atom is observed at 80.06 ppm. The isogamous methyl absorption appears at 23.27 ppm in the ^{13}C and 1.57 ppm in the ^{1}H NMR spectrum.
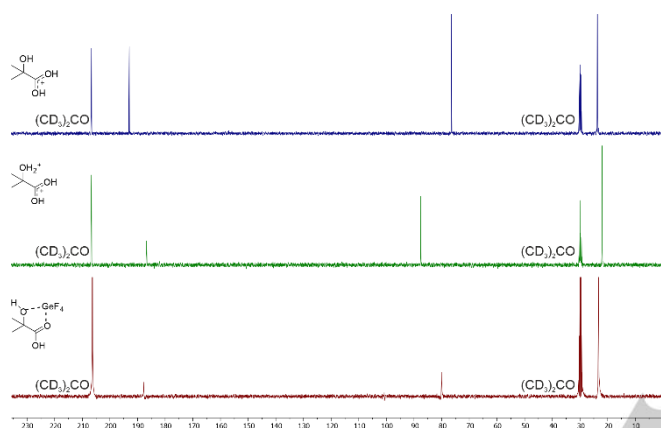
Figure 4. Stacked ^{13}C NMR spectra of [HIBA-1H][SbF$_6$] (top), [HIBA-2H][SbF$_6$]$_2$ (middle), and [HIBA]·GeF$_4$ (bottom).

Table 4. ^{1}H and ^{13}C NMR shifts [ppm] of HIBA, [HIBA-1H]$^+$, and [HIBA-2H]$^{2+}$, and [HIBA]·GeF$_4$.

	HIBA	[HIBA-1H]$^+$	[HIBA-2H]$^{2+}$	[HIBA]·GeF$_4$
δ (^{1}H) (methyl)	1.39	1.27	1.55	1.59
δ (^{1}H) (hydroxy)			9.80	
δ (^{13}C) (carboxylic)	178.35	193.01	186.76	187.70
δ (^{13}C) (tertiary)	72.17	76.44	87.59	80.06
δ (^{13}C) (methyl)	27.70	23.68	21.98	23.27

Theoretical Study

Structural optimizations of the protonated species [HIBA-1H]$^+$ and [HIBA-2H]$^{2+}$ were calculated on the B3LYP/aug-cc-pVTZ level of theory, revealing C_s symmetry for both the mono- and the dication. Two symmetrically independent cations were found in each of the X-ray structure analyses of **1** and **2**, all of which stray from the calculated point group. To investigate why more than one conformer crystallizes, we performed rotational scans of the geometry-optimized structures of [HIBA-1H]$^+$ and [HIBA-2H]$^{2+}$ of 1° around the respective C1−C2 bond. After every step, the structures were optimized. Additionally, at the energetic maxima of the curves, the resulting structures were optimized to a transition state with one imaginary frequency. The energy

differences between these structures and the geometry optimizations represent the rotational barrier. A rotational scan was also performed for the starting material HIBA, discussed in the Supporting Information. In summary, at the energetic minimum, HIBA exhibits an intramolecular O3−H2···O2 hydrogen bond with the hydroxy group as the donating site and the carboxylic O=C group as acceptor, stabilizing the C_s symmetric structure.[6] Similar to HIBA, the scan of [HIBA-1H]$^+$ shows an unsteady curve throughout the rotation (Figure S27, Supporting Information). The energetic minimum is located at a dihedral angle O2−C1−C2−O3 of −3.55°, thus close to a C_s symmetry. At this point, the cation exhibits maximal σ-conjugation of the methyl groups as well as an intramolecular hydrogen bridge O2−H2···O3, similar to HIBA. However, in this case, the protonated carboxy group is the donating unit. Hence, by protonating HIBA, the hydrogen bridge is broken up but rearranged by switching donor and acceptor sites. In the conformer with the highest energy, the dihedral amounts to −79.22°. These two structures are shown in Figure 5. The energy difference between these conformers amounts to 44.7 kJ·mol$^{−1}$. Such a high rotational barrier indicates that the C1−C2 bond in [HIBA-1H]$^+$ is not freely rotatable.
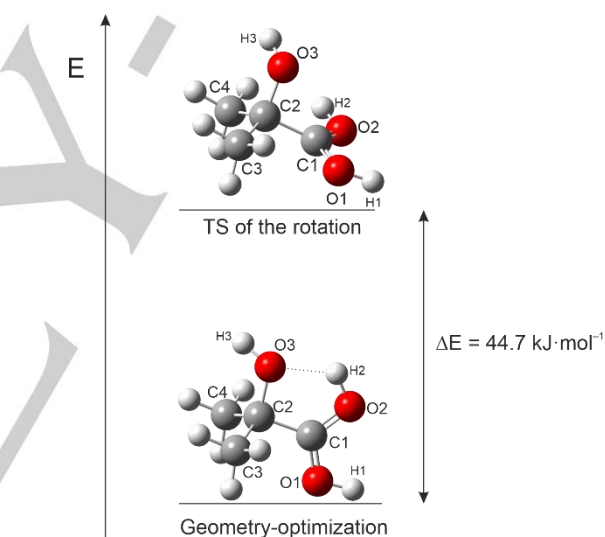
Figure 5. Energy diagram of the optimized structure of [HIBA-1H]$^+$ and the transition state (TS) of the rotation around the C1−C2 bond. Calculated on the B3LYP/aug-cc-pVTZ level of theory.

The rotational scan of [HIBA-2H]$^{2+}$ is displayed in Figure S28 (Supporting Information). The graph shows two minima at a dihedral angle O2−C1−C2−O3 of −0.03° and −179.98°, where the σ-conjugation of the methyl groups is best. At the highest points in the graph, the sterical strain between the OH and CH$_3$ groups is strongest. The geometry-optimization and the calculated transition state are shown in Figure 6.

The rotational barrier amounts to 10.1 kJ·mol$^{−1}$. Therefore, the second protonation drastically lowers the rotational barrier. Since no intramolecular hydrogen bridge can be formed anymore, the C1−C2 bond can be considered freely rotatable. Therefore, the torsion angles of the symmetrically independent cations in the X-ray structure analysis of **2** are easily influenced by packing effects, deviating from the ideal point group C_s.
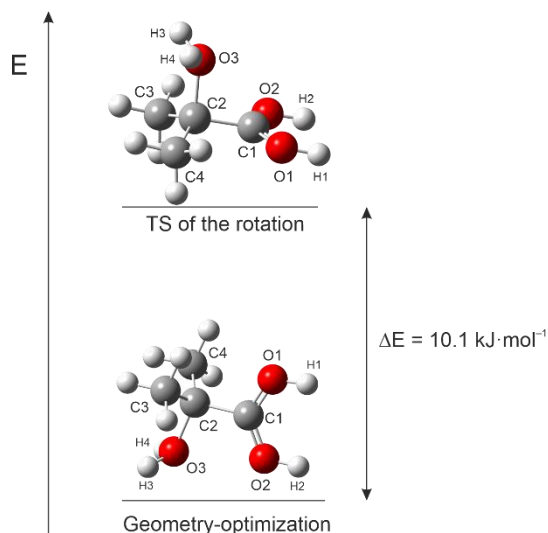
Figure 6. Energy diagram of the optimized structure of [HIBA-2H]$^{2+}$ and the transition state (TS) of the rotation around the C1−C2 bond. Calculated on the B3LYP/aug-cc-pVTZ level of theory.

Conclusions

In the present work, the successive protonation of α-hydroxyisobutyric acid (HIBA) is reported for the first time. The resulting salts [HIBA-1H][SbF$_6$] (**1**) and [HIBA-2H][SbF$_6$]$_2$ (**2**) are stable at room temperature in aHF solution. When GeF$_4$ is applied, a cyclic adduct is formed. The respective X-ray structure analyses of **1** and **2** reveal two independent cations per asymmetric unit, none of which describe the most stable conformers, which have the point group C_s in both cases according to our quantum-chemical calculations. ^{1}H and ^{13}C NMR studies confirm these observations. The successive protonation first reverses the donor and acceptor site of the intramolecular hydrogen bond in HIBA and eventually breaks it completely. This leads to a freely rotatable C1−C2 bond in [HIBA-2H]$^{2+}$, resulting in a significant deviation from the ideal C_s symmetry in the X-ray structure due to packing effects.

Experimental Section

Caution! Avoid contact with any of these materials. Hydrogen fluoride will be formed by the hydrolysis of these compounds. HF burns the skin and causes irreparable damage. Safety precautions should be taken when using and handling these materials.

Apparatus and Materials. All reactions were carried out at standard Schlenk conditions by using FEP/PFA reactors closed with a stainless-steel valve and a stainless-steel vacuum line. All vessels have been dried with fluorine prior to use. Single-crystal X-ray structure investigations were carried out with an Oxford Xcalibur3 diffractometer equipped with a Spellman generator (50 kV, 40 mA) and a KappaCCD detector. The measurements were performed with Mo-K_α radiation (λ = 0.71073 Å). For data collection, the software CrysAlis CCD,[22] for data reduction the software CrysAlis RED[23] was used. The solution and refinement were performed with the programs SHELXT,[24] implemented in the WinGX software package[25] and checked with the software PLATON.[26] The absorption correction was achieved with the SCALE3 ABSPACK multi-scan method.[27] Quantum chemical calculations were performed with the Gaussian 16[28] program package. Calculations were carried out employing the method B3LYP and the basis sets aug-cc-pVTZ. For

visualization of the structures and vibrational modes, the program GaussView 6.0[29] was employed. NMR spectra were recorded either on a Jeol ECX400 NMR or a Bruker AV400 NMR instrument. The spectrometers were externally referenced to CFCl$_3$ for ^{19}F and to tetramethylsilane for ^{1}H and ^{13}C NMR spectra. The spectra were recorded inside 4 mm FEP NMR tube inliners. Acetone-d6 was employed for external shimming when aHF was used as a solvent for the respective compounds. α-Hydroxyisobutyric acid (Aldrich) was used as purchased, antimony pentafluoride (VWR) was distilled three times prior to use.

Deposition Numbers 2150730 ([HIBA]·GeF$_4$), 2150731 ([HIBA-2H]$_2$[SbF$_6$]$_4$·HF), 2150732 ([HIBA-1H][SbF$_6$]), and 2156142 (HIBA) contain the supplementary crystallographic data for this paper. These data are provided free of charge by the joint Cambridge Crystallographic Data Centre and Fachinformationszentrum Karlsruhe Access Structures service.

[1] K. Chandru, I. Mamajanov, H. J. Cleaves, T. Z. Jia, *Life (Basel, Switzerland)* **2020**, *10*.

[2] K. Chandru, N. Guttenberg, C. Giri, Y. Hongo, C. Butch, I. Mamajanov, H. J. Cleaves, *Commun. Chem.* **2018**, *1*.

[3] E. T. Parker, H. J. Cleaves, J. L. Bada, F. M. Fernández, *Rapid communications in mass spectrometry : RCM* **2016**, *30*, 2043.

[4] T. Rohwerder, R. H. Müller, *Microbial cell factories* **2010**, *9*, 13.

[5] Sarita Chauhan, Robert DiCosimo, Robert Fallon, John Gavagan, Leo Ernest Manzer, Mark S. Payne, US 6582943B1, **2003**.

[6] S. Jarmelo, R. Fausto, *Phys. Chem. Chem. Phys.* **2002**, *4*, 1555.

[7] E. T. Peltzer, J. L. Bada, G. Schlesinger, S. L. Miller, *Adv. Space Res.* **1984**, *4*, 69.

[8] E. T. Peltzer, J. L. Bada, *Nature* **1978**, *272*, 443.

[9] U. Feldman, U. Schuhle, K. G. Widing, J. M. Laming, *ApJ* **1998**, *505*, 999.

[10] W. P. J. Gaykema, J. A. Kanters, G. Roelofsen, *Cryst. Struct. Commun.* **1978**, *7*, 463.

[11] M. Schickinger, F. Zischka, K. Stierstorfer, A. Kornath, *Eur. J. Org. Chem.* **2019**, *2019*, 1876.

[12] M. Schickinger, T. Saal, F. Zischka, J. Axhausen, K. Stierstorfer, Y. Morgenstern, A. J. Kornath, *ChemistrySelect* **2018**, *3*, 12396.

[13] A. Virmani, M. Pfeiffer, C. Jessen, Y. Morgenstern, A. J. Kornath, *Z. Anorg. Allg. Chem.* **2022**.

[14] G. A. Jeffrey, *An introduction to hydrogen bonding*, Oxford Univ. Press, New York, **1997**.

[15] E. Wiberg, N. Wiberg, G. Fischer, *Lehrbuch der anorganischen Chemie*, Walter de Gruyter, Berlin, New York, **2007**.

[16] G. A. Olah, S. G. Prakash, Á. Molnár, J. Sommer, *Superacid Chemistry*, Wiley, Hoboken, NJ, **2009**.

[17] G. A. Olah, A. M. White, *J. Am. Chem. Soc.* **1967**, *89*, 7072.

[18] D. Leitz, K. Stierstorfer, Y. Morgenstern, F. Zischka, A. J. Kornath, *Z. Anorg. Allg. Chem.* **2018**, *644*, 483.

[19] N. W. Mitzel, U. Losehand, K. Vojinovic, *Inorg. Chem.* **2001**, *40*, 5302.

[20] G. A. Olah, E. Namanworth, *J. Am. Chem. Soc.* **1966**, *88*, 5327.

[21] G. A. Olah, J. Sommer, E. Namanworth, *J. Am. Chem. Soc.* **1967**, *89*, 3576.

[22] CrysAlisCCD, *Version 1.171.35.11 (release 16-05-2011 CrysAlis 171.NET)*, Oxford Diffraction Ltd, UK, **2011**.

[23] CrysAlisRED, *Version 1.171.35.11 (release 16-05-2011 CrysAlis 171.NET)*, Oxford Diffraction Ltd, UK, **2011**.

[24] G. M. Sheldrick, *Acta crystallographica. Section A, Foundations and advances* **2015**, *71*, 3.

[25] L. J. Farrugia, *J. Appl. Crystallogr.* **1999**, *32*, 837.

[26] A. L. Spek, *J. Appl. Crystallogr.* **2003**, *36*, 7.

[27] SCALE3 ABSPACK, *An Oxford Diffraction Program*, Oxford Diffraction Ltd, UK, **2005**.

[28] M. J. Frisch, G. W. Trucks, H. B. Schlegel, G. E. Scuseria, M. A. Robb, J. R. Cheeseman, G. Scalmani, V. Barone, G. A. Petersson, H. Nakatsuji et al., *Gaussian 16 Rev. C.01*, Wallingford, CT, **2016**.

[29] Roy Dennington, Todd A. Keith, John M. Millam, *GaussView 6*, Semichem Inc., Shawnee Mission KS, **2019**.

Entry for the Table of Contents

Layout 1:

FULL PAPER

The extraterrestrial compound α-hydroxyisobutyric acid (HIBA) reacts with superacids to the mono- and diprotonated species. The intramolecular hydrogen bond of HIBA is reversed and broken up upon successive protonation. What does that mean for the stability of the system? Single-crystal X-ray diffraction and quantum-chemical calculations provide answers.
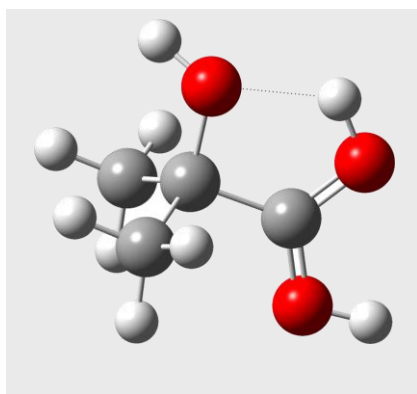
Alan Virmani, Timo F. Manitz, Alexander Nitzer, Christoph Jessen, Andreas J. Kornath*

Page No. – Page No.

Reversing the Intramolecular Hydrogen Bond – Successive Protonation of α-Hydroxyisobutyric Acid

Supporting Information

Reversing the Intramolecular Hydrogen Bond – Successive Protonation of α-Hydroxyisobutyric Acid

Alan Virmani, Timo F. Manitz, Alexander Nitzer, Christoph Jessen, and Andreas J. Kornath*

List of Figures

List of Tables

Experimental Procedure

Caution! Avoid contact with any of these materials. Hydrogen fluoride will be formed by the hydrolysis of these compounds. HF burns the skin and causes irreparable damage. Safety precautions should be taken when using and handling these materials.

Synthesis of [HIBA-1H][SbF$_6$]

For the synthesis of [HIBA-1H][SbF$_6$], first antimony pentafluoride (217 mg. 1.00 mmol) was condensed into a reactor (FEP tube), followed by excess anhydrous hydrogen fluoride at −196°C. The mixture was warmed up to −35°C to form the superacidic medium. α-Hydroxyisobutyric acid (104.1 mg, 1.00 mmol) was added under an inert nitrogen atmosphere. The mixture was warmed up to –35°C for 10 min before being cooled down to −78°C again. After removing excess HF in dynamic vacuum overnight, [HIBA-1H][SbF$_6$] was obtained as a colorless solid in quantitative yields.

Synthesis of [HIBA-2H][SbF$_6$]$_2$

For the synthesis of [HIBA-2H][SbF$_6$]$_2$, first antimony pentafluoride (650 mg, 3.00 mmol) was condensed into a reactor (FEP tube), followed by excess anhydrous hydrogen fluoride at −196°C. The mixture was warmed up to −40°C to form the superacidic medium. α-Hydroxyisobutyric acid (104.1 mg, 1.00 mmol) was added under an inert nitrogen atmosphere. The mixture was warmed up to –40°C for 10 min before being cooled down to −78°C again. After removing excess HF in dynamic vacuum overnight, [HIBA-2H][SbF$_6$]$_2$ was obtained as a colorless solid in quantitative yields.

Synthesis of [HIBA]·GeF$_4$

For the synthesis of [HIBA]GeF$_4$, first germanium tetrafluoride (446 mg, 3.00 mmol) was condensed into a reactor (FEP tube), followed by excess anhydrous hydrogen fluoride at −196°C. The mixture was warmed up to −60°C to form the superacidic medium. α-Hydroxyisobutyric acid (104.1 mg, 1.00 mmol) was added under an inert nitrogen atmosphere. The mixture was warmed up to –60°C for 10 min before being cooled down to −78°C again. After removing excess HF in dynamic vacuum overnight, [HIBA]GeF$_4$ was obtained as a colorless solid in quantitative yields.

NMR Spectroscopy

[HIBA-1H][SbF₆]
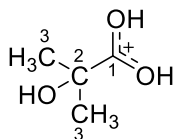
¹H NMR (400 MHz, Acetone-d_6) δ [ppm] = 8.07 - 8.00 (m, 4H, HF), 1.27 (s, 1H, C3−H).
¹³C NMR (101 MHz, Acetone-d_6) δ [ppm] = 193.01 (C1), 76.44 (C2), 23.68 (C3).
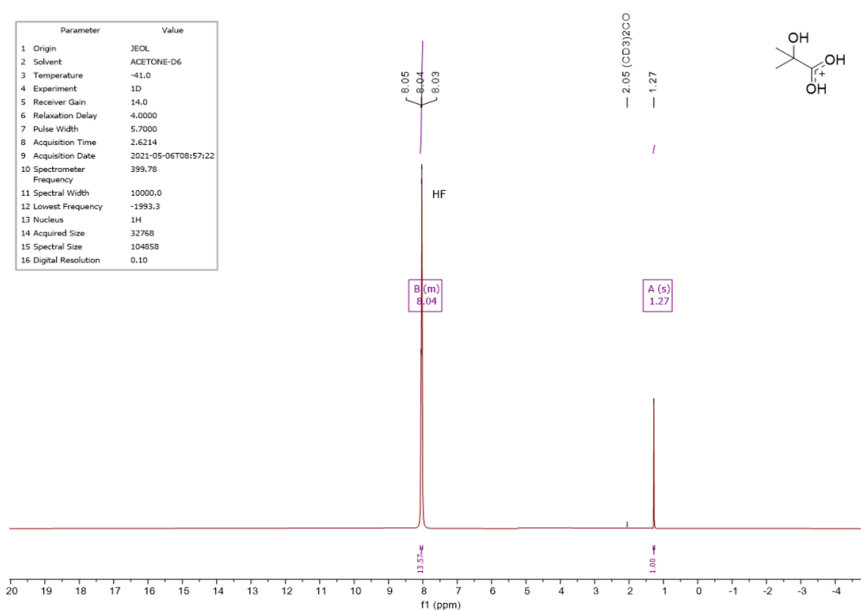
Figure S1. ¹H NMR spectrum of HIBA with one equivalent of SbF₅ in aHF at −40°C.
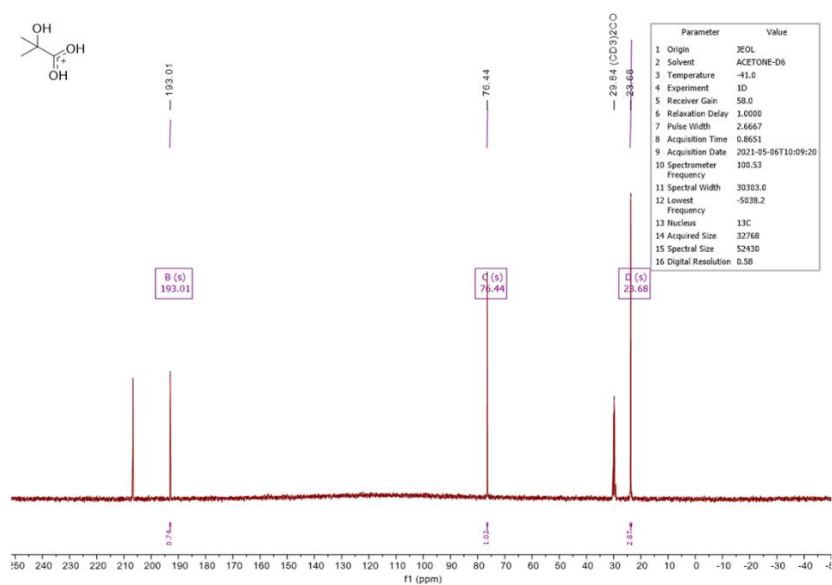
Figure S2. ¹³C NMR spectrum of HIBA with one equivalent of SbF₅ in aHF at −40°C.

S4

[HIBA-2H][SbF₆]₂
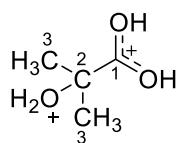
^{1}**H NMR** (400 MHz, Acetone-d_6) δ = 9.80 (s, 0H, [OH$_2$]$^{+}$), 8.01 (s, 19H, HF), 1.55 (s, 1H, C3-H).
^{13}**C NMR** (101 MHz, Acetone-d_6) δ = 186.76 (C1), 87.59 (C2), 21.98 (C3).
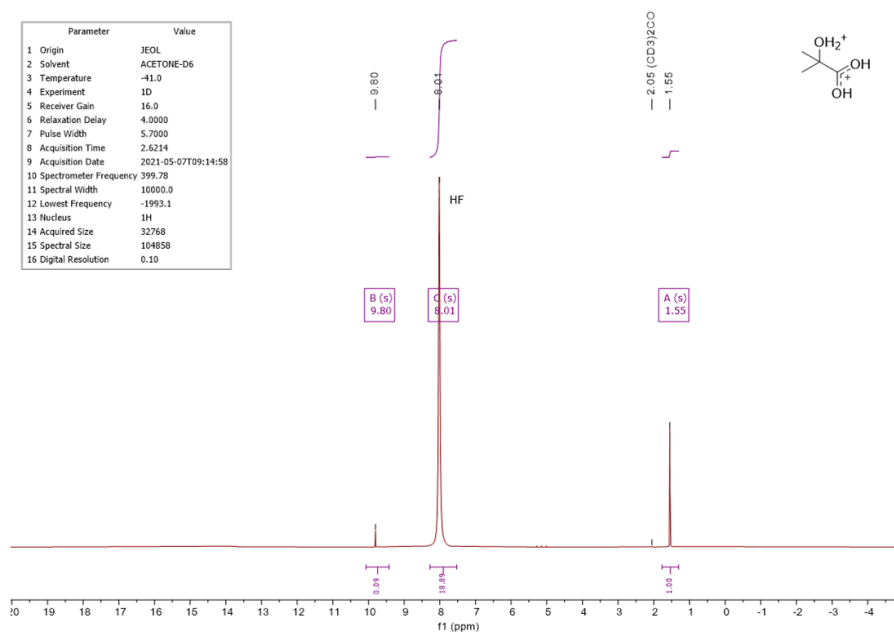
Figure S3. ^{1}H NMR spectrum of HIBA with three equivalents of SbF$_5$ in aHF at −40°C.
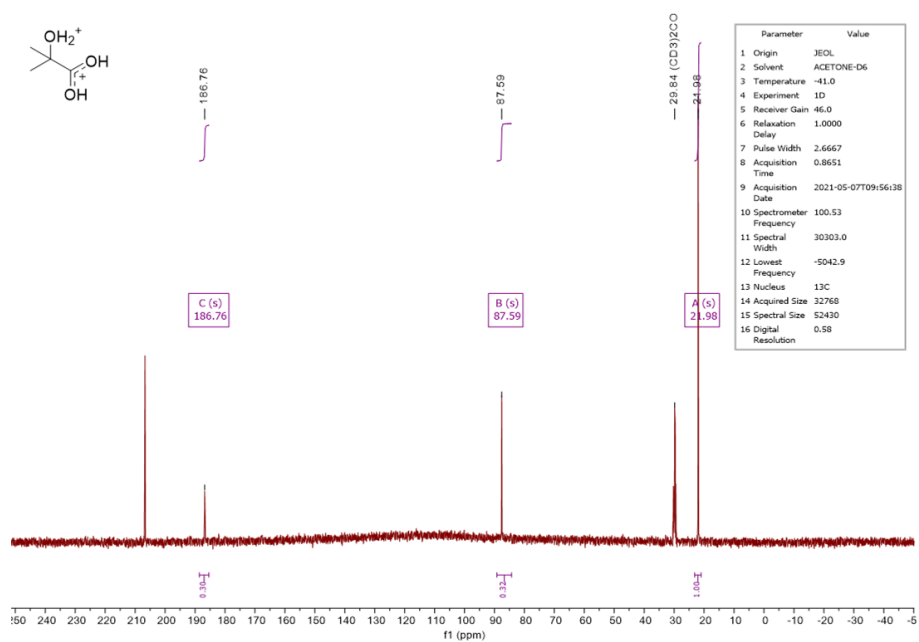
Figure S4. ^{13}C NMR spectrum of HIBA with three equivalent of SbF$_5$ in aHF at −40°C.
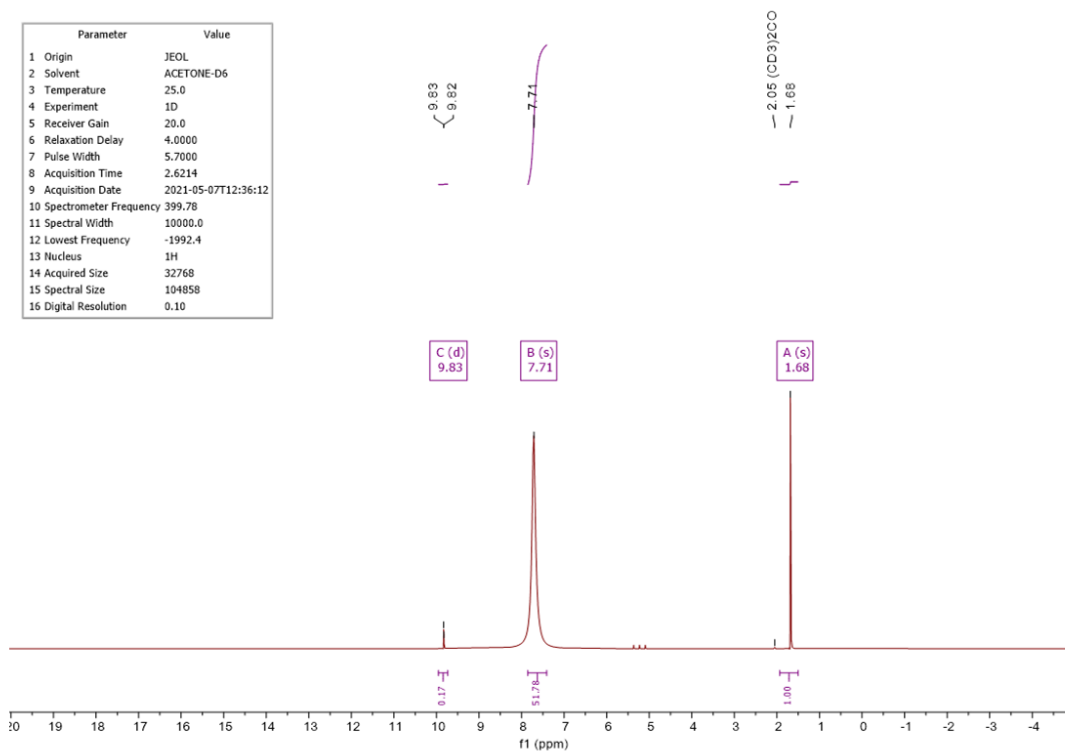
Figure S5. ^{1}H NMR spectrum of HIBA with three equivalents of SbF$_5$ at room temperature.
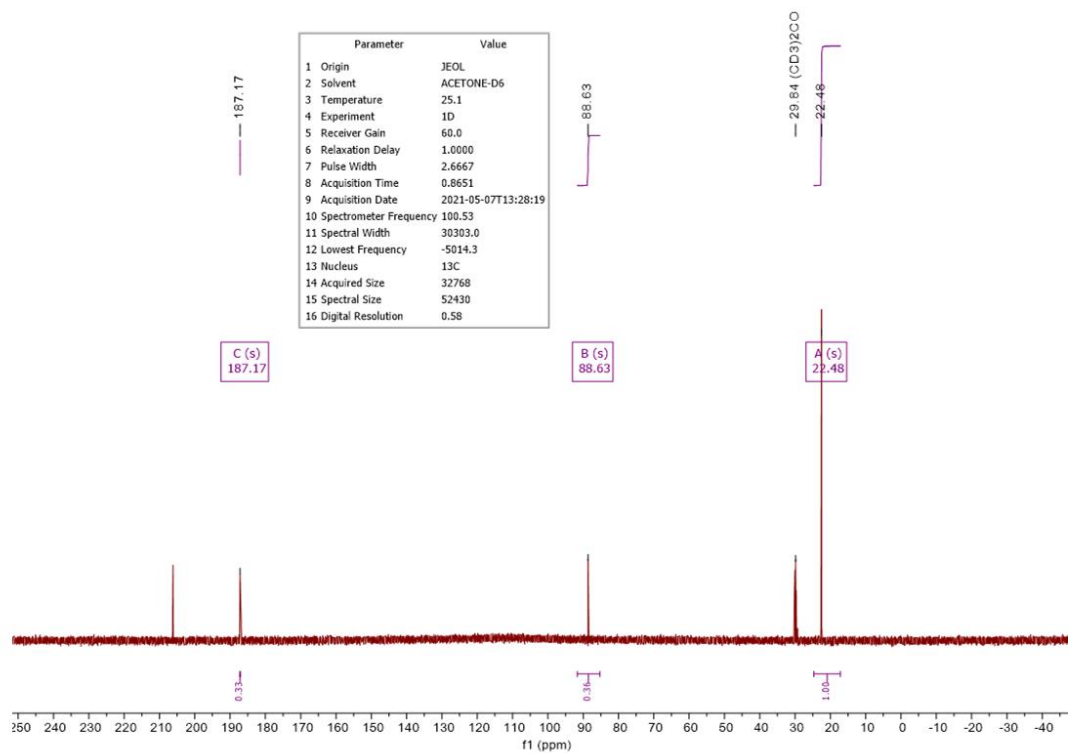
Figure S6. ^{13}C NMR spectrum of HIBA with three equivalents of SbF$_5$ at room temperature.

When two equivalents of SbF$_5$ are employed, the acidity does not suffice to protonate HIBA twice. As discussed, the proton and carbon signals are shifted in a specific direction with successive protonation. Using a twofold amount of Lewis acid leads to resonances in between the mono- and the diprotonated species. A sesquiprotonation is a possible explanation with a bridging proton between the hydroxy groups of two monocations.
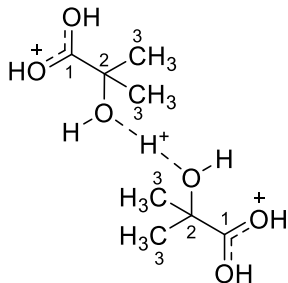
^{1}H NMR (400 MHz, Acetone-d_6) δ = 1.49 (s, 1H, C3−H).
^{13}C NMR (101 MHz, Acetone-d_6) δ = 190.01 (C1), 83.01 (C2), 22.70 (C3).

	Parameter	Value
1	Origin	JEOL
2	Solvent	ACETONE-D6
3	Temperature	-40.9
4	Experiment	1D
5	Receiver Gain	14.0
6	Relaxation Delay	4.0000
7	Pulse Width	5.7000
8	Acquisition Time	2.6214
9	Acquisition Date	2021-05-06T10:18:34
10	Spectrometer Frequency	399.78
11	Spectral Width	10000.0
12	Lowest Frequency	-1993.4
13	Nucleus	1H
14	Acquired Size	32768
15	Spectral Size	104858
16	Digital Resolution	0.10

Figure S7. ^{1}H NMR spectrum of HIBA with two equivalents of SbF$_5$ in aHF at −40°C.
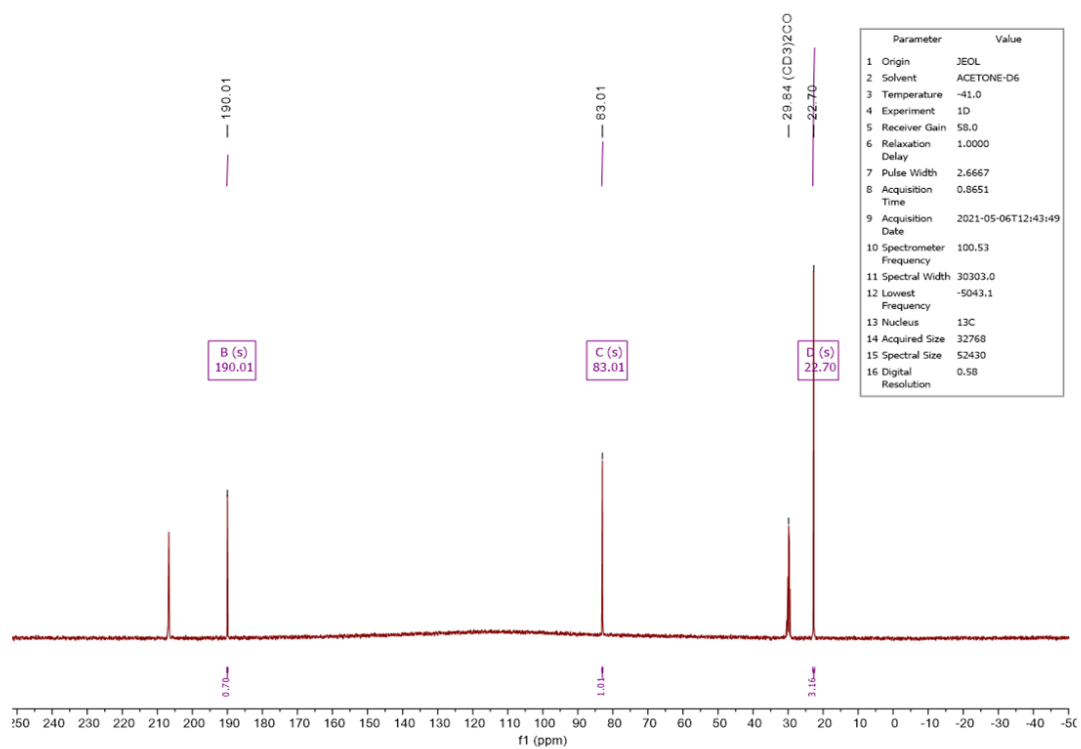
Figure S8. ^{13}C NMR spectrum of HIBA with two equivalents of SbF$_5$ in aHF at $-40°C$.
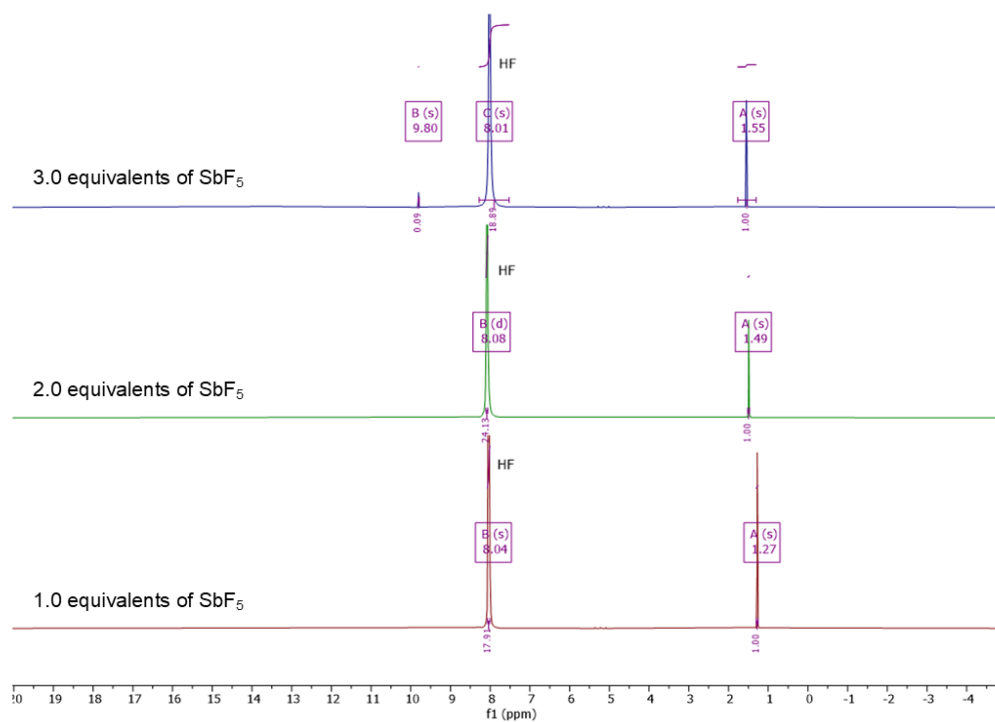
Figure S9. Stack of the ^{1}H NMR spectra of HIBA with the respective amount of Lewis acid at −40°C.
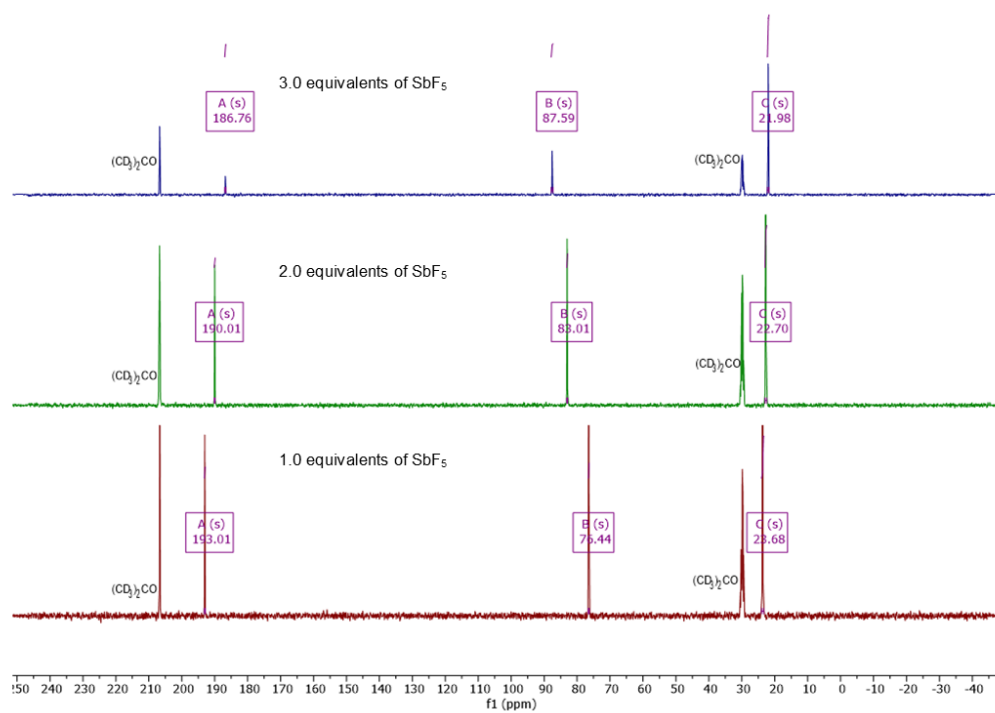
Figure S10. Stack of the ^{13}C NMR spectra of HIBA with the respective amount of Lewis acid at −40°C.

HIBA
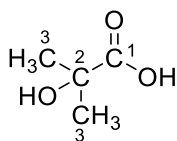
^{1}**H NMR** (400 MHz, Acetone-d_6) δ = 1.39 (s, 1H, C3-H).
^{13}**C NMR** (101 MHz, Acetone-d_6) δ = 178.35 (C1), 72.17 (C2), 27.70 (C3).
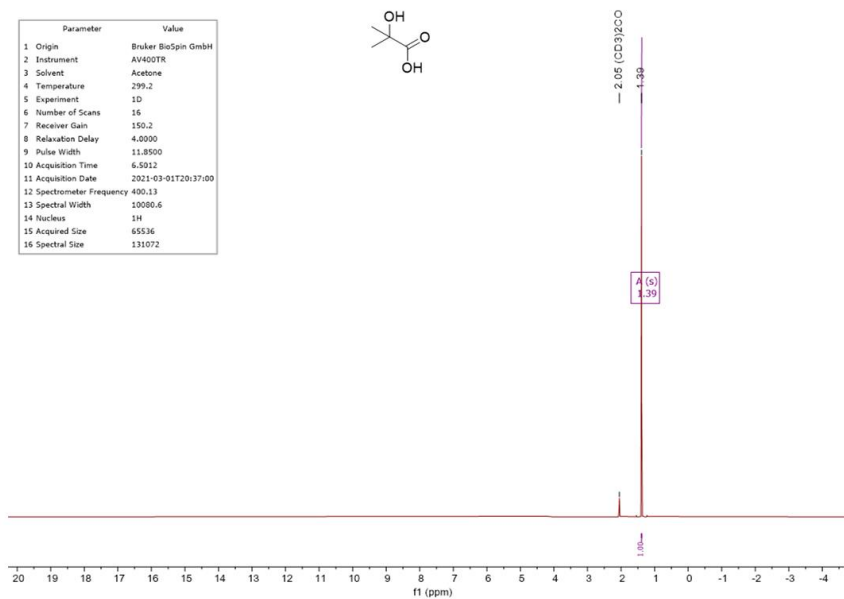
Figure S11. ^{1}H NMR spectrum of HIBA in acetone-d6 at room temperature.
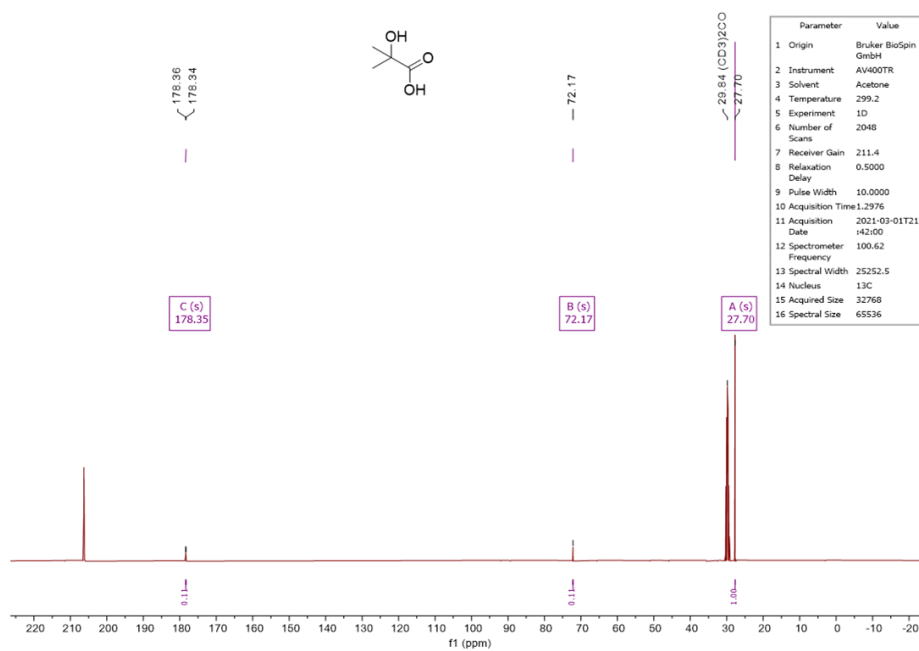
Figure S12. ^{13}C NMR spectrum of HIBA in acetone-d6 at room temperature.

[HIBA]·GeF$_4$

When HIBA is added to a solution of a threefold amount of GeF$_4$ in aHF at −60°C, HIBA chelates to the two acceptor sites of the Lewis acid (Equation S1). The product was analyzed via ^{1}H and ^{13}C NMR spectroscopy at 0°C as well as single-crystal X-ray diffraction (see Chapter X-ray diffraction).
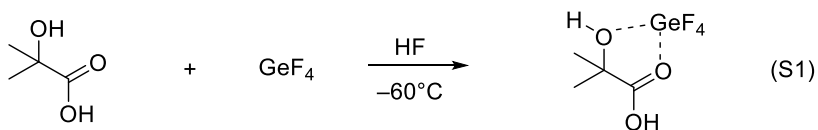
The ^{1}H signal at 7.94 ppm is assigned to the solvent HF. The methyl protons occur at 1.59 ppm and are thus very similar to the doubly protonated species (1.55 ppm). In the ^{13}C NMR spectra, the carboxylic carbon signal is shifted downfield by about 9 ppm to 187.70 ppm compared to HIBA. The C2 atom is moved downfield in the chelated complex (80.06 ppm) than in the starting material (72.17 ppm), whereas the carbon signal of the methyl groups is shifted upfield by about 4 ppm to 23.27 ppm, which is comparable to the monoprotonated species [HIBA-1H][SbF$_6$]. The ^{1}H and ^{13}C shifts of both methyl groups are magnetically equivalent in the formed adduct, indicating C_s symmetry.
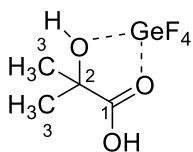
^{1}H NMR (400 MHz, Acetone-d_6) δ [ppm] = 7.94 (s, 41H, HF), 1.59 (s, 1H, C3−H).
^{13}C NMR (101 MHz, Acetone-d_6) δ [ppm] = 187.70 (C1), 80.06 (C2), 23.27 (C3).
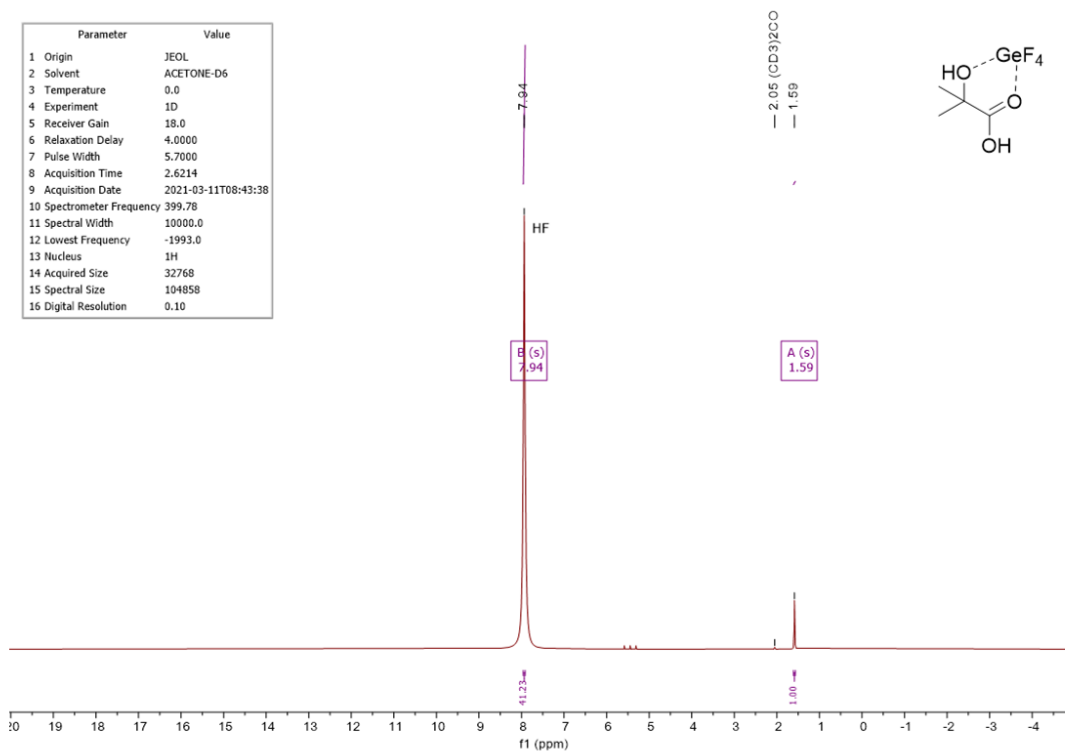
Figure S13. ^{1}H NMR spectrum of HIBA with three equivalents of GeF$_4$ at 0°C.
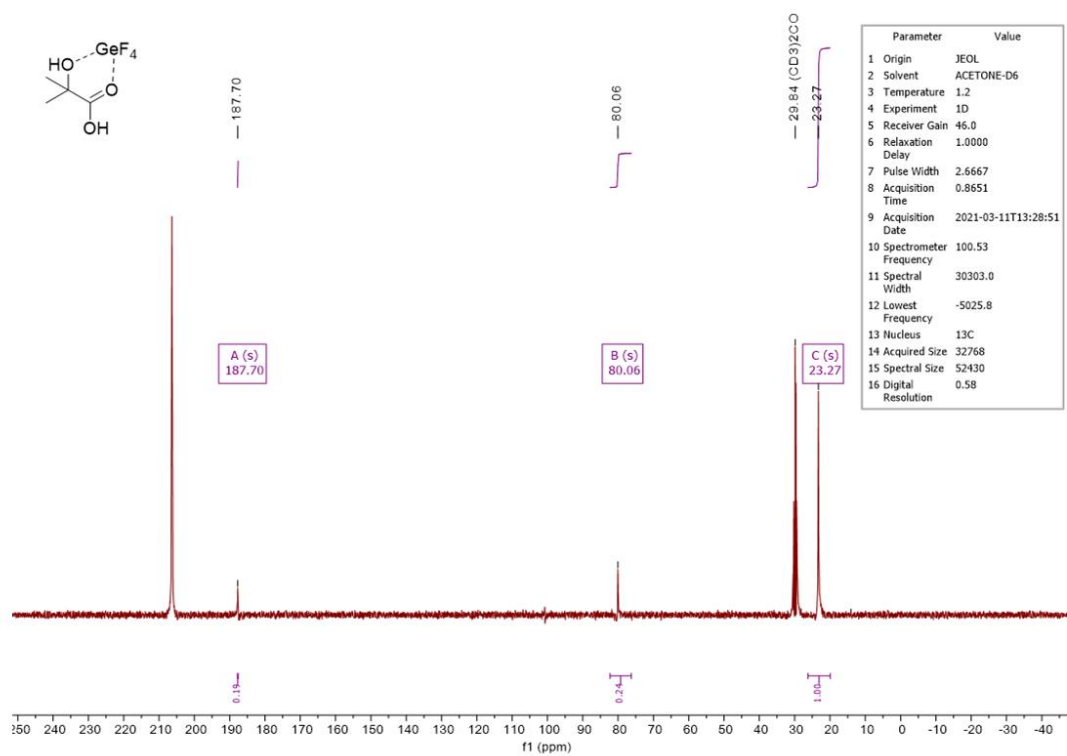
Figure S14. ^{13}C NMR spectrum of HIBA with three equivalents of GeF$_4$ at 0°C.

X-ray diffraction

Table S1. X-ray data and parameters of [HIBA-1H][SbF₆], [HIBA-2H]₂[SbF₆]₄·HF, [HIBA]·GeF₄, and HIBA.

	[C₄H₉O₃][SbF₆]	[C₄H₁₀O₃]₂[SbF₆]₄·HF	[C₄H₈O₃]·GeF₄	C₄H₈O₃[e]
Formula	$C_4H_9F_6O_3Sb$	$C_8H_{21}F_{25}O_6Sb_4$	$C_4H_8F_4O_3Ge$	$C_4H_8O_3$
M_r [g mol⁻¹]	340.86	1175.25	252.69	104.10
Crystal size [mm³]	0.326 × 0.249 × 0.143	0.500 × 0.407 × 0.329	0.416 × 0.383 × 0.263	0.334 × 0.218 × 0.208
Crystal system	monoclinic	orthorhombic	monoclinic	monoclinic
Space group	$P2_1/c$	$Pca2_1$	$P2_1/n$	$P2_1/n$
a [Å]	13.0689(5)	10.5543(2)	5.6782(6)	5.8091(3)
b [Å]	10.9433(4)	14.7516(3)	9.0407(6)	9.3580(5)
c [Å]	13.6410(5)	18.5552(3)	15.1214(11)	9.8933(5)
α [deg]	90.0	90	90	90
β [deg]	101.475(3)	90	90.564(7)	90.133(5)
γ [deg]	90.0	90	90	90
V [Å³]	1911.90(12)	2888.91(9)	776.22(11)	537.81(5)
Z	8	4	4	4
ρ_{calc} [g·cm⁻³]	2.368	2.702	2.162	1.286
μ [mm⁻¹]	2.962	3.886	3.986	0.110
λ(Mo-K$_\alpha$) [Å]	0.71073	0.71073	0.71073	0.71073
F(000)	1296	2184	496	224
T [K]	100(2)	100(2)	102(2)	105(2)
h,k,l range	−12:19; −12:16; −20:19	−15:15; 21:21; −27:27	−7:8; −13:13; −21:22	−7:7; −11:12; −13:13
Refl. Measured	6193	9801	2552	1442
Refl. Unique	4993	9404	2169	1137
R_{int}	0.0318	0.0330	0.0432	0.0388
Parameters	263	453	119	74
R(F)/wR(F^2)[a] (all reflexions)	0.0535/0.0660	0.0235/0.0484	0.0655/0.1316	0.0495/0.0944
Weighting scheme	calc.[b]	calc.[b]	calc.[b]	calc.[b]
S (GooF)[d]	1.034	1.056	1.201	1.052
Residual density [e Å⁻³]	1.142/−0.997	0.900/−0.597	1.390/−1.224	0.398/−0.147
Device type	Oxford Xcalibur	Oxford Xcalibur	Oxford Xcalibur	Oxford Xcalibur
Solution[1]	SHELXT	SHELXT	SHELXT	SHELXT
Refinement[2]	SHELXL-2018/3	SHELXL-2018/3	SHELXL-2018/3	SHELXL-2018/3
CCDC	2150732	2150731	2150730	2156142

[a] $R_1 = \Sigma||F_0|-|F_c||/\Sigma|F_0|$
[b] $w = [\sigma_c^2(F_0^2) + (0.0213P)^2]^{-1}$; $P = (F_0^2 + 2F_c^2)/3$
[c] $w = [\sigma_c^2(F_0^2) + (0.0332P)^2]^{-1}$; $P = (F_0^2 + 2F_c^2)/3$
[d] $GooF = \{\Sigma[w(F_0^2 - F_c^2)^2]/(n-p)\}^{1/2}$ (n = number of reflections; p = total number of parameters)
[e] First published by *Gayekama et al.*[3]

Crystal Structure of [HIBA-1H][SbF$_6$]

Single-crystals of [HIBA-1H][SbF$_6$] were obtained by recrystallizing the colorless solid from aHF at −70°C. The salt crystallizes in the monoclinic space group $P2_1/c$ with eight formula units per unit cell. Bond lengths, bond angles, torsion angles, and intermolecular interaction are listed in Table S2. The asymmetric unit contains two symmetrically independent formula units. The bond lengths and angles of the symmetrically independent cations do not differ significantly, whereas most of the donor-acceptor interactions do. This is probably due to packing effects. In the following, the effects of the protonation are explained by the example of one of the cations. Figure S15 shows the asymmetric unit of **1**. Short contacts are displayed in Figure S16, the crystal packing in Figure S17.

Figure S15. The asymmetric unit of **1**. Thermal ellipsoids set at 50% displacement probability, hydrogen atoms set as spheres of arbitrary radius.
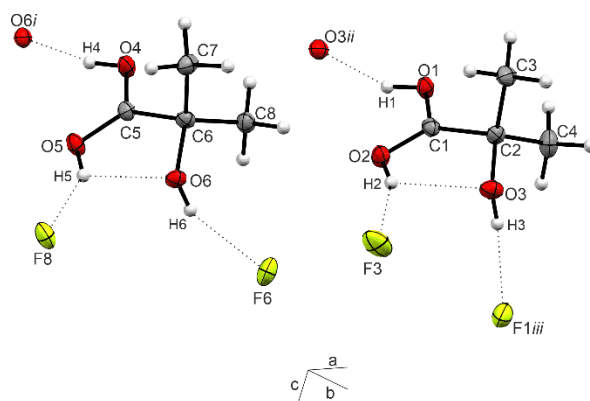
Figure S16. Symmetrically independent cations of **1**. Thermal ellipsoids displacement probability set at 50%, hydrogen atoms as spheres of arbitrary radius. Donor-acceptor interactions are visualized as dashed lines. Symmetry codes: i = 1−x, −0.5+y, 0.5−z; ii = 2−x, −0.5+y, 0.5−z; iii = 2−x, 2−y, 1−z.

The CC bond distances of the C2 atom to the methyl groups for [HIBA-1H]$^+$ (both 1.523(4) Å) are in the same range as in the parent compound (1.522(2) Å and 1.528(2) Å). However, the C1−C2 bond shortens from 1.529(1) Å to 1.507(5) Å. Carboxylic CO bond lengths of 1.257(4) Å (C1−O1) and 1.289(4) Å (C1−O2) are between a formal single and double bond, similar to previous studies in literature.[4],[5] The C2−O3 bond remains unaffected by the protonation (1.439(4) Å against 1.429(1) Å in the starting material). The bond angles around the C2 atom remain unchanged and in the range of a regular sp^3 hybridized carbon atom. The O1−C1−C2 angle widens from 112.7(1)° to 117.5(3)° and O1−C1−O2 shrinks from 123.9(1)° to 119.4(3)°, whereas the O2−C1−C2 angle is the same as in the starting material.

The first symmetrical independent cation of [HIBA-1H]$^+$ has an O2–C1–C2–O3 torsion angle of 13.9(4)°, the respective O5–C5–C6–O6 angle in the second cation amounts to 11.3(4)°. Thus deriving slightly from the ideal C_s symmetry. Both cations form chains with other cations of the same species via the hydrogen bonds O1···O3ii (2.519(3) Å) and O4···O6i (2.540(3) Å), respectively. The first cation strictly interacts additionally with only one of the symmetrically independent anions via the hydrogen bridges O2···F3 (2.699 Å) and O3···F1iii (2.708(3) Å). However, the second cation forms contacts with [(Sb1)F$_6$]$^-$ (O6···F6, 2.752(3) Å) as well as [(Sb2)F$_6$]$^-$ (O5···F8, 2.599(3) Å), which is the only interaction of this anion. Additionally, both cations exhibit intramolecular hydrogen bonds of notable strength as a stabilizing effect (see Theoretical Study in the main article), resulting in a five-membered, nearly planar ring. The donor-acceptor distances amount to 2.644(3) Å (O2···O3) and 2.633(3) Å (O5···O6), respectively.
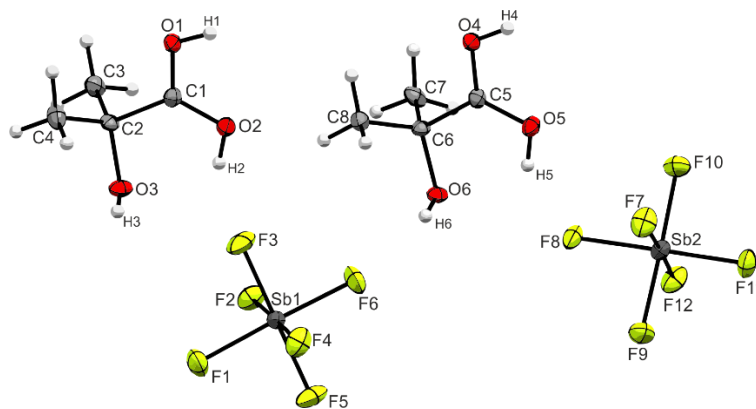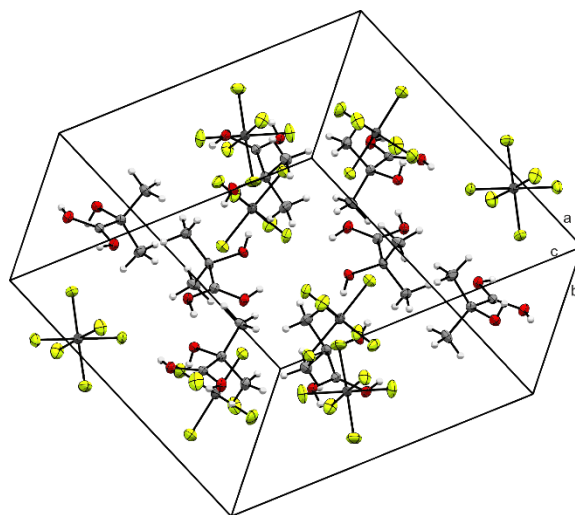
Figure S17. Crystal packing of **1**. Thermal ellipsoids set at 50% displacement probability, hydrogen atoms set as spheres of arbitrary radius.

Table S2. Bond lengths [Å], angles [°], torsion angles [°], and donor-acceptor interactions [Å] of the symmetrically independent cations of **1**. Symmetry operations: *i* = 1−*x*, −0.5+*y*, 0.5−*z*; *ii* = 2−*x*, −0.5+*y*, 0.5−*z*; *iii* = 2−*x*, 2−*y*, 1−*z*.

Bond lengths [Å]			
C1–C2	1.507(5)	C5–C6	1.511(5)
C2–C3	1.523(4)	C6–C7	1.524(4)
C2–C4	1.523(4)	C6–C8	1.522(4)
C1–O1	1.257(4)	C5–O4	1.269(4)
C1–O2	1.287(4)	C5–O5	1.276(4)
C2–O3	1.439(4)	C6–O6	1.442(4)
Bond angles [°]			
O1–C1–O2	119.4(3)	O4–C5–O5	118.4(3)
O1–C1–C2	117.5(3)	O4–C5–C6	118.1(3)
O2–C1–C2	123.0(3)	O5–C5–C6	123.4(3)
O3–C2–C1	106.2(2)	O6–C6–C5	105.7(2)
O3–C2–C3	107.3(2)	O6–C6–C7	108.5(2)
O3–C2–C4	111.1(2)	O6–C6–C8	111.4(2)
C1–C2–C3	106.8(2)	C5–C6–C7	107.6(2)
C1–C2–C4	112.4(3)	C5–C6–C8	111.3(2)
C3–C2–C4	112.7(3)	C8–C6–C7	112.1(2)
Torsion angles [°]			
O1–C1–C2–O3	−170.1(3)	O4–C5–C6–O6	−170.9(3)
O2–C1–C2–O3	13.9(4)	O5–C5–C6–O6	11.3(4)
O1–C1–C2–C3	75.6(4)	O4–C5–C6–C7	73.4(4)
O2–C1–C2–C3	−100.3(3)	O5–C5–C6–C7	−104.4(3)
O1–C1–C2–C4	−48.5(4)	O4–C5–C6–C8	−49.8(4)
O2–C1–C2–C4	135.5(3)	O5–C5–C6–C8	132.4(3)
Donor-acceptor interactions D(−H)···A [Å]			
O1(−H1)···O3*ii*	2.519(3)	O4(−H4)···O6*i*	2.540(3)
O2(−H2)···O3	2.644(3)	O5(−H5)···O6	2.633(3)

| O2(–H2)···F3 | 2.699(3) | O5(–H5)···F8 | 2.599(3) |
| O3(–H3)···F1*iii* | 2.708(3) | O6(–H6)···F6 | 2.752(3) |

Table S3. Bond lengths [Å] and angles [°] of the symmetrically independent anions of **1**.

Bond lengths [Å]

Sb1−F1	1.887(2)	Sb2−F7	1.883(2)
Sb1−F2	1.860(2)	Sb2−F8	1.901(2)
Sb1−F3	1.877(2)	Sb2−F9	1.868(2)
Sb1−F4	1.863(2)	Sb2−F10	1.859(2)
Sb1−F5	1.872(2)	Sb2−F11	1.869(2)
Sb1−F6	1.868(2)	Sb2−F12	1.875(2)

Bond angles [°]

F1–Sb1–F2	89.88(9)	F7–Sb2–F8	88.46(9)
F1–Sb1–F3	91.25(9)	F7–Sb2–F9	87.90(9)
F1–Sb1–F4	88.61(9)	F7–Sb2–F10	90.76(9)
F1–Sb1–F5	89.05(9)	F7–Sb2–F11	91.34(9)
F1–Sb1–F6	178.08(9)	F7–Sb2–F12	177.81(9)
F2–Sb1–F3	89.63(9)	F8–Sb2–F9	89.40(9)
F2–Sb1–F4	178.30(9)	F8–Sb2–F10	89.23(9)
F2–Sb1–F5	90.59(9)	F8–Sb2–F11	179.43(9)
F2–Sb1–F6	90.14(9)	F8–Sb2–F12	89.92(9)
F3–Sb1–F4	89.63(9)	F9–Sb2–F10	178.11(9)
F3–Sb1–F5	179.63(9)	F9–Sb2–F11	90.06(9)
F3–Sb1–F6	90.67(9)	F9–Sb2–F12	90.62(9)
F4–Sb1–F5	90.15(9)	F10–Sb2–F11	91.30(9)
F4–Sb1–F6	91.40(9)	F10–Sb2–F12	90.68(9)
F5–Sb1–F6	89.03(9)	F11–Sb2–F12	90.27(9)

Crystal Structure of [HIBA-2H]₂[SbF₆]₄·HF

Single-crystals of $[HIBA-2H]^{2+}$ were obtained as the $[SbF_6]^-$ salt from aHF at −70°C. The salt crystallizes in the orthorhombic space group *Pca*2₁ with four formula units per unit cell. Similar to the crystal packing of **1**, the asymmetric unit contains two symmetrically independent formula units. Additionally, half an HF molecule co-crystallizes per formula unit, which is why the formula $[HIBA-2H]_2[SbF_6]_4 \cdot HF$ is more appropriate to describe the crystal packing. All bond lengths, bond angles, torsion angles, and donor-acceptor distances are summarized in Table S4. The asymmetric unit is shown in Figure S18, short contacts in Figure S19, and the crystal packing in Figure S20.
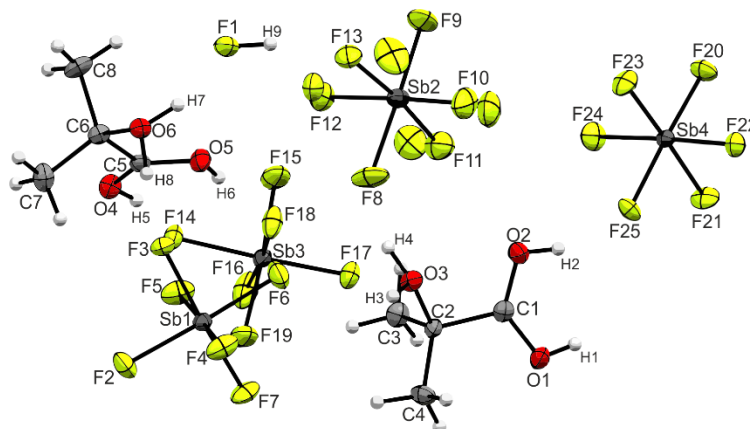

Figure S18. The asymmetric unit of **2**. Thermal ellipsoids set at 50% displacement probability, hydrogen atoms set as spheres of arbitrary radius.
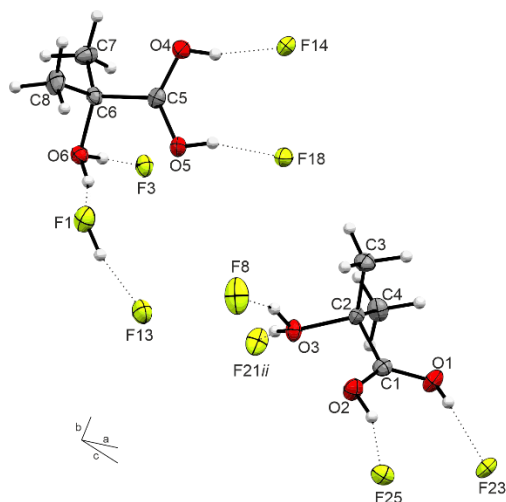
Figure S19. The two symmetrically independent cations of **2**. Thermal ellipsoids displacement probability set at 50%, hydrogen atoms as spheres of arbitrary radius. Donor-acceptor interactions are visualized as dashed lines. Symmetry operations: *i* = 0.5+*x*, −*y*, *z*; *ii* = 1.5−*x*, *y*, −0.5+*z*.

The symmetrically independent cations exhibit in comparison to each other similar bond lengths and angles. In the course of the second protonation, the CC bonds are not affected. However, the CO bond distances of the alcohol group (C2−O3 and C6−O6) significantly elongate from a regular CO single bond[6] in the starting material (1.429(1) Å) and the monoprotonated species (1.439(4) Å/1.442(4) Å) to 1.501(5) Å and 1.484(5) Å. Compared to the monoprotonated species, no intramolecular hydrogen bridge is detected. The protons at the carboxy groups are pointed away from the carbon scaffold, which is very unusual.[7],[8] It is to be noted that the position of protons in the X-ray structure analysis is not significant. Yet, the electron density indicates a high probability of the presence of protons at these positions. Following this, it is not surprising that the O1−C1−O2 (and O4−C5−O6, respectively) widens from 119.5(3)°/118.4(3)° to 127.7(4)°/126.9(4)° while the O1−C1−C2/O4−C5−C6 and the O2−C1−C2/O5−C5−C6 angles decrease. The only significant difference between the symmetrically independent dications regarding the bond angles is found in the O3−C2−C1 (103.3(3)°) and O6−C6−C5 angle (107.0(3)°), respectively. The reason for this is that protons of the $[OH_2]^+$ group are pointed away from the protonated carboxy group in the case of the first cation, in the case of the second cation towards the carboxy group, inherently enhancing steric repulsion. Again, the positioning of protons in the X-ray structure analysis is not significant, but there is a high chance of their presence at this position.
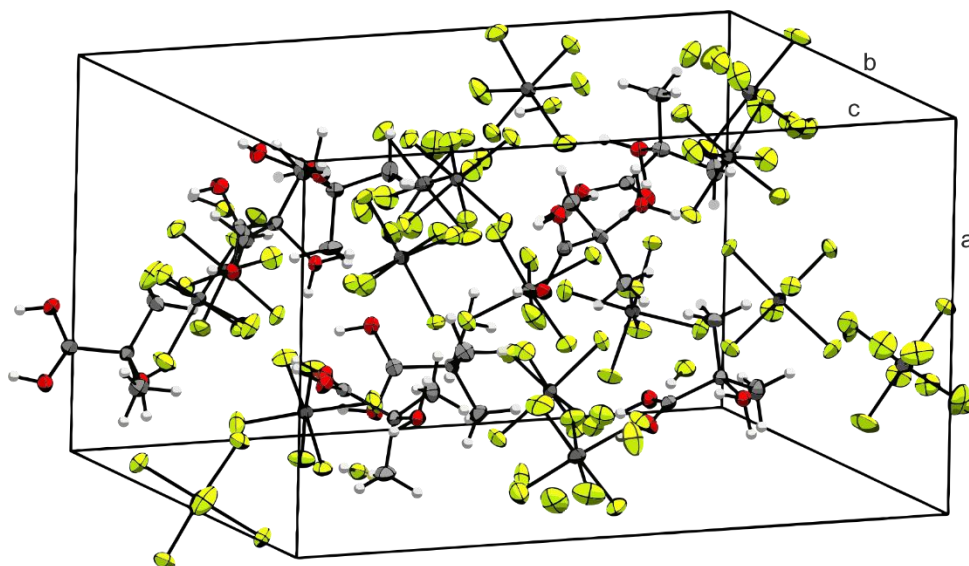
Figure S20. Crystal Packing of **2**. Thermal ellipsoids displacement probability set at 50%, hydrogen atoms as spheres of arbitrary radius.

The biggest difference between the two symmetrically independent cations is the torsion angle around the central C−C bond, which is about 17° smaller in the first cation (e.g. O2−C1−C2−O3: −35.6(5)°) compared to the second cation (O5−C5−C6−O6: −18.0(5)°). Both cations, therefore, derive from the optimal C_s symmetry, likely due to sterical effects and intermolecular interactions. They exhibit strong hydrogen bonds in the range from 2.490(4) Å to 2.576(4) Å. Since no acceptor site is accessible anymore, no cation-cation chains are possible. The first cation is bonded to three different [(Sb4)F$_6$]$^-$ anions via O2···F25 (2.497(4) Å), O1···F23*i* (2.576(4) Å), and O3(−H3)···F21*ii* (2.552(4) Å) contacts. These hydrogen bridges are the basis of the formation of chains throughout the crystal packing. The two cations are distantly linked via the [(Sb2)F$_6$]$^-$ anion, whereby the co-crystallized HF molecule is located between F13 and O6 atoms. At last, [(Sb1)F$_6$]$^-$ forms only one significant contact (O6···F3, 2.571(4) Å), [(Sb3)F$_6$]$^-$ two to the carboxy group of the second cation (O4···F14, 2.547(4) Å and O5···F18, 2.490(4) Å).

Since the four symmetrically independent anions participate in a variety of hydrogen bridges, the [SbF$_6$]$^-$ octahedrons exhibit bond lengths in the range from 1.851(3) Å to 1.919(3) Å. This leads to a deviation from their ideal symmetry in the solid-state.

Table S4. Bond lengths [Å], angles [°], torsion angles [°], and donor-acceptor interactions [Å] of the symmetrically independent cations of **2**. Symmetry operations: *i* = 0.5+*x*, −y, z; *ii* = 1.5−*x*, *y*, −0.5+*z*.

Bond lengths [Å]

C1–C2	1.514(6)	C5–C6	1.516(6)
C2–C3	1.527(6)	C6–C7	1.512(6)
C2–C4	1.514(6)	C6–C8	1.519(6)
C1–O1	1.266(5)	C5–O4	1.266(5)
C1–O2	1.254(5)	C5–O5	1.259(5)
C2–O3	1.501(5)	C6–O6	1.484(5)

Bond angles [°]

O1–C1–O2	127.7(4)	O4–C5–O5	126.9(4)
O1–C1–C2	115.1(4)	O4–C5–C6	115.7(4)
O2–C1–C2	117.2(4)	O5–C5–C6	117.4(4)
O3–C2–C1	103.3(3)	O6–C6–C5	107.0(3)
O3–C2–C3	108.9(3)	O6–C6–C7	107.3(3)
O3–C2–C4	108.0(3)	O6–C6–C8	107.3(3)
C1–C2–C3	108.5(3)	C5–C6–C7	112.0(3)
C1−C2–C4	113.6(3)	C5–C6–C8	109.7(3)
C3–C2–C4	114.1(4)	C7–C6–C8	113.2(4)

Torsion angles [°]

O1–C1–C2–O3	146.9(3)	O4–C5–C6–O6	163.0(3)
O1–C1–C2–C3	−97.7(4)	O4–C5–C6–C8	−80.8(5)
O1–C1–C2–C4	30.3(5)	O4–C5–C6–C7	45.7(5)
O2–C1–C2–O3	−35.6(5)	O5–C5–C6–O6	−18.0(5)
O2–C1–C2–C3	79.8(5)	O5–C5–C6–C8	98.2(4)
O2–C1–C2–C4	−152.3(4)	O5–C5–C6–C7	−135.3(4)

Donor-acceptor distances D(−H)⋯A [Å]

O1(–H1)⋯F23*i*	2.576(4)	O4(–H5)⋯F14	2.547(4)
O2(–H2)⋯F25	2.497(4)	O5(–H6)⋯F18	2.490(4)
O3(–H3)⋯F21*ii*	2.552(4)	O6(–H7)⋯F1	2.549(4)
O3(–H4)⋯F8	2.497(5)	O6(–H8)⋯F3	2.571(4)
F1(–H9)⋯F13	2.551(6)		

Table S5. Bond lengths [Å] and angles [°] of the symmetrically independent anions of **2**.

Bond lengths [Å]

Sb1–F2	1.855(3)	Sb3–F14	1.919(3)
Sb1–F3	1.918(2)	Sb3–F15	1.844(3)
Sb1–F4	1.870(3)	Sb3–F16	1.852(3)
Sb1–F5	1.876(3)	Sb3–F17	1.853(3)
Sb1–F6	1.860(3)	Sb3–F18	1.912(3)
Sb1–F7	1.864(3)	Sb3–F19	1.858(3)
Sb2–F8	1.909(3)	Sb4–F20	1.860(3)
Sb2–F9	1.851(3)	Sb4–F22	1.861(3)
Sb2–F10	1.817(6)	Sb4–F23	1.888(3)
Sb2–F11	1.851(8)	Sb4–F21	1.889(3)
Sb2–F12	1.909(6)	Sb4–F24	1.854(3)
Sb2–F13	1.909(5)	Sb4–F25	1.900(3)

Bond angles [°]

F2–Sb1–F3	89.79(13)	F14–Sb3–F15	88.90(14)
F2–Sb1–F4	89.23(15)	F14–Sb3–F16	90.36(12)
F2–Sb1–F5	89.15(15)	F14–Sb3–F17	174.40(12)
F2–Sb1–F6	177.44(14)	F14–Sb3–F18	84.89(11)
F2–Sb1–F7	93.23(14)	F14–Sb3–F19	86.77(13)
F3–Sb1–F4	88.53(11)	F15–Sb3–F16	90.42(17)
F3–Sb1–F5	87.58(12)	F15–Sb3–F17	91.27(14)
F3–Sb1–F6	87.65(13)	F15–Sb3–F18	89.01(16)
F3–Sb1–F7	176.98(13)	F15–Sb3–F19	175.18(16)
F4–Sb1–F5	175.79(13)	F16–Sb3–F17	95.24(13)
F4–Sb1–F6	90.78(15)	F16–Sb3–F18	175.22(13)
F4–Sb1–F7	91.59(12)	F16–Sb3–F19	91.73(17)
F5–Sb1–F6	90.67(15)	F17–Sb3–F18	89.52(12)
F5–Sb1–F7	92.38(13)	F17–Sb3–F19	92.83(14)
F6–Sb1–F7	89.33(14)	F18–Sb3–F19	88.49(15)
F8–Sb2–F9	178.21(16)	F20–Sb4–F21	90.83(13)
F8–Sb2–F10	85.4(2)	F20–Sb4–F22	90.88(12)
F8–Sb2–F11	88.0(2)	F20–Sb4–F23	92.09(13)
F8–Sb2–F12	89.36(19)	F20–Sb4–F24	92.75(13)
F8–Sb2–F13	86.80(17)	F20–Sb4–F25	177.68(14)
F9–Sb2–F10	95.4(2)	F21–Sb4–F22	89.93(13)
F9–Sb2–F11	93.5(3)	F21–Sb4–F23	176.99(13)
F9–Sb2–F12	89.6(2)	F21–Sb4–F24	90.54(14)
F9–Sb2–F13	91.65(19)	F21–Sb4–F25	88.12(12)
F10–Sb2–F11	94.0(3)	F22–Sb4–F23	89.28(12)
F10–Sb2–F12	173.2(3)	F22–Sb4–F24	176.33(13)
F10–Sb2–F13	89.1(3)	F22–Sb4–F25	87.05(11)

F11–Sb2–F12	90.3(3)	F23–Sb4–F24	90.07(13)
F11–Sb2–F13	173.8(3)	F23–Sb4–F25	88.94(12)
F12–Sb2–F13	86.2(2)	F24–Sb4–F25	89.33(12)

Crystal Structure of HIBA

The solid-state structure of α-hydroxyisobutyric acid (HIBA) was first reported by *Gaykema et al.* in 1978.[3] For better comparison to the mono- and diprotonated species reported in this study, we performed an additional X-ray structure analysis of HIBA at low temperatures. As *Gaykema et al.* reported, HIBA crystallizes in the monoclinic space group $P2_1/n$ with four formula units per unit cell. A list of all bond lengths, angles, torsion angles, and donor-acceptor distances is given in Table S6. The asymmetrical unit is displayed in Figure S21, the intermolecular contacts in Figure S22.
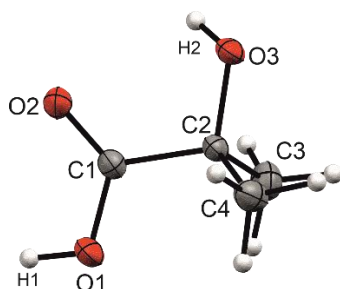

Figure S21. The asymmetric unit of HIBA. Thermal ellipsoid displacement probability set at 50%, hydrogen atoms as spheres of arbitrary size.
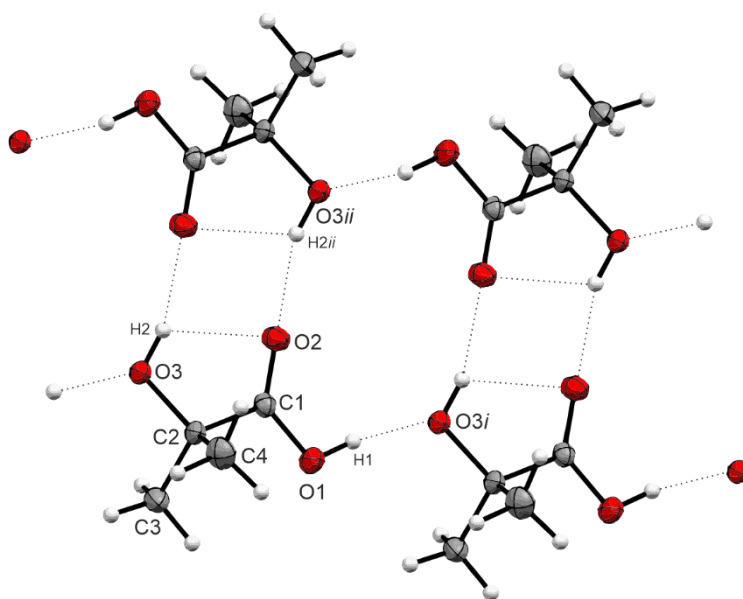
Figure S22. Intermolecular interactions of HIBA. Thermal ellipsoid displacement probability set at 50%, hydrogen atoms as spheres of arbitrary size. Symmetry operation: *i* = 1+*x*, *y*, *z*; *ii* = 1−*x*, 1−*y*, 1−*z*.

HIBA exhibits CC bond distances in the range of a regular single bond.[6],[9] The carboxylic CO bond lengths have the expected values, the C2−O3 bond matches a regular single bond.[9] The O2−C1−C2−O3 torsion angle of 14.3(1)° is approximately the same as in the monoprotonated species. The intramolecular hydrogen bond O3···O2 amounts to 2.680(1) Å with the hydroxy group as the donating site. Individual HIBA molecules form chains via the hydrogen bond O1···O3*i* (2.633(1) Å). Two antiparallel chains are connected by two symmetrical hydrogen bridges per molecular unit (O3*ii*···O2, 2.785(1) Å).

Table S6. Bond lengths [Å], angles [°], torsion angles [°], and donor-acceptor interactions [Å] of α-hydroxyisobutyric acid. Symmetry operation: *i* = 1+*x*, *y*, *z*; *ii* = 1−*x*, 1−*y*, 1−*z*.

Bond lengths [Å]

C1−C2	1.529(1)	C1−O2	1.208(1)
C2−C3	1.528(2)	C1−O1	1.315(1)
C2−C4	1.522(2)	C2−O3	1.429(1)

Bond angles [°]

O1–C1–O2	123.9(1)	O3–C2–C3	110.47(9)
O1–C1–C2	112.69(9)	C1–C2–C4	111.70(9)
O2–C1–C2	123.40(9)	C1–C2–C3	108.31(9)
O3–C2–C1	108.24(8)	C4–C2–C3	111.72(9)
O3–C2–C4	106.36(9)		

Torsion angles [°]

O2–C1–C2–O3	14.3(1)	O2–C1–C2–C4	131.0(1)
O1–C1–C2–O3	−167.31(9)	O2–C1–C2–C3	−105.5(1)
O1–C1–C2–C4	−50.6(1)	O1–C1–C2–C3	72.9(1)

Donor-acceptor distances D(−H)···A [Å]

O1(−H1)···O3*i*	2.633(1)	O3*ii*(−H2)···O2	2.785(1)
O3(−H2)···O2	2.680(1)		

Crystal Structure of [HIBA]·GeF₄

Single-crystals of the adduct of [HIBA]·GeF$_4$ were obtained by recrystallizing the colorless solid from aHF at −70°C. The compound crystallizes in the monoclinic space group *P*2$_1$/*n* with four formula units per unit cell. Crystal data and structure refinements are provided in Table S1, Table S7 contains a full list of bond lengths, bond angles, torsion angles, and intermolecular distances. The asymmetric unit is displayed in Figure S23, the crystal packing in Figure S24. Intermolecular interactions are visualized as dashed lines in Figure S25.

Figure S23. The asymmetric unit of [HIBA]·GeF$_4$. Thermal ellipsoid displacement probability set at 50%, hydrogen atoms shown as spheres of arbitrary radius.
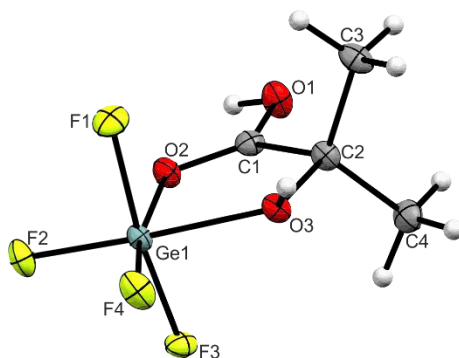
The CC bond distances of the adduct do not change compared to HIBA and are still in the range of a regular single bond.[6] The C1−O1 bond length of 1.273(6) Å is longer than in the starting material (1.208(1) Å), the C1−O2 bond becomes shorter (1.236(5) Å compared to 1.315(1) Å). This is due to the electron-withdrawing effect of the Lewis acid, similar to the protonated species. The C2−O3 bond elongates slightly from 1.429(1) Å to 1.442(6) Å and is thus similar to the respective distance in the cation of **1**. The Ge−F bond lengths are comparable to [GeF$_6$]$^{2-}$ octahedron.[10] The newly formed Ge1−O2 (1.944(3) Å) and Ge1−O3 (1.966(3) Å) bonds are similar to the reported structure of GeF$_4$·2 OEt$_2$.[11] The Ge1−F1 and the Ge1−F3 bonds are equally long within 3σ as well as the C2−C3 and the C2−C4 distances, all of which point away from the plane the adduct exhibits, indicating *C*$_s$ symmetry. This is confirmed by ^{1}H and ^{13}C NMR spectroscopy. The bond angles of the carbon scaffold remain approximately unchanged compared to the starting material. However, the

O3−C2−C1 angle decreases from 108.24(8)° in HIBA to 104.0(4) in the adduct as well as the O2−C1−C2 angle from 123.4(0)° in HIBA to 121.3(4)°. For that, the O1−C1−C2 angle widens from 112.40(9)° to 115.9(4)°. The O2−C1−C2−O3 dihedral drops from 14.3(1)° to 2.2(6)°, likely constrained by the orbital symmetries of the Ge atom.

The two axial F atoms exhibit hydrogen bridged intermolecular interactions to the OH moieties of adjacent adducts (O1(−H1)···F1i, 2.526(5) Å and O3(−H2)···F3ii, 2.576(5) Å). Three-dimensional branched chains are formed that way, visualized in Figure S25.

Figure S24. Crystal packing of [HIBA]·GeF$_4$. Thermal ellipsoid displacement probability set at 50%, hydrogen atoms shown as spheres of arbitrary radius.
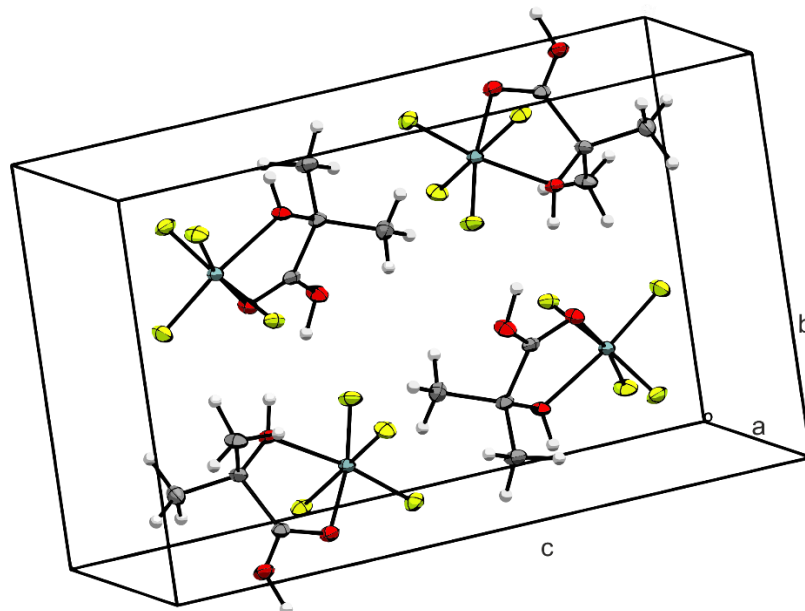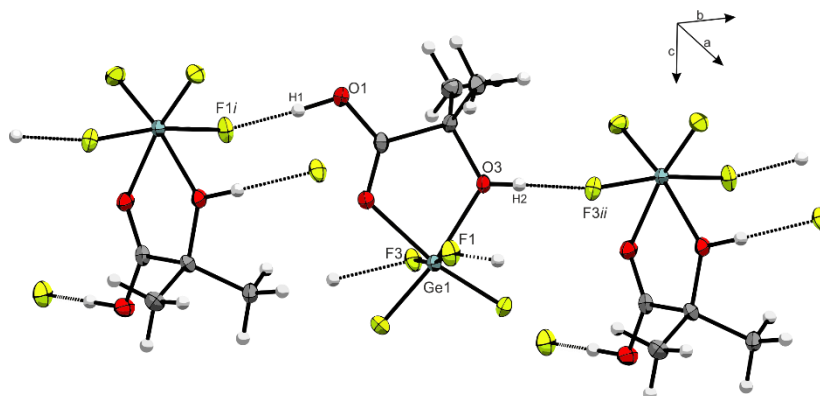

Figure S25. Intermolecular contacts in the crystal packing of [HIBA]·GeF$_4$. Thermal ellipsoid displacement probability set at 50%, hydrogen atoms shown as spheres of arbitrary radius. Symmetry operations: i = 0.5−x,−0.5+y, 1.5−z; ii = 1.5−x, 0.5+y, 1.5−z.

Table S7. Bond lengths [Å], bond angles [°], torsion angles [°], and donor-acceptor distances [Å] of [HIBA]·GeF₄. Symmetry operations: *i* = 0.5−*x*,−0.5+*y*, 1.5−*z*; *ii* = 1.5−*x*, 0.5+*y*, 1.5−*z*.

Bond lengths [Å]

C1−C2	1.515(6)	Ge1−F1	1.793(3)
C2−C3	1.509(7)	Ge1−F2	1.732(3)
C2−C4	1.515(7)	Ge1−F3	1.797(3)
C1−O1	1.236(5)	Ge1−F4	1.726(3)
C1−O2	1.273(6)	Ge1−O2	1.944(3)
C2−O3	1.442(6)	Ge1−O3	1.966(3)

Bond angles [°]

O1–C1–O2	122.8(4)	F1–Ge1–F2	92.45(15)
O1–C1–C2	115.9(4)	F1–Ge1–F3	170.71(14)
O2–C1–C2	121.3(4)	F1–Ge1–F4	92.71(15)
O3–C2–C1	104.0(4)	F1–Ge1–O2	86.25(15)
O3–C2–C4	109.2(4)	F1–Ge1–O3	88.49(15)
O3–C2–C3	109.8(4)	F2–Ge1–F3	91.73(14)
C1–C2–C4	109.8(4)	F2–Ge1–F4	100.46(14)
C1–C2–C3	109.5(4)	F2–Ge1–O2	90.33(15)
C3–C2–C4	113.9(4)	F2–Ge1–O3	170.84(14)
C1–O2–Ge1	116.6(3)	F3–Ge1–F4	94.69(15)
C2–O3–Ge1	117.4(3)	F3–Ge1–O2	85.43(14)
		F3–Ge1–O3	86.08(14)
		F4–Ge1–O2	169.20(15)
		F4–Ge1–O3	88.59(14)
		O2–Ge1–O3	80.64(14)

Torsion angles [°]

O2–C1–C2–O3	2.2(6)	Ge1–O3–C2–C3	115.0(4)
O1–C1–C2–O3	−178.7(4)	Ge1–O3–C2–C4	−119.4(4)
O1–C1–C2–C4	−61.9(5)	Ge1–O3–C2–C1	−2.1(4)
O1–C1–C2–C3	63.9(5)	Ge1–O2–C1–O1	179.7(4)
O2–C1–C2–C4	119.0(5)	Ge1–O2–C1–C2	−1.3(6)
O2–C1–C2–C3	−115.2(5)		

Donor-acceptor distances D(−H)···A [Å]

O1(−H1)···F1*i*	2.526(5)	O3(−H2)···F3*ii*	2.576(5)

Quantum-chemical Calculations

Rotational scan of HIBA

α-Hydroxyisobutyric acid was first structurally examined by *Gaykema et al.* via X-ray structure analysis,[3] but thoroughly investigated by *Fausto and Jarmelo* via vibrational spectroscopy and quantum-chemical calculations.[12] They found the C_s symmetric structure with an intramolecular hydrogen bond O−H$_{(alcohol)}\cdots$O$_{(acid)}$ to be the most stable one. We can confirm these observations by our quantum-chemical calculations on the B3LYP/aug-cc-pVTZ level of theory. Additionally, we performed a rotational scan of 10° per step around the central C−C bond of HIBA (Figure S26), similar to the scans of [HIBA-1H]+ and [HIBA-2H]2+. The importance of this intramolecular hydrogen bond is illustrated by the two significant energy drops of the rotational scan, where hydrogen bonding is possible. It is to be noted that the structure in which the doubly bonded oxygen atom of the carboxy group participates in the hydrogen bridge is most stable.
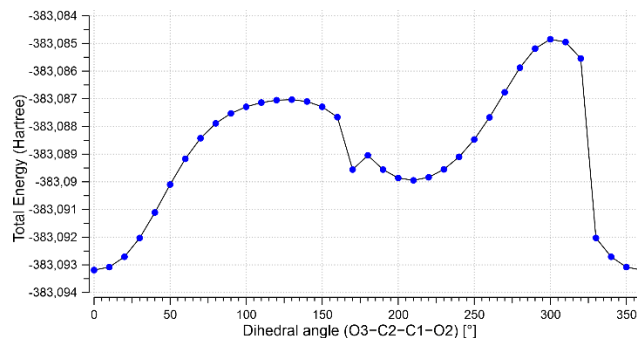

Figure S26. Rotational scan around the central C−C bond of HIBA in steps of 10°. Calculated on the B3LYP/aug-cc-pVTZ level of theory.

Rotational scan of [HIBA-1H]+

Figure S27. Rotational scan around the central C−C bond of [HIBA-1H]+ in steps of 1°. Calculated on the B3LYP/aug-cc-pVTZ level of theory.

Rotational scan of [HIBA-2H]2+

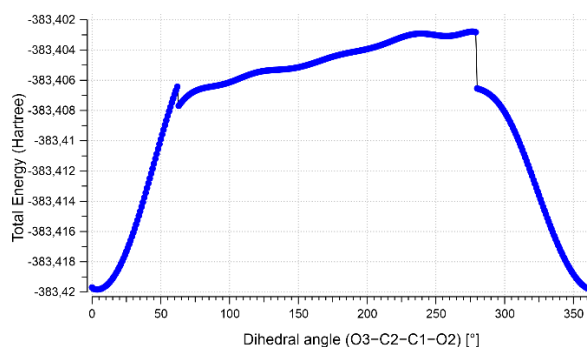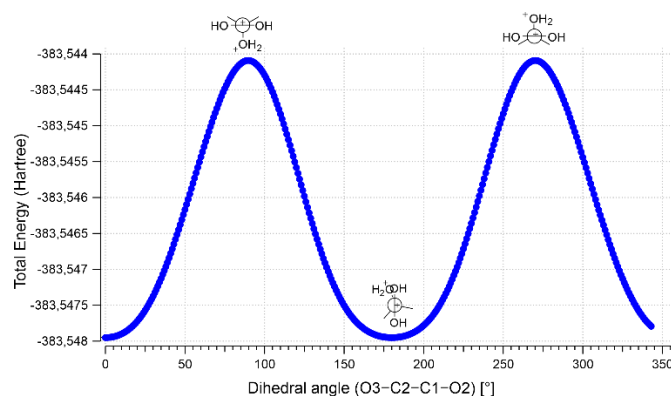**Figure S28.** Rotational scan around the central C−C bond of [HIBA-2H]2+ in steps of 1°. Calculated on the B3LYP/aug-cc-pVTZ level of theory.
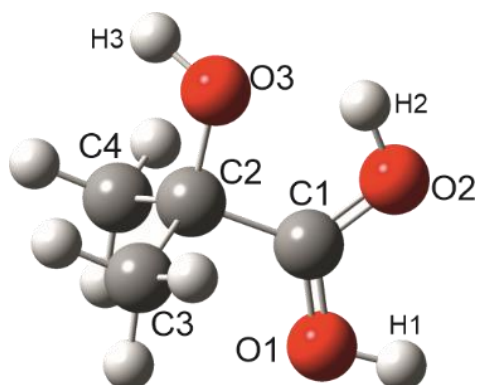
Standard orientations

Figure S29. Optimized gas-phase structure of [HIBA-1H]⁺. Calculated on the B3LYP/aug-cc-pVTZ level of theory.

Table S8: Standard orientation of the geometry-optimization of [HIBA-1H]⁺. Calculated on the B3LYP/aug-cc-pVTZ level of theory.

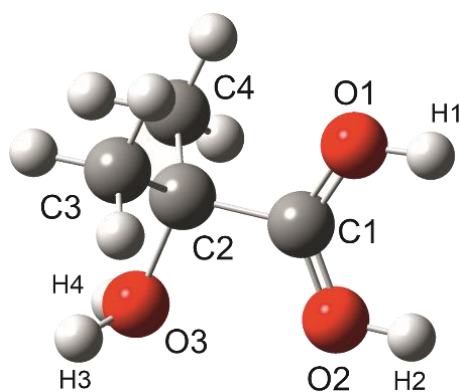| Atomic Type	X	Y	Z
O	-0.842895	1.417437	0.164784
H	-1.650809	1.692560	-0.282955
O	1.579237	1.039142	0.027486
H	0.922036	1.785686	0.067839
O	1.503929	-1.165662	-0.061377
H	2.477285	-1.088766	-0.067157
C	0.904056	-0.037666	-0.009179
C	-1.155382	-0.529667	-1.313201
H	-2.242306	-0.449307	-1.292780
H	-0.900085	-1.579869	-1.437938
H	-0.774913	0.033890	-2.164653
C	-0.608152	0.013730	0.014400
C	-1.129742	-0.761306	1.233231
H	-0.738970	-0.341171	2.158521
H	-0.864155	-1.814809	1.171970
H	-2.214933	-0.676087	1.248502

Figure S30. Optimized gas-phase structure of [HIBA-2H]²⁺. Calculated on the B3LYP/aug-cc-pVTZ level of theory.

Table S9. Standard orientation of the geometry-optimization of [HIBA-2H]²⁺. Calculated on the B3LYP/aug-cc-pVTZ level of theory.

| Atomic Type	X	Y	Z
O	-1.072949	-1.364088	-0.001657
O	1.565814	1.093828	-0.000086
H	2.546109	1.110050	-0.000345
O	1.479338	-1.180130	-0.000436
H	2.457181	-1.260226	-0.000046
C	0.957941	-0.021990	-0.000244
C	-0.572959	0.109301	0.000083
C	-1.068292	0.745308	1.289937
H	-2.156862	0.803940	1.270970
H	-0.685203	1.764407	1.351709
H	-0.736075	0.204590	2.178335
C	-1.069286	0.748568	-1.287626
H	-0.738286	0.209757	-2.177648
H	-0.685609	1.767563	-1.347543
H	-2.157784	0.807846	-1.267407
H	-1.553339	-1.644722	-0.807439
H	-1.552181	-1.647207	0.803947
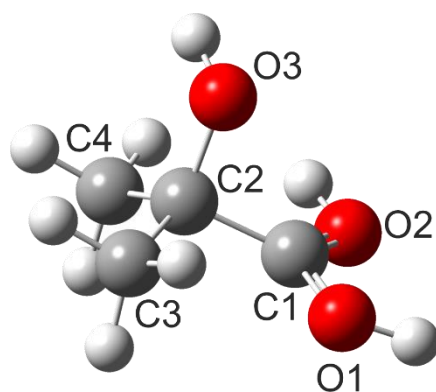
Figure S31. The transition state of the rotation around the C1−C2 bond of [HIBA-1H]⁺. Calculated on the B3LYP/aug-cc-pVTZ level of theory.

Table S10: Standard orientation of the optimization of the transition state of the rotational scan of [HIBA-1H]⁺. Calculated on the B3LYP/aug-cc-pVTZ level of theory.

| Atomic Type	X	Y	Z
C	1.194374	1.385891	-0.362863
H	0.789521	2.170214	0.271394
H	2.273323	1.357827	-0.225505
H	0.982608	1.622032	-1.405486
C	0.631942	0.026648	0.025978
C	1.250471	-1.113567	-0.778722
H	0.896586	-2.101202	-0.466261
H	1.066244	-0.998943	-1.846220
H	2.328244	-1.096761	-0.622587
C	-0.898875	0.004754	-0.085521
O	-1.533470	1.109841	-0.109257
O	-1.607543	-1.066755	-0.078674
O	0.761273	-0.157577	1.438753
H	1.216822	-0.983090	1.643978
H	-2.505222	1.005821	-0.086329
H	-1.077673	-1.882329	-0.062790
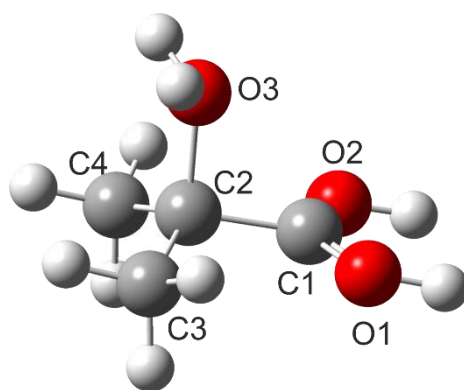
Figure S32. The transition state of the rotation around the C1−C2 bond of [HIBA-2H]²⁺. Calculated on the B3LYP/aug-cc-pVTZ level of theory.

Table S11. Standard orientation of the optimization of the transition state of the rotational scan of [HIBA-2H]²⁺. Calculated on the B3LYP/aug-cc-pVTZ level of theory.

Atomic Type	X	Y	Z
O	0.921392	0.000086	1.437349
O	-1.530441	-1.135412	-0.026667
H	-2.509699	-1.186035	0.014370
O	-1.530436	1.135404	-0.026653
H	-2.509693	1.186031	0.014391
C	-0.964418	-0.000005	-0.051851
C	1.152678	-1.280480	-0.692963
H	2.241779	-1.246718	-0.674679
H	0.852324	-1.362614	-1.741082
H	0.790868	-2.170364	-0.178231
C	0.592239	-0.000007	-0.132841
C	1.152664	1.280401	-0.693122
H	0.790838	2.170345	-0.178504
H	0.852315	1.362395	-1.741255
H	2.241765	1.246657	-0.674826
H	1.383218	-0.802967	1.756161
H	1.383181	0.803191	1.756085

References

[1]   G. M. Sheldrick, *Acta crystallographica. Section A, Foundations and advances* **2015**, *71*, 3.

[2]   G. M. Sheldrick, *Acta crystallographica. Section C, Structural chemistry* **2015**, *71*, 3.

[3]   W. P. J. Gaykema, J. A. Kanters, G. Roelofsen, *Cryst. Struct. Commun.* **1978**, *7*, 463.

[4]   M. Schickinger, F. Zischka, K. Stierstorfer, A. Kornath, *Eur. J. Org. Chem.* **2019**, *2019*, 1876.

[5]   M. Schickinger, T. Saal, F. Zischka, J. Axhausen, K. Stierstorfer, Y. Morgenstern, A. J. Kornath, *ChemistrySelect* **2018**, *3*, 12396.

[6]   E. Wiberg, N. Wiberg, G. Fischer, *Lehrbuch der anorganischen Chemie*, Walter de Gruyter, Berlin, New York, **2007**.

[7]   G. A. Olah, S. G. Prakash, Á. Molnár, J. Sommer, *Superacid Chemistry*, Wiley, Hoboken, NJ, **2009**.

[8]   G. A. Olah, A. M. White, *J. Am. Chem. Soc.* **1967**, *89*, 7072.

[9]   F. H. Allen, O. Kennard, D. G. Watson, L. Brammer, A. G. Orpen, R. Taylor, *J. Chem. Soc., Perkin Trans. 2* **1987**, S1.

[10] D. Leitz, K. Stierstorfer, Y. Morgenstern, F. Zischka, A. J. Kornath, *Z. Anorg. Allg. Chem.* **2018**, *644*, 483.

[11] N. W. Mitzel, U. Losehand, K. Vojinovic, *Inorganic chemistry* **2001**, *40*, 5302.

[12] S. Jarmelo, R. Fausto, *Phys. Chem. Chem. Phys.* **2002**, *4*, 1555.